

New Proton Conducting Membranes for Fuel Cell Applications

Dissertation zur Erlangung des Grades

“Doktor der Naturwissenschaften”

am Fachbereich Chemie, Pharmazie und Geowissenschaften der
Johannes Gutenberg-Universität in Mainz

Prabakaran Reguna Sukumar

geb. in Trichy, India

Mainz 2006

Dekan:

1. Berichterstatter:

2. Berichterstatter:

Tag der mündlichen Prüfung: 23. 10. 2006

Die vorliegende Arbeit wurde in der Zeit von 2002 bis 2006 im Max-Planck-Institute für Polymerforschung in Mainz unter Anleitung von Herrn Prof. Dr. K. Müllen ausgeführt.

Ich danke Herrn Prof. Dr. K. Müllen für seine wissenschaftliche und persönliche Unterstützung sowie für seine ständige Diskussionsbereitschaft

Dedicated to my wife Mrs Charulatha Prabakaran

Index

Theme: New Proton Conducting Membranes for Fuel Cell Applications

Table of contents

1. Introduction and focus of thesis

1.1 Fuel cells	1
1.2 Types of fuel cells	2
1.3 Proton conducting polymers	8
1.4 Polybenzimidazole and its properties	10
1.5 Proton transport mechanism	13
1.6 Multilayers for fuel cell applications	21

2 Motivation

2.1.1 Reactive polybenzimidazole	27
2.1.2 Proton conducting multilayers for fuel cell applications	29
2.1.3 Anhydrous proton conducting homo- and copolymers	29
2.1.4 Synthesis of polybenzimidazole with anthracene structural unit	29

3 Reactive polybenzimidazole

3.1 Modification of PBI	31
3.2 Polybenzimidazole used for the modification experiments	32
3.3 Modification of polybenzimidazole	32
3.4 FTIR spectra of modified PBIs	43
3.5 Viscosity measurements	45
3.6 Solubility	46
3.7 Thermal properties of modified PBIs	47
3.8 Summary	48

4 Polyvinylphosphonic acid grafted PBI

4.1 Poly(vinylphosphonic acid) grafted polybenzimidazole	51
4.2 Preparation of polymer membrane	52
4.3 Proton conductivity measurements	52
4.4 Polymerization in the presence of radical initiator	56
4.5 Proton conducting nature of membranes with increasing temperature	59
4.6 Thermal properties of membranes	60

4.7 Membrane stability in water and oxidative environment	61
4.8 Water uptake and ion exchange capacity	62
4.9 Disadvantages of PVPA grafted PBI membranes	63
4.10 Summary	64
5 Multilayers for fuel cell applications	
5.1 Study on the nature of the interaction between acid-base polymers	68
5.2 Poly(4-vinylimidazole) - poly(benzimidazole) for multilayer fabrication	70
5.3 Multilayers of flexible poly(4-vinylimidazole)	71
5.4 Multilayer of stiff PBI	75
5.5 Properties of LBL film	80
5.6 Proton transport in multilayers	94
5.7 Summary	96
6. Anhydrous proton conducting homo- and copolymers	
6.1 Poly(vinylphosphonic acid)	100
6.2 Poly(vinylbenzyl phosphonate)	105
6.3 Poly(2-vinylbenzimidazole)	111
6.4 Synthesis of poly(styrenesulfonate) by ATRP reaction	115
6.5 Controlled radical polymerisation of 4-vinylimidazole	118
6.6 Proton conducting copolymers	125
6.6 Summary	136
7 Polybenzimidazole with anthracene structural unit	
7.1 Introduction	139
7.2 Synthesis of poly[9,10-bis-(benzimidazole-2-yl)anthracene]	139
7.3. Conductivity of PBA versus N-allyl PBI	143
7.4 General description of making H ₃ PO ₄ blended polymer membranes	145
7.5 Unsuccessful attempt to synthesize Diels-Alder adduct of Vinylphosphonic acid and PBA-1	146
7.6 Summary	147
8 Summary	149

9 Experimental procedure

9.1 General Methods	155
9.2 Materials	156
9.3 Syntheses	157
10 Literature	181

Abbreviation

AIBN	Azobisisobutyronitrile
BPO	Benzoyl peroxide
DMAc	N,N- Dimethylacetamide
DMSO	Dimethylsulfoxide
FTIR	Fourier Transform Infrared Spectroscopy
GPC	Gel Permeation Chromatography
HIm	Protonated Imidazole
Im	Imidazole
ITO	Indium-Tin oxide
NMP	N-Methyl-2-Pyrrolidone
NMR	Nuclear Magnetic Resonance Spectroscopy
PBI	Poly[2,2'-(m-phenylene)-5,5'-bisbenzimidazole]
PBA	Poly[9,10-bis-(benzimidazole-2-yl)anthracene]
PDI	Poly Dispersity Index
PEI	Polyethyleneimine
PEM	Proton Exchange Membrane
PEMFC	Proton Exchange Membrane for Fuel Cell
PSSA	Poly(4-styrenesulfonic acid)
P4VIm	Poly(4-vinylimidazole)
PVSA	Poly(vinylsulfonic acid)
PVPA	Polyvinylphosphonic acid
TEMPO	2,2,6,6- tetramethyl-1-piperdinyloxy
TEMPO adduct	2-(4-(Chloromethyl)phenyl)-2-(2,2,6,6-tetramethylpiperidin-1-yl)oxy)ethyl Ester
UV	Ultraviolet Visible spectroscopy
VBC	Vinylbenzyl chloride

VFT	Vogel-Tamman-Fulcher equation
4-VIm	4- vinylimidazole
VPA	Vinylphosphonic acid

1 Introduction and focus of thesis

1.1 Fuel cells

Fuel Cells have emerged as one of the most promising technologies for the power source of the future. Though Sir William Grove first introduced the concept of a fuel cell in 1839, the fuel cell research has emerged as a potential field in recent decades.

The fuel cell is an electrochemical energy conversion device that converts chemical energy into electrical energy.

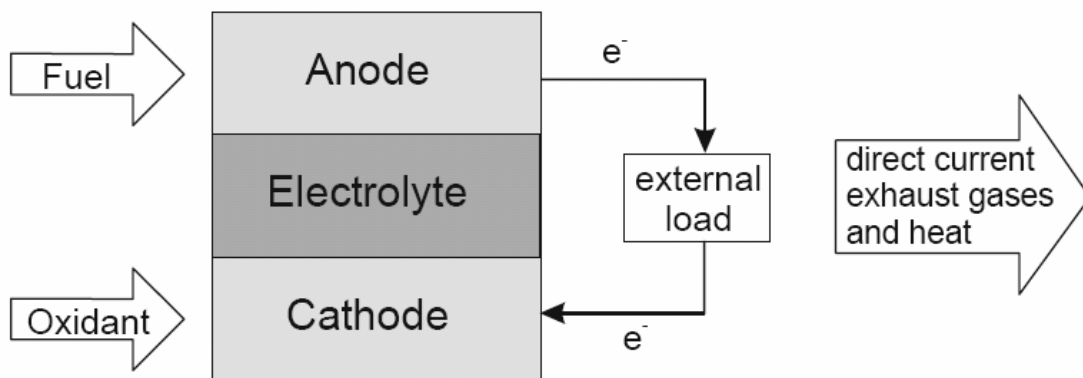


Fig. 1.1: Fuel Cell diagram

A fuel cell consists of a cathode (negatively charged electrode), an anode (positively charged electrode), an electrolyte and an external load. The anode provides an interface between the fuel and the electrolyte, catalyses the fuel reaction, and provides a path through which free electrons are conducted to the load via the external circuit. The cathode provides an interface between the oxygen and the electrolyte, catalyses the oxygen reduction reaction, and provides a path through which free electrons are conducted from the load to the electrode via the external circuit. The electrolyte acts as the separator between hydrogen and oxygen to prevent mixing and therefore, preventing direct combustion. It completes the electrical circuit of transporting ions between the electrodes (Fig.1.1).

The fuel cells are attractive for electricity production⁽¹⁾ due to their properties such as high efficiency and high energy density. Particularly, high energy density (energy per unit weight of the power source), fuel cells are superior to batteries in portable equipment. In fact, the theoretical efficiency of fuel cells is substantially higher than that of the combustion engine- around 90 %. Also, fuel cells are more environmentally friendly in that they reduce carbon dioxide emissions as well as the production of poisonous gases such as nitrogen oxides (NO_x) and sulphuric oxides (SO_x).

1.2 Types of fuel cells

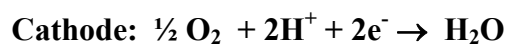
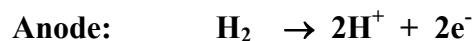
Fuel cell technologies are named by their electrolyte, as the electrolyte defines the key properties of a fuel cell, particularly the operating temperature. Five distinct types of fuel cells have been developed. These fuel cells operate at different temperatures, and each is best suited to particular applications.

The primary fuel cell technologies under development around the world are:

1.2.1 Phosphoric acid Fuel Cells (PAFCs)

A phosphoric acid fuel cell (PAFC) consists of an anode and a cathode made up of finely dispersed platinum catalyst on carbon paper-, and a silicon carbide matrix that holds the phosphoric acid electrolyte. The operating temperature of the fuel cell would be around 150 to 200 °C. The high operating temperature of PAFC can tolerate a CO concentration of about 1.5 percent due to concentrated phosphoric acid (as an electrolyte), which makes PAFC to operate above the boiling point of water, a limitation on other acid electrolytes that require water for conductivity.

The PAFC reactions that occur are:



At the anode, hydrogen is split into two hydrogen ions (H^+) and two electrons, pass to the cathode via electrolyte and via the external circuit (electric load). At the cathode, water is formed and eventually eliminated as shown in the fig. 1.2:

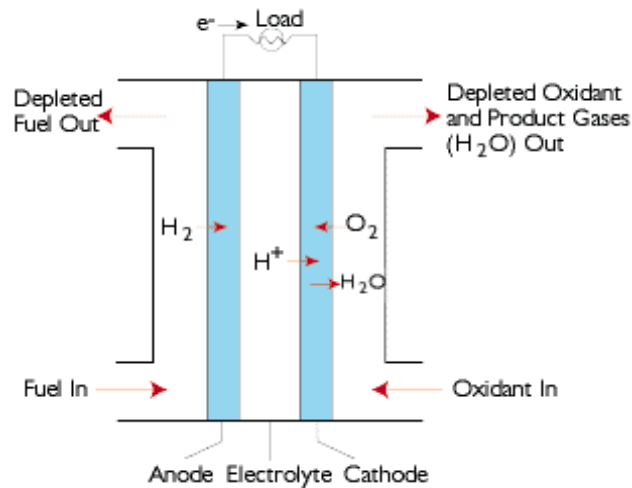


Fig. 1.2: Phosphoric Acid Fuel Cell

This is the most commercially developed type of fuel cell and is being used in hotels, hospitals, and office buildings. The phosphoric acid fuel cell can also be used in heavy automobiles.

1.2.2 Solid Oxide Fuel Cells (SOFC)

Solid oxide fuel cell (SOFC) uses hard ceramic as an electrolyte, which operates at temperatures up to 1,000 °C. Solid oxide fuel cells (SOFC) that are currently under development use a thin layer of stabilized zirconia (zirconium oxide) as a solid ceramic electrolyte-, along with a lanthanum manganate cathode and a nickel-zirconia anode.

In operation, hydrogen or carbon monoxide (CO) in the fuel stream reacts with oxide ions (O^{2-}) at the electrolyte to produce water or CO_2 . In the course of reactions, the electrons are generated and then, travel towards cathode via the external load and get converted into oxide ion. Notably, both CO and H_2 can be used as energy source in solid oxide fuel cell (Fig. 1.3).

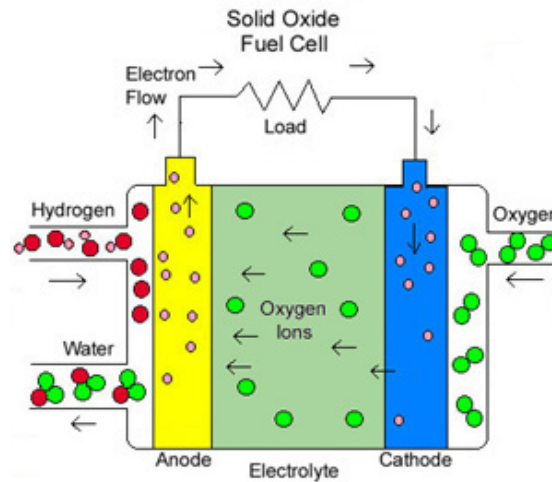
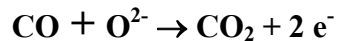
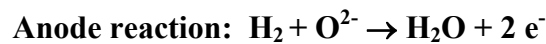


Fig. 1.3: Solid Oxide Fuel Cell

The SOFC reactions that occur include:



This fuel cell is a promising option for high-powered applications, such as industrial uses or central electricity generating stations.

1.2.3 Molten Carbonate Fuel Cells (MCFC)

The Molten Carbonate Fuel Cell (MCFC) designed in 1960's aimed to produce a fuel cell, which would operate directly on coal. The MCFC uses a molten carbonate salt mixture as its electrolyte. The composition of the electrolyte varies, but usually consists of lithium carbonate and potassium carbonate. At the operating temperature of about 650 °C, the salt mixture is liquid and a good ionic conductor. The electrolyte is suspended in a porous, insulating and chemically inert ceramic (LiAlO_2) matrix.

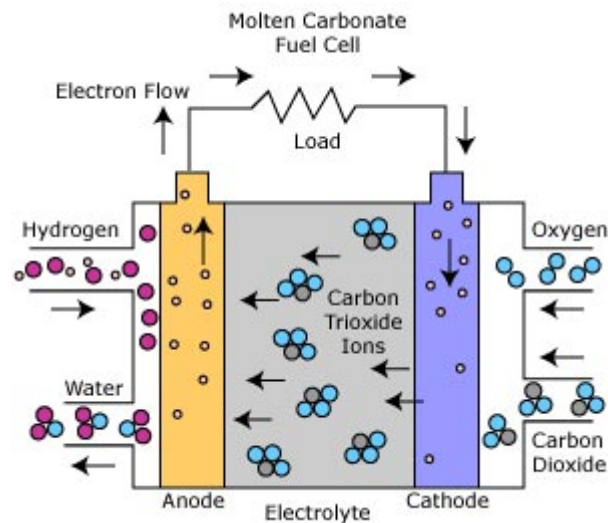
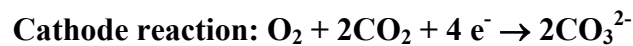
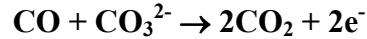


Fig. 1.4: Molten Carbonate Fuel Cell

The MCFC reactions that occur are:



The anode process involves a reaction between hydrogen and carbonate ions (CO_3^{2-}), which produces water and carbon dioxide (CO_2), while releasing electrons to the anode. The cathode combines oxygen and CO_2 from the oxidant stream with electrons to produce carbonate ions, which enter the electrolyte. The need for CO_2 in the oxidant stream requires a system for collecting CO_2 from the anode exhaust and mixing it with the cathode feed stream (Fig. 1.4).

1.2.4 Alkaline Fuel Cells (AFC)

Alkaline fuel cells (AFC) are one of the most developed technologies and have been used since the mid-1960s by NASA in the Apollo and Space Shuttle Programs.

Alkaline fuel cells use an aqueous solution of potassium hydroxide (KOH) in a porous stabilized matrix as an electrolyte. The concentration of KOH can be varied with the fuel cell operating temperature-, which ranges from 65 °C to 220 °C.

The charge carrier for an AFC is the hydroxyl ion (OH^-) that migrates from the cathode to the anode, where it reacts with hydrogen to produce water and electrons. Water formed at the anode migrates back to the cathode to regenerate hydroxyl ions. The chemical reactions at the anode and cathode in an AFC are shown below (Fig. 1.5). This set of reactions in the fuel cell produces electricity and by-product heat.

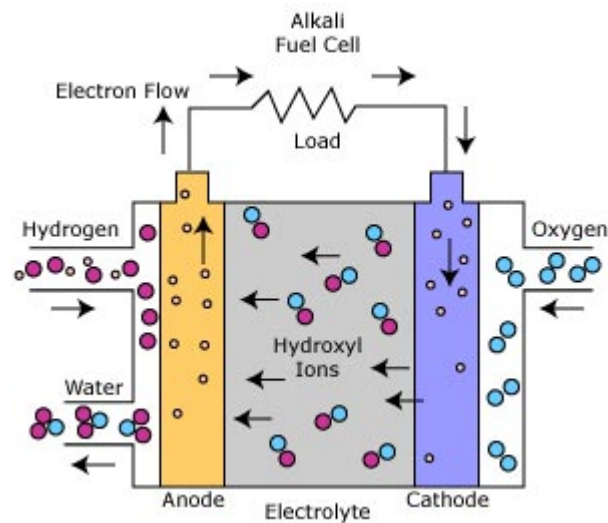
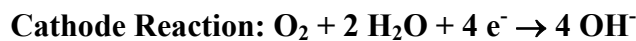
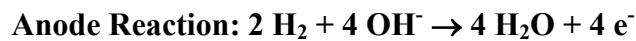


Fig. 1.5: Alkaline Fuel cell (AFC)



AFCs are very sensitive to CO_2 that may be present in the fuel or air. The CO_2 reacts with the electrolyte, poisoning it rapidly, and severely degrading the fuel cell performance. Therefore, AFCs are limited to closed environments, such as space and under sea vehicles, and must be run on pure hydrogen and oxygen.

On the positive side, AFCs are the one of the cheapest fuel cells to be manufactured. This is because the catalyst that is required on the electrodes is inexpensive compared to the catalysts required for other types of fuel cells.

AFCs are not being considered for automobile applications. Their sensitivity to poisoning, which requires pure hydrogen and oxygen, is an insurmountable obstacle at the present time. Conversely, AFCs operate at relatively low temperatures and are among the most efficient fuel cells, characteristics that would enable a quick starting power source and high fuel efficiency, respectively.

1.2.5 Proton-Exchange Membrane (PEM) Fuel Cells

The proton-exchange membrane (PEM) fuel cell uses polymeric membrane as the electrolyte. These cells are the best candidates for light-duty vehicles, for buildings and much smaller applications.

The working principle of hydrogen PEM fuel cell is often described as 'reverse electrolysis'. The hydrogen fuel is supplied to the anode electrode.

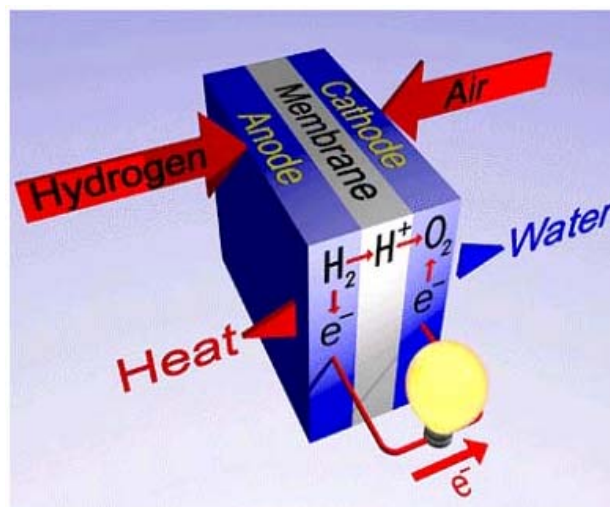
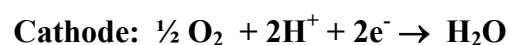


Fig. 1.6: Polymer Electrolyte Membrane Fuel Cell (PEMFC)

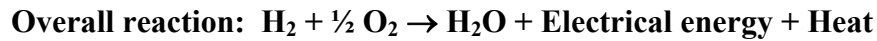
The following reaction takes place at anode, accelerated by a platinum (-containing) catalyst:



The protons (H^+) migrate through the Polymer Electrolyte Membrane (PEM) to the cathode. At cathode, a reaction takes place with oxygen from air:



Notably, the electrons are required for the cathode reaction to produce water. But the electrolyte membrane, which separates the cathode and the anode, is permeable only for protons. Therefore, the electrons have to travel through an external circuit to the cathode.



1.3 Proton conducting polymers

In general, proton-conducting polymers are based on polymer electrolytes, which have negatively charged groups attached to the polymer backbone. Perfluorinated ionomers (NAFION type membranes) have emerged as standard materials for low-temperature fuel cell applications⁽²⁻⁴⁾ due to high proton conductivity and, their excellent chemical and thermal stability.

STATE OF THE ART IN POLYMER ELECTROLYTE MEMBRANES-Nafion and Nafion-like

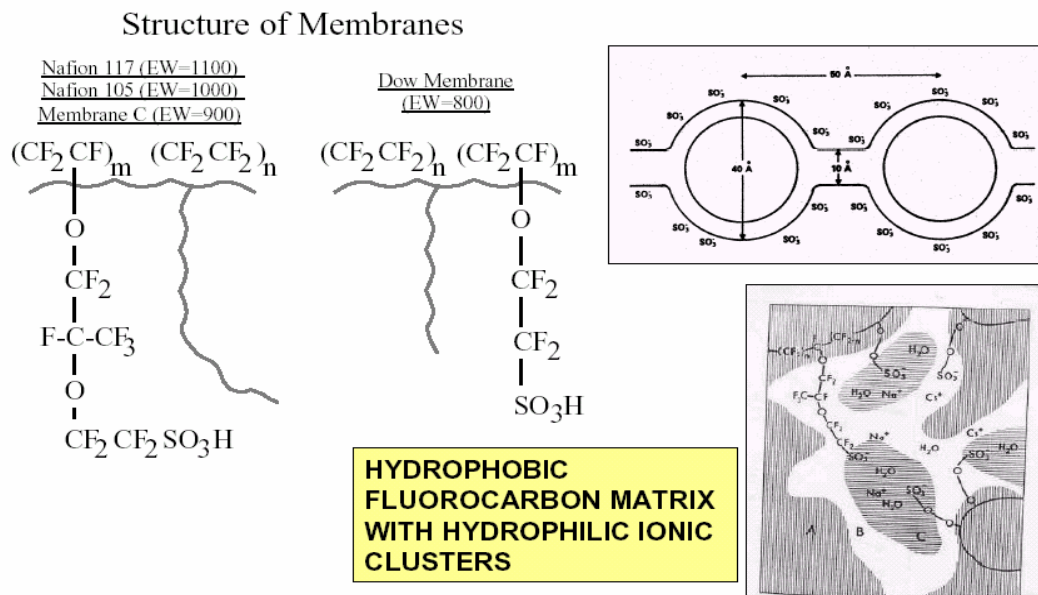
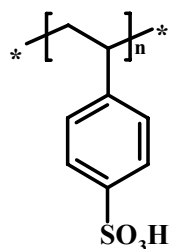
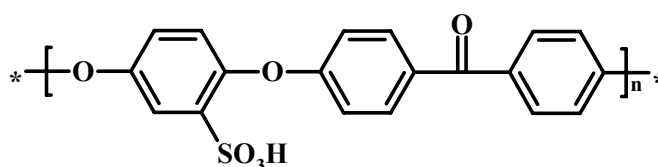
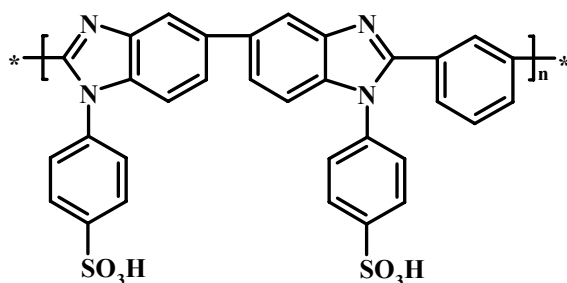
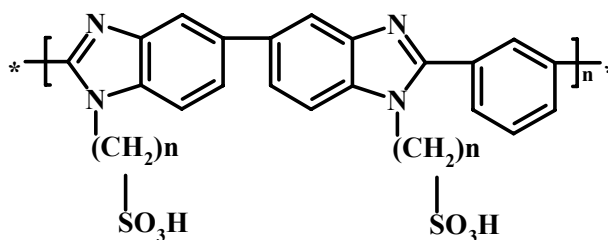


Fig. 1.7: NAFION

No other type of materials could replace perfluorinated ionomers for decades because of inability to provide high proton conductivity with high chemical and thermal stability. The most extensive limitations of NAFION arise from the fact that these materials are proton-conducting only when they are hydrated, which results in a maximum operating temperature of ~ 100 °C that in turn limits activity and CO tolerance of the electro catalyst. Other drawbacks of this type of membrane are the need of permanent humidification (i.e., of additional peripheral devices), high methanol crossover, and limited mechanical stability. In addition to these factors, which decrease the total efficiency of the system, the high price as well as difficult recycling or disposal of the perfluorinated materials, has slowed widespread and economical applications. Accordingly, a variety of alternative approaches using materials that are cheaper and more suitable for higher temperatures have emerged. They are poly(4-styrenesulfonic acid) **(1)**,^(5,6) sulfonated polyetheretherketones **(2)**,⁽⁷⁻¹¹⁾ sulfonated PBI **(3)**,⁽¹²⁾ alkylsulfonated PBI **(4)**,^(4, 13-14) acid-base polymer complexes PEO/H₂SO₄, PEO/H₃PO₄ **(5)**,⁽¹⁵⁾ and PBI/H₃PO₄ **(6)**.⁽¹⁶⁻²⁰⁾

**(1)****(2)****(3)****(4)**

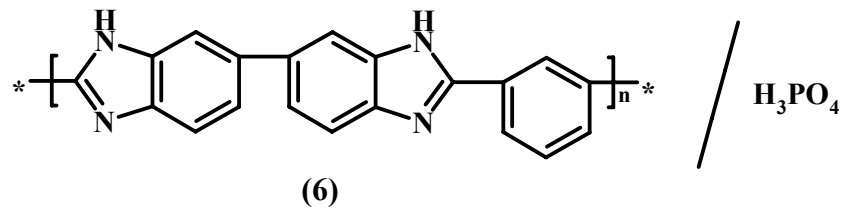
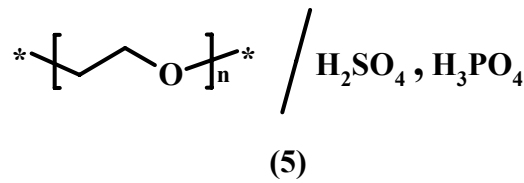


Fig. 1.8: Some of the most prominent polymers used as polymer electrolyte membrane (PEM)

Proton-conducting polymer electrolyte membranes for high performance PEMFCs have to meet several requirements, especially for electrically powered vehicle applications. The most important requirements are:

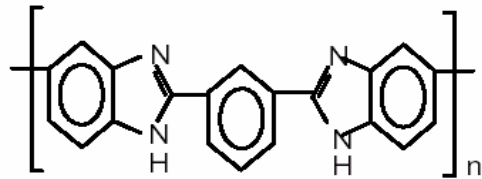
- High proton conductivity
- Low gas permeability
- High mechanical stability
- High chemical stability
- Ability to recycle
- Ease of mass production
- Low cost

1.4 Polybenzimidazole and its properties

Polybenzimidazole (PBI) proposed by Litt⁽²¹⁾ and investigated by Savinell and Wainright⁽²²⁻²⁸⁾ has been studied as a promising electrolyte for high-temperature fuel cells when doped with a strong oxo-acid (i.e., phosphoric acid or sulphuric acid). They have shown that phosphoric acid doped PBI exhibits good proton conductivity,^(22,23) low gas permeability,⁽²⁴⁾ almost zero water electro-osmotic drag,⁽²⁴⁾ excellent oxidative and thermal stability,⁽²⁵⁾ and good mechanical flexibility at elevated temperatures.⁽²⁶⁾

PBI PROPERTIES AND CHARACTERISTICS

- HIGH TEMPERATURE RESISTANT
- GLASS TRANSITION TEMP ~450C
- SMALL MOLECULES ACT AS PASTICIZERS
- ABSORBS ACID, Pka~5.5



poly[2,2'-(m-phenylene)-5,5'-bibenzimidazole]



POLYMER	MOLECULAR WEIGHT AND INHERENT VISCOSITY (I.V.)			
	(5 WT% dI/g	in concentrated sulfuric acid)		
	I.V.	M_n	M_w	MWD (M_w/M_n)
low	.3	6700	11200	1.7
avg	.68	18000	27200	1.5
high	.97	26300	50300	1.9

•Stable in reducing and oxidizing environments to 600 C.

1.4.1 Acid and base doped PBI

Savadogo⁽²⁹⁾ compared the conductivity of PBI membranes doped in various acids, and found that the conductivity changes are in the order of $H_2SO_4 > H_3PO_4 > HClO_4 > HNO_3 > HCl$ for high doping levels. Moreover, they studied alkaline-doped PBI⁽³⁰⁾ (KOH, NaOH, and LiOH). The highest conductivity of KOH-doped PBI⁽³⁰⁾ (9×10^{-2} S/cm, doped in 6 M KOH, measured in doping solution at 60 °C) is higher than those of H_2SO_4 -doped PBI (6×10^{-2} S/cm, doped in 16 M H_2SO_4 solution and measured in 2 M $HClO_4$ solution at 25 °C) and H_3PO_4 doped PBI (2×10^{-3} S/cm, doped in 15 M H_3PO_4 solution and measured in 2 M $HClO_4$ solution at 25 °C).⁽²⁹⁾ Staiti⁽³¹⁾ studied the conductivity of PBI membranes mixed with phosphotungstic acid (PWA) adsorbed on SiO_2 , and obtained 1.5×10^{-3} S/cm at 90-150 °C. They also studied⁽³²⁾ sulfonated PBI and obtained high thermal stability but low proton conductivity (7.5×10^{-5} S/cm, 160 °C, 100 % RH). They attributed this result to strong interaction between protons and nitrogen atoms of the imidazolium ring in PBI, which reduces the proton mobility, producing a slightly semicrystalline polymer.

Akita⁽³³⁾ casted PBI membranes doped with aromatic phosphoric acid mono- and di-esters (i.e., at least one hydrogen atom of phosphoric acid is substituted by a molecule containing a phenyl group) in order to prevent the acid dopants from being leached out by water. They obtained conductivity up to 5×10^{-3} S/cm in a dried state (125 °C, 200 % diphenyl phosphoric acid doped PBI).

1.4.2 PBI and its polymer blends

For composite membranes of PBI with other polymers, Hasiotis and Li⁽³⁴⁻³⁶⁾ studied the conductivity dependence of H₃PO₄ doped PBI/sulfonated polysulfone (SPSF) blends on temperature, acid doping level (dopant molecules per polymer repeat unit), sulfonation degree of SPSF, relative humidity (RH), and blend composition. They obtained conductivities up to 10^{-1} S/cm at 500 % doping level at 160 °C and 80 % RH. Kerres⁽³⁷⁻⁴¹⁾ prepared ionically cross-linked blend membrane by mixing acidic polyaryl membranes such as sulfonated polysulfone (PSU), sulfonated polyetheretherketone (sPEEK), and sulfonated polyetherketone (sPEK), with basic membranes such as PBI. They investigated the strong interactions between acidic and basic components indirectly via ion-exchange capacity of the blend membranes and Fourier Transform Infrared Spectroscopy (FTIR).^(37,38) The conductivity of the blended membranes depends on the composition and ion exchange capacity (ICE) of the membranes. Also, they applied these membranes in H₂ fuel cells⁽³⁹⁾ and direct methanol fuel cells (DMFC),^(37,38,40,41) and concluded that low methanol-permeability makes this membrane suitable for DMFC even at 110 °C.

1.4.3 Acid grafted PBI

Roziere^(42,43) prepared base doped N-benzylsulfonated PBI, which has a conductivity of 2×10^{-2} S/cm at 25 °C and 100 % RH. Bae and Rikukawa⁽⁴⁴⁾ fabricated PBI-PS (propanesultone) as well as PBI-BS (butanesultone) membranes, and measured their conductivity around 1.2×10^{-3} S/cm, T = 100- 160 °C. They also synthesized ethylphosphorylated PBI⁽⁴⁵⁾ with the same procedure for the reactive N-H sites in PBI and showed a high proton conductivity of 10^{-3} S/cm

Therefore, PBIs can be modified to meet high proton conductivity and are promising candidates as materials in high performance fuel cells.

1.5 Proton-transport mechanism

In general, proton conduction occurs in both hydrous and anhydrous state. In hydrous state, proton migration occurs by a combination of Vehicular type mechanism and Grotthuss type mechanism,⁽⁴⁶⁻⁵¹⁾ whereas in anhydrous state, proton conduction occurs either completely by Grotthuss type mechanism⁽⁷⁶⁻⁷⁹⁾ in an ordered environment or combination of Grotthuss and Vehicular type mechanism⁽⁴⁹⁻⁷⁵⁾ in a disordered environment.

1.5.1 Proton conduction in hydrous environment

In Vehicular type mechanism, the protons ride on a carrier molecule; for example, H₂O carries a proton in the form of H₃O⁺ ion. In Grotthuss type mechanism, the proton jump from a donor to a suitable acceptor molecule, for example from H₃O⁺ to H₂O, or from H₂O to OH⁻. Polymers such as NAFION⁽⁴⁶⁾ and the sulphonated polyetheretherketones^(47,48,49) conduct the protons in hydrous state.

1.5.1.1 Microstructures and proton conductivity in hydrous state

According to Kreuer,⁽⁵⁰⁾ perfluorosulfonic polymers (PFSA) have different microstructures from those of sulfonated aromatic polymers, as illustrated in fig.1.9.

NAFION combines the extreme hydrophobicity of the perfluorinated polymer backbone with the extreme hydrophilicity of the terminal sulfonic acid function (-SO₃H). Especially in the presence of water, this gives rise to some amphiphilic nano-separation. The sulfonic acid functional groups aggregate to form a hydrophilic domain. When this is hydrated, only the hydrophilic domain of the nanostructure is responsible for the transport of protons and water, while the hydrophobic domain provides the polymer with the morphological stability (mechanical strength) and prevents the polymer from dissolving in water. As a result, the water uptake by the NAFION membranes is very high.

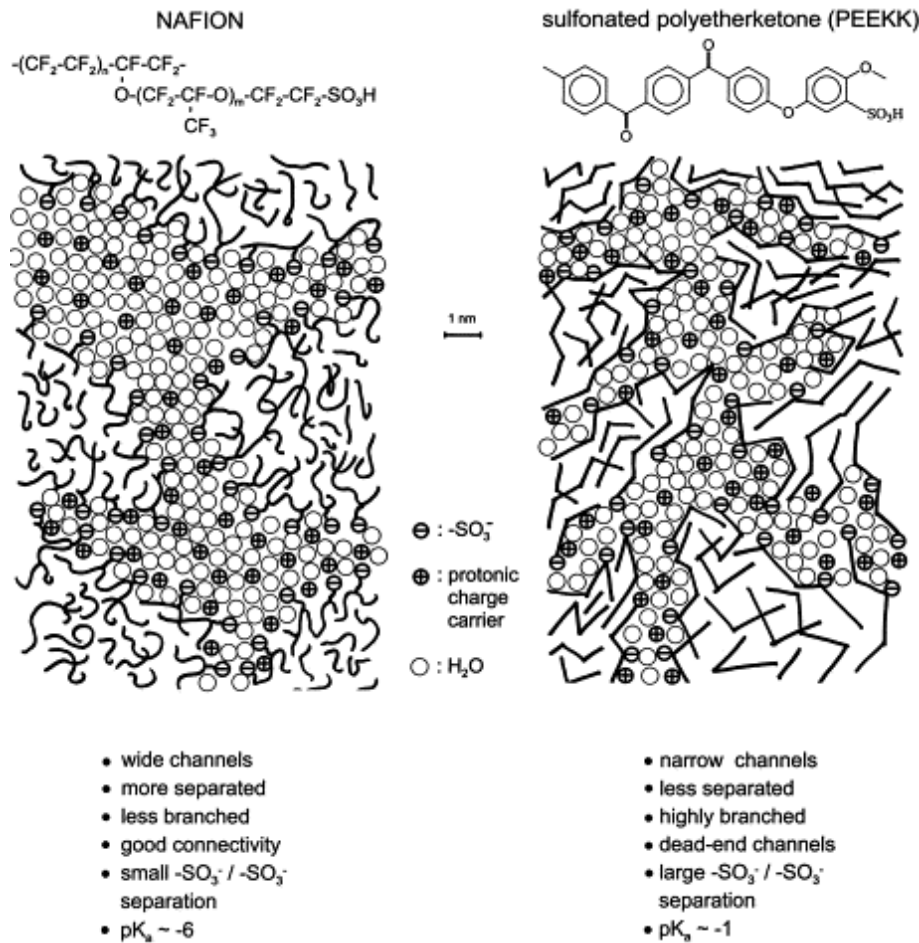


Fig. 1.9: Schematic representation of the microstructures of NAFION and a sulfonated polyetherketone illustrating the less pronounced hydrophobic/hydrophilic separation of the latter compared to the first

The situation in sulfonated aromatic polymers was found to be distinctly different with respect to both transport properties and morphological stability. In the case of sulfonated aromatic polymers, the hydrocarbon backbone is less hydrophobic and the sulfonic acid functional groups are less acidic and polar. As a result, the water molecules of hydration may be completely dispersed in the nanostructures of the sulfonated aromatic polymers.⁽⁴⁷⁾ In general, PFSA and sulfonated aromatic polymers have similar water uptakes at low water activities, whereas at high relative humidity (100 %), PFSA membranes have a much higher water uptake due to the more polar character of the sulfonic acid functional groups. Consequently, the sulfonated polyaromatic membranes in general need more humidification during fuel cell operation in order to maintain the high level of conductivity.

The less hydrophobic nature of the hydrocarbon nanostructure on the other hand may result in less dependence of conductivity on humidity in the low water activity range, allowing for good proton conductivity at high temperatures. For example, polyphenylenesulphide with a sulfonating degree of 200 % exhibits a proton conductivity of the 10^{-2} S/cm level in the temperature range of 30 to 180 °C,⁽⁵¹⁾ whereas in NAFION membranes,⁽⁴⁶⁾ the operating temperature is limited up to the boiling point of water.

1.5.2 Proton conduction in anhydrous state

Anhydrous proton-conducting polymers usually consist of a polymer matrix (base) with an appropriate proton solvent. Swelling the polymer matrix into inorganic acids generally forms disordered molecular arrangements of acid-base complex, and proton conduction in this disordered state reportedly occurs by both Grotthuss and Vehicular type mechanisms; whereas self-assembling of acid-base molecular arrays (ordered acid-base complex) of acid-base complex follows Grotthuss type mechanism.

1.5.2.1 Proton conduction in disordered acid-base complexes

There are different types of anhydrous proton conducting acid-base membranes reported in literature, with a focus on polybenzimidazole (PBI) /H₃PO₄⁽⁴⁹⁾ blends that are currently most suitable for fuel cell applications. In acid-base membranes, the property of the acid (H₃PO₄ or H₂SO₄) to interact via hydrogen bonds facilitates the preparation of blends with a variety of polymers, such as polybenzimidazole,⁽⁴⁹⁾ poly(4-vinylimidazole),⁽⁵²⁾ polyethyleneoxide,⁽⁵³⁾ and poly(vinylpyrrolidone).⁽⁵⁴⁾

Proton conduction in acid-base membranes is strongly dependent on the nature of acid,⁽⁵⁵⁻⁶¹⁾ polymer,⁽⁶²⁻⁶⁹⁾ temperature⁽⁷⁰⁻⁷⁵⁾ and humidity.⁽⁷⁵⁾

1.5.2.2 Nature of acid on conductivity

Phosphoric acid is unique in that its conductivity is remarkably high in the pure state.^(55,56) The first feature is due to the generation of charge carriers by self-dissociation ($5 \text{H}_3\text{PO}_4 = 2 \text{H}_4\text{PO}_4^+ + \text{H}_2\text{PO}_4^- + \text{H}_3\text{O}^+ + \text{H}_2\text{P}_2\text{O}_7^{2-}$ where $\text{H}_3\text{PO}_4 = 16.8 \text{ M}$, $\text{H}_4\text{PO}_4^+ = 0.89 \text{ M}$, $\text{H}_2\text{PO}_4^- = 0.43 \text{ M}$, $\text{H}_3\text{O}^+ = \text{H}_2\text{P}_2\text{O}_7^{2-} = 0.46 \text{ M}$ at 311 K).⁽⁵⁷⁾ The second feature is related to the transport mechanism. The electrical field of extrinsic charge carriers causes a bias on hydrogen bonds and thus suppress fluctuations within the dynamic hydrogen bond network.^(58,59) For example, at a 1.45 molar acid doping concentration, PBI blended with H_3PO_4 has higher conductivity than H_2SO_4 -blended PBI.⁽⁶⁰⁾ For PBI blended with low levels of H_2SO_4 , infrared studies have shown that SO_4^{2-} is the predominant counter-ion; whereas in PBI- H_3PO_4 , the anion associated with the polymer is H_2PO_4^- over a wide range of pH.⁽⁶¹⁾ At high acid concentration, it is found⁽⁶⁰⁾ that the conductivity of H_2SO_4 -blended PBI is higher than that of H_3PO_4 -blended PBI. Above a certain concentration level, the conductivity increases sharply, which corresponds to the appearance of HSO_4^- anions in H_2SO_4 -blended PBI.

Further, conductivity is found to be strongly dependent on the acid-doping level. According to PU,⁽⁶⁰⁾ the conductivities increase by about 3 orders of magnitude when the acid concentration changed from 1.8 to 3.8 molar in PBI-blended phosphoric acid at constant temperature. These results should be understood in terms of the following relation,

$$\sigma (\text{T}) = n (\text{T}) \mu (\text{T}) e$$

Where σ is the proton conductivity, n is the number of charge carriers, μ is their mobility, and e is the unit of electric charge. It means that the number of charge carriers increases rapidly as acid concentration is changed from 1.8 to 3.8 molar in PBI blended H_3PO_4 .

1.5.2.3 Nature of polymer on conductivity

In regard to proton conductivity with imidazoles, imidazole molecules are known to be involved in proton transport across biological membranes.⁽⁶²⁾ In general, the behaviour of imidazole groups toward protons is very similar to that of water: the heterocycles are amphoteric molecules, they exhibit extensive hydrogen bonding interactions that result in a fluctuating network and to some extent undergo self-dissociation. (Fig.1.10)

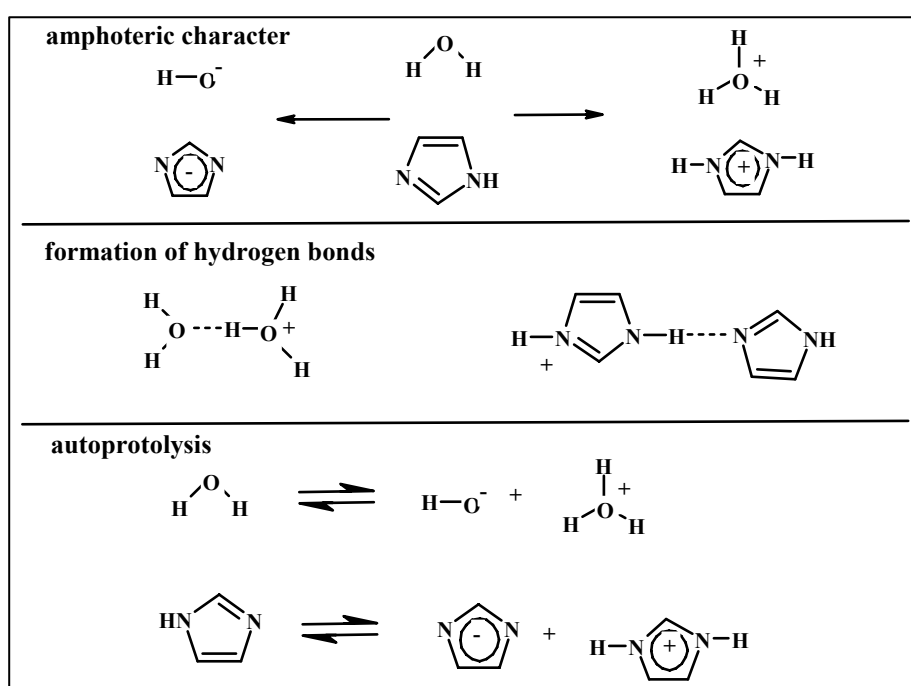


Fig. 1.10: Imidazole and water exhibit similar behavior toward proton

The existence of a Grotthuss-type mechanism (structure diffusion) for pure imidazole and its oligomers has been established experimentally.⁽⁶³⁾ In Grotthuss-type mechanism, the transport of the excess proton in imidazole is described involving proton transfer- and reorientation steps. The proton transfer step assumes proton transport to occur through hydrogen bridges, either as a cooperative process⁽⁶⁴⁾ or by migrating charged defects,⁽⁶⁵⁾ fig. 1.11. The reorientation step in both models would then involve a coherent rotation of all the imidazole molecules in the hydrogen-bonded chains, which involves the breaking of short, strong hydrogen bonds. The suggested time scale of 1 s for the coherent reorientation process⁽⁶⁴⁾ could not be verified experimentally by a recent ¹⁵N NMR study.⁽⁶⁶⁾

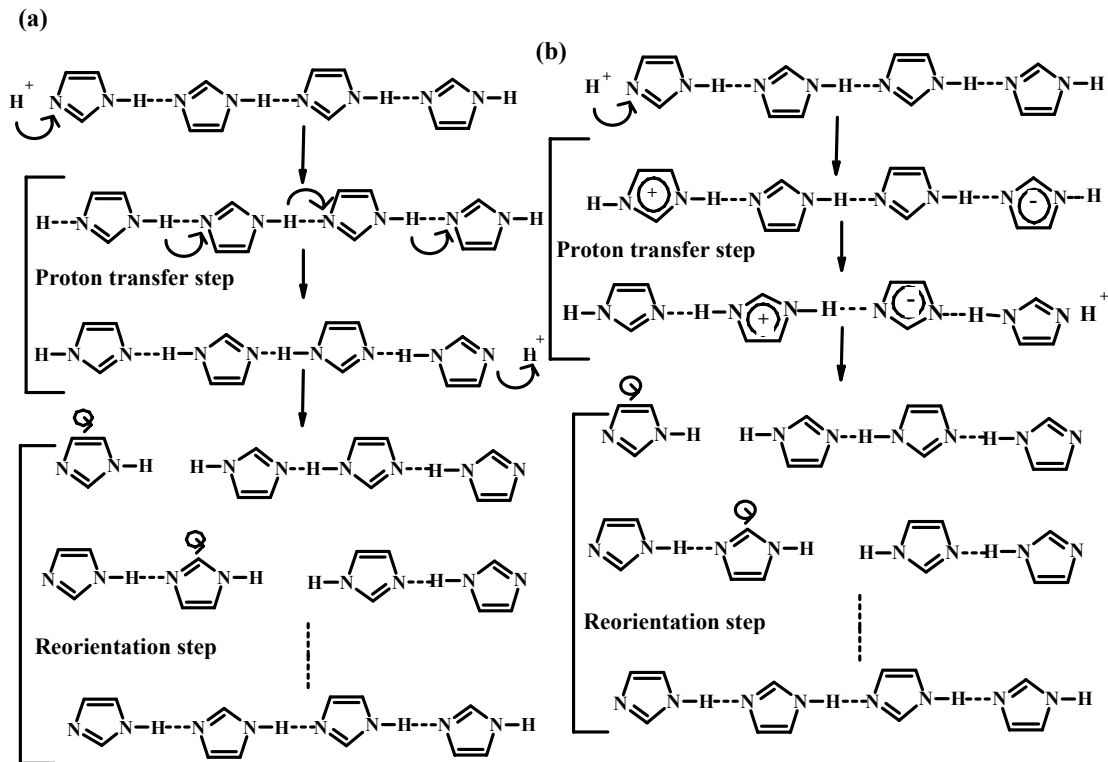


Fig. 1.11: The proton transfer process as proposed (a) by Daycock⁽⁶⁴⁾ (b) by Kawala⁽⁶⁵⁾

However reports on the conductivity of imidazole containing polymers are conflicting. Neutral polybenzimidazole (PBI) films have been described as highly conducting, with values reported up to 6×10^{-3} S/cm at room temperature,⁽⁶⁷⁾ whereas conductivities of different PBIs are also reported around 10^{-12} S/cm in the pure state.^(68,69)

1.5.2.4 Effect of temperature on conductivity

The temperature dependence of the conductivity in polymer electrolytes has been taken as an indication for a particular type of conduction mechanism.^(70,71) A distinction is generally made between systems that fit the Arrhenius equation and those that fit the Vogel-Tamman-Fulcher (VTF) equation. The temperature dependent conductivities of the membranes below the glass transition temperature can be fitted with a simple Arrhenius relation ($\sigma = \sigma_0 \exp[-E_a/RT]$ where σ is the conductivity, σ_0 - pre-exponential factor, E_a - activation energy, R - Boltzmann constant, and T - Temperature of polymer electrolyte).

PBI blended- H_3PO_4 which has a high glass transition temperature, shows Arrhenius type of behavior.⁽⁶⁰⁾ These results are interpreted as the consequences of the two contributions to proton conductivity: one is based on rapid proton exchange (hopping) between phosphate and imidazole moieties via hydrogen bonds (Grotthuss type mechanism), and the other on self-diffusion of phosphate moieties (Vehicular type mechanism). The segmental motion of PBI, as proposed by Frontanella,⁽⁷²⁾ seems to play no role in proton transport.

The deviation from the linear Arrhenius relation of the conductivity has been reported⁽⁷³⁾ in poly(4-vinylimidazole)- H_3PO_4 membranes. The P4VIm membrane with H_3PO_4 concentration of 0.5 M can be fitted with the Arrhenius relation very well, however, the concentration above 0.5 M can be fitted with the Vogel-Tamman-Fulcher (VTF) equation ($\sigma = \sigma_0 [\text{DT}_0/T-T_0]$ where σ is the conductivity, σ_0 and D are constants, T_0 – glass transition temperature, T - temperature of polymer electrolyte). This behaviour was explained by T_g of poly(4-vinylimidazole)- H_3PO_4 membranes. At H_3PO_4 concentration 0.5 molar, poly(4-vinylimidazole)- H_3PO_4 membrane are in its glassy state, since the glass transition temperature of this sample is 126 °C. The glass transition temperature of the polymer-acid blends decreases with increasing acid content; the corresponding data for poly(4-vinylimidazole)- H_3PO_4 membranes are $T_g = 70$ °C (Acid concentration, x = 1.0 M), $T_g = 15$ °C (x = 1.5 M), and $T_g = -23$ °C (x = 2.0 M) according to the literature.⁽⁷⁴⁾ Thus, the deviation from the linear Arrhenius relation of the conductivity curves of the samples with x > 0.5 M are just centred around the glass transition temperatures of the individual samples. When the temperature exceeds T_g , segmental motions of the polymer (blends) are activated. Hence, the proton transport mediated by segmental motion, proton hopping between phosphate - imidazole units via hydrogen bonds, and the self-diffusion of phosphate moieties can contribute to the conductivity. As a result, a crossover in the mechanism from Arrhenius-type in the temperature regime below T_g to a VTF-type in the temperature range above T_g can explain the temperature dependence of the conductivity of the poly (4-vinylimidazole)-x H_3PO_4 blends with x > 0.5 M. Similar behaviour was found in PBI/poly (4-vinylpyridine) doped with H_3PO_4 blends.⁽⁷⁵⁾

The temperature-dependent conductivity of the blends follows a simple Arrhenius relationship when the poly(4-vinylpyridine) content is low (lower than 15 %), while a non-Arrhenius behaviour becomes more and more significant with increasing poly(4-vinylpyridine) content. This means that proton transport in the blends is controlled by both the proton hopping mechanism (Grotthuss type mechanism) and the segmental motion of the polymer (Vehicular type mechanism). The contribution of these two mechanisms depends on the poly(4-vinylpyridine) content.

1.5.2.5 Effect of humidity on conductivity

In general, the protonic conductivity is greatly influenced by the presence of water. For example, when H₃PO₄-blended PBI⁽⁶⁰⁾ was allowed to absorb 12 wt % H₂O, the conductivity of the sample increased dramatically. These water molecules can act as additional proton solvents and contribute to the proton transport either by self-diffusion while carrying a proton (Vehicular type mechanism) or by the rapid exchange of protons via hydrogen bridges (Grotthuss type mechanism). However, water may play a role as a plasticizer of blends that may result in a small change in the proton-transport mechanism and a small deviation from the Arrhenius relation at higher temperatures.

1.5.3 Proton conductivity in ordered acid-base complex

Conductivity in polymer electrolytes has long been confined to the amorphous phase above the glass transition temperature, T_g , where polymer chain motion creates a dynamic, disordered environment. This dynamic nature plays a critical role in facilitating proton transport.⁽⁴⁶⁻⁷⁵⁾ In contrast to this prevailing view, recently, it has been described in the literature⁽⁷⁶⁾ that ionic conductivity in the static, ordered environment can also be higher like disordered arrangement. To support this view, for imidazole single crystals, anisotropic conductivity has been reported and attributed to the directional H-bonding in the crystalline material.⁽⁷⁷⁾

Proton conductivity in ordered self-assembling acid-base complex occurs by Grotthuss type mechanism, where the segmental mobility does not play any role for conductivity. Recently, it has been reported⁽⁷⁸⁾ that a self-assembled acid-base complex consisting of acidic surfactant monododecyl phosphate and basic surfactant 2-undecylimidazole molecules exhibited high proton conductivity of $1 \times 10^{-3} \text{ S cm}^{-1}$ at 150°C under the anhydrous condition.

1.6 Supramolecular chemistry (Multilayers for fuel cell applications)

Supramolecular chemistry is the science of intermolecular association as driven by multiple weak interactions.⁽⁷⁹⁻⁸²⁾ The weak interactions between different molecules are electrostatic attraction between opposite charges and dipoles, hydrogen bonding, aromatic π -stacking, charge transfer, or hydrophobic effects. (Micelle formation and liquid crystals in solution are examples of supramolecular architectures in solution). As a result, the properties of supramolecular architectures depend on the exact arrangement of attractive and repulsive groups of the molecules in a given solvent. However, it is usually difficult to exploit the directionality of the intermolecular interactions since the resulting assemblies normally stay dissolved in an isotropic solution.

Therefore, it is essential that the molecules should be assembled in a stepwise fashion starting from a template, so that the resulting target structures preserve the directionality of the intermolecular interaction. This process is called ‘directed assembly’.

1.6.1 Towards directed assembly

The classical example of a directed assembly procedure is the Langmuir-Blodgett technique, in which amphiphilic molecules are allowed to self-organize at the air-water interface and are subsequently transferred on to solid substrates.⁽⁸³⁻⁸⁵⁾ However, it is a disadvantage that adsorption processes are dependent on the substrate size and topology.⁽⁸⁸⁾

1.6.2 The principle of Layer-By-Layer assembly

Recently, a new technique of constructing multilayer assemblies by alternating adsorption of anionic and cationic polyelectrolytes (Layer-By-Layer) was developed by Decher.⁽⁸⁶⁾ Here the adsorption processes are independent of the substrate size and topology. Layer-by-Layer (LBL) deposition of polyelectrolytes leads to multilayer films in which distances and orientation of the different compounds can in principle be controlled. This approach has the advantage that electrostatic attraction between opposite charges is the driving force for the multilayers built-up. In contrast to chemisorption techniques⁽⁸⁷⁾ that require a reaction yield of 100 % in order to maintain a constant surface functional density after each deposition step, no covalent bonds need to be formed. Additionally, an advantage over the classic Langmuir-Blodgett technique is that one can work even with water-soluble molecules, which is required for many biological macromolecules.

The principle of constructing the LBL assembly is displayed in figure 1.12 and is described as follows:

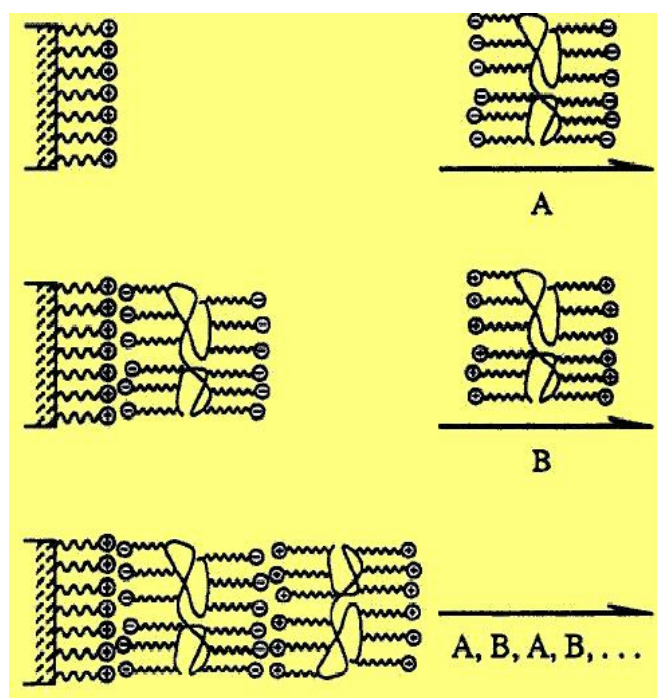


Fig. 1.12: Side-view of the build-up of multilayers assemblies by consecutive adsorption of anionic and cationic polyelectrolytes

A solid substrate with a positively charged planar surface is immersed in the solution containing the anionic polyelectrolyte, and a layer of polyanion is adsorbed (Step A). Since the adsorption is carried out at relatively high concentration of polyelectrolyte, a large number of ionic groups remains exposed to the interface with the solution, and thus the surface charge is effectively reversed. After rinsing with pure water, the substrate is immersed in the solution containing the cationic polyelectrolyte. Again a layer is adsorbed, but now the original surface charge is restored (step B). By repeating both steps (A, B, A, B,) in a cyclic fashion, alternating multilayer assemblies are obtained. The complete reversal of surface charge is the crucial factor for a regular stepwise growth.

However, the resulting structure is not really a layered film as shown in figure 1.13A. This is because profuse interpenetration of successive "layers" occurs during the adsorption process. This is schematically illustrated in figure 1.13B below:

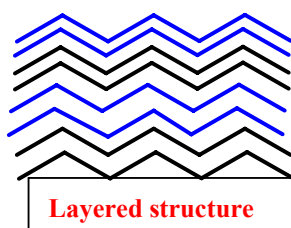


Fig.1.13A: Layered structure of multilayers.

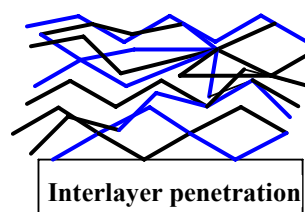


Fig. 1.13B: Interpenetration of layers

1.6.3 Structure and properties of multilayers

Structure and physical properties of LBL films depend on the degree of ionisation of the polyelectrolytes. With weak polyelectrolytes, it is possible to tune charge densities by simple changes in solution pH and therefore to manipulate structure and properties. For example, using the same two polymers assembled under different pH conditions, it is possible to create thin films with dramatically different and quite useful properties.⁽⁸⁹⁾

In exploring growth conditions, it is generally observed that salt has the strongest influence on the amount deposited ('layer' thickness) per cycle.⁽⁹⁰⁾ Polymer concentration, molecular weight and deposition time are known to be less important variables.⁽⁹⁰⁾

1.6.4 Applications of multilayers

Much of the recent work on these polyelectrolyte multilayers has focused on generalizing and expanding the technique to various combinations of charged components including synthetic polyelectrolytes, biopolymers such as proteins,⁽⁹¹⁻⁹²⁾ clay materials,⁽⁹³⁾ dendrimers,⁽⁹⁴⁾ metal colloids,⁽⁹⁵⁾ silica⁽⁹⁶⁾ and other inorganic particles.⁽⁹⁷⁾ Applications have appeared almost simultaneously and include conducting layers,⁽⁹⁸⁾ ion selective membranes,⁽⁹⁹⁻¹⁰⁰⁾ enzyme-active thin films,⁽¹⁰¹⁾ sensors,⁽¹⁰²⁾ light-emitting thin films,⁽¹⁰³⁾ selective area patterning,⁽¹⁰⁴⁾ electro catalysis⁽¹⁰⁵⁻¹⁰⁶⁾ and films for non-linear optics.⁽¹⁰⁷⁾

1.6.5 Advantages of multilayer films as conducting materials

The LBL technique offers unique advantages for the design and development of ionically conductive films for use as solid polymer electrolytes. LBL polymer films are inherently amorphous solids with mechanical properties superior to those of gels and crystalline solids: they do not flow or easily deform, yet they remain flexible. They can be applied very thin and defect-free, which can lead to very thin solid electrolytes in devices, increasing the overall conductance of the electrolyte layer. Unlike roll casting, solvent casting, or spin coating, the LBL technique can uniformly coat non-planar surfaces, allowing for a diverse range of cell geometries. Finally, LBL films can be easily tailored on the nanometer scale to create composition gradients or surface passivation, incorporating a wide variety of materials to achieve chemical compatibility and high performance.

1.6.6 Disadvantages of ion conducting multilayer films

Despite these advantages, early ionic conductivity results were disappointing. The dielectric and ion conduction properties of LBL films were first investigated by Durstock and Rubner,⁽¹⁰⁸⁾ following limited earlier studies on polycation/polyanion complexes.⁽¹⁰⁹⁻¹¹⁰⁾ The first LBL investigation evaluated films of poly(allylamine hydrochloride) (PAH) with poly(styrene sulfonate) (SPS) and poly(acrylic acid) (PAA). These composites demonstrated a maximum ionic conductivity of 2×10^{-7} S/cm at room temperature under high hydration level,⁽¹⁰⁸⁾ which is too low for most electrochemical applications.

The low ionic conductivity of typical electrostatic LBL films can be explained using the general relation

$$\sigma = \sum_{i=1}^{\text{all ion types}} n_i q_i \mu_i$$

where σ is ionic conductivity, i is the ion type, n is the number of mobile ions, q is the ion charge, and μ is the ion mobility. The ion number and mobility are potentially limited by the LBL technique.

The limited number of mobile ions is due to the large extent of polyion pairing and rejection of residual small ions from the bulk LBL film, which is especially notable in strong polyion systems such as poly(diallyl dimethylammonium chloride) (PDAC)/SPS.⁽¹¹¹⁾ In general, an electrostatic LBL film *cannot* contain as many dissociable small counter ions as a neat film of polyion, which would contain one counter ion per monomer unit. In addition, hydrophobic aspects of common model polyelectrolytes such as PAH, PDAC, or SPS limit the potential for residual or added salt to dissolve into the film.

Limited mobility is due to an inherently high cross-link density, which has been shown to decrease ionic conductivity in polyether networks.⁽¹¹²⁾ The underlying mechanism of such poor conductivity is the constraint of small-segment polymer dynamics, which are widely recognized as being coupled to ion mobility.⁽¹¹³⁾

Furthermore, each ion pair within a LBL film can behave as a "Coulomb trap", slowing down migration by temporary association with the migrating ion. An important conclusion from this work was that high ionic cross-link density slowed free ion mobility, presumably due to a hindrance of polymer chain motion, because ion pair sites can behave in a manner similar to ion-exchange resins,⁽¹¹¹⁾ creating "Coulomb traps" or associative sites for mobile ions.

Efforts to increase ionic conductivity by maximizing small ion concentration was addressed by Deanlongscamp and Hammond⁽¹¹⁴⁾ who reported the conductivity value of $\sim 10^{-5}$ S/cm at room temperature for poly(ethylene imine) (PEI) paired with either anionic layer of poly(2-acrylamido-2-methyl-1-propanesulfonic acid) (PAMPS) or poly(acrylic acid) (PAA) films in the presence of salt. In their recent publication,⁽¹¹⁵⁾ they replaced electrostatic interaction with less rigid interaction such as hydrogen bonding to lower cross-link density and reported the conductivity value of $\sim 10^{-11}$ S/cm for poly(ethylene oxide) paired with poly(acrylic acid) for completely dry film in the absence of salt, while addition of salt improves its conductivity value up to $\sim 10^{-5}$ S/cm at room temperature.

The role of polybenzimidazole or poly(4-vinylimidazole) with poly(vinylphosphonic acid) multilayers by noncovalent interaction is an interest of study due to proton conducting properties in anhydrous environment. Thus, with the input from nanoscience, imidazole based multilayers are attracting renewed interest and are about to create exciting challenges for material research on polyelectrolytes.

2.1 Motivation

Acid doped PBIs, which can withstand the temperature up to 200 °C, have been useful as membrane materials in fuel cell applications.⁽²¹⁻³²⁾ However for practical applications, acid doped PBI membranes have a serious drawback in that the water formed as a product during cell operation dilutes the acid in which the membrane is soaked. For example, when PBI membranes are doped with 11 M phosphoric acid at room temperature, the equilibrium uptake is about 5 molecules of H₃PO₄ per repeat unit of PBI and its proton conductivity is around 7.9×10^{-2} S/cm at 200°C.⁽²³¹⁻²³²⁾ After washing the membrane with water, about 2 molecules of H₃PO₄ are hydrogen bonded with the two nitrogens of the PBI monomer unit. The rest of the acid is 'free acid', i.e., not hydrogen bonded with imidazole units, and is easily washed away. Hence, the conductivity of the membrane drops up to 2.5×10^{-4} S/cm at 200°C, and the performance of the cell is reduced.⁽²³¹⁻²³²⁾ To overcome the problem of acid loss from PBI membranes, acids should be attached onto PBI either covalently or by strong noncovalent interaction. For this reason, graft copolymer and polyelectrolyte multilayer are chosen as membrane materials. Further, a systematic comparison of direction oriented proton conductivity in ordered polymer chain arrangements of multilayers with direction independent proton conductivity in disordered polymer chain arrangements of copolymers would enable to better understand the variation in proton-transport properties with architecture.

The ideal protogenic groups have been proposed to be amphoteric in nature and should have a high dielectric constant to facilitate charge separation. Among protogenic groups, phosphonic acids are more interesting units than sulfonic acids and imidazoles for proton exchange membrane applications due to their ability to transport protons even in an anhydrous state.⁽¹⁷¹⁻¹⁷³⁾ As phosphonic acid based materials are becoming important, there is a demand for high molecular weight polymers from the points of view of improving conductivity and thermal stability of the membrane material. More importantly, an understanding of the fundamental relationships between the molecular weight of phosphonic acid polymer and proton conductivity is required.

Sulfonic acid polymers have been the focus of much attention, because of excellent proton conductivity and thermal stability.⁽⁴⁶⁻⁵¹⁾ The proton transport properties of sulfonic acid membranes are largely depending on water and hence, their application is limited to temperatures below the boiling point of water.⁽⁴⁶⁻⁵¹⁾ It is therefore desirable to develop an anhydrous sulfonic acid polymer membrane system which will not suffer from the effects of hydration and dehydration, and will maintain a stable conductivity at elevated temperatures. For this purpose, incorporation of imidazole units into sulfonic acid polymers is of practical significance, because imidazole will play the role of water at higher temperatures.⁽⁶⁴⁻⁶⁵⁾

The excellent thermal stability with good mechanical characterization of benzimidazole-based polymers have been recently used to determine their suitability for use as proton conducting membranes.⁽²¹⁻²⁸⁾ However, neutral imidazole polymers differ from phosphonic acid and sulfonic acid polymers by their poor proton conductivity. In order to increase the proton conductivity of imidazole polymers, its modification with phosphonic acid groups by N-substitution of the imidazole ring have been described in the literature.⁽¹³⁵⁻¹⁴¹⁾ Despite becoming a conducting polymer after grafting, the membrane loses the conductivity to a certain extent due to absence of a proton transport path in the N-substituted imidazole ring. For example, conductivities above 10^{-3} S/cm were measured for imidazole/ $3\text{H}_3\text{PO}_4$ and about 10^{-5} S/cm were reported for N-methyl imidazole/ $3\text{H}_3\text{PO}_4$ membranes.⁽²³⁾

These results should be understood in terms of the following relation:

$$\sigma (\text{T}) = \mathbf{n} (\text{T}) \mu (\text{T}) \mathbf{e}$$

Where σ is the proton conductivity, \mathbf{n} is the number of charge carriers, μ is their mobility, and \mathbf{e} is the unit of electric charge. The number of protons (from H_3PO_4) remains the same in both imidazole and N-methyl imidazole membranes, but mobility of the proton (μ) is higher for the free imidazole ring compared to the N-methyl imidazole. The presence of imidazole ring (without N-substitution) increases the mobility of the proton and therefore creates additional pathway for the proton conduction. This opens the possibility to synthesize new PBI that contains anthracene structural unit, because anthracene unit would prone to undergo modification reaction with olefins such as vinylphosphonic acid and vinylsulfonic acid by ‘Diels-Alder’ reaction without affecting imidazole ring of PBI.

Objectives

2.1.1 Poly(vinylphosphonic acid) grafted PBI membrane

Introduction of allyl groups $[-\text{CH}_2-\text{CH}=\text{CH}_2]$, vinylbenzyl groups $[-\text{CH}_2-\text{C}_6\text{H}_5-\text{CH}=\text{CH}_2]$ and TEMPO-adduct groups $[-\text{CH}_2-\text{C}_{24}\text{H}_{31}\text{NO}_3]$ by N-alkylation of the benzimidazole rings of PBI should lead to new reactive PBIs. These new reactive groups would copolymerise with vinylphosphonic acid and the resulting copolymer membrane could exhibit better performance during fuel cell operating condition.

2.1.2 Proton conducting multilayers for fuel cell applications

In order to study acid attached PBI or P4VIm by strong noncovalent interactions, multilayers of various combinations such as poly(vinylphosphonic acid) - poly(benzimidazole), poly(vinylphosphonic acid) - poly(4-vinylimidazole), poly(vinylsulfonic acid) - poly(benzimidazole), poly(vinylsulfonic acid) - poly(4-vinylimidazole), poly(4-styrenesulfonic acid) - poly(benzimidazole) and poly(4-styrenesulfonic acid) - poly(4-vinylimidazole) are considered for fuel cell applications.

2.1.3 Anhydrous proton conducting homo- and copolymers

Synthesis of homo- and copolymers based on flexible chain backbone (important factor for high conductivity) is an attention of current fuel cell research at elevated temperatures.⁽¹⁹⁹⁻²⁰⁶⁾ Therefore synthesis of various proton conducting polymers such as poly(vinylphosphonic acid), poly(vinylbenzylphosphonic acid), poly(4-styrenesulfonic acid), poly(2-vinylbenzimidazole), poly(4-vinylimidazole), copolymers based on 4-vinylimidazole and vinylphosphonic acid as well as 4-vinylimidazole and 4-styrenesulfonic acid are chosen for this purpose.

2.1.4 Synthesis of polybenzimidazole with anthracene structural unit

In order to avoid grafting reactions in the imidazole ring, PBI that contains anthracene unit should be synthesized, because anthracene would encourage the modification reaction with olefins such as vinylphosphonic acid and vinylsulfonic acid by Diels-Alder reaction.

3.1 Synthesis of reactive PBIs by allyl, vinylbenzyl and TEMPO - adduct grafting

In the previous chapters, it was shown that polybenzimidazoles are promising polymeric materials for high temperature fuel cell applications.⁽²²⁻³²⁾ When doped with phosphoric acid, proton conductivities up to 2×10^{-2} S/cm have been measured.⁽²²⁻³²⁾ However for practical application as a membrane material in real PEMFC, the acid doped PBI exhibits a severe drawback. Since water is formed as a product during cell operation, it dilutes the acid in which the membrane is soaked. In this way, the acid is slowly washed out of the membrane and the performance of the cell goes down.

In order to retain acid in the PBI membrane, it is essential to introduce covalently bound acid groups onto the PBI backbone. This will enhance the performance by retaining acid in the membrane during fuel cell operating conditions. To synthesize PBI membranes with covalently bound acid group, N-substitution of -CH₂-CHPO(OH)₂ groups (Ethyl phosphonic acid) into the benzimidazole ring of PBI has been reported recently.⁽¹⁴¹⁾ The presence of covalently bound phosphonic acid enhances conductivity but depending on the degree of phosphonation, the conductivities are changed. Thus high degree of phosphonation results in conductivity of only up to 10^{-5} S/cm, which is lower than maximum reported conductivities of different membranes around 10^{-2} S/cm.^(15, 34-41) The low proton conductivity could be attributed to lower phosphonic acid concentration in the membrane (i.e., mono phosphonic acid group substitution per imidazole ring of PBI).

To increase the number of phosphonic acid groups per imidazole ring, the poly(vinylphosphonic acid) chain has to be introduced into PBI. Its grafting onto PBI would offer the improved conductivity of the membrane.

Synthesis of PVPA grafted PBI membrane can be done according to "grafting from" and "grafting through" methods. In "grafting through" method (or macromonomer method), monomer (e.g., vinylphosphonic acid) is radically copolymerized with olefin group attached macromonomer (e.g., allyl grafted PBI and vinylbenzyl grafted PBI). This approach is inherently limited to synthesize graft-copolymer with well-defined architectural and structural parameters.

In "grafting from" method, monomer (e.g., vinylphosphonic acid) is polymerized from polymer backbone containing pendant functionalities as initiating sites (e.g., TEMPO-adduct grafted PBI for 'nitroxide mediated controlled radical polymerization'). This approach would allow precisely controlled growth of polymer chains.

In order to introduce olefin groups and TEMPO-adduct groups into PBI, synthesis of allyl grafted PBI, vinylbenzyl grafted PBI and TEMPO-adduct grafted PBI are performed by N-alkylation of polybenzimidazole with allyl chloride, vinylbenzyl chloride and Cl-TEMPO-adducts via 'nucleophilic substitution reaction'. Furthermore, PBI after modification with allyl groups, vinylbenzyl groups and TEMPO-adduct groups should improve its solubility, because commercially available PBI from Hoechst Celanese Corp., has a very poor solubility in most organic solvents with an exception for dimethylacetamide (DMAc) and concentrated sulfuric acid.

In this chapter, the synthesis of functionalised PBIs with different degrees of modification and its viscosity, solubility properties and thermal properties are discussed in detail. The copolymerisation of functionalised PBI with vinylphosphonic acid and proton conducting properties are discussed in Chapter-IV.

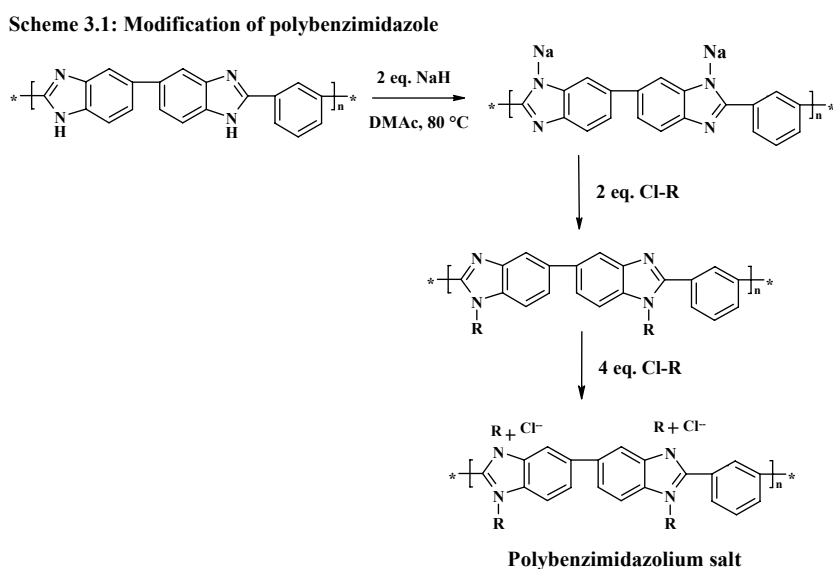
3.2 Polybenzimidazole used for modification experiments

All modification experiments were performed with poly[2,2'-(*m*-phenylene)-5,5'-bisbenzimidazole] (Intrinsic viscosity ~ 0.89 dl/g, $M_n \sim 22 \times 10^3$ g/mol and $M_w/M_n \sim 2.1$), which was obtained as a gift from Celanese Ventures GmbH, Frankfurt.

3.3 Modification of polybenzimidazole

Polybenzimidazoles are ideal candidates for 'nucleophilic substitution reaction', because they possess two potentially reactive N-H bonds per repeating unit of PBI.⁽¹²⁶⁻¹⁴¹⁾ Upon addition of NaH, which deprotonates the nitrogens of the benzimidazole rings in the polymer backbone, there is an initial formation of a polyanion of the parent polybenzimidazole, followed by reaction with an appropriate modifying reagent (allyl chloride, vinylbenzyl chloride and Cl-TEMPO- adduct) to produce N-alkyl derivative.

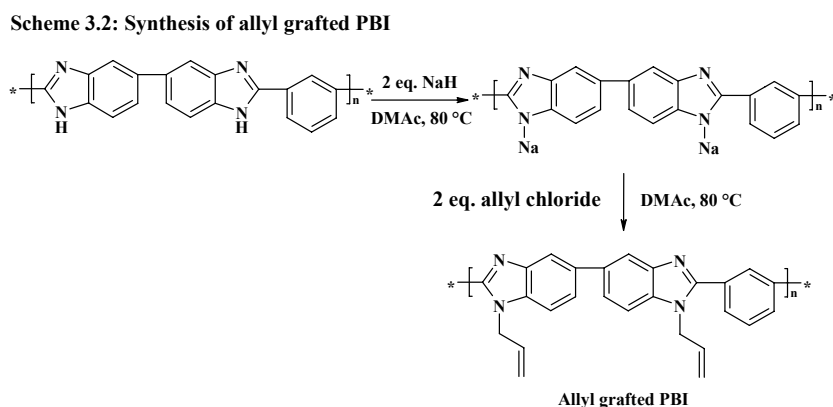
The addition of 4 equivalents of modifying agent per repeat unit of benzimidazole might give a positively charged polybenzimidazolium salt as it was reported for the modification of polybenzimidazole with methyl iodide.⁽²³³⁾ Scheme 3.1 describes the modification of PBI.



From this general procedure, the detailed description of grafting different modifying groups such as allyl groups, vinylbenzyl groups and TEMPO-adduct groups onto PBI are as follows:

3.3.1 Allyl grafted PBI

According to Scheme 3.2, synthesis of allyl grafted PBI was carried out as follows: A 15-wt % DMAc solution of PBI was diluted by adding equal volume of DMAc (because of its high viscosity) and then 2 equivalents of NaH per repeating unit of PBI were added to the mixture at 80 °C. After 3-6 hours, 2 eq. of allyl chloride was added to generate allyl grafted PBI.



The degree of modification for allyl groups grafting was calculated by ^1H NMR spectroscopy. For the sample PBI-A1, the calculation is described below using Fig. 3.1:

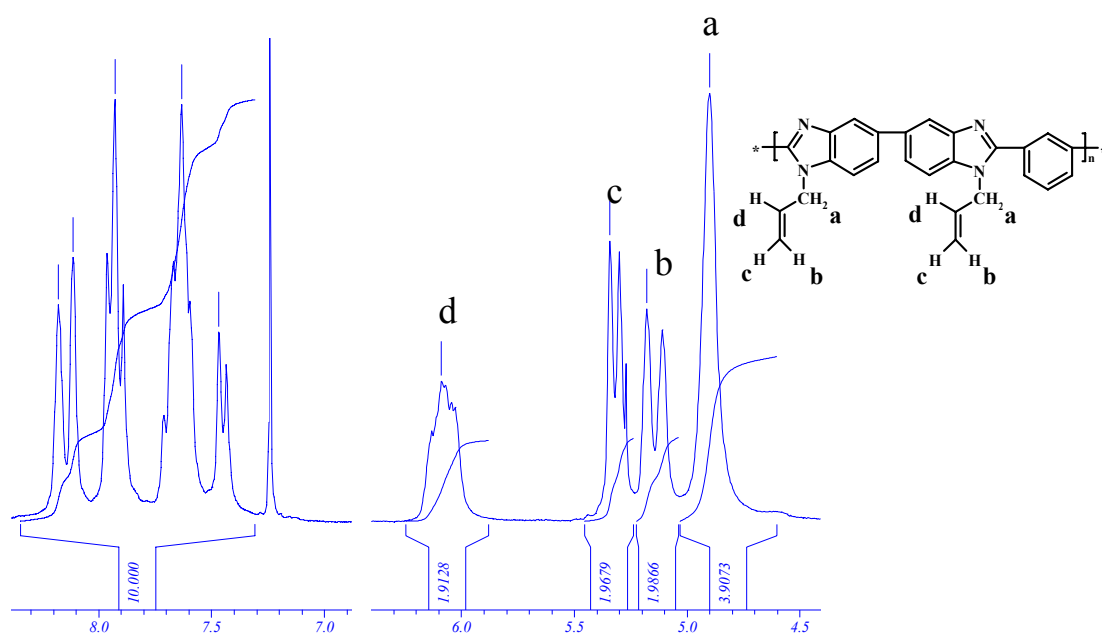


Fig. 3.1: ^1H NMR (250 MHz, CDCl_3) spectrum of allyl grafted PBI (PBI-A1)

The signals appearing at 4.89 ppm ($-\text{N}-\text{CH}_2-$), and 5.1 to 6.08 ppm ($-\text{CH}=\text{CH}_2$) confirm the N-alkylation of the imidazole ring. As PBI has two benzimidazole rings in its repeating unit, 100 % modification means that two equivalents of allyl groups have been covalently bound to each repeating unit of benzimidazole.

In the present study, the degree of modification for allyl grafting ($-\text{CH}_2-\text{CH}=\text{CH}_2$) was calculated from ^1H NMR data using equation 1:

Degree of modification (%) =

$$\frac{\text{Integrated intensity of } -\text{N}-\text{CH}_2 \text{ protons}}{\text{Integrated intensity of all aromatic protons}} \times \frac{10}{4} \times 100 \quad (1)$$

Using equation 1,

$$\text{Degree of modification (\%)} = \frac{3.92}{10} \times \frac{10}{4} \times 100 = 98 \%$$

The allyl grafted PBI prepared with different degrees of modification using NaH as base, $\text{CH}_2=\text{CH}-\text{CH}_2\text{Cl}$ and PBI are summarized in Table 3.1. The error limit of these experiments was within $\pm 2\%$ depending on the moisture content in the reaction mixture.

Table-3.1: Summary of allyl grafted PBIs from $^1\text{H-NMR}$ data

Sample	Reaction conditions	Aromatic protons intensity	Relative intensity of $-\text{N}-\text{CH}_2-$ protons	Degree of modification (%)
PBI-A1	24 hr at 80°C	10	3.9	98
PBI-A2	24 hr at 80°C	10	3.0	75
PBI-A3	24 hr at 80°C	10	3.0	75
PBI-A4	2 hr at 80°C	10	0.5	14
PBI-A5	2 hr at 80°C	10	0.4	10
PBI-A6	1hr at 80°C	10	0.3	8
PBI-A7	1 hr at 80°C	10	0.2	5
PBI-A8	24 hr at 80°C	10	----	----
PBI-A9	24 hr at 80°C	10	3.9	98

*In all experiments, concentration of PBI was 1.3 mmol. Concentrations of NaH from PBI-A1 to PBI-A9 were as follows: 1.3, 1.0, 1.0, 0.2, 0.13, 0.1, 0.07, 0.0 and 1.3 mmol; Concentrations of allyl chloride from PBI-A1 to PBI-A9 were as follows: 1.3, 1.0, 1.3, 0.2, 0.13, 0.1, 0.07, 1.3 and 2.6 mmol.

The study of the data, presented in Table 3.1 reveals that the degree of grafting depends on the reaction time and the concentration of NaH used in the reaction mixture. From samples PBI-A1 and PBI-A2, the degree of modification changes from 98 to 75 % upon decreasing concentration of NaH from 1.3 to 1.0 mmol.

Decreasing the reaction time from 24 hrs to 2 hrs on samples PBI-A1 and PBI-A5 also decreases the degree of grafting from 98 to 10 %. Further, in the absence of NaH, there are no allyl groups grafting on sample PBI-A8 illustrating that the deprotonated polyanion are essential for the grafting reaction. From sample PBI-A9, addition of 2.6 mmol of allyl chloride per repeating unit of benzimidazole did not produce benzimidazolium salt as there is no shift in $-\text{N}-\text{CH}_2-$ proton signal for positively charged benzimidazole ring (benzimidazolium salt) with respect to $-\text{N}-\text{CH}_2-$ proton signal for uncharged benzimidazole ring by ^1H NMR spectroscopy. Furthermore, solubility property of PBI-A9 did not differ from solubility of PBI-A1 demonstrating the absence of positively charged benzimidazole ring on sample PBI-A9.

^{13}C NMR spectrum (Fig. 3.2) shows a peak at 47 ppm corresponding to $-\text{N}-\text{CH}_2-$ group. The peaks for the allyl double bond carbon signals could not be resolved from the aromatic carbon signals that start to appear from 110 ppm.

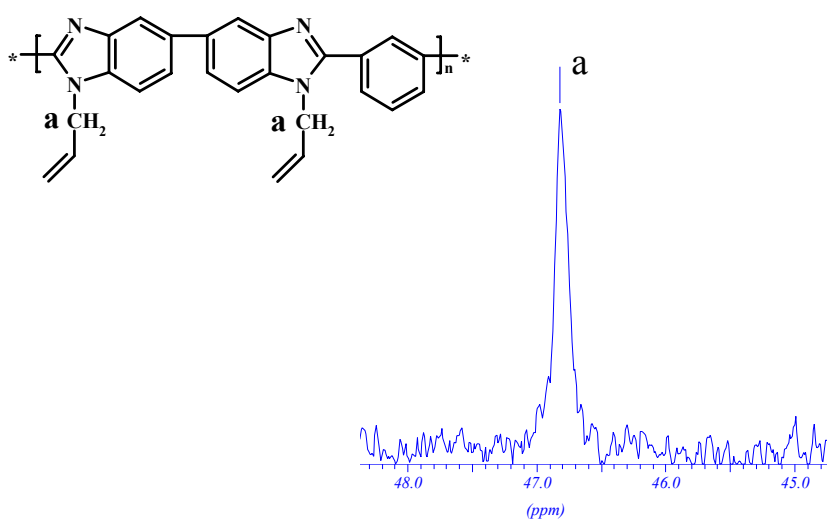


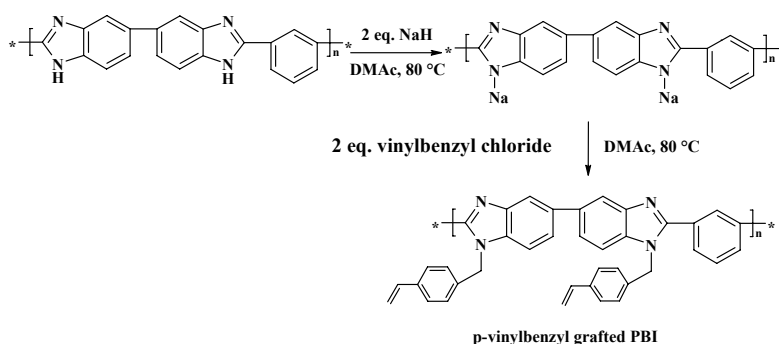
Fig. 3.2: ^{13}C NMR (62.5 MHz, CDCl_3) spectrum of allyl grafted PBI (PBI-A1)

Characterization of allyl grafted PBI by FTIR spectroscopy, viscosity measurement, solubility and thermal properties are discussed in Section- 3.4, 3.5, 3.6 and 3.7.

3.3.2 Vinylbenzyl grafted PBI

The general synthetic procedure for vinylbenzyl grafting is shown in Scheme-3.3. It was carried out with NaH (2eq.) as base and p-vinylbenzyl chloride (2 eq.) as modifying agent. The result of this procedure was the formation of vinylbenzyl grafted PBI. Addition of 4 eq. of vinylbenzyl chloride per repeating unit of benzimidazole failed to give benzimidazolium salt.

Scheme 3.3: Synthesis of vinylbenzyl grafted PBI



The degree of modification for vinylbenzyl grafting was calculated by ^1H NMR spectroscopy. For the sample PBI-V1, the calculation is described below using Fig. 3.3:

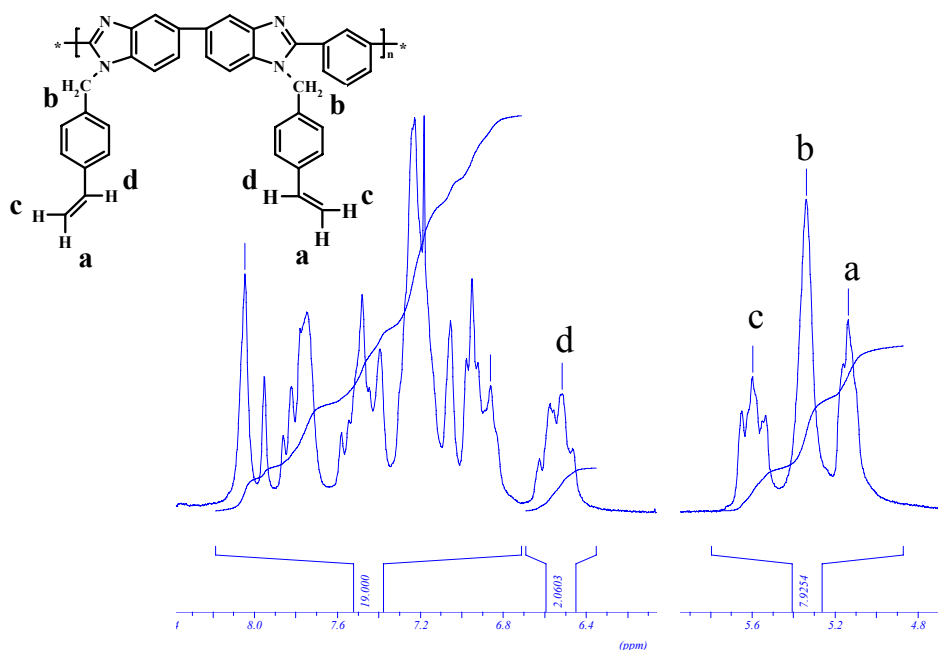


Fig. 3.3: ^1H NMR (250 MHz, CDCl_3) spectrum of p-vinylbenzyl grafted PBI (PBI-V1)

The signals appearing at 5.3 ppm ($-\text{N}-\text{CH}_2-$), 5.1 ppm, 5.6 ppm and 6.5 ppm ($-\text{CH}=\text{CH}_2$) confirm the N-alkylation of the imidazole ring.

The degree of modification for vinylbenzyl grafting was calculated using equation 2:

Degree of modification (%) =

$$\frac{\text{Integrated intensity of one double bond proton}}{\text{Integrated intensity of all aromatic protons}} \times \frac{18}{2} \times 100 \quad (2)$$

Using equation 2,

$$\text{Degree of modification (\%)} = \frac{2}{18} \times \frac{18}{2} \times 100$$

It shows that every repeating unit has two vinylbenzyl groups. The vinylbenzyl grafted PBI synthesized with different degrees of modification are summarized in Table 3.2. The error limit of these experiments was within $\pm 2\%$.

Table-3.2: Summary of vinylbenzyl grafted PBIs from ^1H NMR data

Sample	Reaction conditions	Aromatic protons intensity	Relative intensity of one double bond proton	Degree of modification (%)
PBI-V1	24 hr at 80°C	18	2.0	100
PBI-V2	24 hr at 80°C	18	1.4	70
PBI-V3	12 hr at 80°C	18	1	50
PBI-V4	6 hr at 80°C	18	0.4	20
PBI-V5	2 hr at 80°C	18	0.2	10
PBI-V6	2 hr at 80°C	18	0.1	5
PBI-V7	24 hr at 60°C	18	0.3	14
PBI-V8	24 hr at 80°C	18	2.0	100

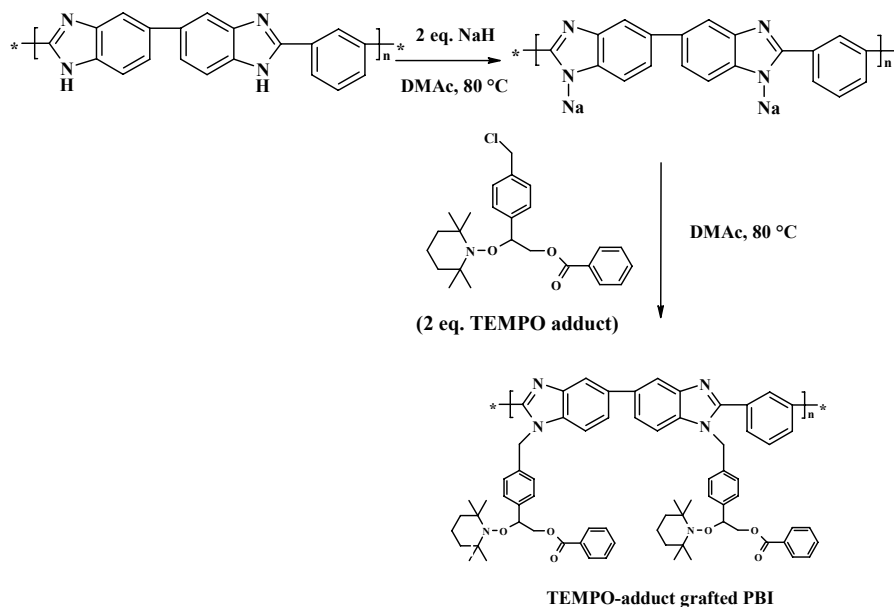
*In all experiments, concentration of PBI was 1.3 mmol; Concentrations of NaH from PBI-VI to PBI-V8 were as follows: 1.3, 0.9, 0.7, 0.3, 0.13, 0.07, 1.3 and 1.3 mmol. Concentrations of vinylbenzyl chloride from PBI-V1 to PBI-V8 were as follows: 1.3, 0.9, 0.7, 0.3, 0.13, 0.07, 1.3 and 2.6 mmol.

As shown in Table 3.2, the degree of vinylbenzyl grafting strongly depends on the number of deprotonated N-H groups as well as temperature of the grafting reaction. From the samples PBI-V1 and PBI-V7, decreasing the reaction temperature from 80 °C to 60 °C lowers the degree of grafting from 100 to 14% while maintaining other conditions such as vinylbenzyl chloride, sodium hydride and PBI concentrations at 1.3 mmol. In PBI-V8, addition of 2.6 mmol of vinylbenzyl chloride per repeating unit of benzimidazole did not produce benzimidazolium salt.

3.3.3 Benzoic acid 2-(4-(chloromethyl) phenyl)-2-(2,2,6,6-tetramethylpiperidin-1-yloxy) ethyl ester [TEMPO-adduct] grafted PBI

Synthesis of TEMPO adduct grafted PBI is presented on Scheme 3.4. Polybenzimidazole was treated with NaH (2 eq. per repeat unit of benzimidazole) with constant stirring for 3 hrs, and subsequent treatment with TEMPO adduct (2 eq.) creates the TEMPO adduct grafted PBI.

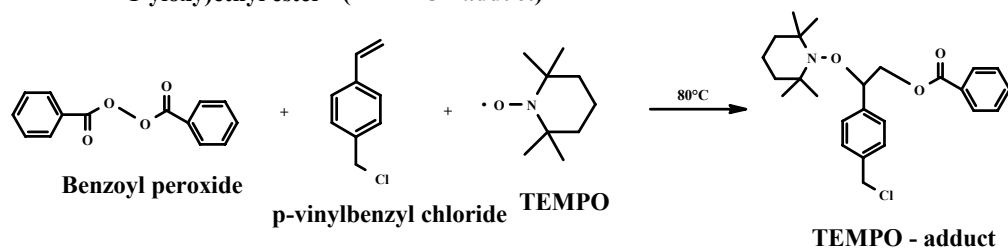
Scheme 3.4: Synthesis of TEMPO adduct grafted PBI



In order to synthesize graft copolymer without cross-linking, the grafting of TEMPO- adduct into PBI is essential, which control the polymerisation and provide well-defined architectures with narrow polydispersity.⁽¹⁹⁰⁻¹⁹⁴⁾ Further TEMPO-adduct grafted PBI is able to initiate polymerisation from poly(benzimidazole) by thermal heating at 125 °C and therefore it would act as 'macroinitiator'.

Unlike commercially available modifying agents such as allyl chloride and vinylbenzyl chloride, the modifying agent TEMPO adduct was synthesized according to the literature procedure.⁽¹⁵²⁾ Benzoyl peroxide, TEMPO and excess of p-vinylbenzyl chloride was heated at 80 °C under an argon atmosphere (Scheme 3.5). The product was purified by column chromatography and the yield was 40 %.

Scheme-3.5: Synthesis of benzoic acid 2-(4-(chloromethyl)phenyl)-2-(2,2,6,6-tetramethylpiperidin-1-yloxy)ethyl ester (TEMPO - adduct)



¹H NMR and ¹³C NMR spectra of TEMPO-adduct are given in Fig. 3.4 and 3.5.

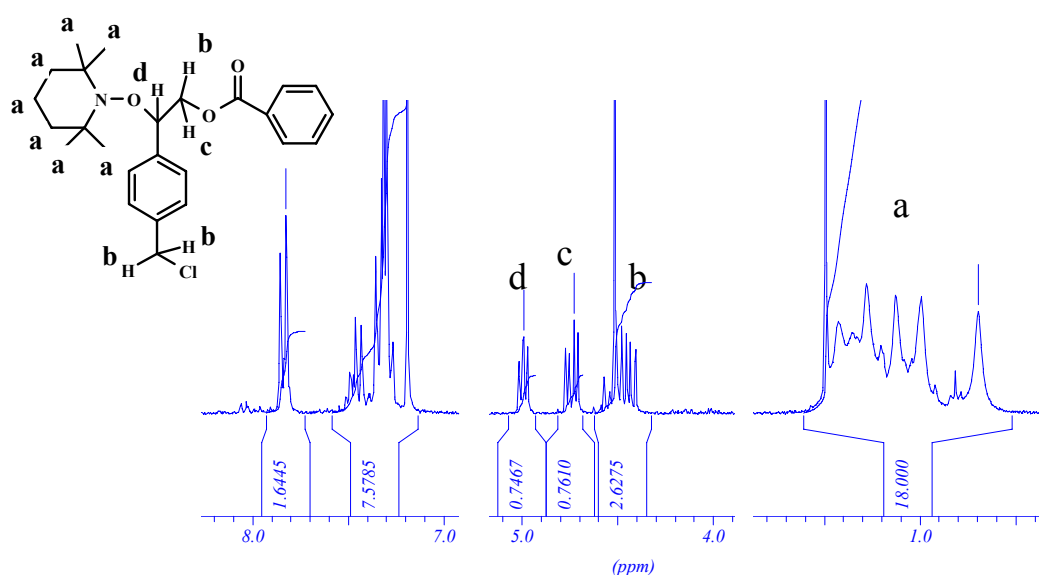


Fig. 3.4: ¹H NMR (250 MHz, CDCl₃) spectrum of TEMPO-adduct

The signals appearing at 0.5 to 1.5 ppm (aliphatic groups from TEMPO), 4.51 ppm for -C₆H₄CH₂Cl, 4.72 ppm for C₆H₅-COO-CH₂- and 4.98 ppm for C₆H₄-CH< confirm the expected structure of TEMPO-adduct. The ¹³C NMR spectrum shows a peak at 60.5 ppm corresponding to -CH₂-Cl, 67 ppm for -O-CH₂-, 84 ppm for >CH- and 166.6 ppm for carbonyl carbon from ester group agree with the structure of the TEMPO-adduct (Fig. 3.5). Analysis by FD mass showed a molecular ion peak at m/e 430 (M⁺) corresponding to TEMPO-adduct.

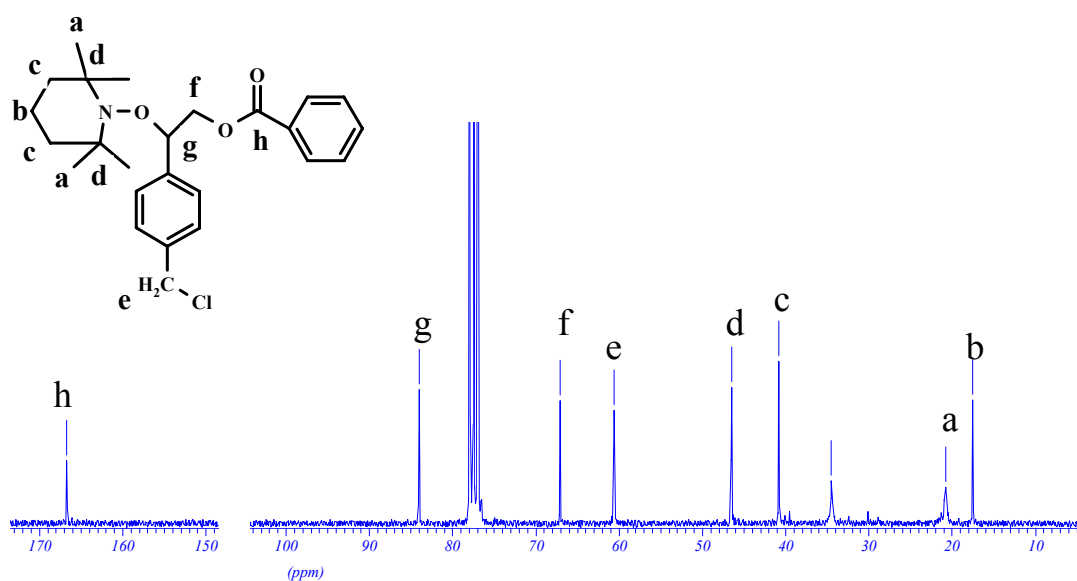


Fig. 3.5: ^{13}C NMR (62.5 MHz, CDCl_3) spectrum of TEMPO-adduct

After synthesizing TEMPO-adduct, it was grafted onto PBI (Scheme 3.4) by nucleophilic substitution reaction at 80°C . The degree of modification for TEMPO-adduct grafted PBI was calculated by ^1H NMR spectroscopy. For the sample PBI-M1, the calculation is described below using Fig. 3.6:

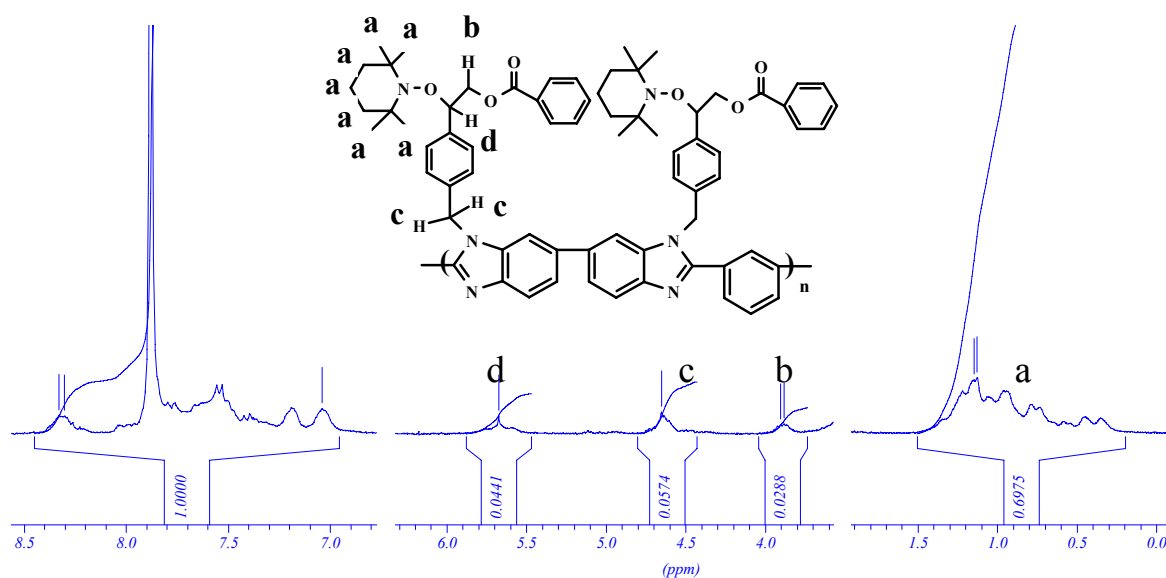


Fig. 3.6: ^1H NMR (250 MHz, $\text{D}_6\text{-DMF}$) spectrum of polybenzimidazole macro initiator (PBI-M1)

The signals (Fig. 3.6) appearing at 0.3 to 1.5 ppm (from TEMPO), 4.6 ppm (-N-CH₂-), 3.9 ppm, (-O-CH₂-), 5.7 ppm (-O-CH-benzene) confirm the N-alkylation of the imidazole ring. The degree of modification for TEMPO adduct grafting was calculated using equation 3:

$$\text{Degree of modification (\%)} = \frac{A}{B - (18 \times C)} \times \frac{28}{36} \times 100 \quad \text{--- (3)}$$

Where A – Integrated intensity of TEMPO - aliphatic protons

B – Intensity of all aromatic protons

C – Integrated intensity of one –CH- proton in the adduct

Using equation 3,

$$\text{Degree of modification (\%)} = \frac{0.07}{(1 - 18 \times 0.02)} \times \frac{28}{36} \times 100 = 83 \%$$

The TEMPO-adduct grafted PBI with different degrees of modification are summarized in Table 3.3. The error limit of these experiments was within $\pm 2 \%$

Table-3.3: Summary of TEMPO-adduct grafted PBIs from ¹H-NMR data

Sample	Reaction conditions	Aromatic protons intensity	Relative intensity of protons from Aliphatic groups	Degree of modification (%)
PBI-M1	24 hr at 80°C	1	0.7	83
PBI-M2	24 hr at 80°C	1	0.7	83
PBI-M3	24 hr at 80°C	1	0.5	56
PBI-M4	8 hr at 80°C	1	0.4	35
PBI-M5	6 hr at 80°C	1	0.2	15
PBI-M6	2 hr at 80°C	1	0.1	7

*In all experiments, concentration of PBI was 1.3 mmol; Concentrations of TEMPO- adduct from PBI-M1 to PBI-M6 were as follows: 1.3, 1.6, 1.0, 1.3, 1.3 and 1.3 mmol; Concentrations of NaH from PBI-M1 to PBI-M6 were as follows: 1.3, 1.6, 1.0, 1.3, 1.3 and 1.3 mmol.

From Table 3.3, the maximum degree of grafting is 83 %. For samples PBI-M1 and PBI-M2, the maximum degree of grafting remains the same (83 %) even when concentrations of TEMPO-adduct and sodium hydride are increased to 1.6 mmol. The reason for this behaviour should be due to steric effect of TEMPO-adduct in the TEMPO-adduct grafted PBI, which restricts the grafting reaction to 100 % completion. However, addition of 4 eq. of TEMPO-adduct per repeating unit of benzimidazole did not produce benzimidazolium salt.

3.4 FTIR spectra of modified PBIs

The chemical structures of allyl groups grafted PBI (PBI-A1) and vinylbenzyl groups grafted PBI (PBI-V1) are characterized by FTIR spectroscopy as shown in Figure 3.7.

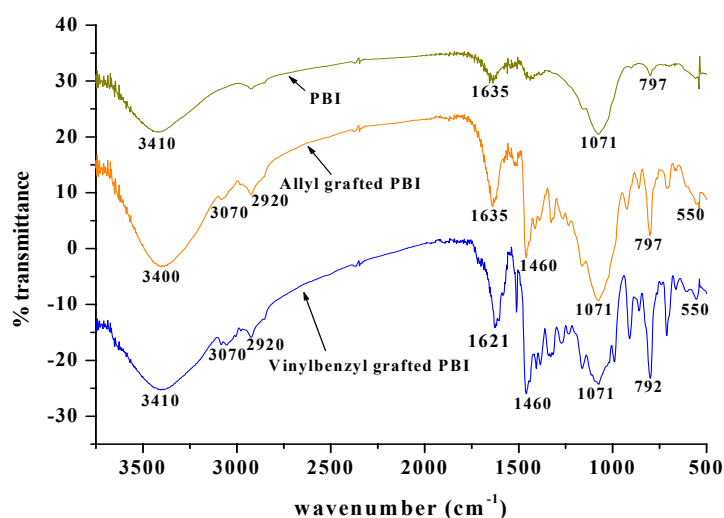


Fig. 3.7: FTIR spectra of PBI, allyl grafted PBI (PBI-A1) and vinylbenzyl grafted PBI (PBI-V1)

3.4.1 Allyl grafted PBI

FTIR spectra of polybenzimidazole and its derivatives have been studied extensively in the past.⁽¹⁵³⁻¹⁵⁶⁾ The strong band from 3200 to 3500 cm⁻¹ in the spectrum of PBI is ascribed to strong hydrogen bonding of the type N-H...N. This band becomes broader with allyl group in the spectrum of allyl grafted PBI due to N-substitution. Bands at 3070 and 2920 cm⁻¹, which correspond to -CH₂- stretching vibrations are from allyl grafting.

Bands derived from aromatic C=C and C=N stretching modes are found in the 1635-1460 cm^{-1} region. Bands from 550 - 1075 cm^{-1} are due to bending frequencies of double bonds in allyl grafted PBI. Further there is significant increase in the -C=C- stretching frequency at 1635 cm^{-1} , which indicates the presence of double bonds in the allyl grafted PBI. No calculation of the degree of modification has been attempted from these data.

3.4.2 Vinylbenzyl grafted PBI

Bands at 3070 and 2920 cm^{-1} , which correspond to -CH₂- stretching vibration, appear with the addition of -CH₂- group from vinylbenzyl grafting. Bands derived from aromatic C=C and C=N stretching modes are found in the 1620-1460 cm^{-1} region. Bands from 550 to 1075 cm^{-1} are due to bending frequencies of double bonds in vinylbenzyl grafted PBI. Further there is significant increase in the -C=C- stretching frequency at 1621 cm^{-1} , which indicates the presence of double bond in the vinylbenzyl grafted PBI. No calculation of the degree of modification has been attempted from these data.

3.4.3 TEMPO adduct grafted PBI

The chemical structures of TEMPO-adduct groups grafted PBI (PBI-M1) are displayed by FTIR spectroscopy in Fig. 3.8.

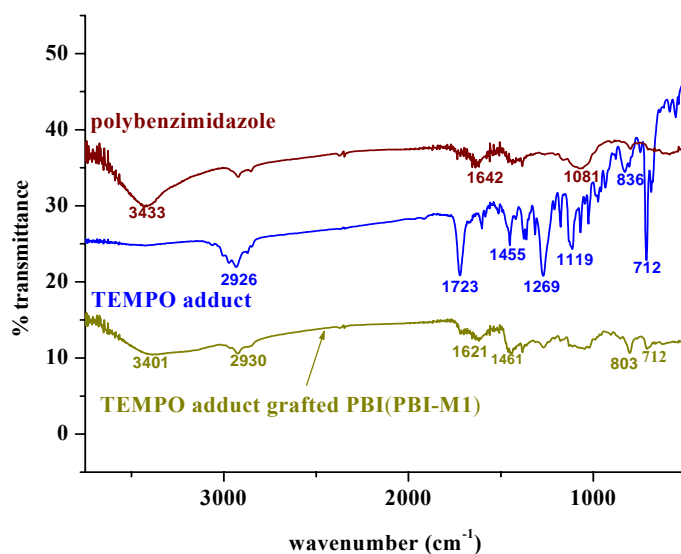


Fig. 3.8: FTIR spectra of PBI, TEMPO-adduct and polybenzimidazole macro initiator (PBI-M1)

The band at 2930 cm^{-1} , which corresponds to $-\text{CH}_2-$ stretching vibration, appears with the addition of $-\text{CH}_2-$ group from TEMPO-adduct grafting. Bands derived from aromatic $\text{C}=\text{C}$ and $\text{C}=\text{N}$ stretching modes are found in the $1620\text{--}1460\text{ cm}^{-1}$ region. Bands from 800 to 1000 cm^{-1} are due to bending and stretching frequencies of TEMPO group. The appearance of characteristic peaks of TEMPO-adduct (peaks at $2930, 803, 712\text{ cm}^{-1}$) clearly proves grafting onto PBI. No calculation of the degree of modification has been attempted from this data.

3.5 Viscosity measurements

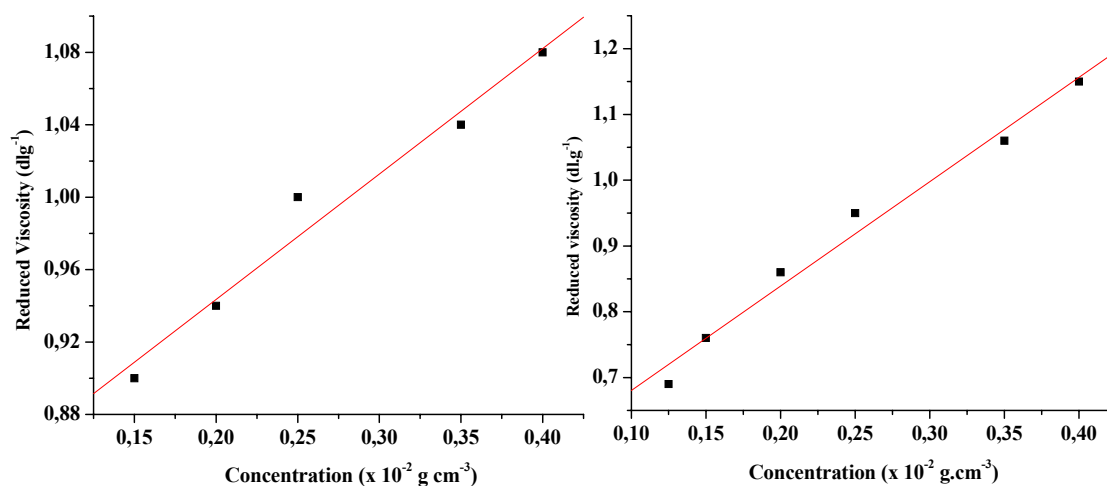


Fig. 3.9A: Determination of the intrinsic viscosity of PBI

Fig. 3.9B: Viscosity of allyl grafted PBI (PBI-A1)

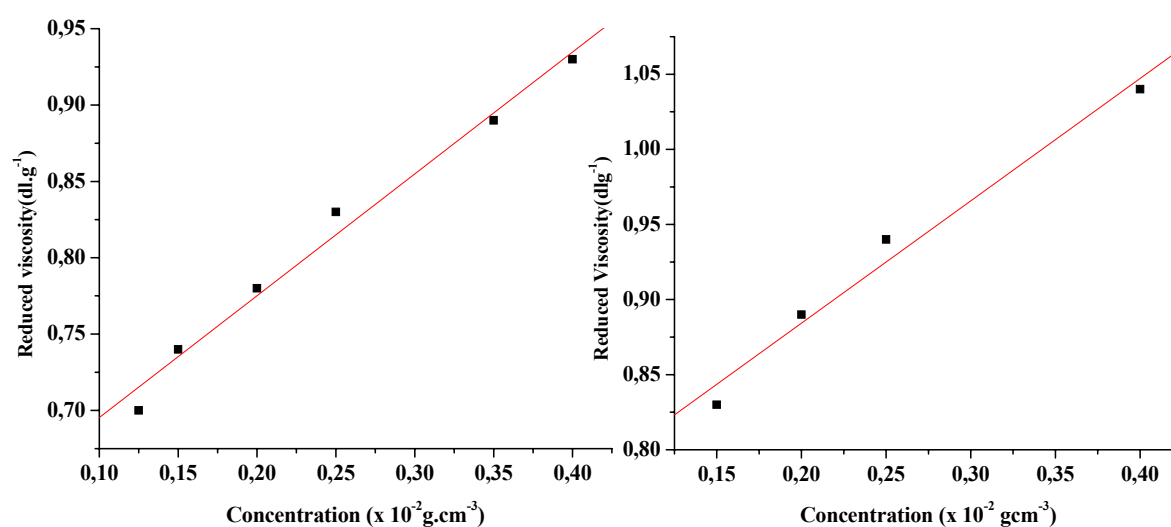


Fig. 3.9C: Viscosity of vinylbenzyl grafted PBI (PBI-V1)

Fig. 3.9D: Viscosity of TEMPO-adduct grafted PBI (PBI-M1)

Solubility was a problem encountered in the characterization of all the products from the starting compound PBI to the modified PBI. Methods such as MALDI-TOF or GPC, which are commonly used for determination of molecular weight and dispersion, are not suitable for PBI due to high insolubility of the polymer in common solvents. In order to get some idea about the molecular weight of the products obtained, their intrinsic viscosities have been determined and compared. The intrinsic viscosity of the PBI, N-allyl PBI, N-vinylbenzyl PBI, and N-TEMPO-adduct PBI were measured by Ubbelohde type viscosimeter (in H₂SO₄ solvent) as given in Fig. 3.9.

The intrinsic viscosity of PBI was 0.89 dl. g⁻¹, and the intrinsic viscosity of allyl grafted PBI (PBI-A1) was 0.69 dl.g⁻¹. The lower viscosities of modified PBIs are related to weaker hydrogen bonding interaction by replacement of –N-H hydrogen by allyl groups, vinylbenzyl groups and TEMPO-adduct groups. However, the viscosity increases with decreasing degree of modification due to increasing hydrogen-bonding interaction between polymer chains.

3.6 Solubility

The modified PBIs (**W**₁) were dissolved in a given solvent by ultrasonification for 3 hrs at room temperature. Insoluble fractions were collected by filtration, then washed several times by a given solvent and dried at 120 °C under vacuum. The weight of the insoluble fraction (**W**) was measured and the solubility was calculated using the following formula below:

$$\text{Solubility} = [(\mathbf{W}_1 - \mathbf{W}) / \mathbf{W}_1] \times 100$$

where **W**₁ is the weight of the polymer used for the solubility measurement

Solubility properties of PBI and modified PBIs are shown in the following Table 3.4 below:

Table-3.4: Solubility properties of modified PBIs

Solvent	% solubility of PBI	% solubility of allyl grafted PBI (PBI-A1)	% solubility of vinylbenzyl grafted PBI (PBI-V1)	% solubility of TEMPO-grafted PBI (PBI-M1)
DMAc	Soluble	Soluble	Soluble	Soluble
DMSO	~ 70 soluble	Soluble	~ 70 soluble	Soluble
NMP	~ 80 soluble	Soluble	~ 80 soluble	Soluble
H ₂ SO ₄	Soluble	Soluble	Soluble	Soluble
CHCl ₃	Insoluble	Soluble	Soluble	Swelling, but insoluble
CH ₂ Cl ₂	Insoluble	Soluble	Soluble	Swelling, but insoluble
CH ₃ OH	Insoluble	Insoluble	Insoluble	Swelling, but insoluble
Water	Insoluble	Insoluble	Insoluble	Swelling, but insoluble

From Table 3.1, the modified PBIs have considerably higher solubility than the PBI due to weaker hydrogen bonding interactions in it. However, the solubility decreases with decreasing degree of grafting due to increasing hydrogen-bonding interactions between polymer chains.

3.7 Thermal properties of modified PBIs

Figure 3.10 displays the thermogravimetric (TG) curves of modified PBIs. PBI and modified PBIs show an initial weight loss of ~ 5 % upon heating from 100 to 140 °C due to water and residual solvent such as DMAc present in the polymer. The decomposition of allyl grafted PBI (PBI-A1) begins at 420 °C, decomposition of vinylbenzyl grafted PBI (PBI-V1) and TEMPO-adduct grafted PBI (PBI-M1) begin at 450 and 380 °C respectively. The lower decomposition temperatures of modified PBIs than PBI (decomposition of PBI begins at 550 °C) must be due to flexible segments of allyl groups, vinylbenzyl groups and TEMPO-adduct groups in the polymer chain.

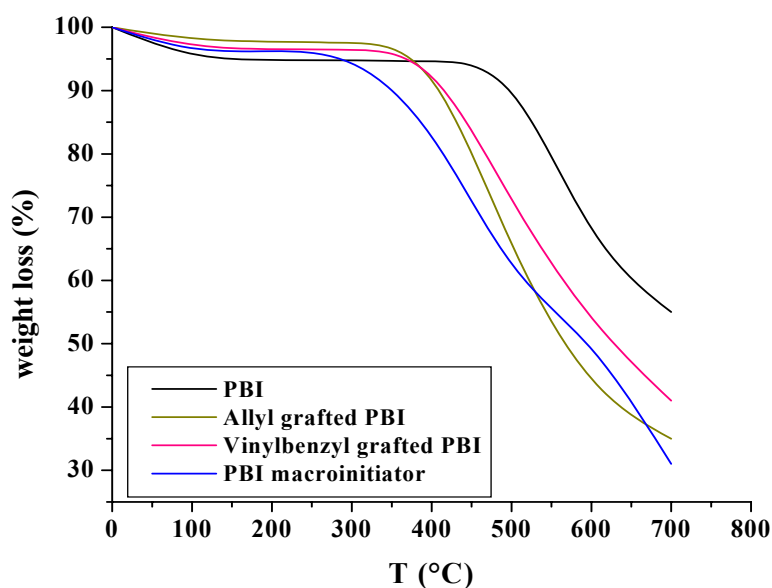


Fig. 3.10: TGA curves of PBI and modified PBIs recorded under N₂ with a heating rate of 10 K/min.

3.8 Summary

Poly(N-allyl polybenzimidazole), poly(N-vinylbenzyl polybenzimidazole) and poly(N-TEMPO-adduct polybenzimidazole) were synthesized through the nucleophilic substitution reaction of PBI with allyl chloride, p-vinylbenzyl chloride and Cl-TEMPO-adduct. It was found that at constant temperature (80 °C for PBI concentration of 1.3 mmol), the modification degree was dependent on the concentration of NaH up to 1.3 mmol and concentration of modifying agent up to 1.3 mmol. Addition of 2.6 mmol of modifying agent did not produce benzimidazolium salt. Modified PBIs were soluble in dichloromethane, chloroform, DMF, DMAc and DMSO. However solubility decreases with decreasing modification degrees due to increasing hydrogen-bonding interaction between polymer chains.

Vinylbenzyl grafted PBI (PBI-V1) becomes an insoluble polymer in all solvents by exposing to air at room temperature for long time period due to cross-linking reactions by electron rich double bonds from vinylbenzyl groups. Whereas allyl grafted PBI (PBI-A1) is a solvent soluble polymer even after prolonged exposure to air at room temperature indicating the absence of electron rich double bonds from allyl groups. Therefore, vinylbenzyl grafted PBI is capable of generating radicals even in the absence of added initiator.

Modified PBIs with higher degree of modification (PBI-AI and PBI-V1) would be useful for synthesizing graft-co-polymer due to its excellent solubility and more reactive centres for copolymerisation reaction with monomer such as vinylphosphonic acid.

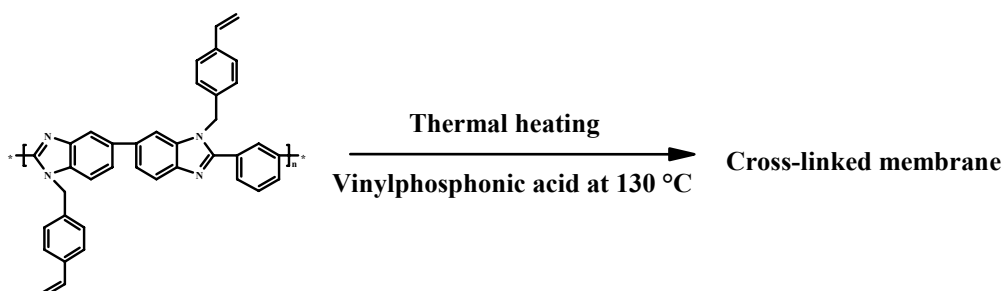
Further, vinylbenzyl groups grafted PBI and allyl groups grafted PBI are not only useful to synthesize membranes with VPA, but the double bonds would also be useful to fabricate composite membranes of PBI with various high performance polymers by cross-linking reactions, which is similar to the conventional cross-linking methods of PBI reported in the literature.⁽²²³⁾

4.1 Poly(vinylphosphonic acid) [PVPA] grafted poly(benzimidazole) as membrane materials for fuel cell applications

Poly(vinylphosphonic acid) is an appropriate alternative for H_3PO_4 to prevent self-condensation of acid groups up to 150 °C.⁽¹⁷¹⁻¹⁷³⁾ Its grafting onto PBI may not only increase the performance of the membrane without self-condensation of acid groups till 150 °C, but possibly avoid the acid leakage in the membrane. In general, two methods can be used for grafting PVPA onto PBI.

In the first method, vinylphosphonic acid was copolymerized with vinylbenzyl grafted PBI by thermal heating. In this method, radicals might be generated from electron rich styrene double bonds by thermal heating at 130 °C, which is well known as ‘auto-initiation of styrene’ in the literature.⁽¹⁹⁶⁻¹⁹⁷⁾ The following Scheme 4.1 explains the copolymerisation reaction.

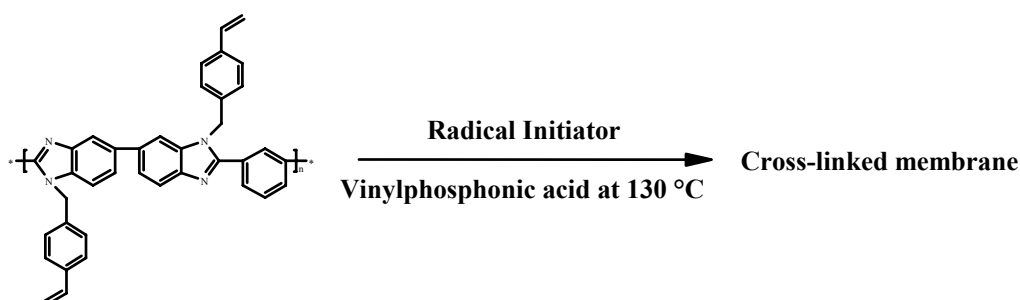
Scheme-4.1: Polymerisation and cross-linking reactions by thermal heating



In addition, the copolymerization was carried out using a radical initiator. In this method, radicals are generated by thermal decomposition of an initiator, for example, azobiscyclohexanenitrile (decomposition temperature of the initiator, 112 °C) as well as by electron rich styrene double bond from vinylbenzyl grafted PBI and hence, both radicals initiate polymerization with vinylphosphonic acid.

Scheme 4.2 presents the copolymerisation in the presence of a radical initiator.

Scheme-4.2: Polymerisation and cross-linking reactions in presence of a radical initiator



4.2 Preparation of polymer membrane

In the present study, membranes were prepared from a vinylbenzyl grafted PBI in N, N'-dimethylacetamide (DMAc) solution, since DMAc is a suitable solvent to make a homogeneous solution with vinylphosphonic acid (VPA).

The DMAc solution of vinylbenzyl grafted PBI (PBI-V1) was first mixed with VPA in a 250 ml conical flask, and placed in an ultrasonification bath for 2 hrs to make a homogeneous solution. Oxygen was removed from the flask by bubbling argon through the solution for 2 h. The conical flask was then closed and placed in an ultrasonification bath for another 2 h.

Membranes were cast using Petri dishes. The thickness and size of the membranes were varied by controlling the volume of the solution according to the diameter of the dishes. The polymerisation reaction as well as solvent evaporation started at 130 °C for 24 h. The products were washed with distilled water at 80 °C in order to remove unreactive monomers as well as residual solvent from the membrane. Traces of solvent molecules were removed by drying at 100 °C.

4.3 Proton conductivity measurements

Proton conductivity measurements were carried out by means of a four-probe cell. A schematic view of the galvanostatic four-point-probe electrochemical impedance spectroscopy is shown below (Fig. 4.1):

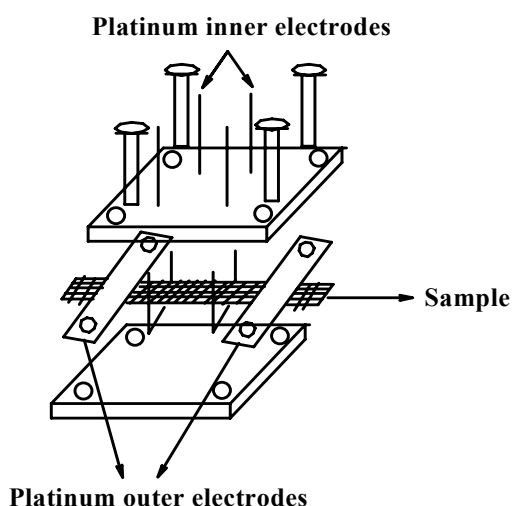


Fig. 4.1: Four-point-probe electrochemical cell

In order to study the proton conductivity of membranes systematically by four-point probe electrochemical cell, attention was focussed on the concentration of vinylphosphonic acid (VPA) and its conversion into the polymeric form. To find more clear dependencies, 0.7 g of vinylbenzyl grafted PBI (**W1**) was taken in all experiments and the weight of vinylphosphonic acid was varied from 1.5 g to 3.5 g. In all experiments, vinylbenzyl grafted PBI with the highest degree of modification (PBI-V1) was used due to its excellent solubility and more available reactive centres for copolymerisation with VPA. After the cross-linking reaction, the membrane was washed with hot water to remove unreactive monomers, and then dried at 100 °C for 24 hrs. Finally, the weight of the membrane (**W2**) was measured. The percentage of vinylphosphonic acid grafted onto PBI (conversion of VPA into polymeric form) was calculated from the following equation:

$$= \frac{100 \times (W2-W1)}{\text{Weight of VPA used for the grafting reaction}}$$

The number of VPA units per repeat unit of benzimidazole was calculated as the ratio of number of moles of VPA that was grafted onto PBI and the number of moles of vinylbenzyl grafted PBI (0.0016 mole) used for all modification experiments.

$$\text{Number of VPA per repeat unit of benzimidazole} = \frac{\text{Number of moles of grafted VPA}}{0.0016}$$

In Tables 4.1 to 4.4, the proton conductivities of the four membranes are described with increasing temperature.

4.3.1 Temperature dependence on proton conductivity of membrane-1

The membrane-1 was synthesized from 1.5g of VPA and the proton conductivity values are given in Table 4.1. Conversion of vinylphosphonic acid into polymeric form is 60 % and the number of VPA units per repeat unit of benzimidazole is 3.

Table-4.1: The temperature dependence on proton conductivity of membrane-1

Ex.No.	Temperature	Conductivity (10^{-2} S/cm)
1	20 °C	0.07
2	40 °C	0.05
3	60 °C	0.04
4	80 °C	0.05
5	100 °C	0.07
6	120 °C	0.13
7	140 °C	0.20
8	160 °C	0.21

As seen in Table 4.1, the proton conductivity of membrane-1 increases with temperature with a maximum conductivity of 2.1×10^{-3} S/cm measured at 160 °C. Further, the maximum conductivity value of membrane-1 was higher than ethyl phosphonic acid grafted PBI⁽¹⁴¹⁾ and ethyl sulfonic acid grafted PBI⁽¹⁵⁾ which can be explained by the higher number of VPA units per benzimidazole in membrane-1. However, the conductivity is lower than those of H₂SO₄ doped PBI membrane,^(34-36, 61) H₂SO₄ doped sulfonated PBI polymer blends,⁽³⁷⁻⁴¹⁾ H₃PO₄ doped PBI membrane,^(29,57-61) KOH doped PBI membrane,⁽³⁰⁾ and NAFION type membranes,⁽²⁻⁴⁾ whose conductivity values are in the range of 10^{-2} S/cm. Therefore, it is essential to increase the number of VPA units per repeating unit of benzimidazole in order to get a membrane with proton conductivity around 10^{-2} S/cm.

4.3.2 Temperature dependence on proton conductivity of membrane-2

The membrane-2 was synthesized from 2.5 g of VPA and the proton conductivity values are recorded in Table 4.2. Conversion of VPA into polymeric form is 56 % and the number of VPA units per repeat unit of benzimidazole is 5.

Table-4.2: The temperature dependence on proton conductivity of membrane-2

Ex.No.	Temperature	Conductivity (10^{-2} S/cm)
1	20 °C	0.03
2	40 °C	0.04
3	60 °C	0.04
4	80 °C	0.05
5	100 °C	0.08
6	120 °C	0.15
7	140 °C	0.21
8	160 °C	0.23

From Table 4.2, the proton conductivity of membrane-2 increases with temperature and a maximum conductivity of 2.3×10^{-3} S/cm was measured at 160 °C. Increasing VPA units per benzimidazole from 3 (membrane-1) to 5 (membrane-2) did not increase the proton conductivity much, and the proton conducting properties of membrane-1 and membrane-2 are almost similar in nature. To improve the proton conductivity further, it is required to graft more VPA units by increasing the acid concentration from 2.5 g to 3.0 g.

4.3.3 Temperature dependence on proton conductivity of membrane-3

The membrane-3 was synthesized from 3 g of VPA and the conductivity values are given in Table 4.3. Conversion of VPA into polymeric form is 50 % and the number of VPA units per repeat unit of benzimidazole is 6.

Table-4.3: The temperature dependence on proton conductivity of membrane-3

Ex.No.	Temperature	Proton conductivity (10^{-2} S/cm)
1	20 °C	0.03
2	40 °C	0.07
3	60 °C	0.08
4	80 °C	0.11
5	100 °C	0.21
6	120 °C	0.39
7	140 °C	0.56
8	160 °C	0.64

As seen in Table 4.3, the proton conductivity increases with temperature and a maximum conductivity of 6.4×10^{-3} S/cm was measured at 160 °C. Membrane-3 shows a uniform increase in proton conductivity from 20 °C to 160 °C and its conductivity values are higher than those of membrane-1 and membrane-2 due to the higher number of VPA units grafted per benzimidazole. However, the conductivity is still lower than the maximum proton conductivity values reported in the literature (around 10^{-2} S/cm).^(2-4, 29-30, 34-41) To improve the conductivity further, it is essential to graft more acid units (more than 6) per benzimidazole in PBI.

4.3.4 Temperature dependence on proton conductivity of membrane-4

The membrane-4 was synthesized from 3.5 g of VPA and the conductivity values are reported in Table 4.4. Conversion of VPA into polymeric form is 43 % and the number of VPA units per repeat unit of benzimidazole is 7.

Table-4.4: The temperature dependence on proton conductivity of membrane-4

Ex.No.	Temperature	Proton conductivity (10^{-2} S/cm)
1	20 °C	0.07
2	40 °C	0.17
3	60 °C	0.22
4	80 °C	0.26
5	100 °C	0.41
6	120 °C	0.69
7	140 °C	1.01
8	160 °C	1.21

From Table 4.4, the conductivity increases with temperature with a maximum conductivity of 1.2×10^{-2} S/cm measured at 160 °C. The conductivity of this membrane is comparable to the reported maximum proton conductivity values in the literature in the range of 10^{-2} S/cm. ^(2-4, 29-30, 34-41) However, membrane-4 is superior than acid doped PBI membranes due to its ability to retain acids in the membrane, whereas acid doped PBI membranes can not retain acids in the membrane during fuel cell operating conditions and Nafion type membranes are useful only below the boiling point of water. The higher conducting nature of membrane-4 was explained by the higher number of VPA units per benzimidazole ring in PBI.

4.4 Polymerization in the presence of radical initiator

As seen from Table 4.1 to 4.4, it is clear that increasing the number of VPA units per benzimidazole in PBI increases its proton conductivity. To increase the conductivity above 1.2×10^{-2} S/cm, it is essential to add initiator to attach higher number of VPA units per repeat unit of benzimidazole.

In order to study the cross-linking reaction in the presence of a radical initiator, 0.7 g of vinylbenzyl grafted PBI (PBI-V1) or 0.7 g of allyl grafted PBI (PBI-A1) was taken along with 0.1 mmol of initiator, and the weight of vinylphosphonic acid was varied from 4.5 g to 5.5 g.

Membranes were also synthesized from initiator concentration of 0.05 mmol, but number of VPA units per repeat unit of benzimidazole (synthesized from vinylbenzyl grafted PBI) remain as 7 and 8, which is not sufficient to increase the proton conductivity of the membrane.

Increasing the initiator concentration at 0.15 mmol is accompanied by increasing rigidity, which develops cracks and voids in the membrane. Therefore membrane becomes useless that no conductivity measurement could be performed. Hence, concentration of initiator was optimised at 0.1 mmol to reduce rigidity of the membrane. Table 4.5 shows the temperature dependence of proton conductivity of membrane-5, membrane-6, membrane-7 and membrane-8.

Table-4.5: The temperature dependence on proton conductivity of membrane-5

Ex.No.	Temp. (°C)	Proton conductivity (10^{-2} S/cm)			
		Membrane-5	Membrane-6	Membrane-7	Membrane-8
1	20	0.08	0.09	0.08	0.08
2	40	0.19	0.20	0.20	0.23
3	60	0.28	0.29	0.27	0.29
4	80	0.32	0.34	0.31	0.33
5	100	0.49	0.46	0.46	0.47
6	120	0.77	0.80	0.80	0.81
7	140	1.71	1.72	1.61	1.78
8	160	2.01	2.81	1.97	2.14

*Membrane-5 was synthesized from vinylbenzyl grafted PBI with 4.5 g of VPA; Conversion into polymeric form = 48 %. Number of VPA units per benzimidazole = 10;

*Membrane-6 was synthesized from vinylbenzyl grafted PBI with 5.5 g of VPA; Conversion into polymeric form = 45 %. Number of VPA units per benzimidazole = 12;

*Membrane-7 was synthesized from allyl grafted PBI with 4.5 g of VPA; Conversion into polymeric form = 40 %. Number of VPA units per benzimidazole = 7.

*Membrane-8 was synthesized from allyl grafted PBI with 5.5 g of VPA; Conversion into polymeric form = 37 %. Number of VPA units per benzimidazole = 8.

As recorded in Table 4.5, the proton conductivity increases with temperature and a maximum conductivity of 2.81×10^{-2} S/cm was measured at 160 °C. The conductivity values are higher in membrane-5, membrane-6, membrane-7 and membrane-8, but not much different from those of membrane-4 even with increasing number of VPA units from seven to twelve per benzimidazole ring. In these membranes (synthesized in presence of radical initiator), the flexibility of polymer chains are lowered by increasing cross-link (because mobility plays an important role to enhance conductivity)⁽²³³⁾ and, as a result, the conductivity did not increase much even though the number VPA units increase from seven to twelve per benzimidazole ring.

On comparing allyl grafted PBI with vinylbenzyl grafted PBI for copolymerisation reaction with VPA (from membrane-5 and membrane-7), vinylbenzyl grafted PBI polymerises with higher VPA units than allyl grafted PBI under similar conditions. This may be due to more radical centres available in vinylbenzyl grafted PBI (where radicals may be generated from electron rich double bonds as well as from added initiator) than allyl grafted PBI (where radicals are generated only by added initiator). Hence membranes synthesized from vinylbenzyl grafted PBI exhibited higher conductivity than those tailored from allyl grafted PBI.

DSC measurements were carried out to determine the glass transition temperature (T_g) of these membranes. Table 4.6 displays T_g of membrane-1 to membrane-8.

Membrane	No of VPA units per imidazole ring	Max. proton conductivity ($\times 10^{-2}$ S/cm)	T_g
Membrane-1	3	0.21	50 °C
Membrane-2	5	0.23	42 °C
Membrane-3	6	0.64	20 °C
Membrane-4	7	1.21	14 °C
Membrane-5	10	2.01	-5 °C
Membrane-6	12	2.81	-10 °C
Membrane-7	7	1.97	2 °C
Membrane-8	8	2.14	-2 °C

From Table 4.6, high VPA contents result in high conductivity but sacrifice mechanical stability, especially lowering T_g of membranes. When the VPA content is higher (membranes- 6, 7 and 8), the plastifying effect of the excessive acid sometimes leads to formation of a soft paste, which is unable to be processed into membranes. Addition of inorganic filler such as high-surface-area SiO_2 would make the membranes stiffer, as demonstrated in systems of $\text{PEI-H}_3\text{SO}_4\text{-SiO}_2$ ⁽²⁵⁰⁾ and $\text{Nylon-H}_3\text{PO}_4/\text{H}_2\text{SO}_4\text{-SiO}_2$.⁽²⁵¹⁾ However, maximum conductivities decreased to 10^{-3} S/cm at 160 °C for membranes -6, 7 and 8 in addition of 1 mg SiO_2 . This is possible because polymer chain mobility is reduced in stiff membranes.

4.5 Proton conducting nature of membranes with increasing temperature

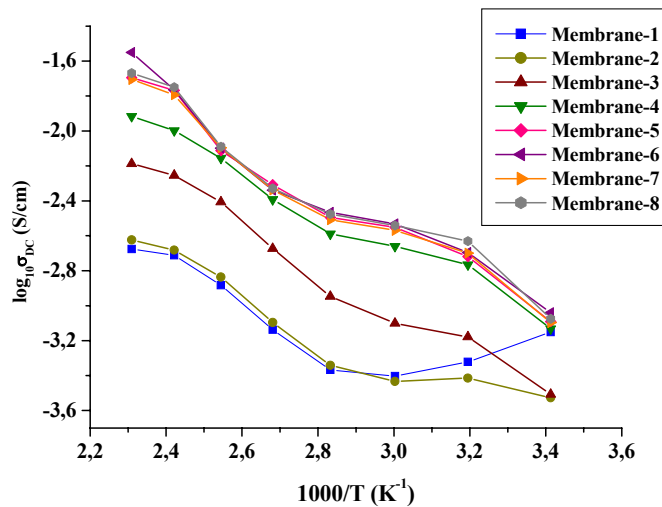


Fig. 4.2: Temperature dependence of DC conductivity of PVPA grafted PBI

Fig. 4.2 summarizes the data from Table 4.1 to Table 4.6 and shows the relation between the proton conductivity and temperature. The starting points with exceptionally high conductivity from membrane-1 at 20 °C could be a result of high moisture content. The data from Table 4.1 as well as Table 4.2 (membrane-1 and membrane-2), display some curvature around 40 to 60 °C.⁽⁷³⁾ This behaviour can be explained in terms of ‘glass transition temperature’ of membrane-1 and membrane-2 which are at 50 and 42 °C respectively. Below T_g , the observed conductivity could be contributed by proton hopping between acid and imidazole units in the membrane. Segmental motion of polymer chain does not play any role as T_g of both membranes is above 40°C. However above T_g , segmental motions of the polymer chains are activated well and that may appear to enhance the conductivity along with proton hopping process.⁽⁷³⁾ As a result, a crossover in mechanism from Arrhenius-type in the temperature regime below T_g (below 60 °C) to a Vogel-Tamman-Fulcher type (VTF) in the temperature range above T_g can be assumed to explain the temperature dependence of the conductivity of membrane-1 and membrane-2.^(75, 141)

The membranes 3, 4, 5, 6, 7 and 8 have glass transition temperatures below room temperature. The membranes obey ‘Vogel-Tamman-Fulcher equation’, which indicate the proton transport mediated by both segmental motions of the polymer chains as well as proton hopping between acid and imidazole units that explains the plateau behaviour of membranes in Fig. 4.2.

4.6 Thermal properties of membranes

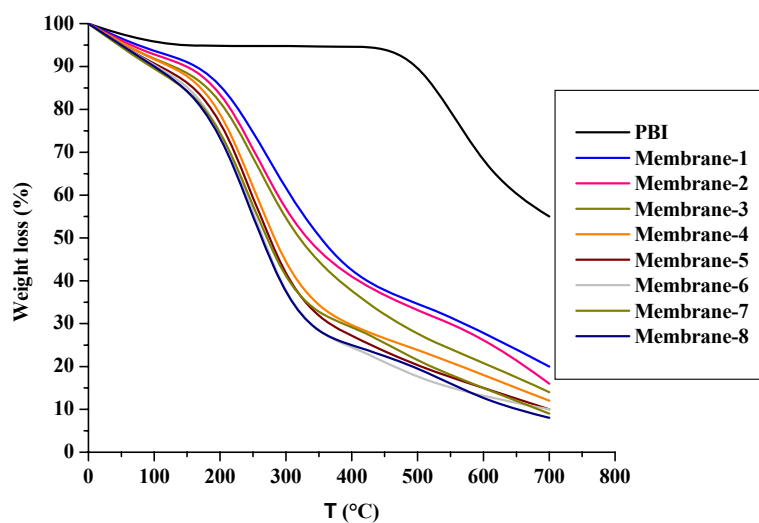


Fig. 4.3: TGA curves of membranes recorded under N_2 with a heating rate of 10 K/min.

The TG curves of the PBI and the membrane samples under nitrogen are represented in Fig. 4.3. Four stages of mass loss are evident in these curves, and the initial weight loss stage is 0 to 100 °C. The reason for this weight loss below 100 °C is due to physically bound water as well as residual DMAc in the membrane. The second degradation stage is from 100 to 200 °C by the decomposition of the VPA repeat units and lead to the gaseous products of ethylene and water, which is detected by combined TG / mass spectrometer.⁽²²⁴⁾

The third degradation regime is between 200 and 400°C. This degradation pathway is probably similar to the behaviour reported in the literature⁽²²⁴⁾ on cleavage of the carbon-phosphorus bond producing a PO_3H_2 radical, which by hydrogen abstraction leads to the formation of phosphoric acid. The final mass loss begins at 400 °C and ends at 600 °C. The degradation of imidazole fragments and further condensation of phosphorus acid occurs within this regime.

Therefore, the membranes are thermally stable up to 175 °C, and start to lose weight above 20 % on further heating by decomposition of phosphonic acid units in the polymer chain.

4.7 Membrane stability in water and oxidative environment

To evaluate the stability of PVPA grafted PBI membranes after poly(vinylphosphonic acid) grafting, time dependent measurements of the proton conductivity at 25 °C and, the weight changes in 3 and 10% H₂O₂ solutions at an elevated temperature of 60 °C were carried out, respectively. As an example, Fig. 4.4 shows the variation in the proton conductivity with time measured at 25 °C for the membrane-6 soaked in pure water. As given in Fig 4.4, PVPA grafted PBI membranes showed an excellent stability toward water for a long time without any decrease in proton conductivity (e.g. for 240 hr, 25 °C). In fact, all the membrane samples exhibited a good hydrolytic stability without any changes in original appearance, flexibility, and toughness even after they had been immersed in 50 °C water more than a week.

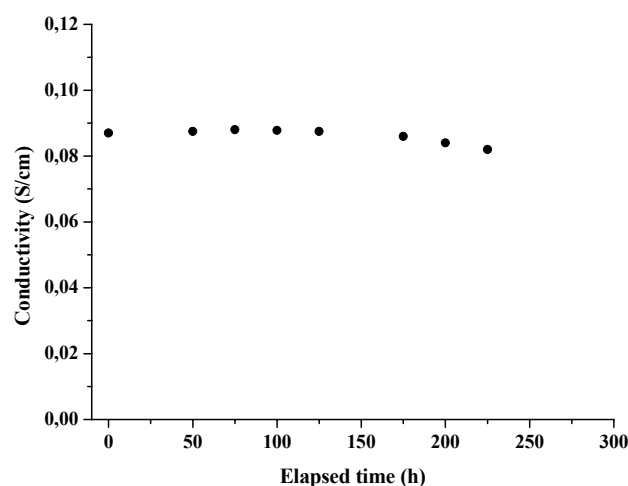


Fig. 4.4: Time course of the proton conductivity for chemically cross-linked PVPA grafted PBI membrane (membrane-6) soaked in pure water at 25±2 °C.

The membrane samples showed a relatively high oxidative durability after they were immersed in H₂O₂ solutions (Fig. 4.5). No noticeable weight change was observed after the membrane sample was immersed in 3% H₂O₂ solution up to 100 h at 60 °C, and about 15% weight loss was observed after 240 h. When the membrane sample was immersed in 10% H₂O₂ solution, an initial sharp decrease in weight percentage (30%) was observed within 20 h, and then the sample weight tends to maintain a constant value of about 69 wt% with no further weight losses again. Obviously, the chemical cross-linking would play an important role in improving the membrane performances.

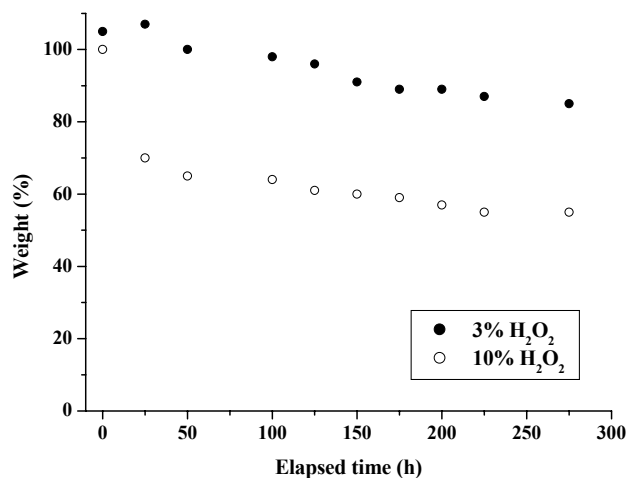


Fig. 4.5: Oxidative durability of the chemically cross-linked PVPA grafted PVPA membrane (membrane-6) in 3 and 10% solutions at 60 °C, respectively.

4.8 Water uptake and ion exchange capacity

The water uptake (WU) of the membranes was evaluated from the mass change before and after the complete dryness of the membrane. A dry membrane was immersed in deionized water for a day, then the surface water was wiped carefully with a filter paper, and it was immediately weighed. After drying the sample overnight in a vacuum oven at 60 °C, the water uptake (WU), was calculated using the expression:

$$WU = \frac{W_{\text{wet}} - W_{\text{dry}}}{W_{\text{dry}}}$$

Where W_{wet} and W_{dry} are the mass of fully hydrated membrane, and of the dry membrane, respectively.

The ion exchange capacity (IEC, mequiv g⁻¹) of the membranes was determined titrimetrically. Square pieces of each membrane were soaked in 20 ml of a 2 M NaCl solution and equilibrated for at least 24 h to replace the protons by sodium ions. The remaining solution was then titrated with a 0.01 M NaOH solution using phenolphthalein as an indicator. The IEC is defined as mequiv of phosphonic groups per gram of dried sample.

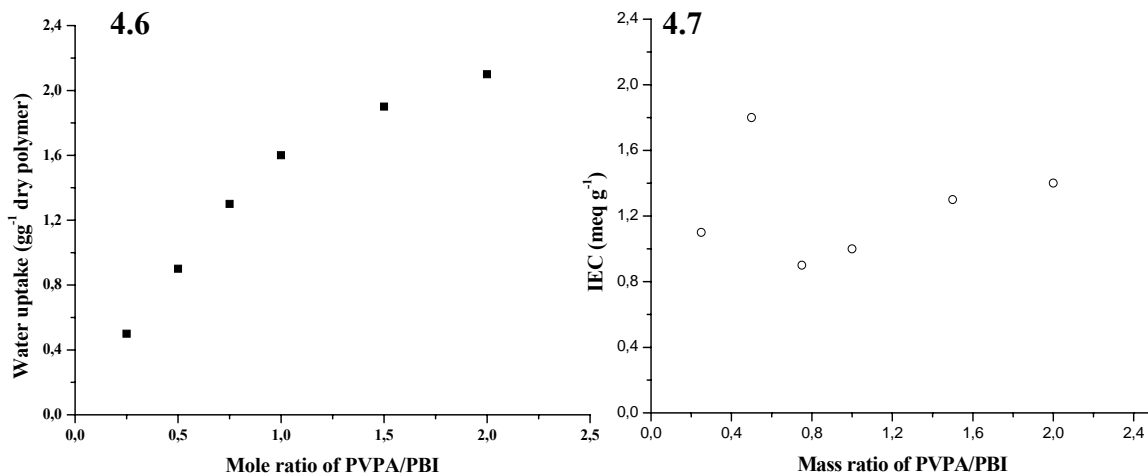


Fig. 4.6: Water uptake of the PVPA cross-linked PBI membranes plotted as a function of PVPA/PBI molar ratio of membranes. **Fig. 4.7:** IEC of the membranes plotted as a function of PVPA/PBI molar ratio of membranes.

WU and IEC are known to have the profound effects on membrane conductivity. The proton conductivity will increase with increasing WU because the mobility of ions in the water phase increases with increasing water content (volume). Also, the proton conductivity increases with increasing IEC because of the high charge density of the membranes. Fig. 4.6 and Fig. 4.7 represent the WU and IEC of the PVPA grafted PBI membranes plotted as a function of PVPA/PBI mole ratio in the membrane, respectively. The water uptake of PVPA grafted PBI membranes increased gradually with PVPA due to the strong hydrophilicity of the phosphonic acid groups (Fig.4.6). The IEC increased with increasing PVPA content in the membrane and then leveled off. This coincides with the proton conductivity as Table-4.5 shows, which indicates that a large PVPA content plays a major role in controlling the proton conduction due to the increased phosphonic acid groups in the membrane.

4.9 Disadvantages of PVPA grafted PBI membranes

1. PVPA grafted PBI membrane's expansion in size after prolonged exposure in water would prevent reuse of the membrane.
2. The potential instability of PVPA grafted PBI membranes above 175 °C should restrict usage for high temperature fuel cell applications.

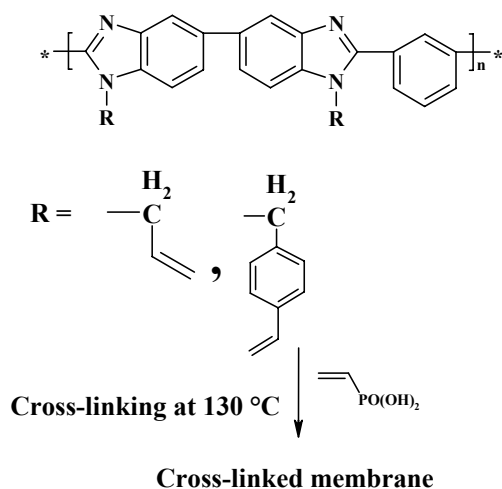
3. The tendency for membranes to become sticky (with increasing phosphonic acid grafting) and, as a result, difficult to handle for proton conductivity measurement in ‘Four-point probe electrochemical impedance cell’.

4. The presence of residual DMAc impurities should affect the proton conductivity of the membrane.

4.10 Summary

The present work of grafting poly(vinylphosphonic acid) onto PBI can be achieved by casting from DMAc solution of vinylbenzyl grafted PBI or allyl grafted PBI with VPA in the presence of a radical initiator by heating at 130 °C as described in Scheme 4.3.

Scheme- 4.3: Polymerisation of VPA with allyl and vinylbenzyl groups grafted PBI



Vinylbenzyl grafted PBI copolymerises with VPA thermally at 130 °C and grafts with higher VPA units than allyl grafted PBI under the same acid and initiator concentration (followed by weight gain of the membrane) indicating that additional radicals generated from electron rich styrene double bonds may be responsible for grafting higher VPA units.

Poly(vinylphosphonic acid) grafted PBI membranes show measured proton conductivities up to 10^{-2} S/cm and the conductivity values are higher than those of membranes based on alkyl sulfonic acid grafted PBI⁽¹⁵⁾ and alkyl phosphonic acid grafted PBI membranes.⁽¹⁴¹⁾

The proton conductivity values are comparable to membranes based on H_3PO_4 doped PBI membranes⁽²⁹⁻³¹⁾ and Nafion type membranes.⁽²⁻⁴⁾ Furthermore, the proton conductivity values were unchanged after several repeated water washings of the membranes indicating that the PVPA cross-linked PBI can retain acids in the membrane during fuel cell operating conditions.

However membrane's expansion in size during continuous presence in water would limit reuse of the membrane. To reuse or reprocess the membrane, future research should focus on synthesizing solvent soluble PVPA grafted PBI membranes from possible methods such as 'Stable Free Radical Polymerisation' of TEMPO adduct grafted PBI with VPA, and synthesizing PVPA oligomer with Br- or I- end groups by 'Telomerization' (Free radical polymerisation of VPA in presence of $CHBr_3$ or CHI_3) and subsequent grafting it onto the polybenzimidazole chain by nucleophilic substitution reaction.

Further, the low thermal stability of poly(vinylphosphonic acid) chain (up to 175 °C) in the graft-copolymer membrane limits performance for high temperature applications above 175 °C. Therefore synthesizing poly(trifluorovinylphosphonic acid) grafted PBI membranes that would withstand high temperatures above 175 °C are recommended for future application.

Despite disadvantages, poly(vinylphosphonic acid) cross-linked PBI membranes would show excellent long-term performance without acid leakage for PEMFC applications. More importantly, the high temperature operation up to 150 °C with less demanding humidification requirement leads to system simplifications. Therefore the development of a low-cost and reliable high-temperature membrane represents a technological breakthrough with important implication for stationary and, more critically, transport applications.

5 Proton Conducting Multilayers for Fuel Cell Applications

Conductivity in polymer electrolytes has long been confined to the amorphous phase above the glass transition temperature, T_g . (above T_g , the dynamic and disordered motion of the polymer chains play a crucial role in facilitating proton transport).⁽¹³⁶⁻¹⁴¹⁾ However, the existence of higher ionic conductivity in the static and well ordered environment has been recently reported⁽¹⁴²⁾ and the measurement of the anisotropic proton conductivity of a crystalline imidazole sample further shows that ‘the conductivity is higher in the ordered environment’.⁽¹⁴³⁾ As discussed earlier in the introduction, the layer-by-layer (LBL) deposition of polymers (introduced by Decher) have been proven to be useful for making ordered architectures.⁽¹⁴⁴⁻¹⁴⁷⁾

Thin, defect free and uniform LBL films offer an advantage to be used as solid polymer electrolyte for fuel cells. The excellent uniformity of LBL films might lower the electrolyte resistance; hence the conductivity of the LBL film would be higher. Further, the multilayer membrane obtained by LBL technique could prevent the acid leakage by strong ionic interaction between polymer chains.

In this chapter, the proton conducting LBL assembly of polymers by various strong acids such as poly(vinylphosphonic acid) [PVPA], poly(vinylsulfonic acid) [PVSA], and poly(styrenesulfonic acid) [PSSA] paired with basic polymers such as poly(4-vinylimidazole) [P4VIm] and poly(benzimidazole) [PBI], which are appropriate for ‘Proton Exchange Membranes for Fuel Cell’ applications have been described. For example, PVPA is a strong acidic polymer⁽¹⁴⁸⁾ and will give higher number of mobile ions [n_i] with proton acceptor such as PBI and P4VIm. Imidazole is well known to transport protons by a hopping mechanism⁽¹⁴⁹⁾ and will increase the mobility [μ_i] in the LBL assembly. Furthermore, LBL is a unique technique for fabricating ordered architectures,⁽¹⁵⁰⁻¹⁵³⁾ which will allow PBI and P4VIm (imidazole unit) to assemble in an ordered fashion suitable for proton hopping between imidazole units, even in an undoped state.^(154,155)

Fig. 5.1 explains the assembling of proton donor polymer such as poly(vinylphosphonic acid) [PVPA] with proton acceptor polymer such as poly(benzimidazole) [PBI] by the LBL technique.

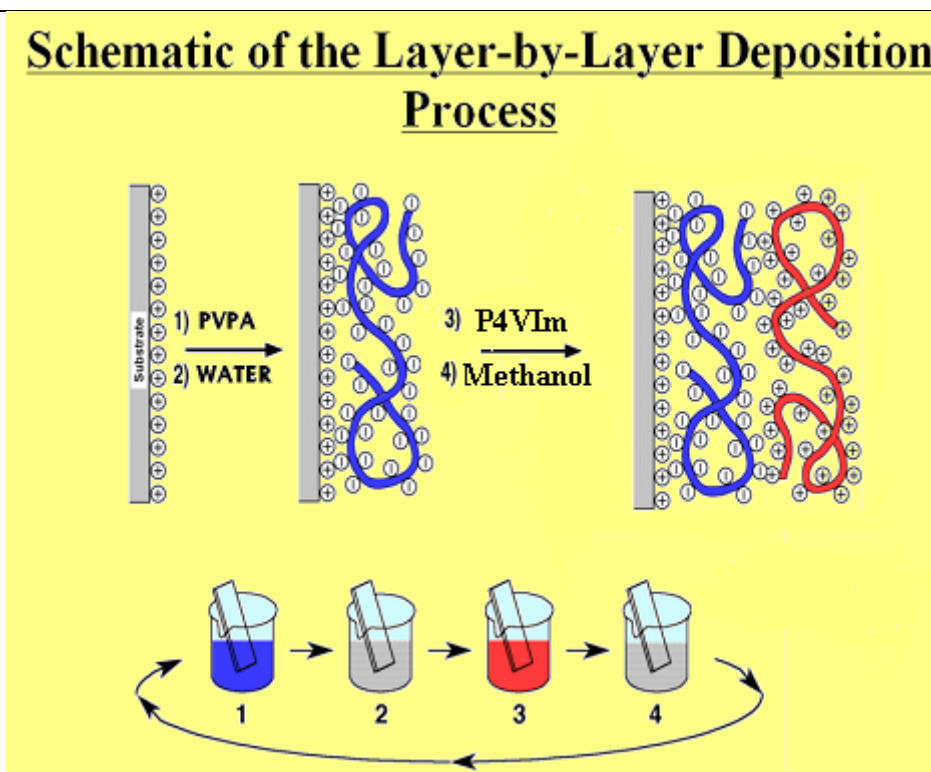


Fig. 5.1: Schematics of the LBL assembly of PVPA-P4VIm. 1- PVPA in water, 2- water, 3- P4VIm in CH_3OH , and 4- CH_3OH

The substrate was first immersed in a proton donor polymer such as PVPA, PVSA and PSSA in aqueous solution for 15 min to create acid layers on the substrate. After rinsing with Millipore water for five minutes and subsequent drying under argon purge, the substrate was transferred in an organic solution of proton acceptor polymer such as PBI and P4VIm and kept for 15 min. After washing with solvent for 5 minutes, the substrate was dried under an argon purge, and then again dipped into a proton donor polymer solution for 15 min to generate a second acid layer. A multilayer film could be obtained by repeating the above steps in a cyclic fashion as illustrated in Fig. 5.1.

5.1 Study on the nature of the interaction between acid-base polymers

Before characterizing multilayers, it is essential to know the nature of interaction between acid-base polymers. FTIR spectroscopy was used to study the nature of the interaction between PVPA and P4VIm.

The donor-acceptor interaction between phosphonic acid and imidazole, results in the formation of strong ionic salts. IR spectroscopy (Fig. 5.2) explains the nature of the interaction between these two polymers:

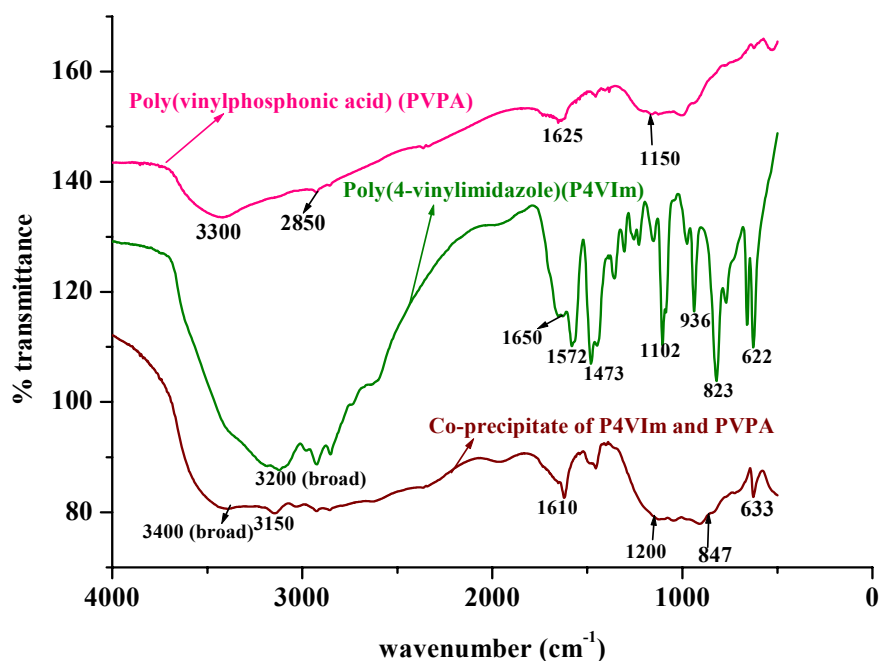


Fig. 5.2: IR spectra of P4VIm, PVPA and the co-precipitate of PVPA-P4VIm

In P4VIm, the heteroaromatic rings (imidazole ring) show several medium strong peaks in the $1650\text{--}1570\text{ cm}^{-1}$ range due to ring stretching vibrations.⁽¹⁵⁷⁾ In addition, the five-membered heteroaromatic rings exhibit a strong absorption at $800\text{--}700\text{ cm}^{-1}$, which can be related to C-H out-of-plane vibrations for unsaturated systems. Hydrogen bond formation between aryl-N-H and aryl-N in the solid-state results in a band broadening at 3200 cm^{-1} .⁽¹⁵⁷⁾ The IR spectrum of the PVPA shows strong bands at $1040\text{--}910\text{ cm}^{-1}$ belonging to asymmetric stretching vibration of (P-O)H group and at 1150 cm^{-1} that corresponds to P=O stretching.⁽¹⁶⁵⁾ Additionally, the O-H stretching of the POH group gives rise to further broad bands at medium intensity at $2850\text{--}2750\text{ cm}^{-1}$.⁽¹⁶⁵⁾ After mixing the PVPA water solution and P4VIm methanol solution, a precipitate is formed, which is unaffected by water washings indicating a very strong ionic interaction between the two polymers. This results in protonation of the ‘free’ nitrogen of the imidazole rings. The broadening of the peak from 910 to 1200 cm^{-1} indicates the deprotonation of phosphonic acid units to form P-O^- . Correspondingly, the protonation of the ‘free’ nitrogen of the imidazole rings to form imidazolium ion is accompanied by the appearance of a strong peak near at 1617 cm^{-1} [$\nu(\text{H-Im}^+\text{-H})$].⁽¹⁶⁵⁾ The N-H stretching peak being relatively increased at 3150 cm^{-1} is another proof of protonation.⁽¹⁶⁵⁾ The frequencies and assignments of several characteristic vibrations of pure compounds and blends are reported in Table-5.1.

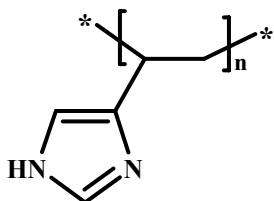
Table-5.1: IR vibrations in wave numbers (cm^{-1})

P4VIm	PVPA	PVPA-P4VIm	Attribution ^(157, 165)
3200 (b)	2850-2750	3400, 3150 (b)	ν (N-H)
1650-1470			ν (PO-H)
820-700	1150	1610	ν (C=N, C=C)
	1040-890	1200-910	ν (H-Im ⁺ -H)
ν_{st} (P=O)			
			ν (P-O ⁻)
			ν_{as} (P-O)H
			ν (C=C)

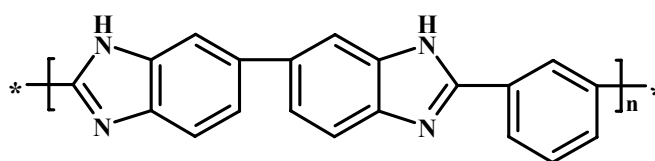
5.2 Poly(4-vinylimidazole) and poly(benzimidazole) for multilayer fabrication

In order to study systematically the ordered architectures, the multilayers of two different imidazole-containing polymers, a flexible poly(4-vinylimidazole) [P4VIm] and a stiff polybenzimidazole [PBI] were generated with various acidic polymers.

The LBL film based on a stiff PBI is expected to form a higher ordered architecture than a flexible P4VIm. In general, highly ordered architectures will provide a more uniform path (easier path) for proton transport, and hence the proton conductivity would be significantly higher than the lower ordered architectures.⁽⁷⁶⁻⁷⁸⁾ Therefore a systematic comparison on PBI and P4VIm based multilayers would enable to better understand the proton transport in terms of ordering, which was followed by UV-visible spectroscopy, reflectivity measurements and profilometry.



Flexible P4VIm chain



Stiff PBI chain

5.3 Multilayers of flexible P4VIm

To compare the proton conductivity of phosphonic and sulfonic acid polymers, it was paired separately with P4VIm and its multilayer built-up was followed by UV-vis spectroscopy, profilometry and X-ray reflectivity.

5.3.1 Poly(4-vinylimidazole) and poly(vinylphosphonic acid) multilayers

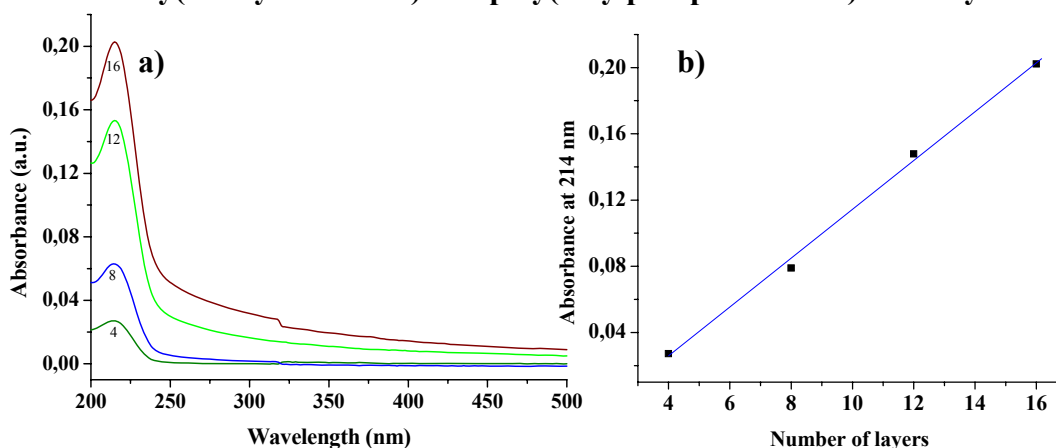


Fig. 5.3: a) UV-vis spectra of P4VIm-PVPA LBL film (absorbance versus wavelength) on NH₂-modified quartz substrate. b) Absorbance at 214 nm versus number of layers (P4VIm-PVPA LBL film).

UV-vis absorption spectroscopy was used to monitor the P4VIm/PVPA multilayer film assembly. The increase in the absorbance of imidazole chromophores (214 nm) with increasing number of layers indicates the stepwise assembly of the multilayers (Fig. 5.3a). A plot of the absorbance maximum against the number of layers yields a straight line indicating a uniform self-assembly about 16 alternate layers as shown in Fig. 5.3b. The linearity breaks down when the number of layers exceeds 16. The uniform assembling of polymers can be explained in terms of the conformation of the polymer chains. The polymers may adopt extended chain conformation (around 16 layers), and therefore absorbance increases linearly. After 16 layers, polymer chains could form a random coil, and hence, the chain adsorbs rather “loopy”.

From the molecular orientation point of view, polymer chains assemble in uniform angle of orientation at lower number of layers, even if few polymer chains deposit in slightly different angle of orientation, it is not sufficient to disturb uniformity up to certain number of layers. However with increasing number of layers, nonuniform orientation dominates over the uniform orientation and hence, linearity lost at higher number of layers.⁽⁹²⁾

The above experimental results were verified using ‘X-ray reflectivity’ as shown in Fig. 5.4. The measurements are in agreement with the UV-vis data as loss in linearity is again observed when the number of layers approaches about 20 layers (~ 53 nm thickness) inferred from its thickness values. The X-ray curves reveal well-defined Kiessig fringes up to scattering angles $2\theta = 0.25^\circ$, which proves that polymeric self-assembled films are uniform and flat. From the oscillation periods, one can estimate the thickness of the film⁽⁹⁰⁻⁹⁵⁾ and the number of visible oscillations is connected with film roughness.

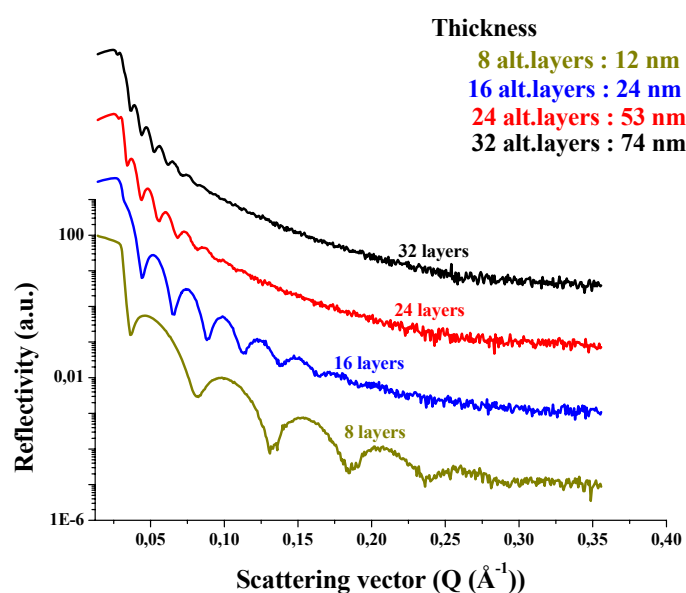


Fig. 5.4: Reflectivity versus scattering vector (P4VIm-PVPA LBL film) on NH_2 -modified quartz substrate.

The thickness is calculated from X-ray reflectivity data using the following equation:

$$\text{Thickness} = 2\pi / \Delta Q^{(90-95)}$$

Where ΔQ is the distance between the minima.

The periodicity of Kiessig fringes decreased with increasing number of layers, reflecting the increasing film thickness and roughness values of the film. With increasing number of layers, the ordering of LBL film was lost by interpenetration of layers into each other that result in roughness increment, thus making the Kiessig fringes difficult to observe. As a consequence, X-ray reflectivity curves show only the film thickness up to 75 nm. In order to measure the thickness of thicker films, profilometry was used as illustrated in Fig. 5.5a.

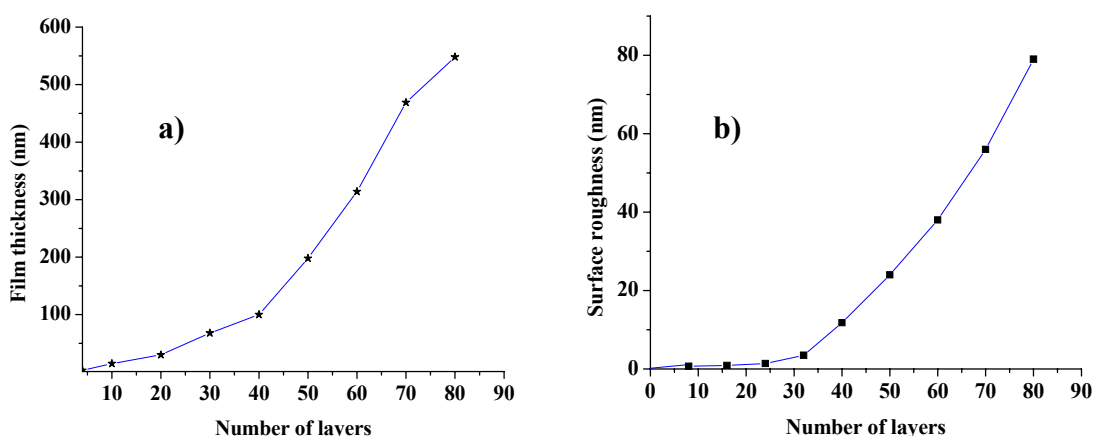


Fig. 5.5: **a)** Film thickness versus number of layers on top of indium-tin oxide (ITO) substrate by profilometry (P4VIm-PVPA LBL film). **b)** Film roughness versus number of layers on top of ITO substrate by profilometry (P4VIm-PVPA LBL film).

The film thickness increases linearly around 20 layers and loses its linearity with subsequent higher number of layers (Fig. 5.5a).⁽⁸⁹⁻⁹⁵⁾ It is again supported by surface roughness measurement, where LBL film is smooth about 25 layers with a measured roughness value of below 1 nm indicating the uniformity of LBL film as shown in Fig. 5.5b. Further, surface roughness increases significantly with higher number of layers due to nonuniform deposition of polymers during multilayer built-up.⁽⁸⁹⁻⁹⁵⁾

Analogous results are long known in the literature that LBL films such as poly(4-vinylpyridine)/poly(acrylic acid),⁽⁸⁹⁾ poly(4-vinylpyridine)/Dendrimer (carboxyl-terminated polyether dendrimer),⁽⁹¹⁾ and poly[4-vinylbenzyl-(*N,N*-diethyl-*N*-methyl)ammonium iodide]/poly(styrenesulfonate)⁽⁹³⁾ exhibit linear increase in absorbance until a certain number of layer and the linearity breaks down with subsequent higher number of layers. Although these polyelectrolyte multilayer fabrications are consistent with poly(4-vinylimidazole)/poly(vinylphosphonic acid) multilayers, they differ in certain environmental effects. In wet condition, water molecules causes to swell certain extent showing noticeable effects of deterioration on the surface of poly(4-vinylpyridine) /poly(acrylic acid)⁽⁸⁹⁾ multilayer. In contrast to this multilayer film, the LBL of imidazole and phosphonic acid offers a film by strong ionic interaction, which is unaffected even after prolonged exposure in water. Therefore, it is promising to employ imidazole and phosphonic acid supramolecular multilayer architectures for PEM application in order to retain poly(vinylphosphonic acid) in the membrane during fuel cell operating condition.

5.3.2 Poly(4-vinylimidazole) [P4VIm] and poly(4-styrenesulfonic acid) [PSSA] multilayers

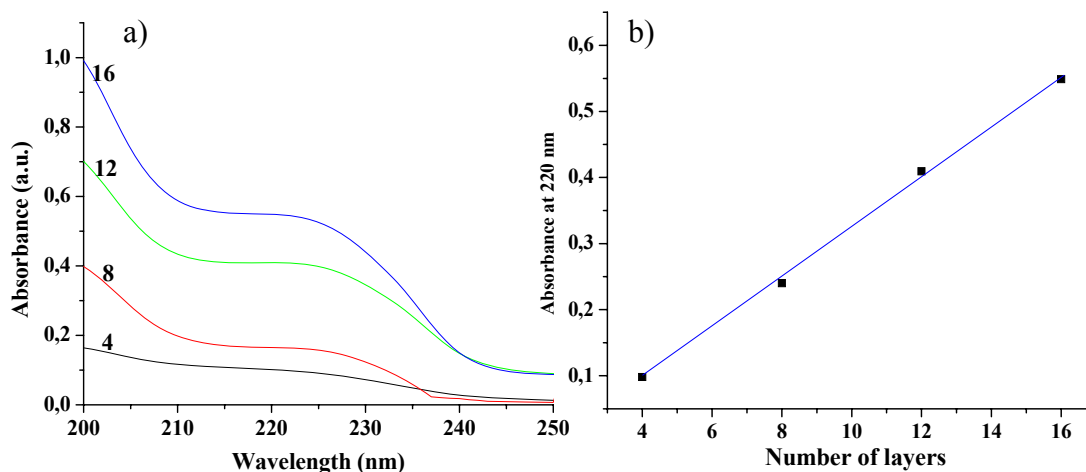


Fig. 5.6: **a)** UV-vis spectra of P4VIm-PSSA LBL film (absorbance versus wavelength) on NH₂-modified quartz substrate. **b)** Absorbance at 220 nm versus number of layers (P4VIm-PSSA LBL film).

Fig. 5.6a presents the UV-vis absorption spectra of P4VIm/PSSA multilayer film. From Fig. 5.6a, the absorbance at 220 nm increases with number of layers demonstrating a stepwise assembling of polymers. Further, a plot of the absorbance at 220 nm against the number of layers displays a straight line illustrating a uniform self-assembly (Fig. 5.6b). However, the observed growth at 220 nm is nonlinear with additional layers indicating aggregate formation within the multilayer.⁽⁸⁹⁻⁹⁵⁾ A similar pattern was observed in the LBL assembly of P4VIm/PVPA.

The change in film thickness and roughness with number of layers was monitored by profilometry (Fig. 5.7). The thickness and roughness values of P4VIm/PSSA multilayers again fit well with similar measurements of P4VIm/PVPA multilayers.

From thickness measurements of P4VIm/PSSA LBL film (Fig. 5.7a), the linear increase in thickness about 20 layers indicate the uniform assembling of polymer layers. Further, the nonlinear increase in thickness with additional number of layers illustrates the nonuniform multilayer built-up.⁽⁸⁹⁻⁹⁵⁾ Also, from surface roughness measurements (Fig. 5.7b), the LBL film is smooth around 20 layers and the surface roughness increases with subsequent higher number of layers shows a nonuniform assembling of polymers.

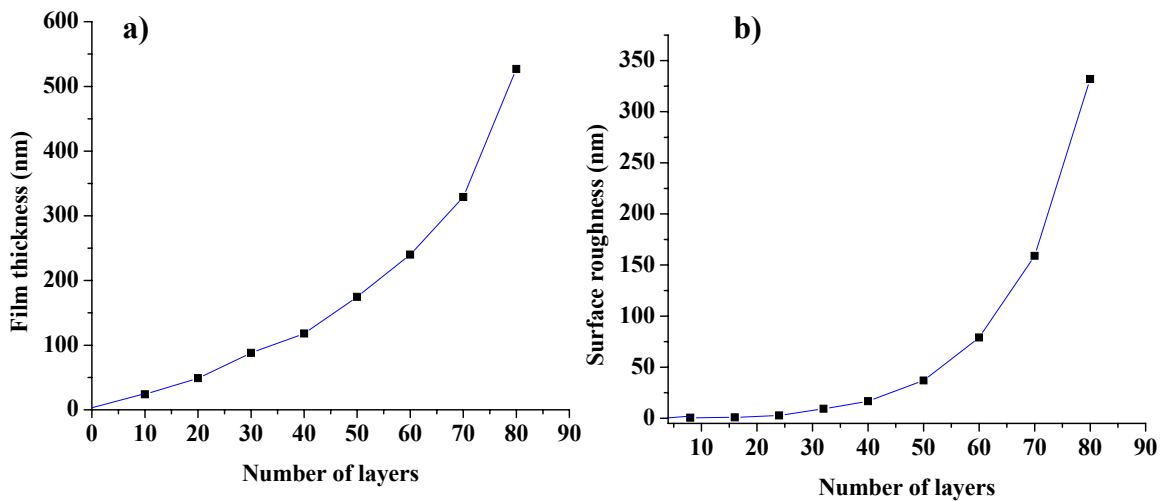


Fig. 5.7: **a)** Film thickness versus number of layers on top of ITO substrate by profilometry (P4VIm-PSSA LBL film). **b)** Film roughness versus number of layers on top of ITO substrate by profilometry (P4VIm-PSSA LBL film)

5.4 Multilayers of stiff poly(benzimidazole)

In order to synthesize multilayer films with better ordering than P4VIm, a stiff PBI is used, because P4VIm adsorption becomes nonuniform above a certain number of layers during multilayer fabrication.

Further, the PBI is paired with polymers such as poly(vinylphosphonic acid), poly(vinylsulfonic acid) and poly(styrenesulfonic acid) in order to compare the proton conductivity of phosphonic acid polymer with two different sulfonic acid polymers in the LBL assembly.

The linear increase in absorbance and thickness were followed by UV-vis spectroscopy and profilometry.

5.4.1 Polybenzimidazole [PBI] and polyvinylphosphonic acid [PVPA] multilayers

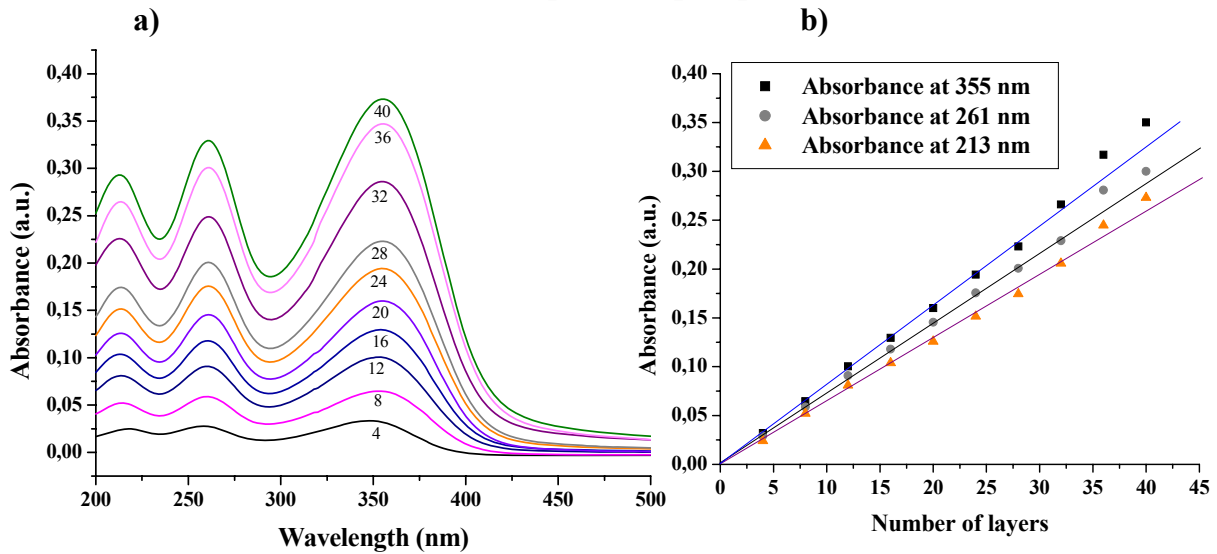


Fig. 5.8: a) UV-vis spectra of PBI-PVPA LBL film (absorbance versus wavelength) on NH₂-modified quartz surface. b) Absorbance at 355, 261 and 213 nm versus number of layers (PBI-PVPA LBL film).

Fig. 5.8a displays the UV-vis absorption spectra of PBI/PVPA multilayers assembled on the NH₂-tailed quartz surface. As illustrated in Fig. 5.8a, the PBI absorption is clearly identified by the characteristic peaks at 213 nm, 261 nm and 355 nm due to its incorporation into the multilayers. Fig. 5.8b demonstrates that the absorbance increases linearly with the increasing number of layers at 213, 261 and 355 nm indicative of uniformly self-assembled layers.^(96-98, 102)

The change in film thickness with increasing number of layers was followed by profilometry (Fig. 5.9a).

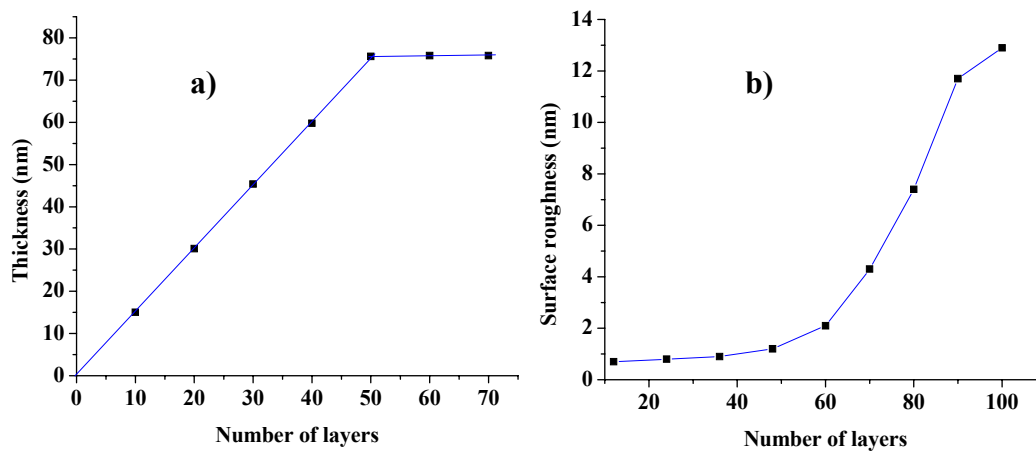


Fig. 5.9: a) Film thickness versus number of layers on top of ITO glass surface by profilometry (PBI-PVPA LBL film). b) Film roughness versus number of layers on top of ITO glass surface by profilometry (PBI-PVPA LBL film).

The thickness increases linearly and reaches its maximum value of 75 nm and remains constant thereafter. The surface roughness of the film remains less than 1% of total film thickness about 50 layers indicative of the smoothness of PBI/PVPA multilayers. However, the roughness increases significantly with additional layers beyond 50 (Fig. 5.9b) due to propagation of surface defects caused by increasing number of layers. Unlike P4VIm, a stiff PBI cannot form coil chain conformation and hence, its thickness increases linearly during the multilayer build-up.

The incorporation of stiff polymers into multilayer assemblies has meanwhile been demonstrated briefly in literature.⁽⁹³⁻⁹⁵⁾ The LBL assembly of polyimide / poly(acrylic acid) and aromatic poly(amide) / poly(acrylic acid) have also observed a well-ordered layers, but these films swell in wet condition. The swelling of LBL film is primarily due to adsorption of significant water molecules inside the hydrogen bonding architectures. Whereas PBI/PVPA film does not swell even after heating in water up to 100 °C indicating that PBI/PVPA multilayers are better suited than polyimide / poly(acrylic acid) and poly(amide) / poly(acrylic acid) multilayers in terms of stability of the film. The strong ionic interaction between PBI and PVPA prevents penetration of significant water molecules inside the multilayer to facilitate swelling of the film.

5.4.1.1 Poly(vinylsulfonic acid) and poly(styrenesulfonic acid) for multilayer fabrication

Sulfonic acid polymers have been the focus of much attention because of their application as separator membranes in high energy density batteries and fuel cells.⁽⁴⁶⁻⁵¹⁾ It is well-known that high proton conductivity of sulfonic acid membranes can also be achieved in solvent environments other than water, such as water-organic mixtures, alcohols, organic acids, and aprotic dipolar solvents.⁽⁶⁴⁻⁶⁵⁾ Another interesting group of solvents with potential to replace water is the heterocycles (e.,g., imidazole, pyrazole, or benzimidazole, containing both proton donor (NH) and acceptor (N)). For example, Sun reported water-free Nafion membranes by swelling them in imidazole and imidazolium salt solutions and achieved conductivities of about 10^{-3} S/cm at around 140 °C.⁽²⁴⁸⁾ This opens the possibility to fabricate multilayer of sulfonic acid polymer with an imidazole polymer such as PBI.

5.4.2 Poly(benzimidazole) [PBI] and poly(vinylsulfonic acid) [PVSA] multilayers

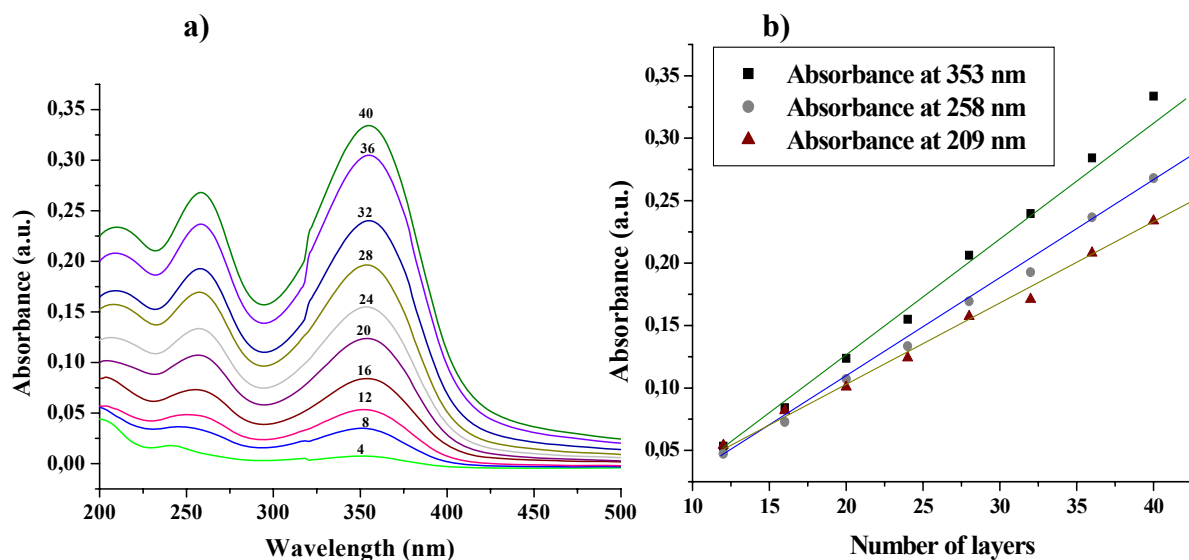


Fig. 5.10: **a)** UV-vis spectra of PBI-PVSA LBL film (absorbance versus wavelength) on NH_2 - modified quartz surface. **b)** Absorbance at 353, 258 and 209 nm versus number of deposition cycles (PBI-PVSA LBL film).

The multilayer deposition process was monitored by UV-vis spectroscopy as shown in Fig. 5.10a. A steady increase of UV-vis absorption is observed with an increase of the number of layers at 209 nm, 258 nm, and 353 nm confirming the successive and uniform growth of the multilayer film. Fig. 5.10b shows that the absorbance of quartz-supported (PBI/PVSA) multilayers film at characteristic wavelength (209, 258 and 353 nm) increases proportionally with the number of deposition cycles. This linear growth of the absorption peaks indicates that an approximately equal amount of PBI-PVSA is deposited for each absorption procedure and that the PBI-PVSA multilayer films grow uniformly with each deposition cycle.

The increase in thickness and roughness of the films was monitored by profilometry. All these measurements are consistent with similar measurements of PBI/PVPA LBL film. Again, the linear increase in thickness up to 53 nm is observed as shown in Fig. 5.11a.

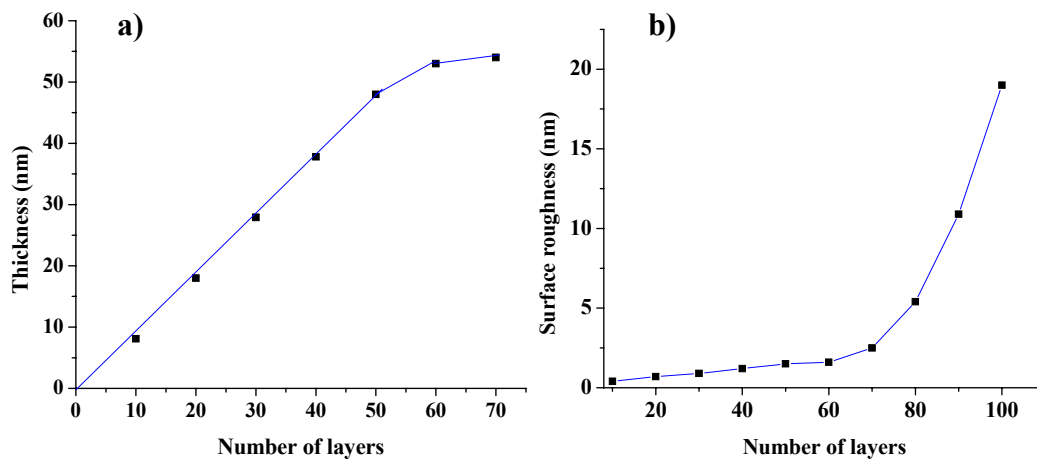


Fig. 5.11 a) Film thickness versus number of layers on top of ITO glass surface by profilometry (PBI-PVSA LBL film). b) Film roughness versus number of layers on top of ITO glass surface by profilometry (PBI-PVSA LBL film).

About 50 layers, surface roughness of the film remains less than 1% of the total film thickness indicative of highly ordered PBI/PVSA LBL film (in Fig. 5.11b). However, the roughness increases significantly with additional layers beyond 60 layers as a result of deterioration of the film surface by increased layer deposition cycles.

Further absence of swelling in PBI/PVSA multilayer film in water is in agreement with PBI/PVPA LBL film.

5.4.3 Poly(benzimidazole) [PBI] – poly(4-styrenesulfonic acid) [PSSA] multilayers

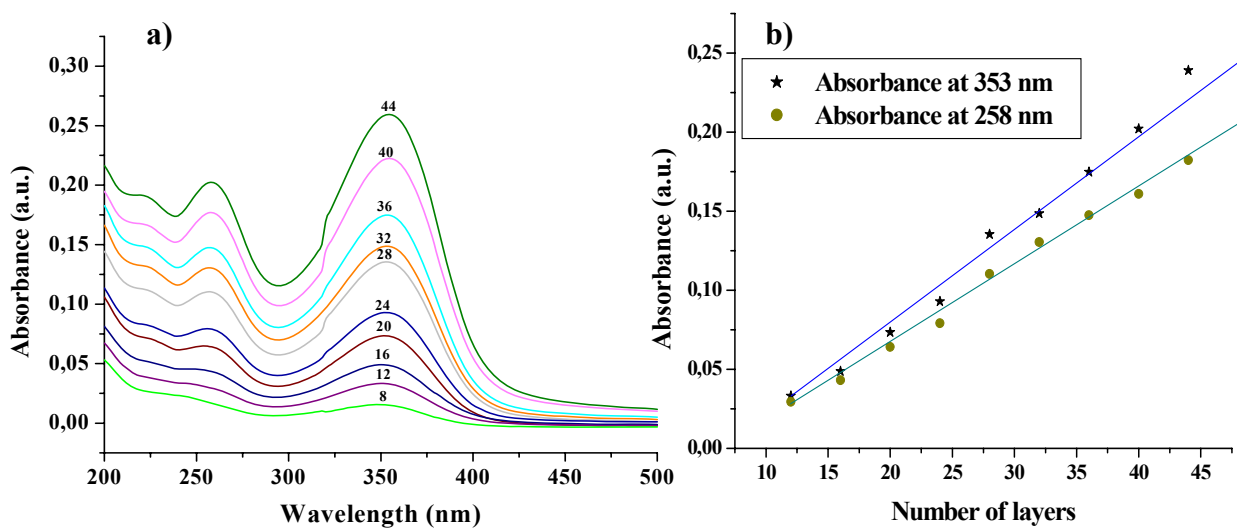


Fig. 5.12: a) UV-vis spectra of absorbance versus wavelength (PBI-PSSA LBL film) on NH₂-modified quartz substrate. b) Absorbance at 353 and 258 nm versus number of layers (PBI-PSSA LBL film).

To monitor the fabrication process of PBI/PSSA multilayers, the absorbance at 258 nm and 353 nm, which are the characteristic of the PBI were determined after each absorption cycle by UV-vis absorption spectra as shown in Fig. 5.12a. The linear increase of the absorbance at 258 and 353 nm with the number of the depositions suggests that a constant amount of PBI/PSSA could be immobilized upon each deposition to form a multilayer on the NH_2 - modified quartz surface as displayed in Fig. 5.12b.

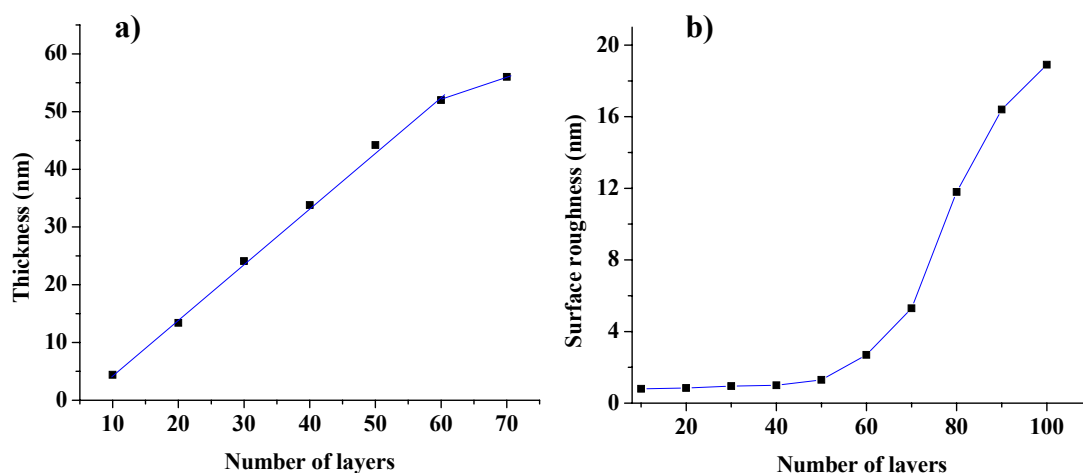


Fig. 5.13: **a)** Film thickness versus number of layers on top of ITO substrate by profilometry (PBI-PSSA LBL film). **b)** Film roughness versus number of layers on top of ITO surface by profilometry (PBI-PSSA LBL film).

The thickness and roughness of PBI/PSSA LBL film were measured by profilometry. Again, all these measurements are consistent with similar measurements of PBI/PVPA and PBI/PSSA multilayer films. The thickness reaches a maximum value of 56 nm for about 70 layers, and remains unchanged thereafter (Fig. 5.13a). The surface roughness was less than 1% of the total film thickness around 60 layers of the film. However, the roughness increases significantly with additional layers beyond 60 layers as illustrated in Fig. 5.13b.^(96-98, 102)

5.5 Properties of LBL film

To study the properties of the multilayers, the proton conductivity measurements were carried out with gold electrodes as well as with indium-tin oxide electrodes.

5.5.1 Gold electrodes for proton conductivity measurements

A quartz substrate (2.5 cm x 2.5 cm x 1 mm) was coated with an adhesive layer of 10 nm of chromium and 300 nm of gold using a thermal evaporator through a custom designed shadow mask of 3 mm width and 2.5 cm length. Gold was evaporated at a slow rate ($< 0.3 \text{ \AA/s}$) with water-cooling and used 90° offset evaporation to get a smooth surface, which had the roughness value of less than 1 nm.

5.5.1.1 Surface modification of gold for multilayer fabrication

The Au-quartz substrates were exposed to a 0.03 M aqueous solution of 2-mercaptoethanesulfonic acid [pH ~ 1.7] for 3 hrs and washed with MilliQ water for 5 mins and dried under an argon purge. Thiols are the most successful chemicals employed as an attachment to metals because it reacts chemically with gold, thus forming very stable gold – sulfur bond as the corresponding thiolates.⁽¹⁵⁸⁻¹⁵⁹⁾ Contact angle measurement and AFM were used to characterize the modified gold electrode.

5.5.1.2 Contact angle measurement

Gold surface became completely hydrophilic with a measured contact angle value of zero after exposing with 0.03 M 2-mercaptoethanesulfonic acid.

5.5.1.3 AFM measurement

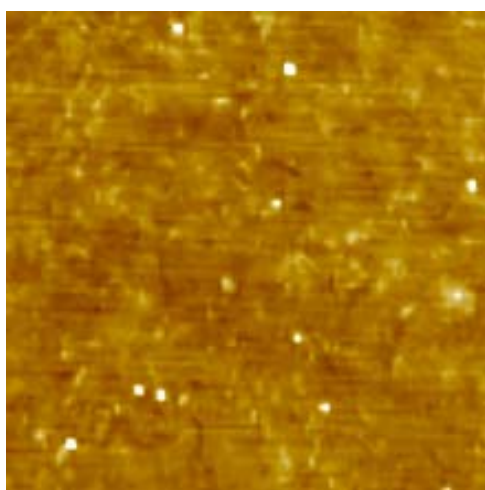


Fig. 5.14: Gold surface

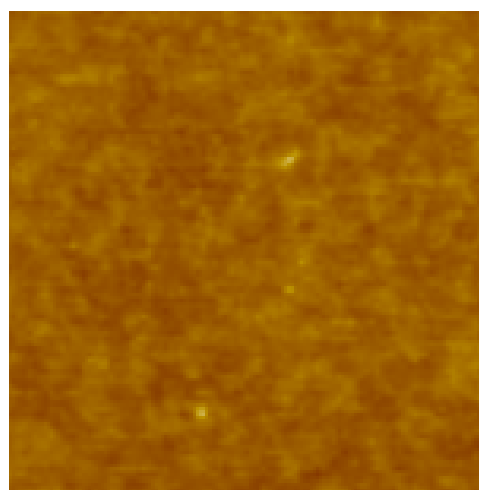


Fig. 5.15: 2-mercaptoethanesulfonic acid modified Au

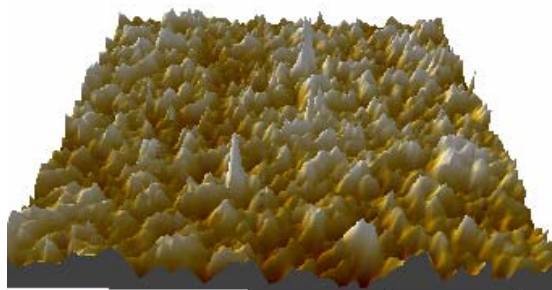


Fig. 5.16: 3D image of 2-mercaptoethanesulfonic acid modified Au surface

The roughness of the gold surface was measured using AFM (Atomic Force Microscopy) before and after surface modification (Fig. 5.14, 5.15 and 5.16). The difference in the surface roughness value of 0.95 nm is in agreement with the chain length of 2-mercaptoethanesulfonic acid. The investigations of monolayers formed from analogous thiols [HS-(CH₂)₂-NH₂,⁽²³⁵⁾ HS-(CH₂)₂-COOH⁽²³⁶⁾ and HS-(CH₂)₂-SO₃N⁽²³⁷⁾] showed that short-chain thiols are more suitable to electrochemical and sensor applications. As a result, 2-mercaptoethanesulfonic acid was chosen to fabricate multilayers with PBI and P4VIm. Furthermore, sulfonic acid functionalisation of gold surface has an advantage of higher compatibility with imidazole polymers, which is required for multilayer fabrication.

5.5.1.4 The LBL assembling of polymers on gold surface for proton conductivity measurement

Multilayers were constructed on top of Au electrode by transferring into 0.02 M poly(4-vinylimidazole) or poly(benzimidazole), followed by washing and drying steps (see Chapter- IX) and then dipping in acid solution. After assembling the multilayers, films for proton conductivity measurements were dried at 100 °C for 48 hours to eliminate solvents from LBL assembled films.

UV-vis spectroscopy was used to follow the LBL assembling of PBI/PVPA multilayers. Fig. 5.17a shows the UV-vis absorption spectra of PBI-PVPA multilayers on Au-quartz substrate.

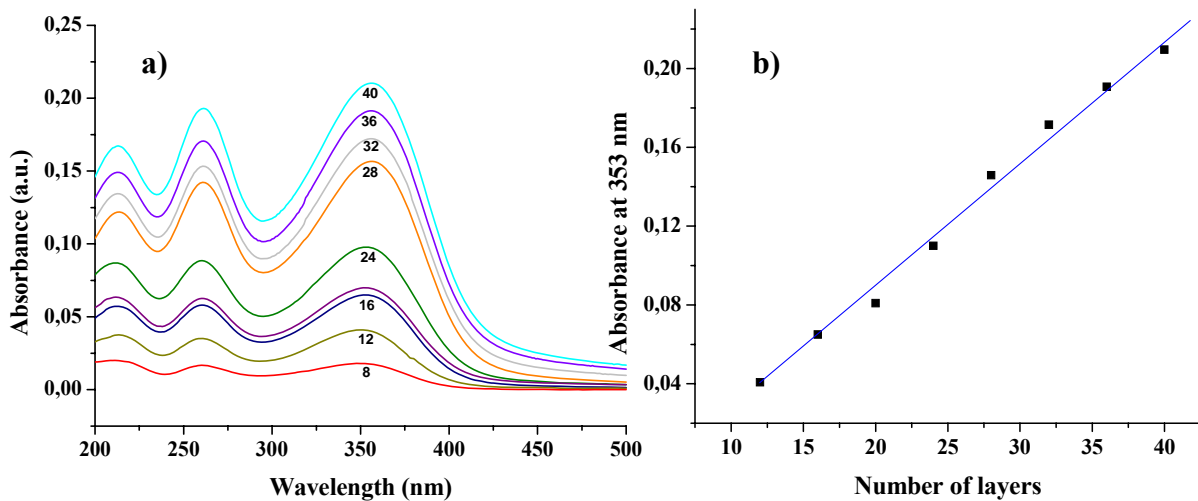


Fig. 5.17: **a)** UV-vis spectra of PBI-PVPA LBL film (absorbance versus wavelength) on SO₃H - modified Au-quartz surface. **b)** Absorbance at 261 nm versus number of layers (PBI-PVPA LBL film).

The increase in absorbance at 353 nm of PBI/PVPA multilayers upon increasing the number of alternate layers indicates the stepwise assembly of the multilayers (Fig. 5.17a). Fig. 5.17b shows a linear increase in absorbance with increasing number of layers at 353 nm indicative of uniformly self-assembled layers.

Similarly, multilayers based on PBI, P4VIm paired with PVSA and PSSA were characterized as described in the Sections 5.3.1, 5.3.2, 5.4.1, 5.4.2 and 5.4.3.

5.5.1.5 Model calculations

Prior to any conductivity measurement, it is essential to know the measurement range of the electrode on the basis of its dimension with respect to the membrane thickness.

Electrodes have their own limit to measure the proton conductivity depending on thickness as well as membrane thickness values. To measure the proton conductivity of the membrane by four-point-probe electrochemical impedance spectroscopy, it is essential to have a membrane thickness in the range of 10^{-6} to 10^{-3} m, which has an electrode (Pt) thickness of 10^{-3} m range.

To measure the conductivity of nanometer thickness membrane materials, Solartron model 1260 Impedance/Gain-Phase Analyser was recently used in the literature.⁽¹⁶⁰⁻¹⁶¹⁾ However, there was no description about the limits on conductivity measurement by this method. In order to better understand the measurement limit of the electrode (see Section 5.5.1 for its dimension), a systematic calculation was carried out as follows:

The resistance (R) of the material is directly proportional to the length (l) and inversely proportional to the cross-sectional area (a).

$$R = \rho (l/a) \quad [1]$$

ρ - Resistivity of the material (for example, Au $\sim 2.44 \times 10^{-6} \Omega \text{ cm}$)

The maximum resistance of the gold electrode, which has 3 mm width, 2.5 cm length and 300 nm thickness, is calculated as follows from equation [1]:

$$\begin{aligned} \text{Maximum resistance} &= 2.44 \times 10^{-6} \Omega \text{ cm} \times 2.5 \text{ cm} / 0.3 \text{ cm} \times 300 \times 10^{-7} \text{ cm} \\ &= 0.677 \Omega \quad [1a] \end{aligned}$$

Rearranging equation (1) leads to specific conductivity

$$\text{Specific conductivity} = 1/\rho = (1/R) \times (l/a) \quad [2]$$

The resistances measured from LBL film below 1 Ω are neglected as the electrode resistance falls in this region [1a]. The reason for this behaviour could be the shortening of the electrode because of direct contact with each other. In order to avoid uncertainty during conductivity measurements, resistances of LBL films obtained above 10 Ω are only taken into consideration.

Further, attempts to measure the proton conductivity of highly ordered films such as 16 alternative layers of P4VIm based LBL film and 50 alternate layers of PBI based LBL film by these methods were not successful due to very low resistance of these films, which fall below 1 Ω . In order to increase the resistance of the LBL film above 10 Ω , the nonuniform LBL films of P4VIm (above 50 alternate layers) and the high surface roughness LBL films of PBI (above 70 alternate layers) were used in all experiments (measuring the ionic conductivity of such type of nonuniform LBL films were reported in recent literatures).⁽¹⁶⁰⁻¹⁶²⁾ Therefore a systematic comparison of multilayers in terms of ordering is neglected in this study due to measurement limits of the instrument.

5.5.1.6 Model calculations for PBI and P4VIm based multilayers

Assuming that PBI based multilayer films (on top of Au electrode with above mentioned dimensions) have a resistance of 10Ω with a thickness of 140 nm (the thickness value was calculated from LBL films of two perpendicular self-assembled Au –electrodes that had a film thickness of $\sim 70 \text{ nm}$ each) and current passing area of 9 mm^2 , the measured conductivity is calculated as follows (using equation-2):

$$\text{Conductivity} = (1/10\Omega) \times (140 \times 10^{-7} \text{ cm} / 9 \times 10^{-2} \text{ cm}^2) = 1.55 \times 10^{-5} \text{ S/cm}$$

It shows that the conductivity is measurable only from $\sim 10^{-5} \text{ S/cm}$ for PBI paired with acid multilayers.

The model calculation for P4VIm multilayers is illustrated below, assuming a value of resistance of 10Ω with a thickness of 1000 nm and an area of 9 mm^2 :

$$\text{Conductivity} = (1/10 \Omega) \times (1000 \times 10^{-7} \text{ cm} / 9 \times 10^{-2} \text{ cm}^2) = 1.11 \times 10^{-4} \text{ S/cm}$$

It indicates that the proton conductivity is measurable from 10^{-4} S/cm for P4VIm based LBL film.

To lower the resistance of the electrode from 0.6Ω (see equation 1a) by increasing its thickness above 300 nm did not make much improvement due to the measurement limit of the instrument (impedance spectroscopy) only up to 1Ω .

5.5.1.7 Proton conductivity measurement of LBL film

Proton conductivity is generally evaluated by measuring along the planes of the membrane. However, in view of the multilayer membrane exhibiting anisotropy in the direction of the membrane thickness compared to measuring along the longitudinal and transversal planes, the need to measure its conductivity in the direction of thickness with high stability, reproducibility and accuracy.

Conductivity measurements can be conducted with either 2- or 4- probe methods, but measuring with 2 probes is much easier than with 4, and this method yields more stable results as fewer inconsistencies occur with multiple specimens.

Impedance spectroscopy was recorded as real (Z') and imaginary (Z'') components of the complex impedance. Raw data plots from this study are displayed in Fig. 5.18a and 5.18b. These plots agree well with impedance plots of ion conducting LBL films sandwiched between blocking electrodes in the literature.⁽¹⁶⁰⁻¹⁶¹⁾

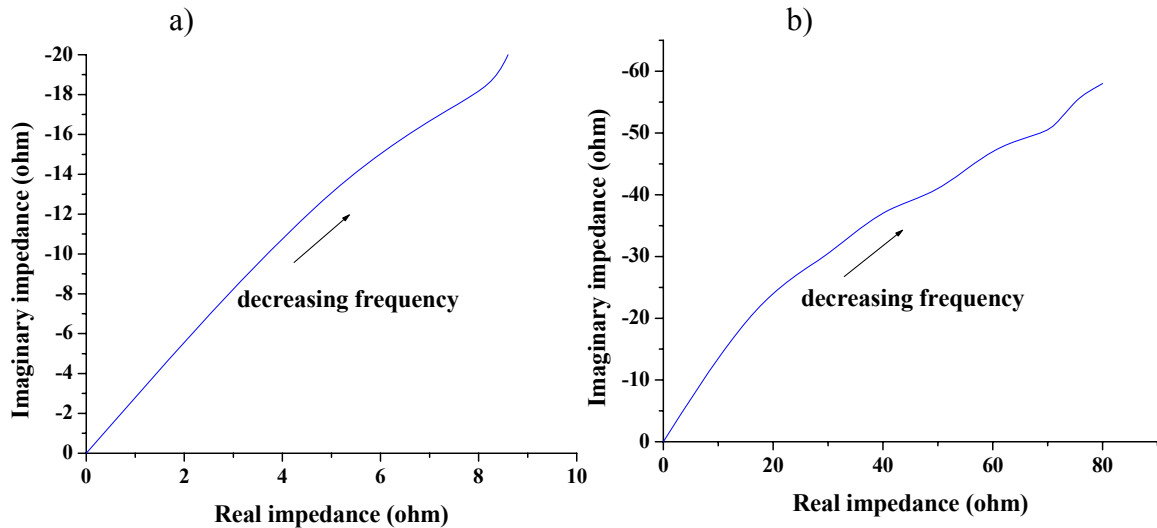


Fig. 5.18: **a)** Complex impedance plots of 70 alternate layers of P4VIm/PVPA multilayer films with measured average roughness of 56 nm. Total film thickness \sim 1020 nm. Measured conductivity value: 1.1×10^{-4} S/cm at 25 °C, \sim 25 % R.H. **b)** Complex impedance plots of 80 alternate layers of PBI/ PVPA multilayer films with measured average roughness value of 3.7 nm. Total film thickness \sim 140 nm. Measured conductivity value: 1.94×10^{-6} S/cm at 25 °C, \sim 25 % R.H.

Resistance of the film can be determined from these plots by fitting to a simple equivalent circuit as shown in Fig. 5.19.⁽¹⁶⁰⁻¹⁶¹⁾

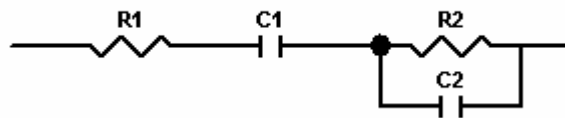


Fig. 5.19: Equivalent circuits used for fitting impedance data

The film response is represented as a parallel RC combination that takes into account the bulk resistance **R2** of the film as well as the bulk capacitance **C2**. The capacitance **C1** arises from the interfacial polarization and double layer formation, and resistance **R1** represents the electrode resistance (**R1**, typically $< 1 \Omega$).

During the measurements, the lowest frequency side of impedance is chosen to avoid the error region of the measurements at the higher frequency region.

Conductivity measurements were carried out by sandwiching two self-assembled Au electrodes perpendicular to each other. During conductivity measurements, the two LBL films on top of Au electrodes that had equal roughness values were taken, so that the contacts between the two films would be smooth and uniform in nature. (The conductivities of these films were in agreement with conductivity measurement of LBL film sandwiched between indium-tin oxide and thermally evaporated Au electrodes indicating that the values obtained from LBL films on top of Au electrodes are reliable [see Section - 5.5.2]). Further, the measurements were repeated several times to be assumed that the error limits of the measurement fall within $\pm 1\%$ range. The conductivity of the LBL film was calculated as follows:

The length was the sum of the film thickness on top of two Au electrodes, which was measured by profilometry, and was converted into cell constant with a total current passing on area of 9 mm^2 . Once the resistance R_2 of the material was measured, the following relation was used to convert it into specific conductivity:

$$\text{Specific conductivity} = (1/R_2) \times \text{Cell constant}$$

For all proton-conductivity measurements, surface roughness films greater than 10% of thickness were studied, which is convenient to measure the resistance of the film. Impedance spectra obtained in at least three different locations on each membrane (L-1, L-2 and L-3) averaged out local variations in thickness for three different samples (Sample-1, Sample-2 and Sample-3). While results for P4VIm/acid multilayers are reproducible to within $\pm 5\%$, results for PBI/acid multilayers membranes are reproducible to within $\pm 3\%$. Membrane conductivity of P4VIm/PVPA and PBI/PVPA from impedance experiments is given in the Table 5.2.

Table 5.2: Proton conductivity of P4VIm/PVPA and PBI/PVPA multilayers

Type	Roughness (nm)	Thickness (nm)	Conductivity (S/cm)		
			L-1	L-2	L-3
P4VIm/PVPA					
Sample-1	58	1020	1.0×10^{-4}	9.0×10^{-5}	1.0×10^{-4}
Sample-2	55	1030	1.0×10^{-4}	2.0×10^{-4}	9.0×10^{-5}
Sample-3	62	1050	1.0×10^{-4}	1.0×10^{-4}	8.0×10^{-5}
PBI/PVPA					
Sample-4	3.4	140	2.0×10^{-6}	9.0×10^{-7}	9.0×10^{-7}
Sample-5	3.1	145	8.0×10^{-7}	3.0×10^{-6}	1.0×10^{-6}
Sample-6	3.6	144	2.0×10^{-6}	1.0×10^{-6}	1.0×10^{-6}

From Table-5.2, the conductivity of sample-1 was similar to those using sample-2 as well as sample-3 for P4VIm/PVPA multilayers, suggesting reproducibility of measurements. In the measurement for PBI/PVPA multilayers, the conductivity of membranes were within the range of 1.0×10^{-6} S/cm, which are similar to values from ITO – membrane – gold electrode studies (see Section- 5.5.2).

Table 5.3 and Table 5.4 display the average proton conductivity results of different high roughness films assembled from 0.02 M polymer solutions at 25 °C (under ~25 % R.H.).

Table-5.3: Room Temperature (25 °C) Proton Conductivity of high roughness P4VIm/PVPA film

S. No	Total film thickness (nm)	Average film roughness values on top of two Au electrode (nm) surfaces	Conductivity (S/cm)*
L-1	1020	56, 60	$\sim 1.0 \times 10^{-4}$
L-2	1000	90, 83	$\sim 6.0 \times 10^{-6}$
L-3	1040	130, 135	$\sim 4.0 \times 10^{-9}$
L-4	1055	180, 187	not measurable**

*All proton conductivity measurements were reproducible after several repeated washing and drying steps.

**Not measurable due to high resistance of the film.

Table-5.4: Room Temperature (25 °C) Proton Conductivity of high roughness PBI/PVPA film

S. No	Total film thickness (nm)	Average film roughness values on top of two Au electrode (nm) surfaces	Conductivity (S/cm)*
L-5	140	3.3, 3.5	$\sim 1.0 \times 10^{-6}$
L-6	142	5.1, 5.3	$\sim 4.0 \times 10^{-9}$
L-7	148	6.4, 6.7	$\sim 2.0 \times 10^{-11}$
L-8	148	10.4, 10.7	not measurable**

*All proton conductivity measurements were reproducible after several repeated washing and drying steps.

**Not measurable due to high resistance of the film.

From Tables 5.3 and 5.4, conductivity of LBL films decrease from 10^{-4} to 10^{-9} S/cm for P4VIm/PVPA multilayers (L-1, L-2, L-3 and L-4) and from 10^{-6} to 10^{-11} S/cm for PBI/PVPA (L-5, L-6, L-7 and L-8) multilayers upon increasing surface roughness of the film. Moreover, the proton conductivity derived from the two-probe method is generally lower using high surface roughness film ($\sim 10^{-11}$ S/cm for ‘Sample L-7’ with roughness of $\sim 20\%$ to its thickness), because the impedance from high roughness films include the contact resistance and the ohmic resistance of the membrane sample causing the steep decrease of the characteristic proton conductivity.⁽²³⁸⁾ Therefore these error sources play an important role for the inaccuracy in the measurement method. As a result, all conductivity values are approximated as whole numbers without decimal digits.

On comparing the maximum proton conductivity of P4VIm/PVPA LBL films with conductivities of different LBL films in literature, P4VIm/PVPA multilayer materials showed higher conductivity ($\sim 10^{-4}$ S/cm) than the multilayers such as poly(allylaminehydrochloride)/poly(styrenesulfonate),⁽¹⁰⁸⁾ poly(ethyleneamine)/poly(2-acrylamido-2-methyl-1-propanesulfonic acid)⁽¹¹⁴⁾ and poly(ethylene oxide)/poly(acrylic acid),⁽¹¹⁵⁾ whose ionic conductivities are in the range of 10^{-5} - 10^{-11} S/cm in presence of salt at room temperature. M. F. Durstock and M. F. Rubner reported conductivities of 10^{-7} S/cm at 110 °C for a poly(acrylic acid)[PAH]/poly(allylaminehydrochloride) [PAA] when plasticizing these films with water.⁽¹⁰⁸⁾ Because water swells the films and solvates the ions thereby increasing their mobility and effective concentration. Whereas in dry film, conductivity of PAH/PAA multilayer decreased to 4×10^{-9} S/cm at about 110 °C.

The same authors also studied on increasing the concentration of ions in the PAH/PAA layers by dipping the film into a high pH salt solution that resulted in an increase in the observed conductivity up to 3×10^{-6} S/cm. The incorporation of a salt was expected to result in a significant improvement of number of ions. This is in accordance with the results of D. M. Delongscamp and P.T. Hammond, who studied the fast ion conduction in poly(ethylene oxide)/poly(acrylic acid), poly(ethyleneamine)/ poly(2-acrylamido-2-methyl-1-propanesulfonic acid) and poly(allylaminehydrochloride)/ poly(styrene- sulfonate) multilayers in addition of LiCF_3SO_3 salt and measured a maximum ionic conductivity of 1.0×10^{-5} at 25°C .⁽¹¹⁴⁻¹¹⁵⁾ Hence they concluded that addition of salt would increase the number of ions to enhance the conductivity in the LBL assembly, but mobility does not play any role, as it was restricted by strong ionic cross-link interaction between polymer chains in the LBL assembly. In contrast to these remarks, strong ionic cross-link in P4VIm/PVPA multilayer offers conductivity up to 10^{-4} S/cm in the absence of any added salt.

This is possible, because mobility plays an important role in the imidazole LBL film and can be explained by the general relation,

$$\sigma (\mathbf{T}) = n (\mathbf{T}) \mu (\mathbf{T}) e$$

where σ is conductivity, n is the number of mobile ions, e is the ion charge, and μ is the mobility.

After accepting the proton (n) from poly(vinylphosphonic acid), the imidazole ring migrates proton (μ) to the inside of the multilayer by proton hopping, which improves conductivity of the multilayer despite strong cross-link interaction between imidazole - phosphonic acid. Hence, the number of protons from acidic poly(vinylphosphonic acid) as well as its mobility may explain the conductivity of imidazole based multilayers.

The proton migration in P4VIm/PVPA multilayers would possibly occur by a Grotthuss type mechanism, which explains the conductivity of ordered architectures in recent literatures.^(76-78, 142-143)

Table 5.5 shows proton conductivities of multilayer films assembled from 0.02 M polymer solutions.

Table-5.5: Proton conductivity values of LBL film on gold electrode

S. No	Basic polymer	B.C (M)	Acid Polymer	pH	No. of layers	T (nm)	S.D	R (nm)	S.Cond (S/cm)
L-9	PBI	0.02	PVSA	1.7	100	110	1.63	3.0	4.0×10^{-6}
L-10	PBI	0.02	PSSA	2.2	100	130	1.12	3.7	1.0×10^{-6}
L-11	P4VIm	0.02	PVSA	1.7	50	1080	1.37	60	3.0×10^{-4}
L-12	P4VIm	0.02	PVSA	1.7	50	870	1.81	70	2.0×10^{-5}
L-13	P4VIm	0.02	PVSA	1.7	50	900	1.97	90	5.0×10^{-6}
L-14	P4VIm	0.02	PSSA	2.2	60	920	1.56	62	2.0×10^{-5}
L-15	P4VIm	0.02	PSSA	2.2	60	1000	1.65	90	1.0×10^{-6}
L-16	P4VIm	0.02	PSSA	2.2	60	975	1.60	110	1.0×10^{-8}

B.C. – Concentration of PBI or P4VIm (M)

R – Roughness of the multilayer (nm)

S.D – Standard deviation

T – Thickness of the multilayer (nm)

From Table 5.5, it can be seen that the proton conductivity of PBI/PVSA (L-9) or P4VIm/PVSA (L-11) multilayer membrane is higher than PBI/PSSA (L-10) or P4VIm/PSSA (L-14) multilayer membrane. The higher acidity of PVSA makes the multilayer better conducting than PSSA based multilayers. On comparing the conductivity of PVSA with PVPA against PBI or P4VIm multilayers (L-9 with L-5 and L-11 with L-1), the higher conductivity values of PVSA based multilayers could again be explained by higher acidity of PVSA than PVPA. These findings in accordance with the observations of Munson and Lazarus,⁽²⁴⁹⁾ who studied the conductivity of benzimidazole/H₂SO₄ and benzimidazole/H₃PO₄ blends. The conductivity of pure sulfuric acid increased by a factor of 7 to 8 upon the addition of benzimidazole, similar attempts failed for phosphoric acid, the conductivity of which decreased by a factor of about 2 upon addition of 10 % benzimidazole. These results were interpreted owing to the higher acidity of H₂SO₄ than H₃PO₄.

To compare the proton conductivity of PBI and P4VIm multilayers in terms of ordering of LBL films, model calculations indicated that electrode could measure the proton conductivity starting from 10^{-5} S/cm for PBI based multilayers and from 10^{-4} S/cm for P4VIm based multilayers. Therefore comparing the conductivity of PBI and P4VIm multilayers would not be appropriate unless the proton conductivity of thin films is measured by a method suitable for highly ordered thin films.

5.5.2 Indium-tin oxide (ITO) glass for conductivity measurements

Substrates were 2.5 cm × 5 cm of ITO coated glass and patterned in a strong acid medium to form multiple 3-mm ITO stripes. ITO film resistance was measured to be 20 Ω/ square after patterning. The ITO substrates were cleaned by ultrasonification in solvents such as detergent, deionized MilliQ-filtered water, acetone, methanol, and 1,1,1-trichloroethane for 15 min each. Immediately before use, the ITO glass substrates were plasma-etched in a Harrick PCD 200G plasma cleaner with oxygen bleed for 5 min. Substrates were exposed to polymer solutions for 15 min, followed by rinsing in solvent baths. After assembly, films for ionic conductivity evaluation were dried at 140 °C for 24 h, which has been shown to effectively remove water and DMAc from LBL assembled films. Drying was followed by thermal evaporation through a custom designed shadow mask of 2-mm wide, 100 nm thick Au electrodes perpendicular to the 3-mm wide patterned ITO stripes. The cells were profiled to verify the absence of significant gold penetration into the LBL film.

5.5.2.1 Proton conductivity measurement of LBL film by ITO-electrode

Impedance spectroscopy is recorded as real (Z') and imaginary (Z'') components of the complex impedance as displayed in Fig. 5.19. Data analysis and conductivity values were calculated as described in the Section 5.5.1.7.

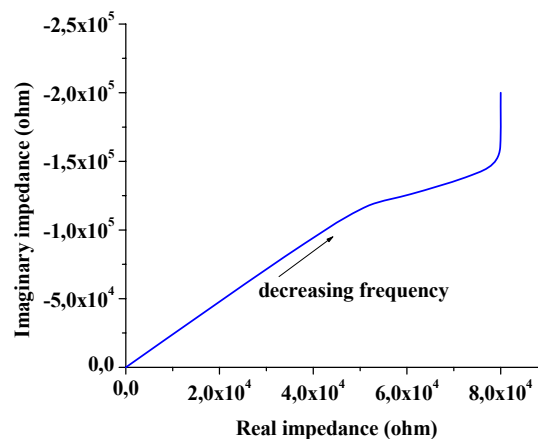


Fig. 5.19: Complex impedance plot of 70 alternate layers of PBI/ PVPA multilayer films with measured average roughness of 7 nm with thickness of 70 nm. Conductivity value: 1.45×10^{-8} S/cm at 25 °C, ~25 % R.H.

Once the resistance (R_2) of the material was measured, the following relation was used to convert it into specific conductivity:

$$\text{Specific conductivity} = (1/R_2) \times \text{Cell constant}$$

Table 5.6 shows proton conductivity measurement using ITO electrode

Table-5.6: Proton conductivity values of LBL film on ITO electrode

S.No	Basic polymer	B.C (M)	Acid Polymer	pH	No. of layers	T (nm)	S.D	R (nm)	S.Cond (S/cm)
M-1	PBI	0.02	PVPA	2.2	100	55	1.21	4.0	9.0×10^{-7}
M-2	PBI	0.02	PSSA	2.2	100	77	1.40	4.2	8.0×10^{-7}
M-3	P4VIm	0.02	PVSA	1.7	50	404	1.57	54	7.0×10^{-6}
M-4	PBI	0.02	PVSA	1.7	100	73	1.31	4.3	1.0×10^{-6}
M-5	P4VIm	0.02	PSSA	2.2	50	380	1.87	40	8.0×10^{-6}
M-6	PEI	0.02	PVPA	2.2	70	534	1.74	43	7.0×10^{-6}
M-7	P4VIm	0.02	PVPA	2.2	50	335	1.47	58	5.0×10^{-6}
M-8	PBI	0.02	PVSA	1.7	100	77	1.90	5.3	3.0×10^{-9}
M-9	PBI	0.02	PVPA	2.2	100	60	1.34	6.0	6.0×10^{-9}

B.C. – Concentration of P4VIm or PBI (M) from 0.02 M solution; *R* – Roughness of the multilayer (nm)

A.C. – Concentration of acid Polymer (M)

S.Cond – Specific conductivity

T – Thickness of the multilayer (nm)

S.D – Standard deviation

From Table 5.6, the proton conductivity measurements by ITO- electrodes also indicate that the surface roughness plays a critical role on proton transport properties of multilayers. For example, in the case of PBI/PVPA multilayer films (M-1 and M-9), an increase in the surface roughness lowers the proton conductivity from 10^{-6} to 10^{-9} S/cm at room temperature. The proton conductivity of uniform PBI/PVSA multilayer exceeds 10^{-6} S/cm and with increasing uniformity, the benefits of measuring the conductivity of the PBI based LBL film are lost. Therefore, the proton conductivity of the PBI/PVSA or PBI/PVPA is not comparable to the proton conductivity of P4VIm based LBL films, H_3PO_4 doped PBI⁽⁵⁸⁻⁵⁹⁾ or H_2SO_4 doped PBI⁽⁶⁰⁻⁶¹⁾ membranes. On the basis of these results, it is clear that further development of LBL polymer electrolytes should focus on measuring proton conductivity of highly uniform PBI based LBL films.

With increasing surface roughness, the effect of contact resistance on proton conductivity was predominant in the measurement using the two-point probe. As a result, the conductivity decreases up to 10^{-9} S/cm.

5.6 Proton conducting properties of multilayers

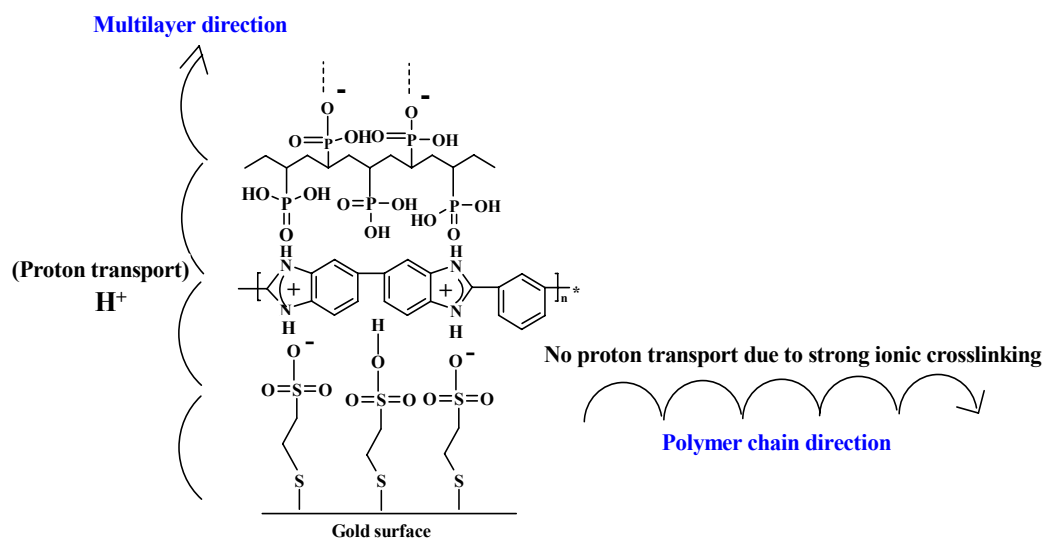


Fig. 5.20: Probable structure of PBI/PVPA LBL film

In the P4VIm/PVPA or PBI/PVPA multilayers, the imidazole (P4VIm or PBI) is expected to provide a migration path for protons emerging from the dissociation of the PVPA (Imidazole nitrogen acts as a strong proton acceptor thus forming protonic charge carriers). The proton is rapidly transferred to the neighbouring molecule and hence, the proton migrates in the multilayers. In these cases, a Grotthuss type diffusion mechanism may explain the proton diffusion process within protonated and unprotonated imidazoles. The protonic defect may cause local disorder by forming ($--HIm-(HImH^+)-ImH...$) configuration.^(162,163) Further, the proton conducting properties of LBL film vary with the direction. The directionality of proton transport in the multilayer can be explained by the donor and acceptor interaction between phosphonic acid and imidazole units leading to the formation of phosphonate anion and imidazolium ion along the multilayer direction. The strong ionic interaction along the multilayer direction supersedes any proton transfer mechanism through hydrogen bonding along the polymer chain direction. This accounts for the high resistance observed in the polymer chain direction, which is different from the measured low resistance of multilayer direction. Attempts to measure resistance value in the polymer chain direction by impedance spectroscopy were not successful, indicating a very high resistance (beyond instrument limit to measure the resistance) in the chain direction (Fig. 5.20).

In acid-doped polyelectrolyte membranes (PBI/H₃PO₄), the conductivity is independent of direction. Hence, the conducting properties of acid-doped membranes are scattered equally in all directions, and maximum conductivity might be lower than the conductivities for the multilayer systems. For example, in H₃PO₄ doped P4VIm, the maximum reported conductivity was 10⁻⁴ S/cm at ambient temperatures,⁽¹⁶⁴⁾ whereas P4VIm/PVPA multilayers showed conductivity in the range of 10⁻⁴ S/cm at room temperature (under dry condition). Similarly, multilayers are superior to copolymers with conductivities in the range from 10⁻⁶ to 10⁻¹² S/cm for poly(vinylphosphonic acid-co-4-vinylimidazole) [see Section-6.5.2 of chapter-6].

Furthermore, the difference between the conductivity of the self-assembled membranes and the membranes from random⁽¹⁶⁵⁾ or graft copolymers⁽¹⁴¹⁾ or acid doped membranes⁽¹⁶⁴⁾ lies in the connectivity of the conduction pathways. In a membrane made from these materials, conductivity occurs above a minimum acid concentration,^(141, 164-165) where there is enough connection between charged regions for a continuous pathway to exist. This leads to minimal conduction at low acid concentration, for example, for H₃PO₄ doped poly(4-vinylimidazole) membranes, the conductivity varies from ~ 10⁻⁶ S/cm to ~ 10⁻⁴ S/cm when changing the concentration of H₃PO₄ from 0.5 M to 3 M.⁽¹⁶⁴⁾ For multilayer membranes, the channels are expected to form by proper ordering as the surfaces of imidazole and acid units touch and provide continuous pathways even at low charge content similar to the ion-conducting membranes formed through the self-assembly of surface charged latex nanoparticles.⁽²²⁰⁾ However, specific applicability of styrene and acrylate⁽²²⁰⁾ type monomers for latex particle synthesis makes the multilayer membrane more suitable for applications.

In terms of acid retention ability in the membrane, both PBI/PVPA multilayer membrane and PVPA cross-linked PBI membrane would retain acids in the membranes during fuel cell operating conditions. However, the high stability of PBI/PVPA LBL membrane materials without any swelling even after prolonged exposure in water medium indicates its suitability for commercial applications.

Nevertheless, multilayers are not so perfect and often show patches of different interference colors on different regions of a substrate, clearly visible to the naked eye, especially when substrates such as an ITO glass is being used. These spots correspond to regions of slightly different thickness, which might originate from improper layer deposition of polymer chains during LBL fabrication. The presence of these inhomogeneities clearly indicates that the multilayer properties are not entirely controlled by the choice of materials and deposition conditions. This causes the high surface roughness of films sometimes even with lower number of layers.

5.7 Summary

The applications of LBL films have been extended to PBI, P4VIm, PVPA and PVSA polymer electrolytes that are appropriate for proton exchange membrane. For PBI/ acid multilayers, the linear increase in absorbance and thickness were followed by UV-vis spectroscopy and profilometry indicating the highly ordered polymer chain arrangements in LBL assembly. With P4VIm / acid multilayers, the polymer chains were arranged in an ordered fashion till 16th layers and the ordering was lost with additional number of layers as followed by UV-vis spectroscopy, X-ray reflectivity and profilometry.

Thin films such as nonuniform P4VIm films and high surface roughness PBI films have been studied extensively for proton conductivity in terms of observed resistance above $10\ \Omega$, which is convenient to measure by instrument, but there still remain a conductivity of highly ordered films that need to be addressed for a complete understanding. The proton conductivity increases with smoothness of the film on the surface, and the measured maximum conductivities were in the range of 10^{-4} S/cm at room temperature (under dry state) for P4VIm/PVPA LBL films, which is one order of magnitude greater than those of poly(ethylene oxide)/poly(acrylic acid)⁽¹¹⁵⁾ and poly(ethyleneamine)/poly(2-acrylamido-2-methyl-1-propanesulfonic acid)⁽¹¹⁴⁾ LBL films, whose maximum ionic conductivities of about 10^{-5} S/cm. In P4VIm/PVPA multilayers, the number of free protons from acidic poly-(vinylphosphonic acid) as well as the mobility allowed by the poly(4-vinylimidazole) after accepting proton from PVPA may appear to enhance proton conduction.

This suggestion is contradicted by comparison with the literature,^(108, 114-115) which demonstrates that it is the number of ions that determines the conductivity and not mobility, as it is restricted by strong ionic interaction in the multilayer. Whereas in P4VIm based multilayers, the proton hopping nature of imidazole is largely responsible for the proton mobility.

For PBI/PVPA and PBI/PVSA based multilayer films, the conductivity was measured only from 10^{-6} S/cm preventing the comparison with other polymer electrolyte membranes that are known in the literature.^(108, 114-115) With regard to the conductivities of PVPA and PVSA, the higher acidity of the latter led to a proton conductivity up to 7×10^{-6} S/cm. However, brittleness of sulfonic acid multilayers would restrict its applicability as membrane materials. Therefore PVPA based PBI LBL film would emerge as a potential membrane material for commercial applications due to its excellent uniformity and high thermal stability.

The LBL films are superior due to acid retention in the membrane at various fuel cell operating temperatures and hence, the proton conductivity would not change with time. Unlike the swelling behaviour of PVPA cross-linked PBI membrane materials in water medium, the high stability of PBI/PVPA LBL films even after prolonged exposure to water for 10 days indicates the suitability of the membrane material for fuel cell applications.

Future work should focus on constructing LBL thin films atop a porous polycarbonate membrane.⁽²²¹⁾ The porous framework would provide a highly conductive matrix for the passage of protons from one electrode to the other. An important advantage of this approach is that the LBL thin-film membrane constructed on either side of a nano- or micro-porous polycarbonate membrane would serve as the PEM for the fuel cell. Further, this design would utilize a cheap layer-by-layer technology to assemble a separate micrometer-sized fuel cell. Patterned layer-by-layer fuel cells would provide access to low-cost, readily available, and easily mass-produced micro-power devices analogous to, but much cheaper than, the traditional microelectronic processes.

The effect of contact resistance on proton conductivity was severe with increasing surface roughness of the film and this factor decreases the proton conductivity till 10^{-9} S/cm for P4VIm/PVPA LBL film and 10^{-11} S/cm for PBI/PVPA LBL film. To neglect contact resistance completely, measuring proton conductivity of highly uniform film should be seriously considered in the future.

6 Anhydrous proton conducting homo- and copolymers

Proton-conducting polymers have a key function in many important technical devices, such as polymer electrolyte fuel cells (PEMFCs), electrochemical sensors, and electrochromic devices.⁽²⁰⁷⁻²⁰⁸⁾ PEMFC technology has attracted considerable interest due to its high energy efficiency and environmental compatibility.⁽²⁰⁹⁻²¹⁰⁾ The polymer membranes in PEMFCs should facilitate fast proton conduction and at the same time be thermally and mechanically stable. It is considerably more favourable to operate PEMFCs at high temperatures, e.g., above 100 °C, due to the many advantages at the system level.⁽²⁰⁹⁻²¹¹⁾ The high proton conductivities reached by the membranes is mainly facilitated by water or other volatile low molecular weight compounds present in the polymer membrane. Consequently, a loss of these species will immediately result in a parallel loss of conductivity. For example, Nafion, the most widely used polymer membrane, quickly loses conductivity at temperatures above 100 °C due to the evaporation of water. The replacement of water by less volatile compounds can enable the membrane to operate above 100 °C. For example, strong oxo acids like phosphoric and sulfuric acid, have been complexed with basic polymers such as polybenzimidazole to improve long-term stability.⁽²¹²⁻²¹³⁾ However, self-condensation of oxo acids is a problem at operating temperatures above 120 °C. There is consequently a need to explore new concepts and new polymeric materials that are capable of fast proton conduction in the absence of any volatile compounds and are durable at elevated temperatures.⁽²¹⁴⁾

Recently, anhydrous proton-conducting membranes with flexible structural backbones, which show proton-conducting properties comparable to Nafion have been reported in the literature.⁽¹⁹⁹⁻²⁰⁶⁾ The flexible backbone of polymer chains allow for a high segmental mobility and thus, a sufficiently low glass transition temperature (T_g), which is an essential factor to reach highly conductive systems. Using a series of model compounds with imidazole tethered to the chain ends of oligo(ethylene oxide)s, Schuster⁽²¹⁵⁻²¹⁶⁾ showed that it is possible to reach conductivities in the range of 20-80 S/cm at 120 °C. In addition, similar oligomers based on benzimidazole tethered to both ends of oligo(ethylene oxide)s have recently been studied and were found to reach conductivities of the order of 10^{-1} - 10^1 S/cm at 110 °C, depending on the length of the oligo(ethylene oxide) spacer.⁽²¹⁷⁾

Furthermore, two fully polymeric proton conductors consisting of imidazole tethered to polystyrene and benzimidazole tethered to a branched siloxane network has recently been reported by Hertzl.⁽²¹⁸⁾ Conductivities as high as 700 S/cm at 200 °C were obtained for the former system.

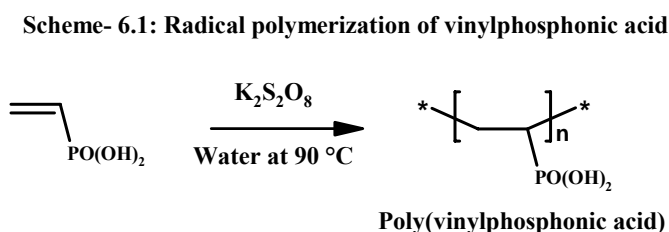
Among the polymers with a flexible chain backbone, poly(vinylphosphonic acid), poly(vinylbenzylphosphonic acid), poly(2-vinylbenzimidazole), poly(4-styrenesulfonic acid), poly(4-vinylimidazole), poly(4-vinylimidazole-co-vinylphosphonic acid) and poly(4-vinylimidazole-co-4-styrenesulfonic acid) are interesting materials for fuel cell applications. Hence there is both academic as well as industrial interest to develop and improve optimal synthetic routes to these materials.

6.1 Poly(vinylphosphonic acid)

Polymer electrolyte membranes were obtained by doping of polymers bearing basic units with strong acids such as H₃PO₄ or H₂SO₄.⁽¹⁶⁶⁻¹⁶⁸⁾ Although these types of polymer blends show high proton conductivity in the anhydrous state, self-condensation of acidic units (H₃PO₄) is a problem at higher operation temperatures.⁽¹⁶⁹⁾ Replacing H₃PO₄ with poly(vinylphosphonic acid), which can withstand higher operating temperatures⁽¹⁷⁰⁾ without self-condensation is of practical significance. The homopolymerisation of vinylphosphonic acid and its ester derivative have been mentioned briefly in the literature with molecular weight (M_n) in the range of 1.5 × 10³ g/mol⁽¹⁷¹⁻¹⁷³⁾ and concluded that chain transfer is an important factor for the observed low polymerisation of the monomer. Therefore a systematic study on the polymerisation of vinylphosphonic acid and its ester derivative to improve its molecular weight is of utmost importance.

6.1.1 Synthesis of polyvinylphosphonic acid

Vinylphosphonic acid was polymerized in presence of potassium persulfate at 90 °C for 15 hrs in 40% yield as shown in Scheme 6.1.



The polymer was purified by dissolving in water and then precipitated in excess of acetone. The precipitated polymer was dried at 100 °C for two days under vacuum. Details of polymerisation of vinylphosphonic acid under different reaction conditions are presented in Table 6.1.

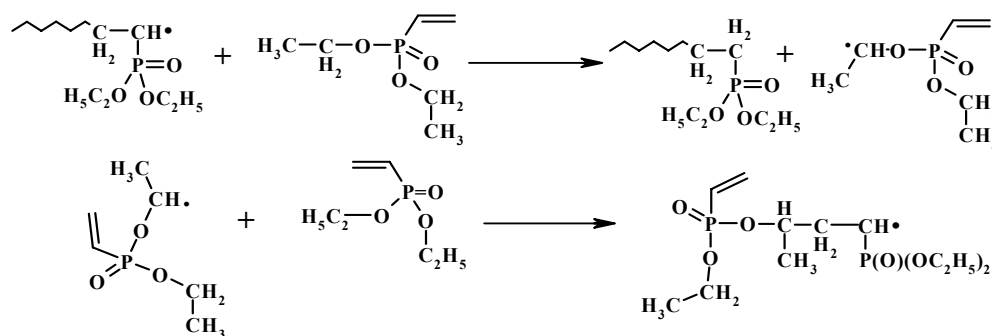
Table-6.1: The polymerisation of VPA in bulk and water medium

Sample	VPA (g)	Water (ml)	Initiator (mg)	$M_n \times 10^3$ (g/mol)	$M_w \times 10^3$ (g/mol)	M_w/M_n	Yield (%)
PVPA-1	2	0	Peroxide*, 30	1.7	2.4	1.4	23
PVPA-2	2	0	AIBN, 30	1.4	2.2	1.3	37
PVPA-3	2	5	$K_2S_2O_8$, 30	1.5	2.2	1.5	40
PVPA-4	2	10	$K_2S_2O_8$, 30	2.1	3.6	1.7	35
PVPA-5	2*	10	$K_2S_2O_8$, 30	1.8	3.4	1.9	31

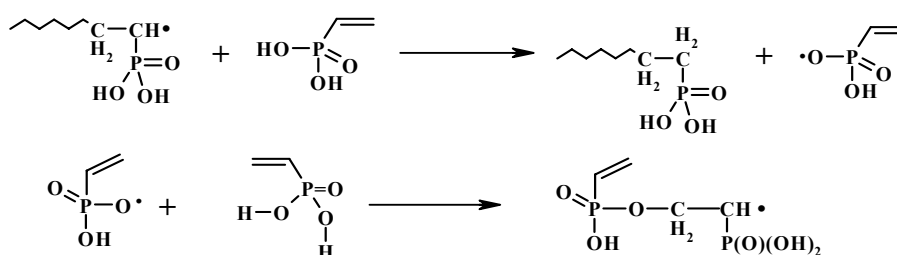
VPA – Vinylphosphonic acid; **Peroxide*** - benzoyl peroxide; **2*** - Diethyl vinylphosphonate

As recorded in Table 6.1, PVPA-1 and PVPA-2 were synthesized in the bulk medium. Due to chain transfer reactions by monomer molecules and propagating chains (as given in Scheme 6.2 and 6.3),⁽¹⁷¹⁻¹⁷³⁾ only low molecular weight of polymers were obtained.

Scheme-6.2: Chain transfer reactions in polymerisation of diethyl vinylphosphonate



Scheme-6.3: Chain transfer reactions in polymerisation of vinylphosphonic acid



To minimize chain transfer reaction, a solution polymerisation was carried out in water medium. However, the low molecular weight polymers PVPA-3, PVPA-4 and PVPA-5 were again obtained. A possible explanation is that when water was used as a solvent, the probability of frequent collision between the propagating polymer chain and the monomer is more due to high solubility, and as a result, chain transfer reaction plays vital to reduce molecular weight in highly polar water medium. In order to study polymerization in less polar solvent, the polymerization was performed in ethyl acetate and ethanol. Table 6.2 displays polymerization of vinylphosphonic acid in ethyl acetate and ethanol medium.

Table-6.2: Radical polymerization in ethyl acetate and ethanol medium at 80 °C

Sample	VPA (g)	Ethyl acetate (g)	Ethanol (g)	AIBN (g)	$M_n \times 10^3$ (g/mol)	$M_w \times 10^3$ (g/mol)	M_w/M_n	Yield (%)
PVPA-6	2	3.3	0	0.06	5.2	46.0	8.7	100
PVPA-7	2	0	2.8	0.06	3.4	6.0	1.7	42
PVPA-8	2	3.0	0.4	0.06	5.4	27.0	5	82
PVPA-9	2	1.7	1.7	0.06	3.7	16.0	4.2	74

*VPA – Vinylphosphonic acid

As shown in Table 6.2, using ethyl acetate as solvent, PVPA-6 was synthesized in excellent yield with molecular weight (M_w) of 4.6×10^4 g/mol, but with broad molecular weight distribution due to precipitation of the polymer in the reaction medium during polymerisation. To suppress molecular weight distribution (by preventing precipitation of the polymer), PVPA-7 was synthesized using more polar ethanol solvent, but molecular weight (M_w) reduced to 6.0×10^3 g/mol. In an attempt to optimise molecular weight and its distribution, the polymerisation was done in a mixture of ethyl acetate – ethanol medium, and the molecular weights (M_w) of 2.7×10^4 g/mole (PVPA-8) and 1.6×10^4 g/mol (PVPA-9) were obtained depending on the ratio of each solvent. The chain transfer reaction was significantly lowered by polymerising VPA in ethyl acetate and ethanol medium; however there is still a need to control molecular distribution.

In order to control molecular weight distribution, the anionic polymerization of diethyl vinylphosphonate was carried out in dry THF under argon atmosphere as given in Table 6.3.

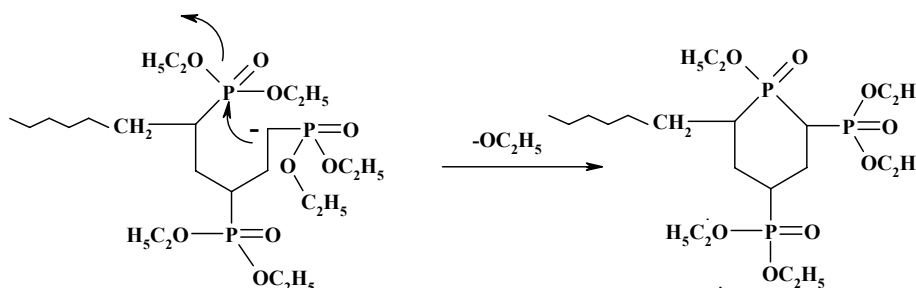
Table-6.3: The anionic polymerisation of diethyl vinylphosphonate at $-80\text{ }^{\circ}\text{C}$

Sample	VPA (g)	THF (ml)	n-buLi (mg)	$M_n \times 10^3$ (g/mol)	$M_w \times 10^3$ (g/mol)	M_w/M_n	Yield (%)
PVPA-10	2	10	30	2.6	3.0	1.1	30
PVPA-11	2	10	40	2.3	2.7	1.1	26
PVPA-12	2	10	50	1.9	2.2	1.1	20

VPA – Diethyl vinylphosphonate; n-buLi – n-butyl lithium.

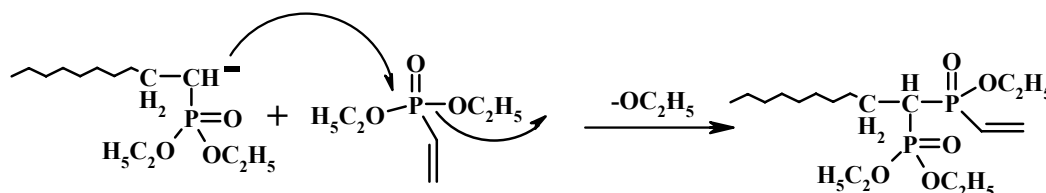
As recoded in Table 6.3, the low molecular weight polymers PVPA-10, PVPA-11 and PVPA-12 were obtained by this method. The reason could be due to nucleophilic substitution by intramolecular backbiting attack of a propagating carbanion terminating the polymerisation as shown in Scheme 6.4.

Scheme-6.4: Intramolecular backbiting attack



Also nucleophilic attack by a propagating carbanion on the monomer to displace ethoxide ion can lead to chain termination as illustrated in Scheme 6.5.

Scheme-6.5: Intermolecular nucleophilic attack



From anionic polymerization, the broad molecular weight distribution was suppressed, but molecular weight was reduced drastically; In an attempt to synthesize high molecular weight polymer with reduced polydispersity, the polymerization was carried out by ‘Stable Free Radical Polymerisation’ using TEMPO.

To study the TEMPO-mediated controlled radical polymerisation of diethyl vinylphosphonate (VP), six experiments were performed with different concentration of camphorsulfonic acid (Table 6.4).

S. NO	VPA/AIBN/ TEMPO/CSA	(M _n) g/mol	Reaction time (hrs)
PVP-1	100: 2: 0: 0	1.6×10^3	15
PVP-2	100: 2: 1: 0	-----	15
PVP-3	100: 2: 1: 0.5	-----	15
PVP-4	100: 2: 1: 1.0	-----	15
PVP-5	100: 2: 1: 1.5	-----	15
PVP-6	100: 2: 1: 2.0	-----	15

*CSA- camphorsulfonic acid

In the absence of TEMPO and CSA, the molecular weight of 1.6×10^3 was achieved using AIBN as initiator (PVP-1, Table 6.4). When TEMPO was solely used, VP did not undergo polymerisation (PVP-2). This interesting finding shows that stronger electron-withdrawing $-\text{PO}(\text{OC}_2\text{H}_5)_2$ group in vinylphosphonate prevents the double bond for the nitroxide controlled free-radical polymerisation. Even using CSA as an additive with four different molar ratio of TEMPO/CSA did not activate the double bond for the polymerisation of diethyl vinylphosphonate (Samples PVP-3, PVP-4, PVP-5 and PVP-6). Reactions were also performed at 130 and 135 °C in this initiating system, but diethyl vinylphosphonate failed to undergo polymerization. In comparison with nitroxide controlled free-radical polymerisations reported in literature,⁽²³⁹⁻²⁴¹⁾ it is most efficient for the polymerisation of styrene and acrylate up to the present. These types of monomers, which have electron-releasing groups, have been proved to be useful for nitroxide-mediated living free-radical polymerisation.⁽²³⁹⁾

In conclusion, PVPA was synthesized in the range of molecular weights up to 4.6×10^4 g/mol. All efforts to polymerise VPA in the presence of TEMPO failed due to electron-withdrawing effect from phosphorus atom rendering the double bonds less reactive.⁽¹⁶⁶⁻¹⁷³⁾ Approaches to activate the double bond in vinylphosphonates towards polymerisation include the identification of suitable monomer.⁽¹⁷⁴⁻¹⁷⁸⁾ Among the best-known vinyl phosphorus derivatives, diethylvinylbenzyl phosphonate shows high reactivity under different radical polymerisation methods. In the literature, different methods have been reported for the synthesis of diethylvinylbenzyl phosphonate from vinylbenzyl chloride(VBC).⁽¹⁷⁹⁻¹⁸²⁾ However yields were poor (~ 10 %) due to high temperature (145 °C) used for the synthesis of the monomer. Therefore, it is essential to optimize the reaction condition to get high yield of monomer and to study its polymerizability under different conditions.

6.2 Monomer synthesis

The VBC can be obtained commercially and was easily converted into its phosphonated derivative as described in literature⁽¹⁸⁰⁾ by heating with triethyl phosphite at 95 °C for three days. The yield was 70% using 6-tert-butyl-2,4-dimethylphenol as inhibitor (Scheme 6.6).

Scheme- 6.6: Synthesis of diethylvinylbenzyl phosphonate

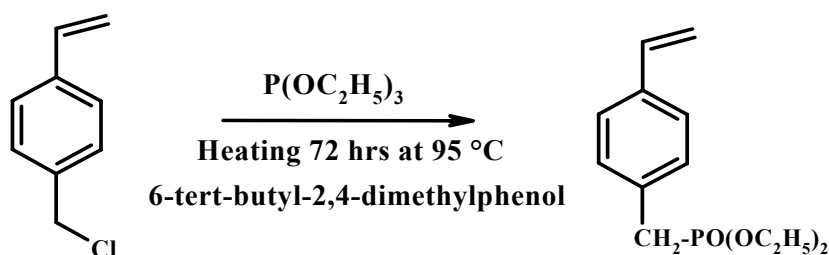


Fig. 6.1 shows the ^1H NMR spectrum of diethylvinylbenzyl phosphonate monomer.

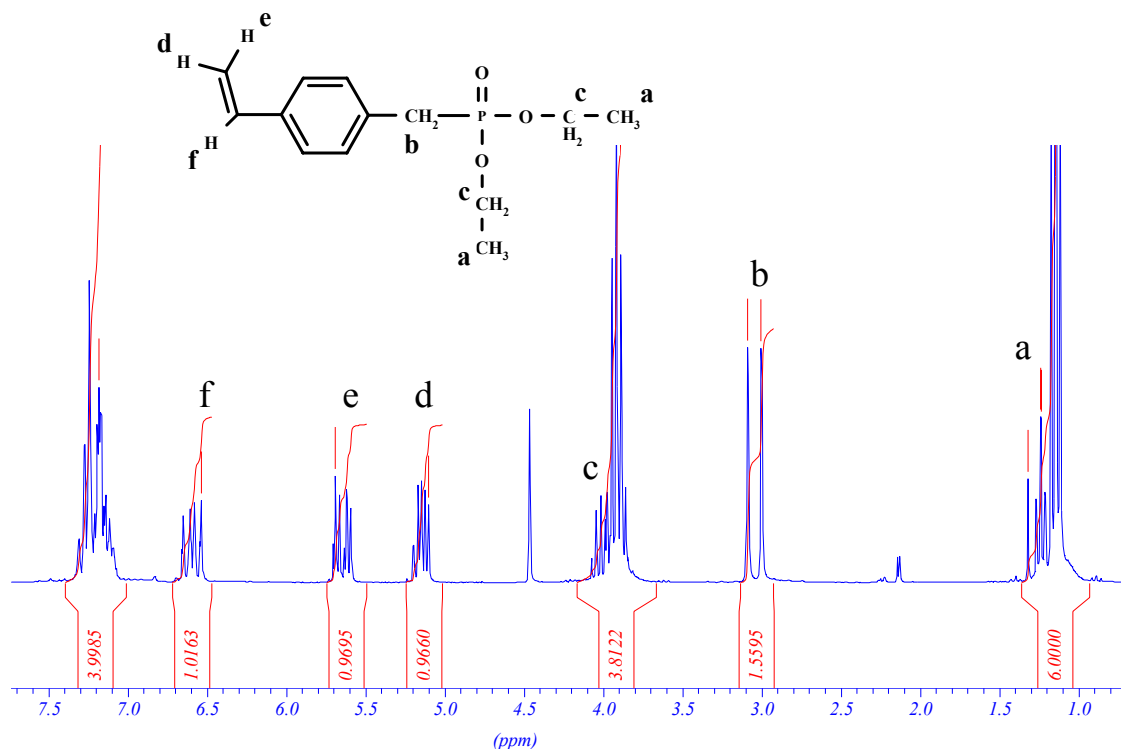


Fig. 6.1: ^1H NMR (250 MHz, CDCl_3) spectrum of m/p-diethylvinylbenzyl phosphonate

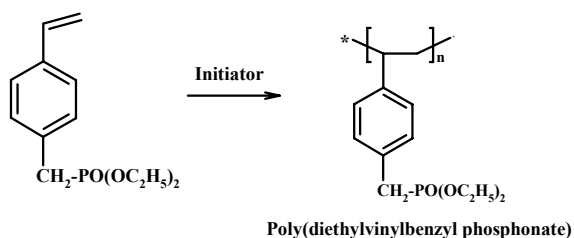
The signals appearing at 1.2 ppm for CH_3 , 3.0 ppm for $\text{C}_6\text{H}_4\text{CH}_2$, 3.9 ppm for CH_2 , 5.1 ppm, 5.6 ppm, and 6.5 ppm correspond to vinylic hydrogen atoms as assigned above and 7.1 ppm for aromatic hydrogen atoms agree well with the expected structure of diethylvinylbenzyl phosphonate monomer.

6.2.1 Synthesis of poly(diethyl vinylbenzylphosphonate)

Initiator (BPO or AIBN) was dissolved in vinylbenzyl phosphonate monomer, and the solution was degassed and sealed under vacuum at $-78\text{ }^\circ\text{C}$. The polymerisation was carried out at $90\text{ }^\circ\text{C}$ under argon atmosphere. After few hours, the polymer was dissolved in CHCl_3 , and then precipitated in an excess of hexane. It was dried in vacuum for 48 hrs and the yield was 90 %. The same polymerization procedure was used in the presence of TEMPO, however, the reaction was carried out at $125\text{ }^\circ\text{C}$ for 15 hrs. The molecular weight was determined by GPC.

Scheme 6.7 presents the radical polymerisation of diethylvinylbenzyl phosphonate monomer.⁽¹⁷⁹⁻¹⁸²⁾

Scheme- 6.7: Radical polymerization reaction of diethylvinylbenzyl phosphonate



Details of bulk polymerization of diethylvinylbenzyl phosphonate under different reaction conditions are given in Table 6.5.

Table-6.5: Bulk polymerisation of diethylvinylbenzyl phosphonate at 90 °C

Sample	VBP (g)	Initiator (mg)	$M_n \times 10^3$ (g/mol)	$M_w \times 10^3$ (g/mol)	M_w/M_n	Yield (%)
PVBP-1	2.0	AIBN, 5	35.0	10.5	3.0	94
PVBP-2	2.0	BPO, 5	43.0	97.0	2.26	96
PVBP-3	2.0	T/A*, 1.5	58.0	73.0	1.25	80
PVBP-4	2.0	T/B*, 1.5	80.0	98.0	1.22	85

*Mole percentage of TEMPO with respect to AIBN= 1.5; Amount of AIBN = 3 mg; polymerisation temperature = 125 °C; *Mole percentage of TEMPO with respect to Benzoyl peroxide = 1.5; Amount of AIBN = 3 mg; polymerization temperature = 125 °C;

As shown in Table 6.5, the bulk polymerization was carried out at 90 °C in the presence of a radical initiator and at 125 °C with TEMPO and the molecular weight was measured by GPC. In the radical polymerisation of PVBP-1 and PVBP-2, the polymerisation reaction was fast and difficult to control, which led to high molecular weight distribution. In the presence of TEMPO (PVBP-3 and PVBP-4), the polymerisation reaction was slow due to controlled addition of monomer units to growing polymer chains that led to narrow molecular weight distribution. The radical polymerization of vinylbenzylphosphonate has been discussed in the literature.⁽¹⁷⁹⁻¹⁸²⁾ In those studies, a molecular weight of 55×10^3 g/mol with polydispersity of 2.7 was reported. This could be attributed to the presence of impurity in the monomer used. However using high purity monomer (from ¹H NMR spectroscopy and FD mass spectroscopy), the molecular weight of 9.8×10^4 g/mol with an excellent polydispersity of 1.22 was achieved in this study.

The influence of temperature was also studied for the polymerisation of vinylbenzyl phosphonate (VBP) with CSA as an additive in TEMPO-mediated controlled radical polymerisation. The reactions were performed at three different temperatures (110, 115 and 120 °C), and the molar ratio of CSA to TEMPO was 2:1. In presence of CSA, the reaction rate increased with temperature (Table 6.6). Even at 110 °C, the conversion of the polymerisation reached 40% within 1 hr. In comparison with the conversion of the polymerisation without additives under the same conditions (16% within 1 hr at 125 °C), the increase in the rate was distinct. This meant that CSA not only enhanced the rate greatly but also decreased the temperature of the reaction. From Table 6.6, the polydispersity stayed relatively low indicating the absence of autoinitiation of VBP at 110 °C. A similar experiment with styrene under the same conditions only 8% conversion was reached in 1 hr.⁽²⁴⁰⁾ Because VBP has active –CH₂- substitution in p-position, which could enhance the rate and this resulted in better conversion (40%) than styrene (16%).

Table-6.6: Temperature dependent nitroxide mediated polymerization

Sample	Temperature	$M_n \times 10^3$ (g/mol)	PDI	Conversion	Time (hr)
PVBP-5	110 °C	16.0	1.12	40	1
PVBP-6	115 °C	23.0	1.19	48	1
PVBP-7	120 °C	31.5	1.25	53	1
PVBP-8	125 °C	45.0	1.32	56	1
PVBP-9	130 °C	47.0	1.47	72	1

*Molar ratio of VBP/AIBN/CSA/TEMPO = 100: 1: 2: 1

Fig. 6.2 shows that the conversion increases almost linearly with temperature in the range of 110-125 °C. This meant that the increase in the rate of polymerisation did not lose the living character of the polymerisation. However at 130 °C, the conversion rate increases significantly indicating the thermal radical auto-generation of vinylbenzyl phosphonate. Obviously, the polydispersity illustrated in Fig. 6.3 measured by GPC, increases significantly and the living characteristic is minimized at 130 °C. This is the same phenomenon as observed in the polymerisation of p-vinylbenzyl chloride reported in the literature indicating ‘auto initiation affect living character of the polymerisation’.⁽²⁴⁰⁾

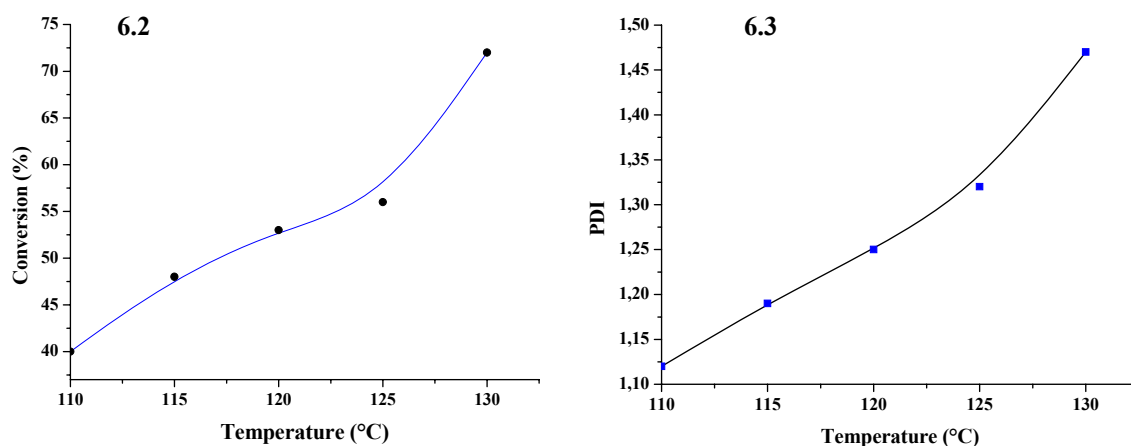
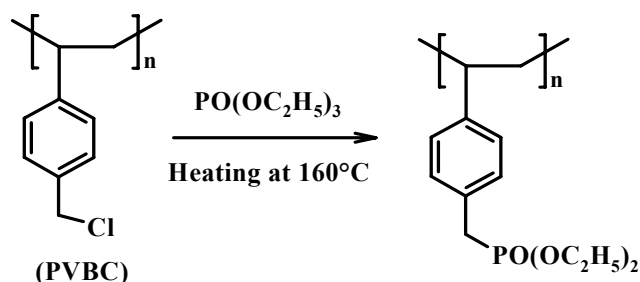


Fig. 6.2: The dependence of conversion on temperature. Molar ratio of VBP/AIBN/CSA/TEMPO = 100: 1: 2: 1. **Fig. 6.3:** The dependence of polydispersities on temperature. Molar ratio of VBP/ AIBN/ CSA/ TEMPO = 100: 1: 2: 1

6.2.2 Synthesis of PVBP from poly(vinylbenzylchloride)

In an attempt to synthesize poly(vinylbenzylphosphonate) from poly(vinylbenzylchloride), the modification experiments were reported in the literature by Michaelis-Arbuzov reaction⁽¹⁸⁰⁾ as given in Scheme 6.8. However, the maximum conversion from chloro to phosphonate derivative was in the range of 80 % at 120 °C. In order to get 100 % conversion, the reaction was carried out at 160 °C in bis(2-ethoxyethyl) ether solvent.

Scheme- 6.8: Michaelis-Arbuzov reaction



To synthesize poly(diethylvinylbenzyl phosphonate) from poly(vinylbenzyl chloride), the synthesis of poly(4-vinylbenzyl chloride) was carried out from vinylbenzyl chloride by radical polymerisation technique at 90 °C. The polymer was purified by dissolving in chloroform and then precipitated in hexane. The yield was 80 %.

Details of polymerization of vinylbenzyl chloride under different conditions are reported in Table 6.7.

Table-6.7: Bulk polymerisation of diethyl vinylbenzylphosphonate at 90 °C

Sample	VBC (g)	Initiator (mg)	$M_n \times 10^3$ (g/mol)	$M_w \times 10^3$ (g/mol)	M_w/M_n	Yield (%)
PVBC-1	2.0	AIBN, 3	28.6	95.3	3.3	87
PVBC-2	2.0	AIBN, 5	23.0	88.0	3.8	83
PVBC-3	2.0	AIBN, T = 3	33.0	43.0	1.3	84
PVBC-4	2.0	AIBN, T = 5	24.0	32.8	1.4	78

*VBC-Vinylbenzylchloride; AIBN- Azobisisobutyronitrile; T – TEMPO

As shown in Table 6.7, the bulk polymerisation was carried out at 90 °C in the presence of a radical initiator and at 125 °C in the presence of TEMPO and the molecular weight was measured by GPC. In PVBC-1 and PVBC-2, the radical polymerisation of vinylbenzyl chloride was very fast, which ended with high molecular weight distribution.

In the presence of TEMPO in PVBC-3 and PVBC-4, the polymerization reaction was slow and controlled that led to narrow molecular weight distribution. Therefore, samples PVBC-3 and PVBC-4 were used to convert into poly(diethylvinylphosphonate). The conversion was 100 % after heating for 24 hrs at 160 °C under argon atmosphere. After cooling up to room temperature, the reaction mixture was precipitated in hexane. The dried polymer samples were verified by ^1H NMR spectroscopy.

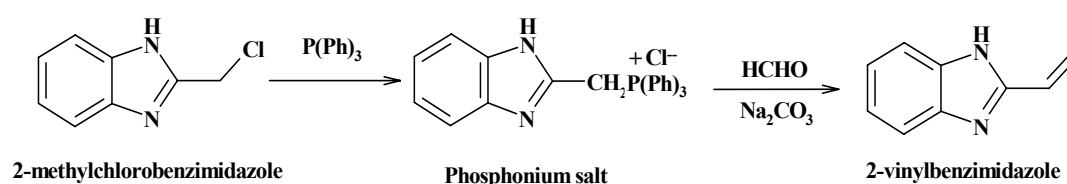
Thus, it may be concluded that vinylbenzylphosphonate is a better monomer than vinylphosphonate or vinylphosphonic acid for the polymerization reaction and the resulting poly(vinylbenzylphosphonate) have molecular weights up to 9.8×10^4 g/mol with polydispersity of 1.2. From another side, the polymer chain mobility will play a very important role to enhance proton conductivity and hence, in terms of segmental mobility of the polymer chain, poly(vinylphosphonic acid) may give rise to better results than poly(vinylbenzylphosphonic acid).

6.3 Poly(2-vinylbenzimidazole)

The poly(2-vinylbenzimidazole) was first introduced by C.G. Overberg⁽¹⁸³⁻¹⁸⁴⁾ in 1967 by thermal heating of 2-vinylbenzimidazole monomer at 120 °C. However, it was carried out by a multi-steps synthetic process that restricted the yield of the product. In order to achieve high yield with minimum possible steps, the reaction was carried out as follows:

2-methylchlorobenzimidazole and triphenylphosphine was refluxed in dioxane for 14 h. Then, formaldehyde was added, and converted into 2-vinylbenzimidazole. Sublimation at 120 °C under reduced pressure afforded 80% of 2-vinylbenzimidazole. Scheme 6.9 shows the synthesis 2-vinylbenzimidazole monomer.

Scheme-6.9: Synthesis of 2-vinylbenzimidazole



¹H NMR spectrum of 2-vinylbenzimidazole is given in Fig. 6.4.

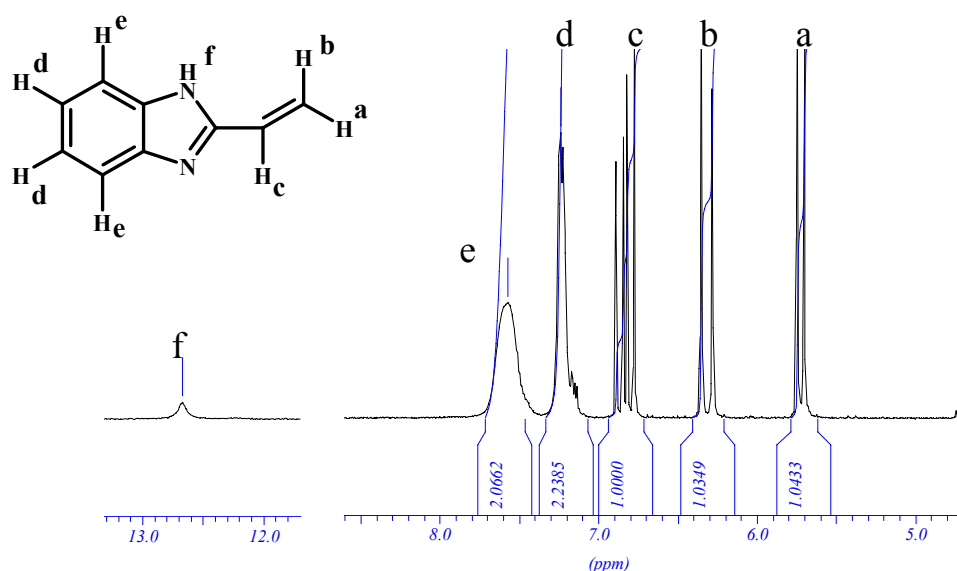


Fig. 6.4: ¹H NMR (250 MHz, d₆-DMSO) spectrum of 2-vinylbenzimidazole

The signals appearing at 5.7 ppm, 6.3 ppm, and 6.7 ppm corresponding to vinylic hydrogen atoms as assigned above, 7.2 ppm and 7.5 ppm for aromatic hydrogen atoms agree well with the structure of 2-vinylbenzimidazole. Analysis by mass spectrometry under EI mode showed a molecular ion peak at m/e 144 (M^+).

6.3.1 Polymerisation of 2-vinylbenzimidazole

Freshly sublimed monomer and AIBN were dissolved in methanol in a small polymerisation tube. The polymerisation was carried out by heating at 70-80 °C for 48 hr. After cooling, the polymer was precipitated in hexane and dried.

Scheme 6.10 explains the polymerisation of 2-vinylbenzimidazole.

Scheme- 6.10: Synthesis of poly(2-vinylbenzimidazole)

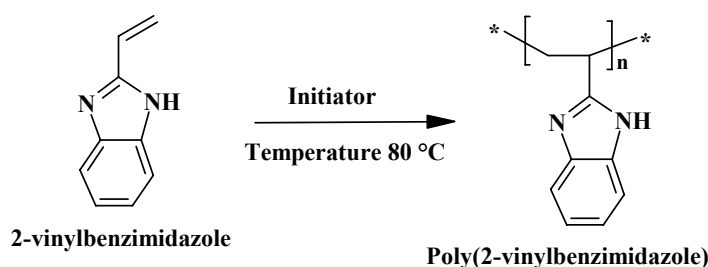


Table 6.8 shows the synthesis of poly(2-vinylbenzimidazole) under various reaction conditions.

Table-6.8: Synthesis of poly(2-vinylbenzimidazole)

Sample	2-VBIm (grams)	Initiator	Sol./Temp (°C)	Yield (%)	Nitrogen content (%)	D.T _o (°C)	Intrinsic viscosity (dl. g ⁻¹)
PVBIm-1	0.3	AIBN	Methanol/80	83	16.83	423	1.23
PVBIm-2	0.3/ DVB* (0.03g)	AIBN	Methanol/80	94	16.08	417	Cross-link. poly.
PVBIm-3	0.3	TEMPO/AIBN =1.5	m-xylene/125	20	18.27	401	1.04
PVBIm-4	0.3	TEMPO/AIBN = 1.5	DMSO/125	25	19.38	414	1.12
PVBIm-5	0.3	TEMPO (1mmol)	m-xylene/125	40	18.23	406	1.06
PVBIm-6	0.3	TEMPO (1.5 mmol)	m-xylene/125	28	18.61	412	1.12
PVBIm-7	0.3	TEMPO (2 mmol)	m-xylene/125	17	17.76	414	1.14

Note: All viscosity measurements in sulfuric acid medium; D.T_o – Decomposition Temperature.

In all experiments, amount of AIBN ~ 3 mg; DVB*-Divinylbenzene

From Table 6.8, the polymerisation was carried out in methanol using AIBN as an initiator. In PBIm-1, the radical polymerisation was very fast at 90 °C and the polymer was precipitated within 30 minutes in the reaction medium. In PVBIIm-2, the radical copolymerisation was carried out with divinylbenzene at 90 °C, and the copolymer was precipitated within few minutes in the reaction medium. The homopolymer was also synthesized in the presence of TEMPO (Stable Free Radical Polymerisation), which was initiated either by AIBN (PVBIIm-3 and PVBIIm-4) or by thermal heating (PVBIIm-5, PVBIIm-6 and PVBIIm-7); In the presence of TEMPO, the polymerisation was slow and precipitation started after 5 hrs due to slow addition of monomer units to growing polymer chain in a controlled fashion.

But all the products were insoluble in common solvents, which restricted ability to synthesize block-co-polymer. The poor solubility can be explained in terms of strong hydrogen bonding interactions between imidazole repeating units in polymer chains. In an attempt to synthesize solvent soluble poly(2-vinylbenzimidazole), the radical copolymerization was carried out with vinylphosphonate in methanol solvent, but homopolymer of 2-vinylbenzimidazole was precipitated due to significant difference in reactivity ratio between two monomers.

Further, the poor solubility of 2-vinylbenzimidazole (except methanol and DMSO) restricted copolymerization with water-soluble monomers such as 4-styrenesulfonate, vinylphosphonic acid and vinylsulfonic acid. So its functional derivatives (N-substituted imidazole) have to be synthesized in order to increase the solubility of poly(2-vinylbenzimidazole).

6.3.2 Conductivity measurement

The film for proton conductivity measurement was prepared from casting a solution of PVBIIm in DMAc/H₃PO₄ mixture. Three different compositions of membranes were synthesized according to the number of phosphoric acid per repeat unit of imidazole in PVBIIm.

The conductivities of the polymer electrolytes were measured with an alternating-current (ac) impedance technique. The film was sandwiched between two platinum blocking electrodes, and the conductivity was measured as a function of frequency. Fig. 6.5 exhibits the conductivity of PVBIIm 3H₃PO₄ film versus frequency with temperature as the parameter.

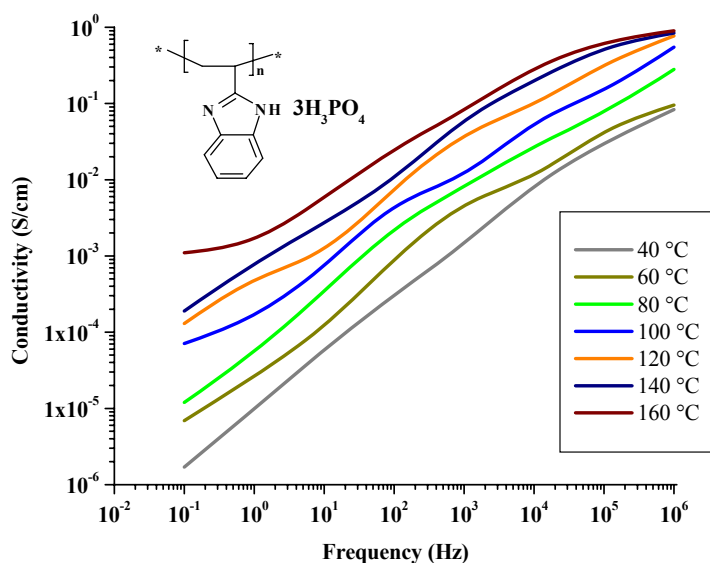


Fig. 6.5: Frequency dependent AC conductivity of poly(2-vinylbenzimidazole). $3\text{H}_3\text{PO}_4$ film

The conductivities of samples prepared from $\times = 1, 2, 3$ H_3PO_4 units per imidazole unit in poly(2-vinylbenzimidazole) are listed in Table 6.9.

Table-6.9: The proton conductivity of PVBIIm membranes

Sample	Number of H_3PO_4 per imidazole unit	Conductivity (S/cm) at 160 °C	T_g
PVBIIm-1	1	7.4×10^{-4}	75 °C
PVBIIm-2	2	9.0×10^{-4}	18 °C
PVBIIm-3	3	1.1×10^{-3}	-24 °C

As seen in Table 6.9, the proton conductivity increases with increasing phosphoric acid concentration with a maximum conductivity of 2.7×10^{-4} S/cm measured at 160 °C. The proton conductivity of samples PVBIIm-1, PVBIIm-2 and PVBIIm-3 can be attributed to proton transport between phosphoric acid and imidazole units along with segmental motion of the polymer chains. Among reports in the literature, H_3PO_4 doped PBI has been most extensively studied for conductivity measurement.⁽²¹⁻³²⁾ Depending on the temperature in PBI $3\text{H}_3\text{PO}_4$ complex, the conductivity was up to 3.5×10^{-4} S/cm at 160 °C. The improved conductivity of PVBIIm $3\text{H}_3\text{PO}_4$ complex can be explained by higher segmental mobility of PVBIIm than stiff PBI, which enhances the conductivity of the membrane.

For fuel cell application, poly(2-vinylbenzimidazole) membrane will be applied within 400 °C. More importantly, a flexible film of moderate tensile strength and T_g would also be helpful to enhance conductivity of the membrane. In terms of development, poly(2-vinylbenzimidazole) modified with PO_3H or PO_3R_2 groups should be highly soluble polymer and then directly useful for PEM application. The resulting polymers would have well defined grafting functional groups that would retain acid and thus improve the performance during fuel cell operating conditions.

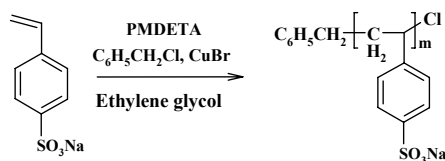
6.4 Synthesis of poly(4-styrenesulfonate) by ATRP reaction

Atom transfer radical polymerisation (ATRP) is a controlled radical polymerisation process that provides well-defined polymers with low polydispersities.⁽¹⁹⁰⁻¹⁹⁴⁾ Control over the radical polymerisation is obtained by using a transition metal complex which induces an extremely fast, reversible activation of the propagating chains. The end groups of the polymers are determined by the initiator, mostly an alkyl halide. The alkyl group of the initiator is transferred to one chain end, the halogen to the other chain end. The halide end groups can further be used in several ways. The polymer chain can be extended with the formation of block copolymers⁽¹⁹⁵⁾ or the halogen end group can be replaced by hydrogen or by other functional groups such as azides.⁽¹⁹⁶⁾ It is reported that the bromine end groups in the polymers were used for nucleophilic substitution reactions.⁽¹⁹⁷⁾ Recently, an important type of core-shell particle (the composite particle made of two different polymers, one forming the core and the other the shell) was prepared in the water phase from ATRP reaction.⁽²³⁰⁾

Therefore synthesizing proton conducting polymers such as poly(styrenesulfonic acid) by ATRP reaction with chloro- or bromo- end groups would be useful to synthesize graft and block copolymers for fuel cell applications. There have been reports in the literature on ‘Stable Free Radical Polymerization’ of styrenesulfonate using TEMPO,⁽⁵⁻⁶⁾ but no indication of ATRP with styrenesulfonate monomer.

To synthesize poly(styrenesulfonate) by ATRP reaction, a reaction was carried out in ethylene glycol medium. The yield was 90 %, and molecular weight (M_n) was in the range of $60 \times 10^3 \text{ g mole}^{-1}$. Scheme 6.11 explains the polymerisation reaction.

Scheme-6.11: Synthesis of poly(4-styrenesulfonate) by ATRP reaction



PMDETA: N, N, N', N', N''-pentamethyldiethylenetriamine

Details of polymerisation of 4-styrenesulfonate under different reaction conditions are given in Table 6.10.

Table-6.10: ATRP polymerisation of 4-styrenesulfonate

Sample	Initiator (mol)	Copper halide (mol)	PMDETA (mol)	M_n, M_w ($\times 10^3$ g/mol)	M_w/M_n	Yield (%)	Time (hrs)
PSSA-1	PECl* (0.02)	CuCl (0.02)	0.02	60.0 70.2	1.2	80	16
PSSA-2	PECl (0.02)	CuCl (0.02)	0.12	65.0 94.1	1.4	92	4
PSSA-3	PEBr* (0.02)	CuBr (0.02)	0.02	55.7 67.0	1.2	83	10
PSSA-4	PEBr (0.02)	CuBr (0.02)	0.12	56.0 78.2	1.4	85	2

PECl• 1-phenylethyl chloride; PEBR 1-phenylethyl bromide

As recorded in Table 6.10, PSSA-1 was synthesized in the presence of stronger binding ligand, such as the tridentate *N,N,N',N',N''*-pentamethyldiethylenetriamine (PMDETA). When a 1:1 ratio of PMDETA to CuBr was used, the polymerisation reaction was slow, which can be explained by controlled addition of monomer units to growing polymer chains. In contrast, at a PMDETA to CuBr ratio of 6:1, the polymerisation was approximately 4 times faster as shown in PSSA-2. This could be explained by the strong catalyzing effect of PMDETA when it is in excess. The polymerisation reactions were carried out using 1-phenylethyl bromide as the initiator and CuCl/PMDETA as the catalyst under similar conditions used for the synthesis of PSSA-1 and PSSA-2. However, the reaction was faster than when chlorine was used as the halogen, presumably due to the higher activation/deactivation equilibrium constant of alkyl bromide and CuBr/PMDETA as shown in samples PSSA-3 and PSSA-4.

In comparison with ATRP of ‘styrene’ reported in literature,⁽²⁴⁴⁻²⁴⁵⁾ styrene polymerises with enhanced polymerisation rate and conversion. Using styrene/1-PEBr/ CuBr/PMDETA molar ratio of 100:1:1:5 at 90 °C, a 65% conversion was obtained within 30 minutes. With styrenesulfonate under the same conditions, only 20% conversion is reached in 30 minutes, documenting electron-withdrawing effect of $-\text{SO}_3\text{Na}$ group retarding the rate of polymerisation. To increase polymerisation rate, the reactions were performed at higher temperatures. Polymerisations at 105 and 125 °C were faster as compared to the analogous experiments at 90 °C, using styrenesulfonate/1-PEBr/CuBr/PMDETA molar ratio of 100:1:1:5. However, polymerisations were not controlled ($\text{PDI} > 1.9$). At high temperatures, autoinitiation of styrenesulfonate may be high and that could compete with ATRP polymerisation of styrenesulfonate. Therefore, high polydispersities were obtained in those experiments. A similar picture was observed for the ATRP polymerisation of styrene at 125 °C.⁽²⁴⁴⁾

The influence of reaction time on conversion was illustrated in Fig 6.6. The conversion increases almost linearly with time at 90 °C meaning that the living characteristic is maintained. However, the linearity was lost at 125 °C indicate the deterioration of the living nature of the polymerisation.

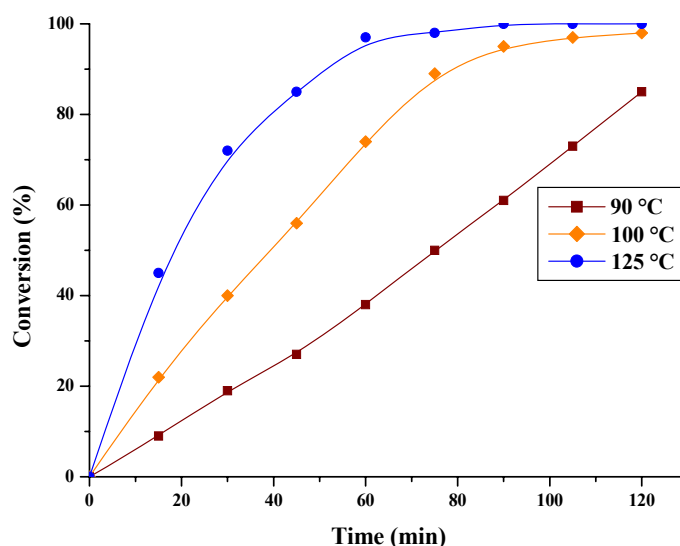


Fig. 6.6: The dependence of conversion on reaction time, [styrenesulfonate]/[1-PEBr]/[CuBr]/[PMDETA] = 100: 1: 1: 5.

In conclusion, the ATRP of sulfonic acid monomer is a significant development, because it is expected that the most durable, performing, and viable membranes will result from fine-tuning the chemical composition and the architecture of the chloro or bromo- terminated sulfonic acid polymer chain for PEM applications.

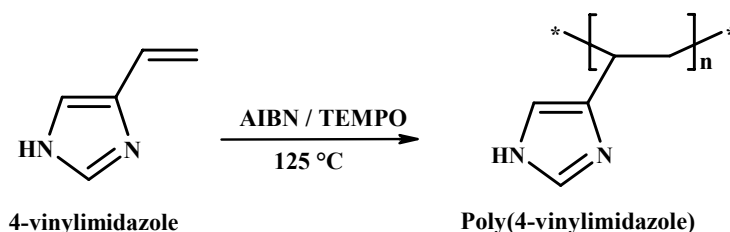
6.5 Controlled radical polymerisation of 4-vinylimidazole

Free radical polymerisation is one of the most important methods to produce mass polymers like poly(4-vinylimidazole), poly(vinylphosphonic acid), polystyrene, polyacrylates and poly(vinyl chloride). However, one of the major drawbacks of these processes is the low control over the reaction, which leads to a broad molecular weight distribution.

During the past decade, several methods for controlled living free radical polymerisation such as ATRP (atom transfer radical polymerisation),⁽¹⁹⁰⁻¹⁹⁴⁾ RAFT (reversible addition – fragmentation chain transfer polymerisation),⁽²⁴⁶⁻²⁴⁷⁾ and NMP (nitroxide mediated polymerisation)⁽²³⁹⁻²⁴¹⁾ have been developed. These new methods allow the synthesis of polymers with defined molecular weights and polydispersities far below the theoretical limit ($PDI < 1.5$).

In the present study, synthesis of 4-vinylimidazole by NMP and ATRP are described to control the polymerisation. These methods would provide the opportunity to synthesize functional polymers such as graft-co-polymer and block-co-polymer for proton exchange membrane application. Scheme 6.12 describes TEMPO-mediated polymerisation of 4-vinylimidazole.

Scheme-6.12: TEMPO-mediated polymerisation of 4-vinylimidazole



The PDI of the poly(4-vinylimidazole) prepared by TEMPO-mediated polymerisation using AIBN as initiator is shown in Table 6.11.

Table-6.11: NMP of 4-vinylimidazole

S. No.	Solvent	4VIm/ AIBN/ TEMPO	($M_n \times 10^3$) g/mol)	PDI	Yield (%)	Reaction time (hrs)
P4VIm-1	Benzene	100: 2: 0	5.1	2.4	63	2
P4VIm-2	Benzene	100: 2: 0	10	3.7	91	4
P4VIm-3	Ethylene glycol	100: 2: 1	3.0	1.19	8	15
P4VIm-4	Ethylene glycol	100: 2: 1	3.1	1.21	8	30
P4VIm-5	m-xylene	100: 2: 1	2.6	1.30	6	15
P4VIm-6	m-xylene	100: 2: 1	2.7	1.31	6	30
P4VIm-7	DMSO	100: 2: 1	4.4	1.35	12	15
P4VIm-8	DMSO	100: 2: 1	4.5	1.38	12	30

*P4VIm-1 and P4VIm-2 were carried out at 70 °C; Other polymerisation reactions were carried out at 125 °C;

When neither TEMPO nor CSA is employed, that is typically in the radical polymerisation, the high conversion of 91% is achieved for 3 hr because of the high polymerisation rate (P4VIm-2, Table 6.11). When 2.0 molar ratio of [AIBN]/[TEMPO] is used at 125 °C in ethylene glycol medium, the PDI decreases to 1.19 with 8% conversion in P4VIm-3. Because heating at 125 °C, the monomer was decomposed at faster rate than polymerisation, which restricted both yield and molecular weight of the polymer. Increasing reaction time up to 30 hr in sample P4VIm-4 did not increase the molecular weight compare to sample P4VIm-3, meaning that the monomer is decomposed completely after heating for 15 hr. The polymerisation was also carried out in xylene and DMSO medium (from samples P4VIm-5 to P4VIm-8). In sample P4VIm-7, the molecular weight of 4.4×10^3 g/mol is achieved with enhanced conversion and polymerisation rate, presumably due to higher solubility of monomer and polymer in the DMSO medium. For comparison of TEMPO-mediated polymerisation of 4-VIm with styrene and n-butyl acrylate, polymerization of 4-vinylimidazole was far slower under the same conditions indicating the absence of electron rich double bond in 4-VIm.⁽²³⁹⁻²⁴¹⁾ Further, the influence of temperature was studied for the polymerisation of 4-vinylimidazole in TEMPO-mediated controlled radical polymerisation. The reactions were performed at three different temperatures (105, 110 and 115 °C), and the molar ratio of 4-vinylimidazole to TEMPO was 100:2, but no polymer was obtained;

Whereas polymerisation of styrene and n-butyl acrylate have been reported at 105 °C in the presence of TEMPO.⁽²⁴⁰⁾

To improve the rate of polymerisation as well as reduce the rate of 4-vinylimidazole decomposition at 125 °C, camphorsulfonic acid (CSA) was added to accelerate the rate of nitroxide-mediated polymerisation.⁽²⁴⁰⁻²⁴¹⁾ Table 6.12 represents the conversion of the TEMPO-mediated polymerisation of 4-vinylimidazole in the presence of CSA in DMSO medium.

Table-6.12: NMP of 4-vinylimidazole in presence of CSA at 125 °C

S.No.	4VIm/AIBN/ TEMPO/CSA	($M_n \times 10^3$ g/mol)	PDI	Reaction time (hrs)	Yield (%)
P4VIm-9	100: 2: 1: 0.5	5.4	1.41	15	16
P4VIm-10	100: 2: 1: 1	6.2	1.47	15	18
P4VIm-11	100: 2: 1: 1.5	6.8	1.51	15	21
P4VIm-12	100: 2: 1: 2	7.1	1.59	15	22
P4VIm-13	100: 1: 2: 1	5.0	1.32	15	19
P4VIm-14	100: 1: 2: 2	5.5	1.37	15	20

As seen in Table 6.12, CSA in TEMPO-mediated dispersion polymerisation efficiently accelerates the polymerisation rate. The presence of CSA in the polymerisation suppresses the thermal degradation of 4-vinylimidazole. When 1.5 molar ratio of [CSA]/[TEMPO] is used, the PDI increases to 1.59 with 22% conversion for sample P4VIm-12. Although with the incorporation of CSA the PDI slightly increases, the molecular weight up to 7.1×10^3 are obtained. However the PDIs of 1.32 and 1.37 are achieved for 0.5 and 1.0 molar ratios of [CSA]/[TEMPO], respectively (P4VIm-13 and P4VIm-14). These polymerisation characteristics indicate that CSA serves as an efficient rate-enhancing agent in the TEMPO-mediated polymerisation by minimizing the monomer decomposition.

Fig. 6.7 displays the conversion of the TEMPO-mediated polymerisation under various conditions. The linearity in reaction time versus conversion is a characteristic of living nature of polymerisation for samples P4VIm-7, P4VIm-12 and P4VIm-14, since the number of growing radicals is maintained constant throughout the polymerisation. In the absence of TEMPO and CSA, a nonlinear kinetics is observed for sample P4VIm-2.

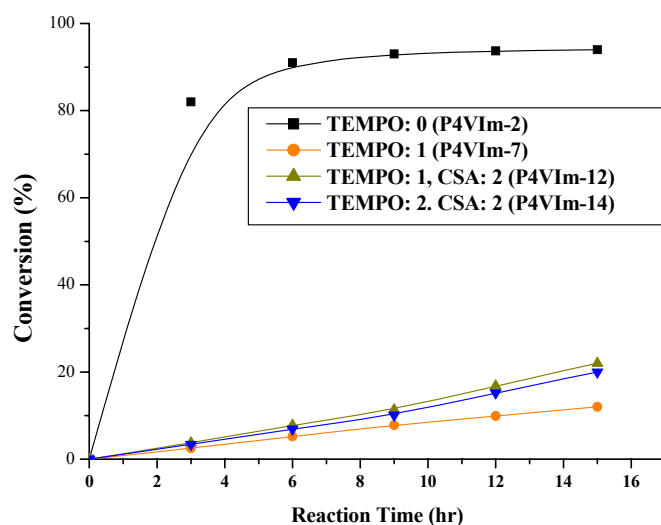
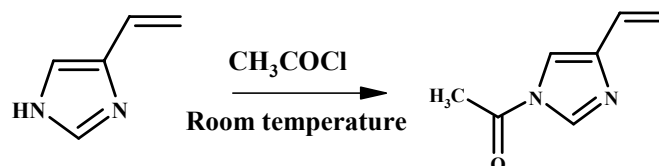


Fig. 6.7: The influence of the addition of CSA on the conversion of TEMPO-mediated polymerisation of 4-vinylimidazole at 125 °C.

To improve the thermal stability of 4-vinylimidazole, the modification of 4-vinylimidazole was carried out in benzene medium at room temperature using acetyl chloride (Scheme 6.13).

Scheme-6.13: Reaction of 4-VIm and acetyl chloride

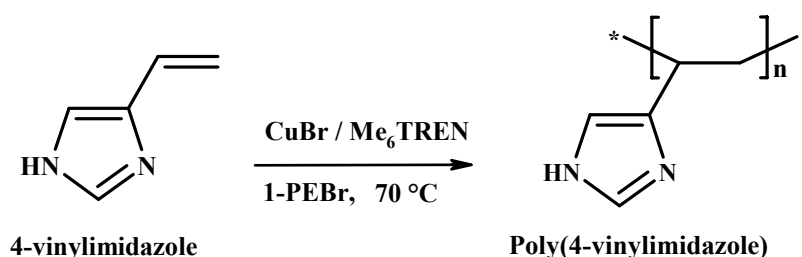


The acetylated product was isolated in 50% yield, but acetylated 4-vinylimidazole failed to undergo radical polymerisation as well as TEMPO-mediated polymerisation due to steric effect of acetyl groups inhibit the polymerisation.

In conclusion, the TEMPO-mediated controlled radical polymerisation of 4-vinylimidazole in the presence of CSA is carried out using AIBN as an initiator. The molecular weight of 7.1×10^3 g/mol was achieved with 22% conversion. The poor thermal stability of 4-vinylimidazole restricted the yield of polymerisation at 125 °C.

To synthesize poly(4-vinylimidazole) with narrow polydispersity at lower temperatures, polymerisation was also carried out by ATRP at 70 °C. Scheme 6.14 presents ATRP polymerisation of 4-vinylimidazole.

Scheme-6.14: ATRP polymerisation of 4-vinylimidazole



The polymerisation of 4-vinylimidazole poses a very challenging problem for ATRP because both 4-vinylimidazole and poly(4-vinylimidazole) are strong coordinating ligands that can compete for the binding of the metal catalysts in polymerisation system. The monomer 4-vinylimidazole is normally present in large excess over the ligand used, the complexation of 4-vinylimidazole with copper might occur. When polymerisation of 4-vinylimidazole with 1-phenylethylbromide /CuBr/2,2'-bipyridine (bpy) as initiation system was performed at 70 °C for 10 h, only a monomer conversion of 5% was achieved with number average molecular weight of 800 g/mol (Table 6.13). Probable reason for low conversion is the high accessibility of the nitrogen in 4-vinylimidazole compared to 2,2'-bipyridine ligand (The imidazole coordinated copper complexes are not effective catalyst for ATRP).⁽²⁴⁵⁾ In comparison with ATRP of nitrogen containing monomer such as 4-vinylpyridine in literature,⁽²⁴²⁾ Matyjaszewski pointed out that a stronger binding ligand, N,N,N',N',N''-pentamethyldiethylene triamine (PMDETA) was used instead of bipyridine ligand, the competitive coordination of 4-vinylpyridine to copper evident, although faster polymerization rate was observed. Therefore polymerisation of 4-vinylimidazole was studied using 1.0, 0.5 and 0.2 molar ratio of CuBr/PMDETA as catalyst and 1-PEBr as initiator and the result are listed in Table 6.13.

Table-6.13: ATRP of 4-vinylimidazole

Sample	4VIm (mol)	CuBr (mol)	Ligand (mol)	$M_n \times 10^3$ (g/mol)	PDI	Yield (%)	Time (hr)
P4VIm-15	0.007	0.00014	Bpy (0.00028)	0.8	1.10	8.0	10
P4VIm-16	0.007	0.00014	PMDETA (0.00014)	1.2	1.18	11.0	10
P4VIm-17	0.007	0.00014	PMDETA (0.00028)	1.3	1.22	13.5	10
P4VIm-18	0.007	0.00014	PMDETA (0.0007)	1.5	1.24	15.0	10
P4VIm-19	0.007	0.00014	Me ₆ -TREN (0.00014)	1.8	1.21	18.0	10
P4VIm-20	0.007	0.00014	Me ₆ -TREN (0.00021)	1.9	1.17	19.5	10
P4VIm-21	0.007	0.00014	Me ₆ -TREN (0.00028)	2.3	1.29	21.0	10
P4VIm-22	0.007	0.00014	Me ₆ -TREN (0.0007)	2.5	1.30	20.0	10
P4VIm-23	0.007	0.00014	Me ₆ -TREN (0.00098)	2.6	1.26	21.0	10

*Initiator: 1-phenylethyl bromide; Temperature of the polymerisation reactions: 70 °C; Solvent: Cyclohexane.

As shown in Table 6.13, when the molar concentration of PMDETA increased from 0.00014 to 0.0007 mole, there was a distinct increase in the rate of polymerisation and conversion (P4VIm-16, P4VIm-17 and P4VIm-18). The molecular weights were slightly increased up to 1.5×10^3 g/mol. All these results indicate that the excess ligand with high complexation constant to copper is very important for ATRP of 4-vinylimidazole, although other factors, such as, halide initiator and solvent, also play significant role of the polymerisation.⁽²⁴³⁻²⁴⁵⁾ When more stronger binding ligand tris[2-(dimethylamino)ethyl]amine (Me₆TREN) was used with increasing concentration of 0.00014 to 0.00098 mole in the solution ATRP of 4-vinylimidazole, the linear increase of molecular weight with conversion was observed (P4VIm-19, P4VIm-20, P4VIm-21, P4VIm-22 and P4VIm-23). However the molecular weight remained quite low of 2.6×10^3 g/mol even though ligand concentration was increased from 0.00098 to 0.0013 mole. The reason may be due to termination reaction of chain radical when excess of CuBr/Me₆TREN present in the polymerisation medium.

In comparison with the polymerisation of 4-vinylpyridine⁽²⁴⁵⁾ using CuBr/Me₆TREN as catalyst under the same conditions of P4VIm-23, the molecular weight of poly(vinylimidazole) was lower than that obtained from poly(4-vinylpyridine). It demonstrates that 4-vinylimidazole or poly(4-vinylimidazole) has stronger coordinative ability to copper ions than 4-vinylpyridine and hence, decrease both molecular weight as well as conversion of the polymerisation. Further removal of copper complexes after polymerisation of 4-vinylimidazole was not successful illustrating the strong coordination between copper and imidazole.

Studies on the ATRP polymerisation of 2-vinylbenzimidazole (2-VBIm) also lead to the similar results to those of 4-vinylimidazole. 2-vinylbenzimidazole was polymerized in propanol using 1-PEBr as the initiator, [CuBr/Me₆TREN] as the catalyst. The conditions and results are listed in Table 6.14.

Table-6.14: ATRP of 2-vinylbenzimidazole at 90 °C

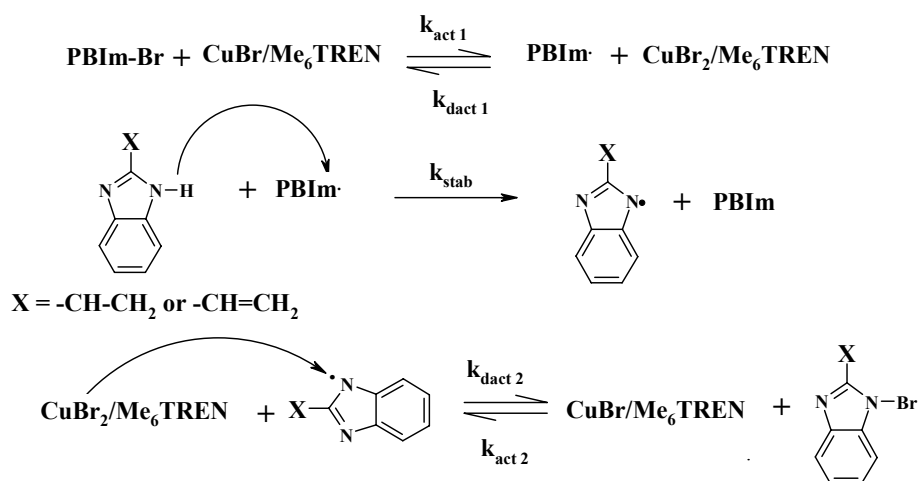
S. No.	[CuBr/Me ₆ TREN] :2-VBIm	M _n (× 10 ³ g/mol)	PDI	Time (hr)	Conversion (%)
PVBIIm-1	1.0: 100	3.8	1.14	7	18.0
PVBIIm-2	1.5: 100	4.1	1.15	7	24.0
PVBIIm-3	2.0: 100	4.4	1.20	7	28.0
PVBIIm-4	2.5: 100	3.9	1.35	7	19.0
PVBIIm-5	3.0: 100	2.7	1.54	7	14.0

*4-vinylimidazole:1-PEBr = 100:1 (molar ratio); Solvent: Propanol.

As shown in Table 6.14, when the molar ratio of [CuBr/Me₆TREN]:2-VBIm was increased from 1.0: 100 to 2.0: 100, there was a distinct increase in the molecular weight in the range of 4.4×10^3 g/mol for samples PVBIIm-1, PVBIIm-2 and PVBIIm-3. The molecular weight distributions were slightly broadened. However, the molecular weights decrease gradually till 2.7×10^3 g/mol with increase in molar ratio of [CuBr/Me₆TREN] :2-VBIm from 2.5: 100 to 3.0: 100, also the polydispersities increase from 1.35 to 1.54 (PVBIIm-4 and PVBIIm-5). These results imply the occurrence of radical couple termination.

A possible explanation is that when excess of [CuBr/Me₆TREN] was used, the dynamic equilibrium of the reaction, as shown Scheme 6.15, would shift to the right direction and the concentration of poly(2-vinylbenzimidazole) radical would increase. As a result of the increased radical concentration, couple termination of poly(2-vinylbenzimidazole) occurred readily.

Scheme-6.15: Termination reaction in the ATRP of 2-vinylbenzimidazole



A similar pattern of reaction was also observed in the reaction imidazole with metal complexes.⁽²⁴³⁾ These polymerization characteristics indicate that the living nature of the ATRP of 4-vinylimidazole or 2-vinylbenzimidazole is marginally affected by the chain transfer reaction.

In conclusion, synthesis of poly(4-vinylimidazole) and poly(2-vinylbenzimidazole) by ATRP were ended with low molecular weight oligomers, presumably due to chain transfer reaction. In addition, imidazole coordination with copper ion⁽¹⁷⁾ complicates the purification of the polymer. Because of the problem of side reactions, more new derivatives substituted with alkyl chains are needed to be synthesized and that would result in better chemistry of such materials.

6.6 Proton conducting copolymers

Copolymers based on flexible structural backbone is a good approach for the development of novel proton conducting polymers in which the segmental mobility of the polymer chains has a significant contribution to the proton conductivity.⁽¹⁹⁷⁻²¹⁷⁾ In this effort, proton-conducting copolymers were synthesized by free-radical copolymerisation of vinylphosphonic acid (VPA) with 4-vinylimidazole and 4-styrenesulfonate with 4-vinylimidazole (4-VIm).

6.6.1 Synthesis of 4-vinylimidazole

The synthesis of 4-vinylimidazole was carried out by thermal heating of urocanic acid as described in the literature.⁽¹⁵⁷⁾ The following Scheme 6.16 explains the synthesis of 4-vinylimidazole. The yield was 53%. The low yield is in part due to thermal decomposition of the starting material at this temperature to give an insoluble black material.

Scheme-6.16: Synthesis of 4-vinylimidazole

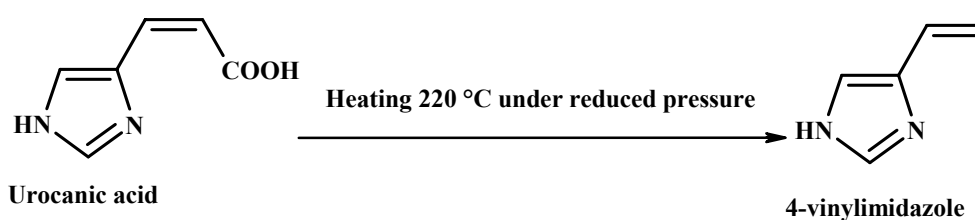


Fig. 6.8 presents the ^1H NMR spectrum of 4-vinylimidazole in CDCl_3 solvent.

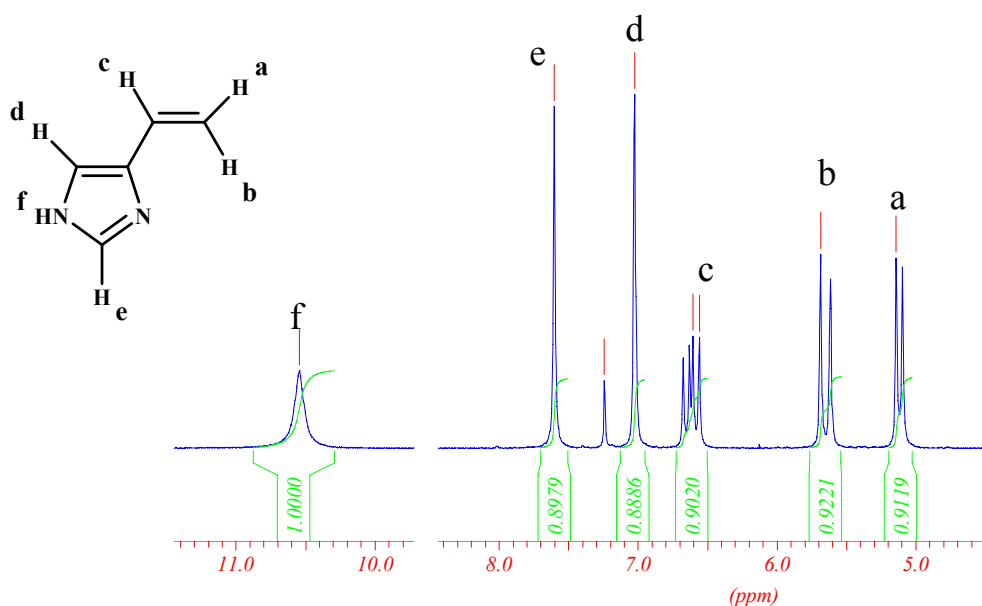


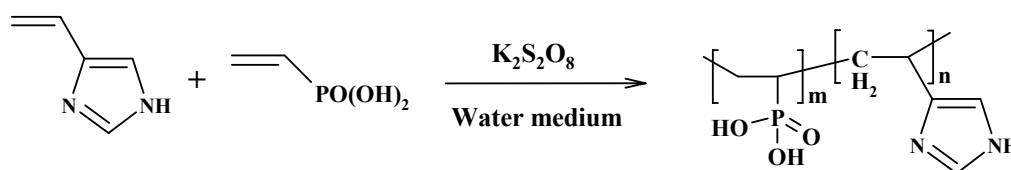
Fig. 6.8: ^1H NMR spectrum (250 MHz, CDCl_3) of 4-vinylimidazole in CDCl_3

The signals appearing at 5.13 ppm, 5.68 ppm and 6.60 ppm correspond to vinylic hydrogen atoms as assigned above, 7.02 ppm for $=\text{N}-\text{CH}=\text{N}$ from imidazole ring, 7.60 ppm for $\text{N}=\text{CH}-\text{NH}$ from imidazole ring and 10.54 ppm for NH hydrogen, agree with 4-vinylimidazole structure. Analysis by mass spectrometry under EI mode showed a molecular ion peak at m/e 94 (M^+) corresponding to 4-vinylimidazole.

6.6.2 Radical copolymerisation of 4-vinylimidazole with vinylphosphonic acid [Poly(4-VIm-co-VPA)]

The radical copolymerisation of vinylphosphonic acid with 4-vinylimidazole (4-VIm) was carried out in water medium at 80°C. The copolymer was purified by dissolving in water and then precipitated in acetone as shown in Scheme 6.17. The yield was 70 % using 1:1 feed ratio of monomers.

Scheme- 6.17: Radical co-polymerisation



GPC analysis of the polymer against polystyrene standard gave a number average molecular weight of 3.2×10^4 g/mol. The copolymer was further characterized by ^1H NMR spectroscopy as shown in Fig.6.9.

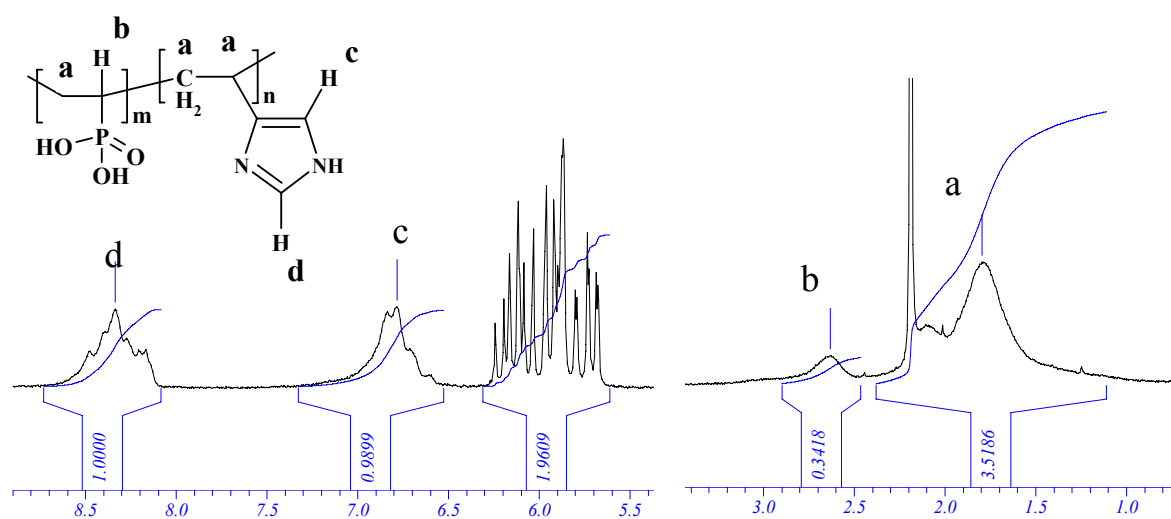


Fig. 6.9: ^1H NMR (250 MHz, D_2O) spectrum of poly(4-vinylimidazole-co-vinylphosphonic acid) The signals appearing at 8.3 ppm for ($-\text{N}=\text{CH}-\text{NH}-$), and 6.7 ppm ($-\text{CH}=\text{C}$) can be assigned to the imidazole ring hydrogen atoms as shown above. Further, the signal representing at 2.6 ppm for ($-\text{CH}-\text{PO}(\text{OH})_2$) agrees with the covalently bound vinylphosphonic acid and presence of signals at 5.6 to 6.4 ppm for double bond corresponding to the unreactive vinylphosphonic acid in the copolymer.

Copolymer composition =

$$\frac{\text{Integrated intensity of an imidazole ring}}{\text{Integrated intensity of a proton from covalently bound vinylphosphonic acid}} = \frac{1}{0.34} = 3$$

It clearly shows 3:1 ratio of imidazole and phosphonic acid units in the copolymer.

Integrated intensity of 1-hydrogen from vinylphosphonic acid monomer = $1.96/3 = 0.65$.

Unreactive vinylphosphonic acid hydrogen (**1H**) has two times higher intensity than covalently bound vinylphosphonic acid hydrogen in the copolymer ($0.34 \times 2 \sim 0.65$). Therefore, 3: 1 ratio of imidazole and acid units in the copolymer composition contains two unreactive VPA units in order to equalize imidazole and acid unit composition as 3:3. And hence, all imidazole units in the copolymer are saturated with equal number of acid units.

The copolymers were also produced with a 4-VIm/VPA mole ratio ranging from 4:1 to 1:2 in the feed. The copolymer samples, which were obtained at higher ratios of 4-VIm, are partially swelling in water. As the feed content of VPA increases, the resultant copolymers become soluble in water.

The actual composition of the copolymers, which were calculated from ^1H NMR spectra are summarized in Table 6.15.

Table-6.15: Calculation of copolymer composition by ^1H NMR spectroscopy

Sample	Feed ratio of 4-VIm/VPA	Ratio of 4-VIm/VPA	Number of unreactive VPA per repeat unit of copolymer	Nitrogen content (%)
S-1	3:1	3.7: 0.3	1	63
S-2	2:2	3.0:1.0	2	57
S-3	1:3	2.4: 1.6	2	50
S-4	1:4	2.0: 2:0	1	46

The composition of the copolymer is depending on the monomer feed ratio. When 4-VIm in the feed ratio is varied from 25% to 75%, the 4-VIm content in the copolymer is changed from 46% to 63%.

The copolymer was also characterized by FTIR spectroscopy.

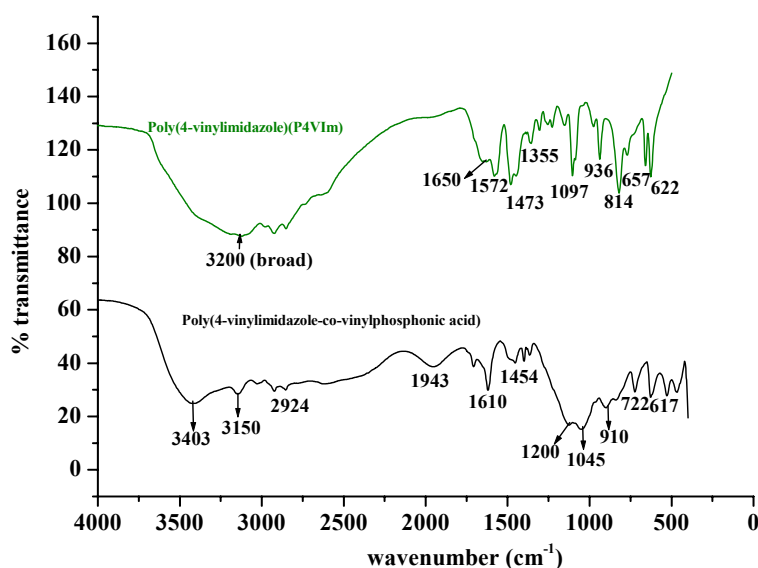


Fig. 6.10: FTIR spectra of P4VIm and copolymer

Fig. 6.10 shows the IR spectra of pure P4VIm and its copolymer. In P4VIm, the heteroaromatic rings (Imidazole ring) show peaks in the 1650-1570 cm^{-1} range due to stretching vibrations. In addition, the five-membered heteroaromatic rings exhibit a strong absorption at 800-700 cm^{-1} , which can be related to C-H out-of-plane vibrations at the double bond of the imidazole ring.⁽¹⁵⁷⁾ Hydrogen bond formation between aryl-N-H and aryl-N in the solid-state results in a band broadening at 3200 cm^{-1} .⁽¹⁵⁷⁾ The IR spectrum of PVPA shows strong bands at 1040-910 cm^{-1} that belongs to asymmetric stretching vibration of P-OH group and at 1150 cm^{-1} that corresponds to P=O stretching.⁽¹⁶⁴⁾ Additionally, the O-H stretching of the POH group gives rise to broad bands at medium intensity at 2850-2750 cm^{-1} .⁽¹⁶⁴⁾ Copolymer shows a very strong interaction between phosphonic acid and imidazole unit. This results in protonation of the 'free' nitrogen of the imidazole rings. The broadening of peak from 910 to 1200 cm^{-1} indicates the deprotonation of phosphonic acid units to form P-O^- .⁽¹⁶⁴⁾ Correspondingly, the protonation of the 'free' nitrogen of the imidazole rings to form imidazolium ion can be indicated by the appearance of a strong peak near 1617 cm^{-1} ($\nu(\text{H-Im}^+-\text{H})$).⁽¹⁶⁴⁾ The N-H stretching peak being relatively increased at 3150 cm^{-1} is another proof of protonation. The frequencies and assignments of several characteristic vibrations of pure compound and copolymers are reported in Table 6.16.

Table-6.16: IR Vibrations in wave numbers (cm^{-1})

P4VIm	PVPA	Copolymer	Attribution ^(157, 164)
3200 (b)		3400, 3150 (b)	ν (N-H)
	2850-2750		ν (PO-H)
1650-1570			ν (C=N, C=C)
		1610	ν (H-Im ⁺ -H)
	1150		ν_{st} (P=O)
		1200-910	ν (P-O)
	1040-910		ν_{as} (P-O)H
800-700			ν (C=C)

Thermogravimetric analyses were performed under an inert atmosphere (Fig. 6.11).

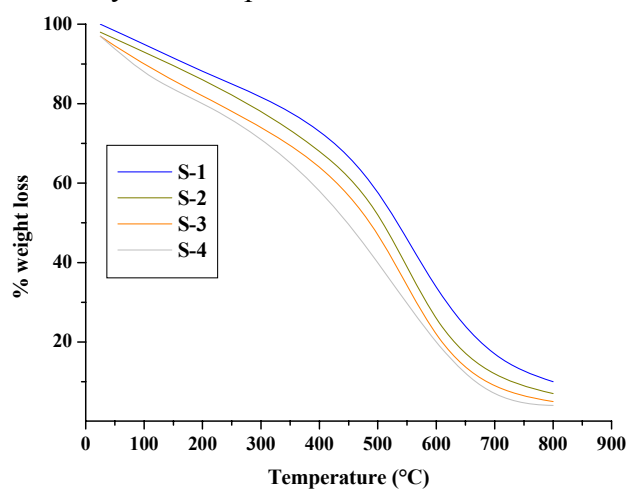


Fig. 6.11: TGA curves of poly(4-VIm-VPA) which were recorded under N₂ with a heating rate of 10 K/min.

The samples were dried 2 days at 70 °C prior to measurement. The initial weight reduction starts around 170 °C because of condensation of the phosphonic acid units. At 200 – 300 °C, the carbon-phosphorus chains decompose by becoming dark. The degradation of imidazole fragments occurs in the temperature of 300 – 400 °C. It has previously been noted that poly(vinylphosphonic acid) cross-linked PBI membranes are stable up to 175 °C (Chapter – IV, Sec- 4.6).

6.6.3 Proton conductivity properties of poly(4-VIm-co-VPA)

The proton conductivity measurement of the copolymer was carried out by impedance spectroscopy as shown in Table 6.17. Membranes were prepared by casting the water solution of copolymer and dried at 100 °C for 48 hrs.

Table-6.17: Proton conductivity measurements of poly(4-VIm-co-VPA)

No.	Temp.	S-1 (S/cm)	S-2 (S/cm)	S-3 (S/cm)	S-4 (S/cm)
1	20 °C	1.2×10^{-12}	2.7×10^{-12}	4.6×10^{-12}	7.1×10^{-12}
2	40 °C	4.1×10^{-11}	8.9×10^{-11}	1.4×10^{-10}	3.8×10^{-10}
3	60 °C	3.7×10^{-10}	6.1×10^{-9}	8.1×10^{-9}	2.1×10^{-8}
4	80 °C	7.5×10^{-9}	5.8×10^{-8}	6.9×10^{-8}	9.8×10^{-8}
5	100 °C	6.9×10^{-8}	2.3×10^{-7}	4.7×10^{-7}	6.3×10^{-7}
6	120 °C	2.9×10^{-7}	9.7×10^{-7}	2.5×10^{-6}	4.7×10^{-6}
7	140 °C	8.1×10^{-7}	1.3×10^{-6}	3.9×10^{-6}	5.6×10^{-6}
8	160 °C	1.7×10^{-6}	7.3×10^{-6}	8.7×10^{-6}	9.7×10^{-6}

*The glass transition temperature of the membrane was 10 °C.

As recorded in Table 6.17, the conductivities range from 10^{-6} to 10^{-12} S/cm within the measured regime. The poor conductivity of poly(4-VIm-co-VPA) may be due to ionic cross-linking by phosphonic acid and imidazole units, which restricts the mobility of the proton. Fig. 6.12 shows a comparison of the temperature-dependent conductivities of poly(4-VIm-co-VPA) samples. Clearly, the DC conductivities of the copolymer samples increase with increasing phosphonic acid in the copolymer.

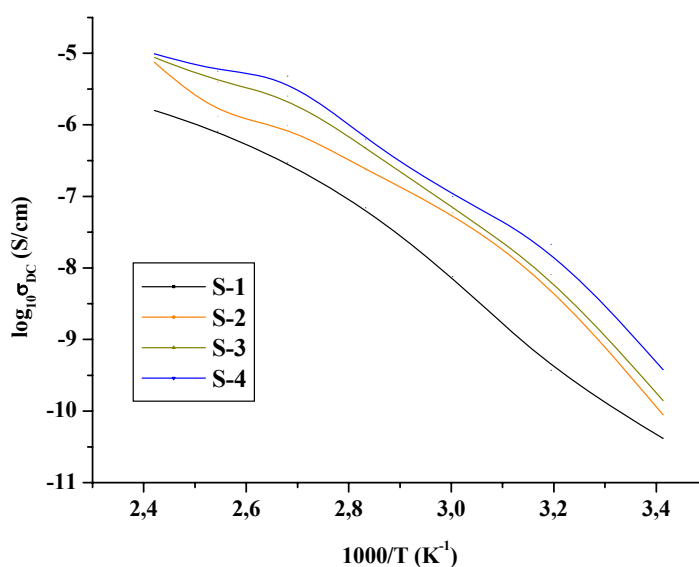


Fig. 6.12: Temperature dependence of DC conductivity of poly(4-VIm-co-VPA)

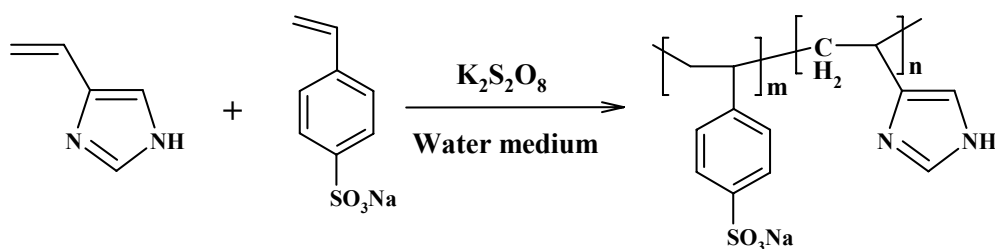
Recently, Hertz presented synthesis of flexible polymer membrane containing imidazole terminated polysiloxane architectures. Conductivities of 6×10^{-4} S/cm at 200 °C were obtained for the undoped polystyrene-based material. This in accordance with the results of Münch, who synthesized highly flexible imidazole-terminated ethyleneoxide oligomers,⁽²³³⁾ gave proton conductivities up to 5×10^{-3} S/cm at 120 °C indicating the segmental motion of the polymer chain to be the dominant conduction process. Because of absence of segmental mobility in poly(4-VIm-co-VPA), the proton conductivity reduced up to 10^{-6} S/cm.

With respect to the development of new separator materials in a low humidity environment, the possibility to introduce phosphonic acid functions into ethylene oxide oligomer should be considered. In addition, thermal stability of the membrane must be improved to get an ideal membrane for fuel cell application.

6.6.4 Radical copolymerisation of 4-styrenesulfonate and 4-vinylimidazole [poly(4-SSA-co-4-VIm)]

The radical copolymerisation of 4-vinylimidazole with 4-styrenesulfonate was carried out in water medium at 80°C as shown in Scheme- 6.18. The copolymer was purified by dissolving it in water and then precipitated in acetone. Yield was more than 90 % using 1:1 feed ratio of monomers.

Scheme- 6.18: Radical co-polymerization of 4-vinylimidazole with 4-styrenesulfonate



The copolymer was characterized by GPC with a number average molecular weight of 6.5×10^4 g/mol. The copolymer was further characterized by ^1H NMR spectroscopy as illustrated in Fig. 6.13.

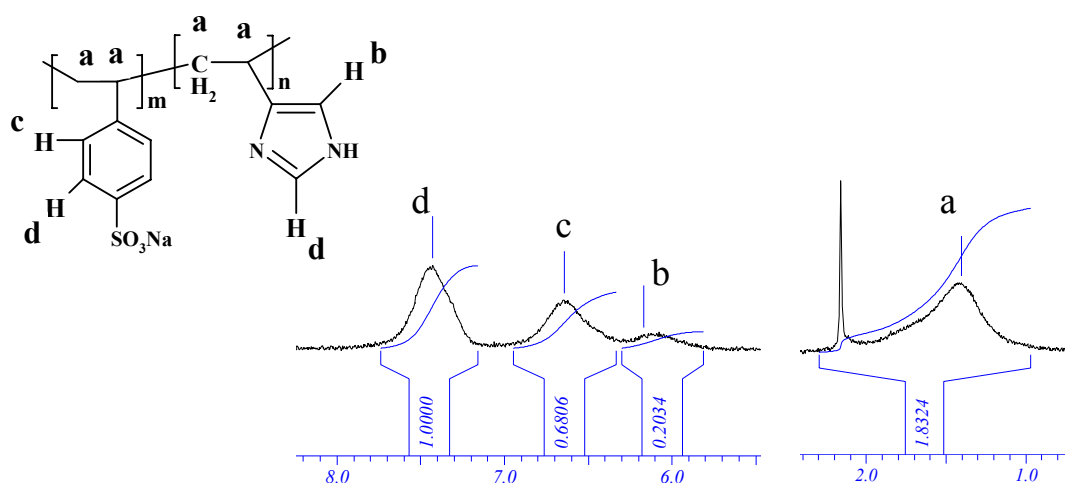


Fig. 6.13: ^1H NMR (250 MHz, D_2O) spectrum of poly(4-vinylimidazole-co-styrenesulfonate)

The signal appearing at 7.4 ppm corresponds to two hydrogen atoms from benzene sulfonate ring, as well as hydrogen atom from $(-\text{N}=\text{CH}-\text{NH}-)$ imidazole ring. Further, the signals representing at 6.2 ppm agree for $(-\text{CH}=\text{C})$ hydrogen atom from imidazole ring and at 6.6 ppm for two hydrogen atoms agree well with benzene sulfonate ring.

From Fig. 6.9, intensity of a hydrogen in the benzene sulfonate ring = $0.68/2 = 0.34$.

Intensity of a hydrogen from imidazole ring = 0.20.

Copolymer composition =

$$\frac{\text{Integrated intensity of a proton in the benzene sulfonate ring}}{\text{Integrated intensity of a proton from imidazole ring}} = \frac{0.34}{0.2} = 1.7$$

Therefore the copolymer contains 2:1 ratio of 4-styrenesulfonate and 4-vinylimidazole.

The copolymer was also characterized by FTIR spectroscopy.

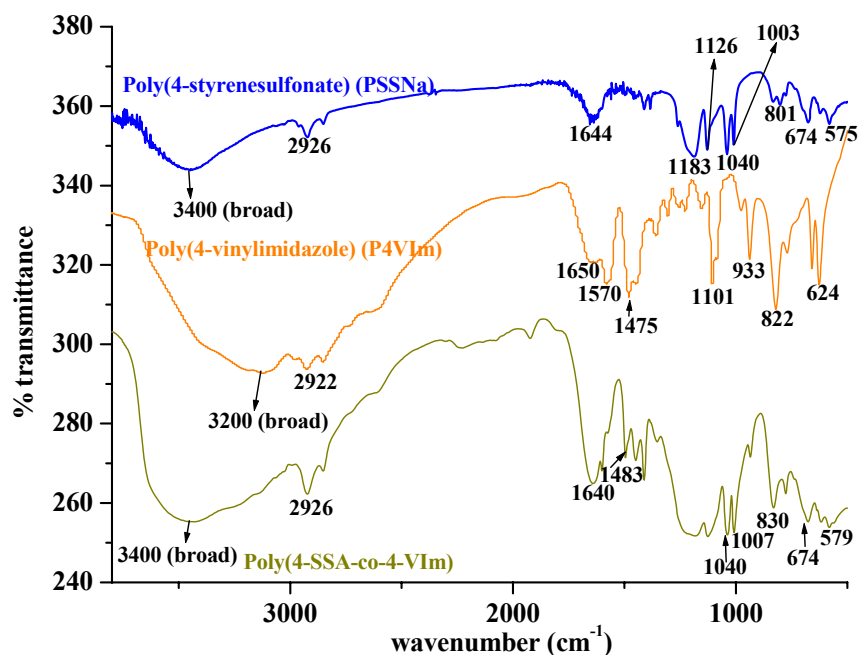


Fig. 6.14: FTIR spectra of PSSNa, P4VIm, and copolymer

Fig. 6.14 presents the IR spectra of PSSNa, P4VIm and its copolymer. In PSSNa, the peak at 1003 cm^{-1} is assigned to in-plane bending of the para-substituted benzene ring, normally appears at 1013 cm^{-1} in completely dry sample.⁽²²⁶⁾ The sharp peak at 1040 cm^{-1} is assigned to symmetric stretching of SO_3^- ;⁽²²⁶⁾ Hydrogen bond formation between aryl- SO_3Na and (residual) water in the solid state results in a band broadening at 3400 cm^{-1} .⁽²²⁶⁾

In the copolymer, broad absorption band in the region at $3500\text{--}2800\text{ cm}^{-1}$ indicates the hydrogen bonding between $-\text{SO}_3\text{Na}$ and $-\text{NH}$ group. The characteristic imidazole ring stretching vibrations appear in the region at $1650\text{--}1570\text{ cm}^{-1}$ and the appearance of C-H out-of-plane vibrations in an unsaturated double group of the imidazole ring at $800\text{--}700\text{ cm}^{-1}$ confirm the imidazole ring in the copolymer. The presence of the styrene sulfonate group in the copolymer is verified by the appearance of band at 1040 cm^{-1} for symmetric stretching of $-\text{SO}_3^-$ group and a band at 1007 cm^{-1} for a para-substituted benzene ring.

The frequencies and assignments of several characteristic vibrations of pure compound and blends are reported in Table 6.18:

Table-6.18: IR vibrations in wave numbers (cm^{-1})

P4VIm	PSSNa	Copolymer	Attribution ^(157, 226)
3200 (b)			ν (N-H)
	3400 (b)		ν ($\text{SO}_3^- \text{Na}-\text{H}_2\text{O}$)
		3500 (b)	ν (N-H- SO_3^-)
1650-1570		1650-1570	ν (C=N, C=C)
	1040	1040	ν_{st} (SO_3^-)
	1003	1007	ν_{ben} (p- C_6H_5)
800-700		800-700	ν (C=C)

6.6.5 Proton conductivity properties of poly(4-SSA-co-4-VIm)

The proton conductivity measurements of the copolymer were carried out by impedance spectroscopy as shown in Table 6.19. Membranes were prepared by casting a water solution of the copolymer after converting the sodium salt of 4-styrenesulfonate into 4-styrenesulfonic acid by passing through Amberlite IR-120 (Plus) Ion Exchange Resin as water solution.

Table-6.19: Proton conductivity measurements of poly(4-SSA-co-4-VIm)

Ex.No.	Temperature	Proton conductivity (S/cm)
1	20 °C	8.0×10^{-11}
2	40 °C	7.2×10^{-10}
3	60 °C	5.7×10^{-9}
4	80 °C	2.9×10^{-8}
5	100 °C	8.7×10^{-8}
6	120 °C	1.4×10^{-6}
7	140 °C	8.3×10^{-6}
8	160 °C	1.3×10^{-5}

*The glass transition temperature of the membrane was 132 °C.

As recorded in Table 6.19, at low temperatures, the conductivity of the copolymer is very low due to strong ion-pair interaction between acid and imidazole units. However, the conductivities increase gradually with temperature due to decreasing degree of ion-pair interaction.

The conductivities range from 10^{-5} to 10^{-11} S/cm within the measured regime. From the glass transition temperature (132 °C), the segmental motion will not play any role till 120 °C, therefore the proton hopping between the imidazole and acid units could possibly decide the conductivity in this measured regime. Comparing it with poly(styrene)-g-poly(styrenesulfonic acid),⁽²²⁶⁾ the conductivity of the graft copolymer is two order of magnitude higher indicating that absence of ionic cross-linking improves the conductivity significantly.

Hence, it should be recognized that imidazole based copolymer membranes such as poly(4-vinylimidazole-co-vinylphosphonic acid) and poly(4-styrenesulfonic acid-co-4-vinylimidazole), are unsuitable for high power density fuel cells because of poor proton conductivity due to strong ionic cross-link interaction. This work demonstrates unambiguously that segmental mobility can play a strong role in determining proton conductivity.

On the basis of these results, synthesis of triazole terminated flexible polymer chains, graft or block copolymers containing hydrophilic and hydrophobic segments should be focussed in future.

6.7 Summary

Vinylphosphonic acid was polymerized in solvents such as water, THF, ethyl acetate and ethanol. The highest molecular weight around 46×10^3 g/mol was achieved in ethyl acetate medium. From polymerization reactions of VPA, the chain transfer reaction decreases with decreasing polarity of the solvent, but increases polydispersity of the resulting polymer. In an effort to develop new phosphonic acid based membranes, synthesis and polymerization of trifluorovinylphosphonic acid should be considered, because fluorinated polymer backbone would provide good thermal stability and mechanical strength. And hence, the resulting polymer might be used directly as a membrane material in PEM applications.

Vinylbenzyl phosphonate was synthesized with excellent yield (95 %) in the presence of 6-tert-butyl-2,4-dimethylphenol (inhibitor) from vinylbenzyl chloride and triethyl phosphite. Vinylbenzyl phosphonate is a highly reactive monomer and molecular weight greater than 10×10^4 g/mol was obtained by radical polymerisation.

In terms of proton transport properties, the polymer chain mobility will play a very important role to enhance conductivity and hence, poly(vinylphosphonic acid) may give rise to better results than poly(vinylbenzylphosphonic acid).

2-Vinylbenzimidazole was synthesized with high yield (~ 80 %) at room temperature from triphenylphosphonium ylide by a Wittig reaction. It was polymerized by radical polymerization and resulting polymer has a very poor solubility in organic solvents. To improve the solubility of the polymer, the introduction of PO₃H containing alkyl groups should be considered.

Narrow disperse poly(4-styrenesulfonate) was synthesized by ATRP reaction in ethylene glycol solvent with excellent yield at 80 °C. The polymerisation reaction was very fast by the strong catalyzing effect of PMDETA when it is in excess during polymerisation. Further, a core-shell architecture based on polystyrene core with polystyrenesulfonate shell particles using ATRP reaction could be recommended for future work.

ATRP and TEMPO mediated controlled radical polymerization of 4-vinylimidazole led to low molecular weight polymers up to 7.1 g/mol. Due to poor thermal stability and side reactions, more new derivatives substituted with alkyl chains are needed to be synthesized and that would result in better chemistry of such materials.

Copolymers of 4-vinylimidazole and vinylphosphonic acid as well as 4-styrenesulfonic acid and 4-vinylimidazole were produced via radical copolymerisation of the corresponding monomers. The conductivities of the dry copolymers are between 10⁻⁵ and 10⁻¹² S/cm within the measured temperature regime. The poor conductivity of the copolymer might be due to absence of segmental mobility by strong ionic cross-link between the imidazole and phosphonic acid units. These results essentially demonstrate that random copolymers based on imidazole and acid units may not be a suitable membrane material. On the basis of this consideration, synthetic effort should be focused on (i) polymers with phosphonic acid or imidazole terminated side chains, and (ii) block and graft copolymers containing hydrophilic and hydrophobic segments for PEM applications.

7.1 Introduction

Poly[2,2'-(m-phenylene)-5,5'-bibenzimidazole] (PBI) is one of the most promising polymeric materials for high temperature fuel cell applications.⁽²²⁻²⁸⁾ It has excellent thermal and oxidative stability, nonflammability, chemical resistance, and good mechanical flexibility at elevated temperatures. However PBI has very poor solubility in most organic solvents with an exception for dimethylacetamide (DMAc) and concentrated sulphuric acid.

Modification of the structure of PBI to improve its solubility and proton conductivity without compromising the mechanical properties of PBI has been the focus of a lot of recent research efforts.⁽¹²⁶⁻¹³¹⁾ The most common approach to improve these properties is through the introduction of side chains.⁽¹³²⁻¹³⁹⁾ The NH group on the imidazole is easily functionalised to introduce side chains, such as N-alkyl sulfonic acid PBI, N-benzene sulfonic acid PBI, N-ethyl phosphonic acid PBI and their derivatives.⁽¹²⁶⁻¹⁴⁰⁾ Although PBI becomes a better conducting polymer after grafting, it loses the conductivity to a certain extent due to absence of proton transport path in N-substituted imidazole ring.⁽¹⁴¹⁾ In order to avoid grafting reaction in the imidazole ring, PBI that contains anthracene repeating unit (PBA) should be synthesized, because anthracene would encourage the modification reaction with an olefin by Diels-Alder reaction.

7.2 Synthesis of poly[9,10-bis-(benzimidazole-2-yl)anthracene] (PBA)

In order to study the polymerisation of 9,10-dicyanoanthracene with 3,3'-diaminobenzidine, a model reaction was carried out in polyphosphoric acid medium by condensation of 9,10-dicyanoanthracene with orthophenylene diamine at 200 °C as shown in scheme 7.1. The yield of the reaction was 70 %.

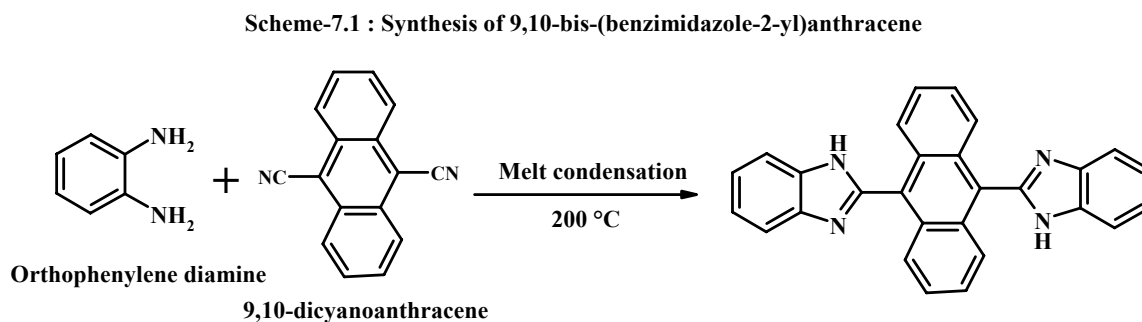


Fig. 7.1 displays the spectrum of 9,10-bis-(benzimidazole-2-yl)anthracene.

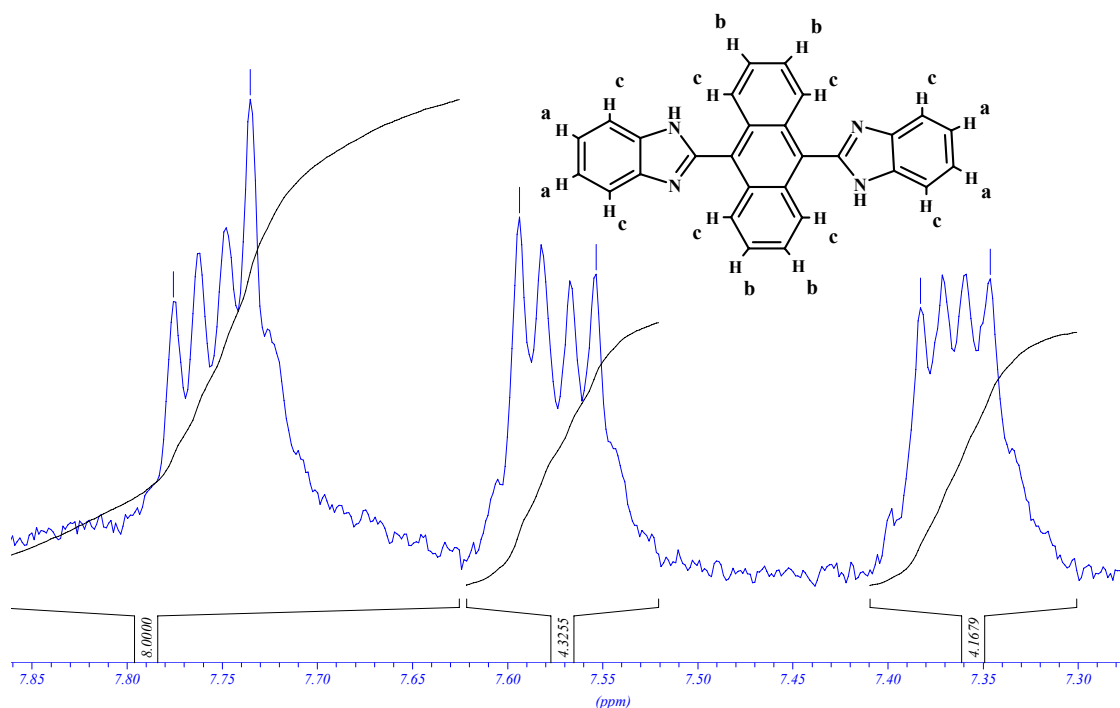


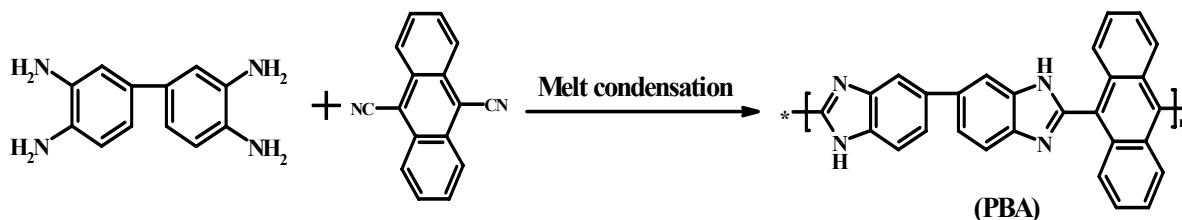
Fig. 7.1: ^1H NMR (250 MHz, $\text{D}_6\text{-DMSO}$) spectrum of 9,10-bis-(benzimidazole-2-yl)anthracene

The signals appearing for aromatic hydrogen at 7.3 ppm (4H), 7.5 ppm (4H), 7.7 ppm (4H) and 7.8 (4H) agree well with the structure of 9,10-bis-(benzimidazole-2-yl)anthracene.

Analysis by FD mass showed a molecular ion peak at m/e 410 (M^+), corresponding to 9,10-bis-(benzimidazole-2-yl)anthracene.

Following the conditions from the model reaction, the polymer was synthesized in polyphosphoric acid medium at 200 °C by melt condensation of 3,3'-diaminobenzidine with 9,10-dicyanoanthracene as given in scheme 7.2.

Scheme-7.2: Synthesis of PBA from 3,3'-diaminobenzidine and 9,10-dicyanoanthracene



The polymerization was carried out for different mole ratios of reactants as reported in Table 7.1.

Table-7.1: Stoichiometric control and molecular weights

Samples	Dicyano anthracene (mmol)	3,3'-diamino benzidine (mmol)	Reaction time (hrs)	Yield (%)	D.T* (°C)	Intrinsic viscosity (dl. g ⁻¹)
PBA-1	0.4	0.4	8	75	425	0.30
PBA-2	0.4	0.4	16	80	430	0.35
PBA-3	0.4	0.4	24	85	430	0.40
PBA-4	0.4	0.4	48	90	430	0.44
PBA-5	0.5	0.4	48	85	445	0.60
PBA-6	0.6	0.4	48	85	450	0.75

Note: D.T*- Decomposition temperature; All viscosity measurements were carried out in sulfuric acid;

As recorded in Table 7.1, when a 1:1 ratio of monomers was used at 200 °C, a low molecular weight polymer (PBA-1, PBA-2, PBA-3 and PBA-4) was obtained with intrinsic viscosities in the range of 0.3 to 0.4 dl/g. This can be attributed to stoichiometric imbalance created by sublimation of 9,10-dicyanoanthracene and hence, the excess of 3,3'-diaminobenzidine terminates the polymerization. As a result, the polymer contains amino end groups (Fig. 7.2).

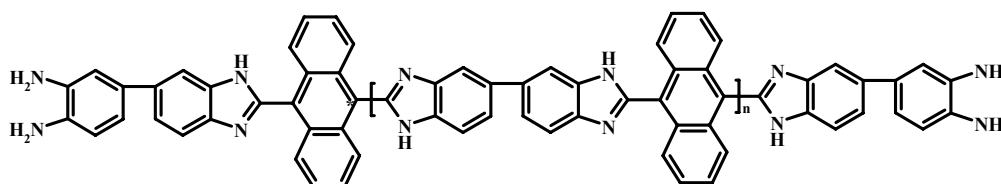


Fig. 7.2: PBA with amino end groups

Further, NMR spectroscopy confirms the presence of amino end groups as shown in Fig. 7.3.

In order to control stoichiometric imbalance, the polymerization reactions were also carried out in the presence of excess amounts of dicyanoanthracene in samples PBA-5 and PBA-6. The higher intrinsic viscosity values of samples PBA-5 and PBA-6 indicate that the molecular weight was increased in the presence of excess dicyanoanthracene during polymerization. Further, the samples (PBA-5 and PBA-6) were completely insoluble in common solvents with an exception for sulfuric acid.

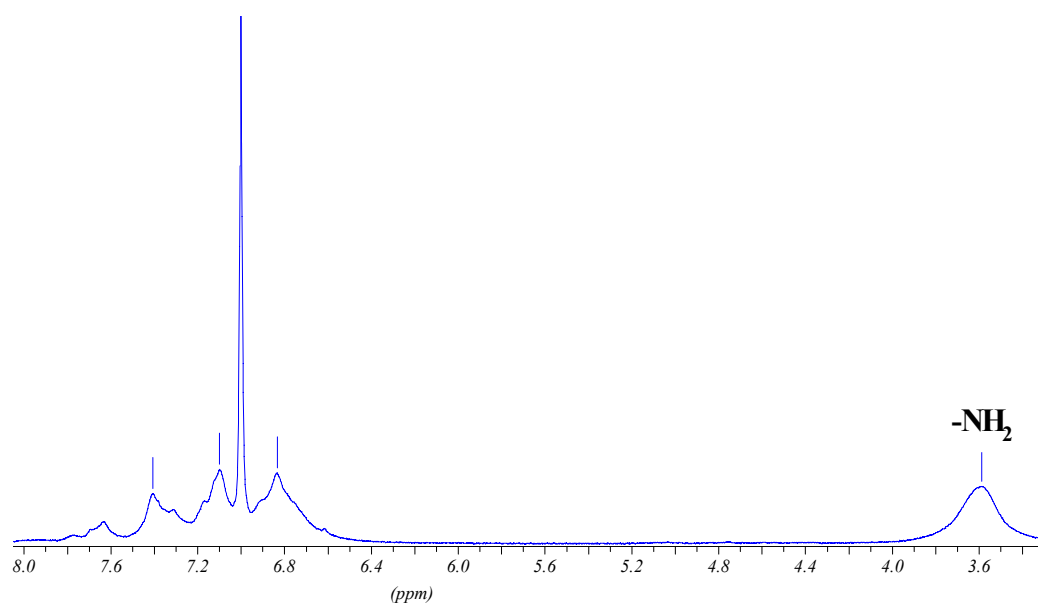


Fig. 7.3: ^1H NMR (250 MHz, $\text{D}_6\text{-DMSO}$) spectrum of poly(9,10-bis-[benzimidazole-2-yl]anthracene)

FT-IR spectroscopy was used to characterize the polymer as displayed in fig. 7.4.

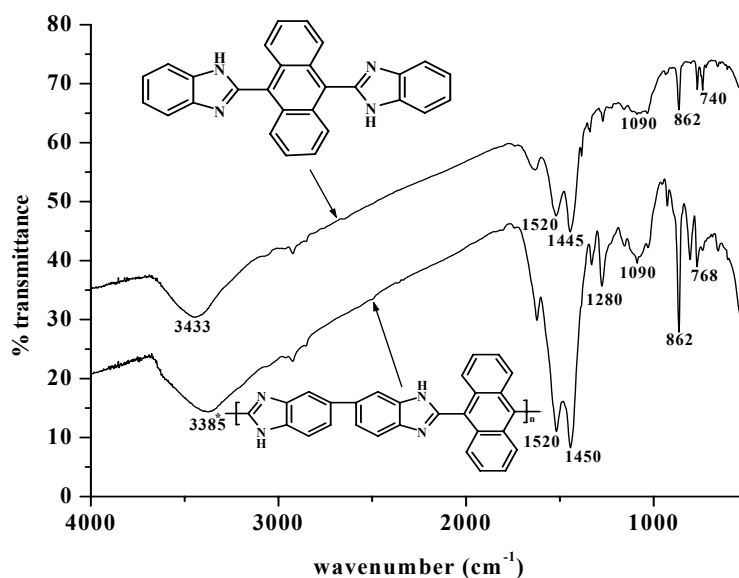


Fig. 7.4: FTIR spectra of model compound and PBA

The broad band at 3400 cm^{-1} in the spectrum of PBA and model compound are due to strong hydrogen bonding of the type $\text{N-H}\cdots\text{N}$. Bands derived from aromatic $\text{C}=\text{C}$ and $\text{C}=\text{N}$ stretching modes are found in the $1520\text{-}1450\text{ cm}^{-1}$ region. Bands from 700 to 1100 cm^{-1} are due to bending frequencies of aromatic rings.

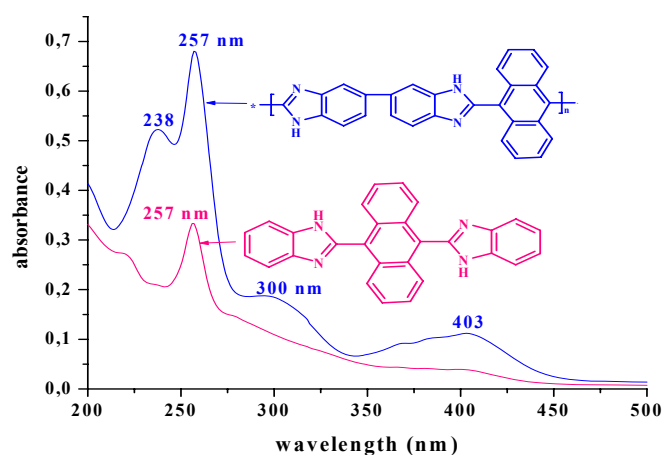


Fig. 7.5: UV-absorption of PBA and model compound

Fig. 7.5 shows the UV-vis absorption spectroscopy of PBA and model compound. PBA shows four different absorption peaks at 403 nm, 300 nm, 257 nm and 238 nm, whereas 9,10-bis-(benzimidazole-2yl)anthracene (model compound) shows the maximum absorption peak at 257 nm, 300 nm and 400 nm. The model compound and PBA are yellow in color due to visible light absorptions at 400 nm.

The thermal stability of polymers is very high, and its decomposition starts at 420 °C;

7.3. Conductivity of pure anthracene unit containing PBA versus N-allyl PBI

In order to compare the proton transport properties of PBA/H₃PO₄ membrane with N-allyl PBI/H₃PO₄ membrane, the conductivity measurement of parent polymer films were carried out to determine the difference in proton conductivity values in terms of ‘free imidazole’ with ‘N-substituted imidazole ring’.

The AC conductivities of the pure N-allyl PBI film (100 % modified sample) and PBA film are displayed in Figs. 7.6 and 7.7 versus frequency with temperature as the parameter. The measured conductivities were in the range of 10⁻¹⁸ – 10⁻¹⁵ S/cm with increasing temperature (10⁻¹ Hz - frequency region) for N-allyl PBI indicating that no proton conductivity can be expected in the absence of NH-groups in PBI. Whereas the observed conductivity of PBA was in the range of 10⁻¹³ – 10⁻⁹ S/cm with increasing temperature (10⁻¹ Hz - frequency region) illustrating the presence of NH group is an additional advantage for synthesizing highly conducting membrane materials with H₃PO₄.

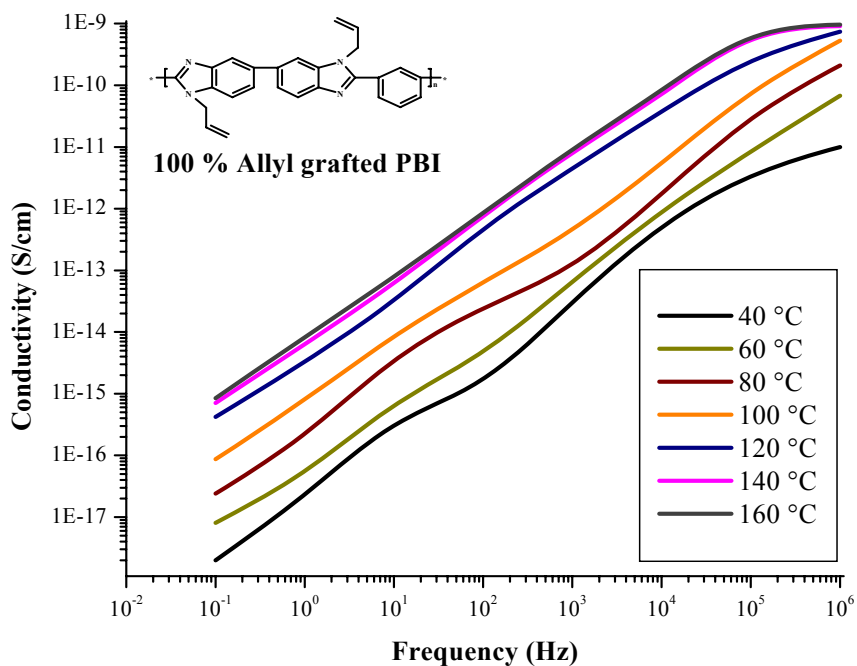


Fig. 7.6: Frequency dependent AC conductivity of 100 % allyl grafted PBI at different temperatures.

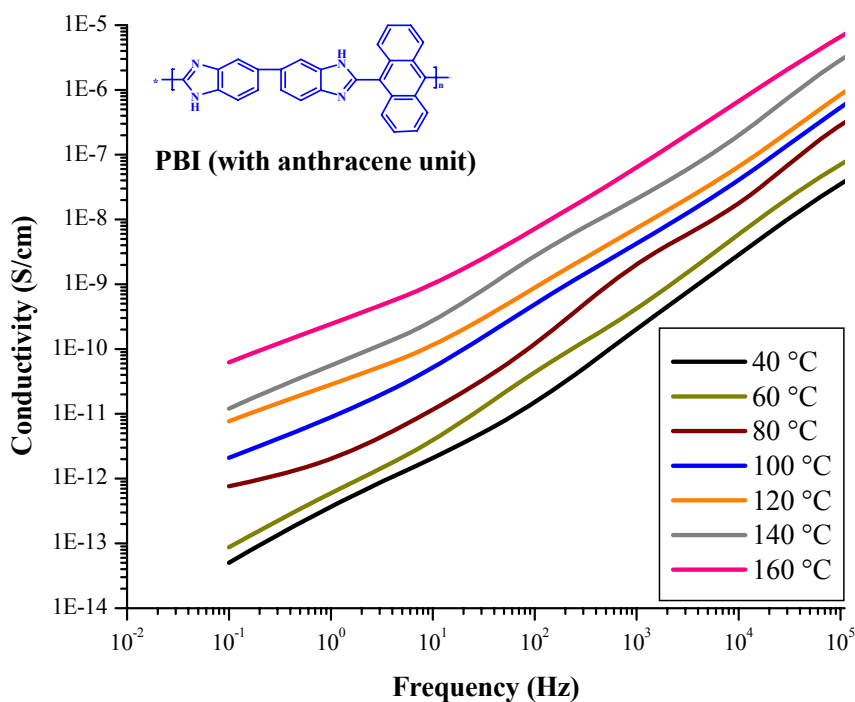


Fig. 7.7: Frequency dependent AC conductivity of PBA

On the basis of these measurements, the conductivity of the ‘free imidazole’ polymer was 10^6 times higher than the ‘N-substituted imidazole’ in the same temperature range.

7.4 General description of making H₃PO₄ blended polymer membranes

In order to measure the proton conductivity of H₃PO₄ doped PBA and H₃PO₄ doped N-allyl PBI, the DMAC solution of both polymers were taken separately in a 250 ml conical flask and mixed with H₃PO₄ solution to get an imidazole and acid composition ratio as 1:0.5. Then, it was placed in an ultrasonification bath for 2 hrs to make a homogeneous solution.

Membranes were cast using Petri dishes and then dried at 120 °C for 48 hrs to remove DMAC and water from membranes. DSC measurements were carried out to determine the glass transition temperature (T_g) of membranes. The proton conductivity was measured using impedance spectroscopy.

The proton conductivity of N-allyl PBI ½ H₃PO₄ membrane is given in Table 7.2.

Table-7.2: The temperature dependence on proton conductivity of acid blended N-allyl PBI

Ex.No.	Temperature	Conductivity of N-allyl PBI ½ H ₃ PO ₄ (S/cm)	Conductivity of PBA ½ H ₃ PO ₄ (S/cm)
1	20 °C	2.7 x 10 ⁻⁷	1.2 x 10 ⁻⁵
2	40 °C	3.4 x 10 ⁻⁷	4.7 x 10 ⁻⁵
3	60 °C	5.3 x 10 ⁻⁷	8.7 x 10 ⁻⁵
4	80 °C	7.0 x 10 ⁻⁷	2.0 x 10 ⁻⁴
5	100 °C	8.6 x 10 ⁻⁷	3.6 x 10 ⁻⁴
6	120 °C	1.2 x 10 ⁻⁶	4.1 x 10 ⁻⁴
7	140 °C	2.7 x 10 ⁻⁶	4.7 x 10 ⁻⁴
8	160 °C	6.3 x 10 ⁻⁶	5.4 x 10 ⁻⁴

*The glass transition temperature of the membrane: 165 °C.

As seen in Table 7.2, the conductivity of N-allyl PBI ½ H₃PO₄ membrane increases with temperature with a conductivity of 6.3 x 10⁻⁶ S/cm measured at 160 °C. The proton transport can be expected to occur by Grotthuss and Vehicular type mechanisms from phosphoric acid molecules. The segmental motion of the polymer chains would not play any role for proton transfer process due to high T_g of the membrane.

Further, the proton conductivity of PBA $\frac{1}{2}$ H₃PO₄ membrane increases with temperature and a maximum conductivity of 5.4×10^{-4} S/cm was measured at 160 °C. The proton transport process may be explained by phosphoric acid molecules as well as proton hopping between imidazole and acid molecules. The segmental motion of the polymer chain may not play any role for proton transfer process due to high T_g of the membrane (210 °C). Further, the reported proton conductivity of membrane synthesized from $\frac{1}{2}$ H₃PO₄ per imidazole molecules in PBI was in the range of 10^{-4} S/cm.⁽²²⁸⁾

On comparing the proton conductivity of N-allyl PBI $\frac{1}{2}$ H₃PO₄ with PBA $\frac{1}{2}$ H₃PO₄, the absence of proton hopping between imidazole and phosphoric acid units in N-allyl PBI membrane lowers the conductivity significantly.

However, when the number of H₃PO₄ molecules is increased to three per imidazole ring, there is no significant difference in proton conductivity values from both N-allyl PBI and PBA membrane materials (The maximum proton conductivity were in the range of 10^{-3} S/cm at 160 °C).

At high acid concentration, the proton transport occurs entirely by phosphoric acid molecules and therefore the contribution from proton transport by imidazole ring becomes insignificant. And hence, the conductivity differences are not high in both membranes; but at low acid concentration, the proton hopping from imidazole units also play an important role and therefore, the conductivity of PBA $\frac{1}{2}$ H₃PO₄ blend is higher than N-allyl PBI $\frac{1}{2}$ H₃PO₄ blend.

7.5 Unsuccessful attempt to synthesize Diels-Alder adduct of vinylphosphonic acid and PBA-1

PBA-1 and diethyl vinylphosphonate were dissolved in o-dichlorobenzene and heated at 180 °C. Unfortunately, vinylphosphate turns into brownish liquid due to thermal decomposition above 160 °C.

To perform this reaction, it would be appropriate to use trifluorovinylphosphonic acid, which could withstand at high temperatures without any change. Further the nitrogen atoms in the imidazole ring might undergo the Michael addition above 150 °C and hence, the imidazole ring should be protected before Diels-alder addition reaction.

7.6 Summary

The low molecular weight PBA was synthesized with the intrinsic viscosity ranging from 0.3 – 0.4 dl/g using 1:1 ratio of reactants. To synthesize high molecular weight polymer, the polymerization was also carried out in presence of excess 9,10-cyanoanthracene and its intrinsic viscosity was in the range of 0.6 - 0.75 dl/g.

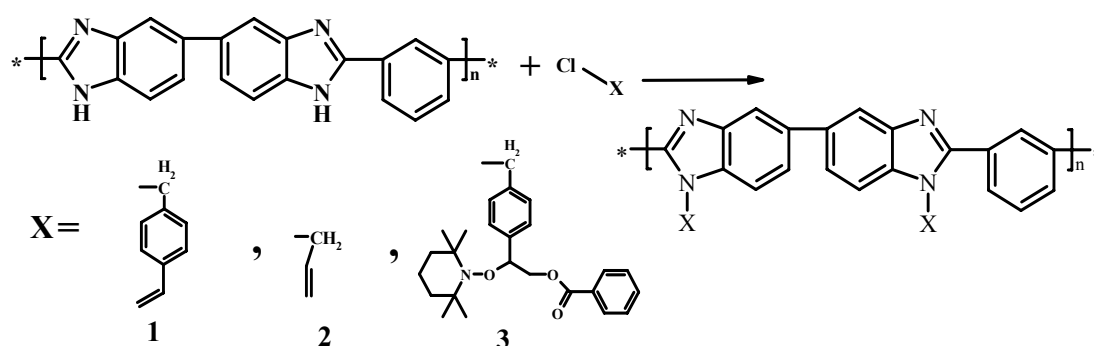
The proton conductivity of pure polymer and its acid blend was measured and compared with N-allyl grafted PBI and its acid blends. The conductivity of pure PBA and PBA $\frac{1}{2}$ H₃PO₄ polymer blend was higher than those of N-allyl grafted PBI and N-allyl PBI $\frac{1}{2}$ H₃PO₄ polymer blend. Whereas changing the blend composition to PBA 3H₃PO₄ and N-allyl PBI 3H₃PO₄, then the conductivity difference becomes insignificant. Therefore, this work demonstrates that modification of PBI by nucleophilic substitution reaction (N-substituted PBI) would lower the proton conductivity significantly at low acid concentration level. Further, the anthracene unit containing PBI would encourage the modification reaction by an anthracene ring with trifluorovinylphosphonic acid after protecting NH group of imidazole ring.

Summary

In order to synthesize proton-conducting materials which retain acids in the membrane during fuel cell operating conditions, the synthesis of poly(vinylphosphonic acid) grafted PBI as well as the fabrication of multilayer membranes are main focus of this thesis.

To synthesize graft-copolymers from PBI, it was functionalised with various reactive groups such as allyl groups, vinylbenzyl groups and TEMPO adduct groups as shown in scheme 8.1 below:

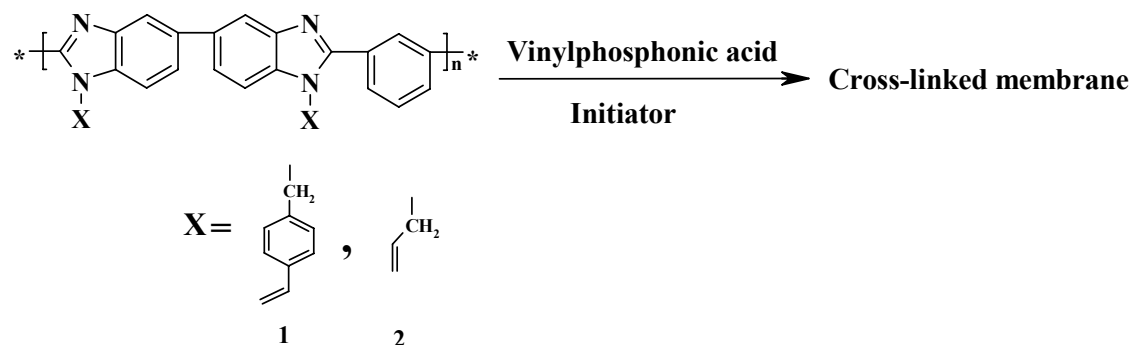
Scheme-8.1: Functionalisation of polybenzimidazole



Polybenzimidazole with degrees of modification ranging from 4 to 100 % were synthesized by nucleophilic substitution reactions. It was found that at constant temperature (80 °C), the modification degree (N-alkylation reactions in polybenzimidazole system) was mainly dependent on the deprotonation degree of PBI. Further, the modified PBIs were soluble in dichloromethane, chloroform, DMSO, DMAc and DMF.

The membrane was synthesized from allyl grafted PBI as well as from vinylbenzyl grafted PBI with VPA as given in scheme 8.2:

Scheme-8.2: PVPA grafted PBI



The membranes prepared from these modified PBIs exhibited the conductivities in the range of 10^{-5} S/cm to 10^{-2} S/cm. Maximum proton conductivity around 10^{-2} S/cm was reached for membranes that had VPA units of seven or more per benzimidazole ring and is comparable with H_2SO_4 doped PBI membrane,^(34-36, 61) H_2SO_4 doped sulfonated PBI polymer blends,⁽³⁷⁻⁴¹⁾ H_3PO_4 doped PBI membrane,^(29,57-61) KOH doped PBI membrane,⁽³⁰⁾ and NAFION type membranes,⁽²⁻⁴⁾ whose conductivity values are in the range of 10^{-2} S/cm. Further, the proton conductivity values were unchanged after several repeated water washings of the membranes indicating that the PVPA cross-linked PBI can retain acids in the membranes during fuel cell operating conditions. Unfortunately, the swelling of PVPA cross-linked PBI membranes after prolonged exposure in water and the thermal stability of the PVPA chains up to 175 °C limit its potential application as membrane materials.

To reuse the membrane, there is a need to synthesize a solvent soluble PVPA grafted PBI membrane by reacting TEMPO adduct grafted PBI with VPA in presence of acetic anhydride as an activator.⁽²²⁹⁾ Further, synthesizing PVPA oligomer with Br- or I- end groups by 'Telomerization' (Free radical polymerisation of VPA in presence of CHBr_3 or CHI_3) and subsequent grafting onto polybenzimidazole chain by nucleophilic substitution reaction would also be a suitable method to synthesize solvent soluble poly(vinylphosphonic acid) grafted PBI membrane.

The low thermal stability of poly(vinylphosphonic acid) chain (up to 175 °C) in the graft-copolymer membrane prevents the performance for high temperature applications above 175 °C. To replace poly(vinylphosphonic acid), the future research should be focused on synthesizing poly(trifluorovinylphosphonic acid) grafted PBI membranes as poly(trifluorovinylphosphonic acid) chain would increase the thermal stability of graft copolymer.

The applications of LBL films have been extended to PBI, P4VIm, PVPA and PVSA polymer electrolytes that are appropriate for proton exchange membrane. For a stiff polymer such as PBI, the LBL films were highly smooth and uniform which were followed by UV absorbance and thickness measurement by profilometry. However in flexible polymer such as poly(4-vinylimidazole), the LBL films were smooth and uniform till 16-layer film and the linearity was lost with additional number of layers indicating the nonuniform assembling of polymers.

From proton conductivity measurements of LBL films, the surface roughness plays a critical role in proton transport process. For all proton-conductivity measurements, high surface roughness films (greater than 10 % of thickness) were studied, which is convenient to measure the resistance of the film. The proton conductivity increases with smoothness of the film on the surface, and the measured maximum conductivities were in the range of 10^{-4} S/cm at room temperature (under dry state) for P4VIm/PVPA LBL films, which is one order of magnitude greater than any LBL polymer electrolyte studied thus far.^(108, 114-115) From proton transport properties, the number of protons as well as the mobility may appear to enhance proton conduction. This suggestion is contradicted by comparison with the literature, which demonstrates that it is the number of ions that determine the conductivity and not mobility, as it is restricted by strong ionic interaction between polymer chains in the multilayer. Whereas in imidazole based multilayers, the imidazole ring could allow the proton mobility by Grotthuss type mechanism.

For PBI/PVPA and PBI/PVSA based multilayer films, the conductivity was measured only from 10^{-6} S/cm preventing the comparison with other polymer electrolyte membranes that are known in the literature. With regard to the conductivities of PVPA with PVSA based multilayers, the higher acidity of the latter led to a proton conductivity up to 7×10^{-6} S/cm. Despite the high conductivity of PVSA based multilayer membranes, the brittle nature of PVSA would restrict its application. Therefore PVPA based PBI LBL film would emerge as a suitable membrane material in PEM applications due to its excellent uniformity and high thermal stability. Further, the membranes were unaffected in water indicating LBL membranes are more suitable for fuel cell applications than PVPA cross-linked PBI materials.

Future work should focus on constructing LBL thin film on top of porous polycarbonate membrane.⁽²²¹⁾ An important advantage of this approach is that the LBL thin-film membrane constructed on either side of a nano- or micro- porous polycarbonate membrane would serve as the PEM for the fuel cell. Further, there is a need to explore on measuring the proton conductivity of highly ordered thin LBL films by a suitable method.

For the synthesis of anhydrous proton conducting homo and copolymers, the poly(vinylphosphonic acid) was synthesized with molecular weights in the range of 3.0×10^3 g/mol to 46×10^3 g/mol. From polymerization reactions of VPA, the chain transfer reaction decreases with decreasing polarity of the solvent, but polydispersity was increased significantly. To replace VPA, synthesis and polymerization of trifluorovinylphosphonic acid could be suggested in PEM applications. This polymer would exhibit high thermal stability and so might be used in PEMFC directly.

Vinylbenzyl phosphonate was synthesized in high yield (70 %) in the presence of 6-tert-butyl-2,4-dimethylphenol (inhibitor) from vinylbenzyl chloride and triethyl phosphite. Further, poly(vinylbenzyl phosphonate) having the molecular weights up to 10.0×10^4 g/mol were synthesized with excellent dispersity by radical polymerisation of vinylbenzyl phosphonate. For PEM applications, poly(vinylphosphonic acid) may give better results than poly(vinylbenzylphosphonic acid) in terms of mobility of the polymer chain is concerned.

2-Vinylbenzimidazole was synthesized with high yield (~ 80 %) at room temperature from triphenylphosphonium ylide by a Wittig reaction. It was polymerized by radical polymerization and resulting polymer has a very poor solubility in organic solvents. To improve the solubility of the polymer, the introduction of PO_3H containing alkyl groups should be considered.

Poly(4-styrenesulfonate) was synthesized by ATRP reaction in ethylene glycol solvent with excellent yield at 80 °C. On the basis of this reaction, a core-shell particle of PS (core) with PSSNa (shell) could be recommended to replace Nafion type membranes for fuel cell applications.

ATRP and TEMPO mediated controlled radical polymerization of 4-vinylimidazole led to low molecular weight polymers up to 7.1 g/mol. Because of poor thermal stability and side reactions, more new derivatives substituted with alkyl chains are needed to be synthesized and that would result in better chemistry of such materials.

For the synthesis of proton conducting copolymers, the radical copolymerisation reactions were carried out with vinylphosphonic acid and 4-vinylimidazole as well as 4-styrenesulfonic acid and 4-vinylimidazole. The proton conductivities of the copolymers were between 10^{-5} and 10^{-12} S/cm. Comparing with poly(styrene)-g-poly(styrenesulfonic acid), the conductivity of the graft copolymer was two order of magnitude higher indicating that absence of ionic cross-linking improves the conductivity significantly. These results indicate that imidazole based random copolymers may not be a suitable membrane material for fuel cell applications. In order to achieve better performance, synthesis of (i) polymers with phosphonic acid or triazole terminated side chains, and (ii) block and graft copolymers containing hydrophilic and hydrophobic segments should be considered for PEM applications.

Polybenzimidazole with anthracene structural units (PBA) were synthesized having intrinsic viscosities in the range of 0.3 - 0.75 dl/g. The proton conductivity of pure PBA and PBA $\frac{1}{2}$ H₃PO₄ polymer blend were higher than pure N-allyl grafted PBI and N-allyl PBI $\frac{1}{2}$ H₃PO₄ polymer blend. Further, the anthracene unit containing PBI would encourage the modification reaction by an anthracene ring with trifluorovinylphosphonic acid after protecting NH group in the imidazole ring.

9.1 General Methods

^1H NMR and ^{13}C NMR spectra were recorded in CDCl_3 , DMSO-d_6 and D_2SO_4 on a Bruker DPX 250, Bruker AMX 300 or Bruker DRX 500 spectrometer with use of the solvent proton or carbon signal as internal standard. Infrared spectra were recorded on a Nicolet FT-IR 320 spectrophotometer as KBr pellets or as films between NaCl discs. Absorption spectra were recorded on Elmer Lambda 9 UV-vis-NIR spectrometer at room temperature. Mass spectra were obtained on a VG Instruments ZAB 2-SE-FPD. Melting points were determined on a Büchi hot stage apparatus and are uncorrected. Elemental analyses were carried out on a Foss Heraeus Vario EL.

Differential scanning calorimetry (DSC) was measured on a Mettler DSC 30 with heating and cooling rates of 10 K/min. First order transition temperatures were reported as the minima of their endothermic peaks during heating. Ubbelohde viscosimeter was employed to measure intrinsic viscosity. A Zeiss Axiophot with a nitrogen flushed Linkam THM 600 hot stage was used to characterize the polarization microscopy textures.

X-ray reflectivity measurements were conducted at a Seifert XTD 3003 TT X-ray diffraction system operated in reflectivity mode equipped with a Goebel Mirror as a monochromator at a fixed wavelength of $\lambda = 1.54 \text{ \AA}$. The thickness and the roughness of films were measured using a Tencor P-10 surface profiler. Gold lines that were 3 mm wide and 300 nm in thickness were evaporated using a Blazers-BAE 250 coating system at a base pressure of 2×10^{-6} Torr.

Impedance measurements were carried out on a Solartron model 1260 Impedance/Gain-Phase Analyser that has a frequency range of 10 μHz to 32 MHz. The AC amplitude was 25 mV with no DC bias. Data analysis and simulations were done using the ZView program made by Scribner Associates, Inc.;

9.2 Materials

9.2.1 Poly(benzimidazole) [PBI]

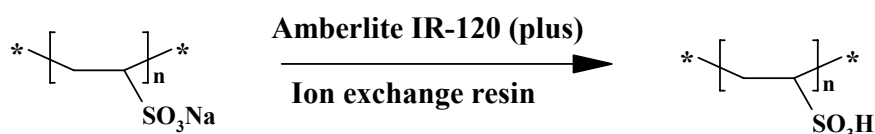
Commercial poly(benzimidazole) [PBI] was obtained as a gift from Celanese Ventures GmbH, Frankfurt has an intrinsic viscosity of 0.89 dl/g indicating the number average molecular weight around 22×10^3 g/mol with polydispersity of 2.1.

9.2.2 Poly(vinylphosphonic acid) [PVPA]

Poly(vinylphosphonic acid) (PVPA) was purchased from Polysciences and has an average molecular weight of 2.00×10^4 g/mol.

9.2.3 Poly(vinylsulfonic acid) [PVSA]

Poly(vinylsulfonic acid) was purchased from Aldrich Inc, as sodium salt solution in water (25 wt. %, estimated molecular weight $\sim 980 - 1100$ g/mol; $M_n \sim 8.0-10.0 \times 10^3$ g/mol). It is converted into poly(vinylsulfonic acid) by passing through Amberlite IR-120 (Plus) Ion Exchange Resin as 25 % water solution.



25% water solution, pH~1.2

9.2.4 Poly(4-styrenesulfonic acid) [PSSA]

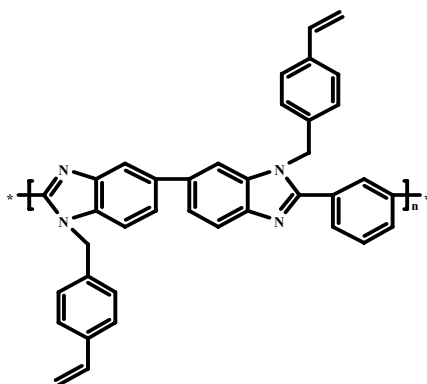
Poly(4-styrenesulfonic acid) was purchased from Aldrich Inc., as 18 wt. % in water with $M_w \sim 7.5 \times 10^4$ g/mol.

9.2.5 Other materials

N,N-Dimethylacetamide [DMAc], 3-(ethoxydimethylsilyl)propylamine, 2-mercaptoethanesulfonic acid (as $3.0 \text{ M} \pm 0.1 \text{ M}$) solution was purchased from Sigma-Aldrich Inc. Quartz microscope slide ($76.2 \times 25.4 \times 1.00$ mm) was purchased from Alfa Aesar Inc.

9.3 Syntheses

9.3.1 Synthesis of vinylbenzyl grafted PBI



In a 250 mL round bottom flask, 10% PBI in N,N-Dimethylacetamide (DMAc) solution was diluted by addition of equal volume of DMAc. Then the solution was mixed with sodium hydride (2 equivalence per benzimidazole repeat unit) and refluxed at 80 °C for 4 h creating the PBI polyanion. With deprotonation, the previously dark-brown PBI solution changed to a very deep red with a noticeably higher viscosity. Subsequent treatment of this polyanion with p-vinylbenzyl chloride (2 eq.) for 15 hrs at 80 °C resulted in the vinylbenzyl grafted PBI. The reaction mixture was cooled to room temperature and was precipitated in hexane. The precipitate was dissolved in dichloromethane and then again precipitated in hexane to remove DMAc completely from the grafted polymer. The modified PBI with different degrees of modification were synthesized by changing NaH and vinylbenzylchloride concentrations are as follows- NaH- 1.3, 0.9, 0.7, 0.3, 0.13, 0.07 and 1.3 mmol; VBC- 1.3, 0.9, 0.7, 0.3, 0.13, 0.07 and 1.3 mmol. Amount of PBI-1.3 mmol.

^1H NMR (250 MHz, CDCl_3 , 298 K) δ [ppm]: 5.1 (s, 1H), 5.3 (s, 2H), 5.6 (s, 1H), 6.5 (s, 1H), 6.8 - 8.0 (m, 18H).

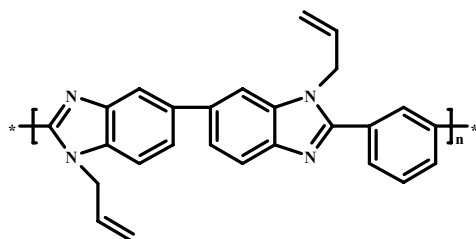
IR (KBr) [cm^{-1}]: 3070 and 2920 ($-\text{CH}_2-$), 1620 and 1460 (Ar);

EA: Calcd for 100 % vinylbenzyl grafted PBI $-(\text{C}_{38}\text{H}_{30}\text{N}_4)_n$ - : C, 84.1; H, 5.57; N, 10.32. Found: C, 80.81; H, 5.97; N, 10.55. (Difference in values due to presence of water in polymer).

Intrinsic viscosity (Degree of modification ~ 100 %): 0.68 $\text{dl}\cdot\text{g}^{-1}$.

TGA/DSC (± 10 K/min): 450 °C.

9.3.2 Synthesis of allyl grafted PBI



In a 250 mL round bottom flask, 10 % PBI solution in N,N-Dimethylacetamide (DMAc) was diluted by addition of equal volume of DMAc. Then the solution was mixed with sodium hydride (2 equivalence per benzimidazole repeat unit) and refluxed at 80 °C for 4 h. Subsequent treatment of this polyanion with allyl chloride (2 eq.) for 15 hrs at 80 °C resulted in the allyl grafted PBI. The reaction mixture was cooled to room temperature and was precipitated in hexane. The precipitate was dissolved in dichloromethane and then again precipitated in hexane to remove DMAc completely from the grafted polymer. The modified PBI with different degrees of modification were synthesized by changing NaH and allylchloride concentrations are as follows- NaH- 1.3, 1.0, 1.0, 0.2, 0.13, 0.01 and 0.07 mmol; A.C- 1.3, 1.0, 1.3, 0.2, 0.13, 0.1, 0.07 and 1.3 mmol. Amount of PBI-1.3 mmol.

^1H NMR (250 MHz, CDCl_3 , 298 K) δ [ppm]: 4.9 (s, 2H), 5.17 (dd, $J = 5.6$, 1H), 5.34 (dd, $J = 4.1$, 1H), 6.1 (s, 1H), 7.4-8.1 (mm, 10H).

IR (KBr) [cm^{-1}]: 3070 and 2920 ($-\text{CH}_2-$), 1635 and 1460 cm^{-1} (Ar);

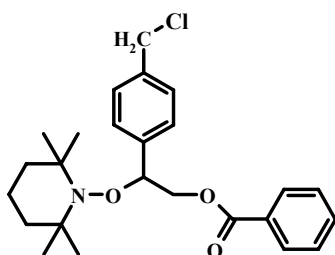
EA: Calcd for 100 % allyl grafted PBI $-(\text{C}_{26}\text{H}_{20}\text{N}_4)_n-$: C, 80.39; H, 5.19; N, 14.42.

Found: C, 78.11; H, 6.17; N, 14.64. (Difference in values due to presence of water in polymer).

Intrinsic viscosity (Degree of modification ~ 100 %): 0.69 dl. g^{-1} .

TGA/DSC (± 10 K/min): 420 °C.

9.3.3 Synthesis of benzoic acid 2-(4-(chloromethyl)phenyl)-2-(2,2,6,6-tetramethylpiperidin-1-yloxy)ethyl ester [TEMPO – adduct]¹⁵²



TEMPO - adduct was synthesized as described in the literature.⁽¹⁵²⁾ Benzoyl peroxide (2.0 g, 8.3 mmol) and TEMPO (2.84 g, 18.2 mmol) were dissolved in 4-vinylbenzyl chloride (80 mL). The mixture was heated for 24 h at 80 °C. The reaction mixture was cooled to room temperature and the excess 4-vinylbenzyl chloride was removed by a rotatory evaporator under high vacuum. The recovered 4-vinylbenzyl chloride had a reddish color due to some codistilled TEMPO. The crude dark-colored residue was chromatographed over silica gel using a gradient elution which was started with 30 % CH₂Cl₂ in hexane and gradually increased to 100 % CH₂Cl₂. The pure product was isolated as clear colourless oil with a 40 % yield. b.p. 217 °C.

¹H NMR (250 MHz, CDCl₃, 298 K) δ [ppm]: 1.8 (s, 3H), 1.1 (s, 3H), 1.4 (s, 3H), 1.2-1.6 (m, 6H), 4.5 (dd, *J* = 11, 6.4 Hz, 1H), 4.6 (s, 2H), 4.8 (dd, *J* = 11, 4.6 Hz, 1H), 5.0 (dd, *J* = 5.2, 5.2 Hz, 1H), 7.3 - 7.6 (m, 7H), 7.9 (m, 2H).

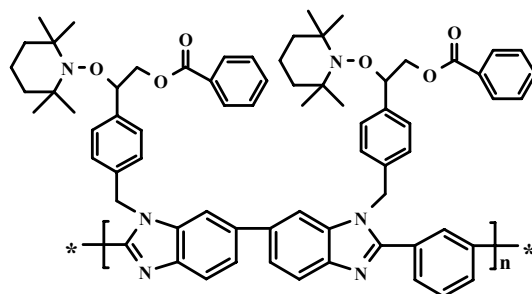
¹³C NMR (62.5 MHz, CDCl₃, 298 K) δ [ppm]: 17, 21, 41 and 46 (Carbons from TEMPO ring), 60.5 (-CH₂-Cl), 67 (-O-CH₂-), 84 (>CH-) and 166 (C=O).

IR (KBr) [cm⁻¹]: 1620 – 1460 (Ar), 2930, 803 and 712 (TEMPO group), 800 – 1000 (Bending frequencies of TEMPO group);

Analysis by FD mass showed a molecular ion peak at *m/e* 430 (M⁺).

EA: Calcd for C₂₅H₃₂ClNO₃: C, 69.83; H, 7.50; Cl, 8.25; N, 3.26. Found: C, 69.61; H, 7.60; Cl, 8.15; N, 3.4.

9.3.4 Synthesis of polybenzimidazole macro initiator



In a 250 mL round bottom flask, 10 % PBI solution in N,N-Dimethylacetamide (DMAc) was diluted by addition of equal volume of DMAc. Then the solution was mixed with sodium hydride (2 equivalence per benzimidazole repeat unit) and refluxed at 80 °C for 4 h. Subsequent treatment of this polyanion with TEMPO – adduct (2 eq. in 2 ml DMAc) at 80 °C results in the macro initiator after 15 hrs. Upon addition of the TEMPO – adduct to the anion solution, an immediate decrease in the viscosity and a lightening to orange occurs. The macro initiator was precipitated in an excess of water, collected by vacuum filtration, and then washed for several days with acetone-water mixture to remove DMAc from the macro initiator. The modified PBI with different degrees of modification were synthesized by changing NaH and TEMPO-adduct concentrations are as follows- NaH- 1.3, 1.6, 1.0, 0.7, 0.2 and 0.1 mmol; TEMPO adduct- 1.3, 1.6, 1.3, 1.0, 0.7, 0.2 and 0.1 mmol. Amount of PBI-1.3 mmol.

^1H NMR (250 MHz, CDCl_3 , 298 K) δ [ppm]: 0.3-1.5 (m, 18H), 3.9 (s, 1H), 4.6 (s, 2H), 5.7 (s, 1H), 7.0 - 8.3 (m, 19H).

^{13}C NMR (62.5 MHz, CDCl_3 , 298 K) δ [ppm]: 15-50 (Aliphatic carbons from TEMPO adduct), 57.9 ($-\text{CH}_2\text{-Cl}$), 71.5 ($-\text{O}-\text{CH}_2-$), 79.1 ($>\text{CH}-$), 115.9, 127, 127.2, 128.5, 129, 129.4, 129.7, 130.5, 136.6 and 138.4 (Ar) and 170.6 (C=O).

IR (KBr) [cm^{-1}]: 1620 – 1460 (Ar), 2930, 803 and 712 (TEMPO group), 800 – 1000 (Bending frequencies of TEMPO group);

Intrinsic viscosity (Degree of modification ~ 83 %): 0.84 dl. g^{-1} .

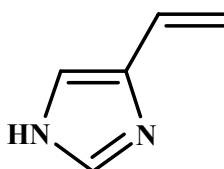
TGA/DSC (± 10 K/min): 380 °C.

9.3.5 Preparation of PVPA cross-linked PBI membrane

The DMAc solution of p-vinylbenzyl grafted PBI was first mixed with VPA in a 250 ml conical flask, and placed in an ultrasonification bath for 2 hrs to make a homogeneous solution. Oxygen was removed from the flask by bubbling argon through the solution for 2 h. The conical flask was then closed and placed in an ultrasonification bath for another 2 h. Membranes were cast using Petri dishes.

The thickness and size of the membranes were varied by controlling the volume of the solution according to the diameter of the dishes. The cross-linking reactions as well as solvent evaporation started at 130 °C for 24 h. Membranes were then washed with distilled water at 80 °C in order to remove unreactive monomers as well as residual solvent from the membrane. Traces of solvent molecules were removed by drying at 100 °C.

9.3.6 Synthesis of 4-vinylimidazole¹⁵⁷



4-vinylimidazole was synthesized as described in the literature.⁽¹⁵⁷⁾ Anhydrous urocanic acid (5.0 g., 0.053 mole) was heated in vacuum in a distilling apparatus. At a temperature of 220 °C, the material melted and began to decompose at 240 °C, as noticed by a decreased vacuum. At a temperature of 220 °C, urocanic acid starts undergoing decarboxylation to generate the desired 4-vinylimidazole. On careful heating at 220-240 °C, the product distilled as a colorless sirup, which crystallized in the receiver; 1.8 g. (53 %), m.p. 83.2 – 84.5 °C. b.p. 118 °C. The low yield is in part due to thermal decomposition of the starting material at this temperature to give an insoluble black material.

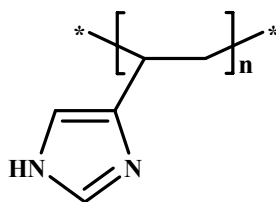
¹H NMR (250 MHz, CDCl₃, 298 K) δ [ppm]: 5.13 (dd, 1H), 5.68 (dd, 1H), 6.6 (m, 1H), 7.02 (s, 1H), 7.6 (s, 1H), 10.54 (broad, 1H).

¹³C NMR (62.5 MHz, CDCl₃, 298 K) δ [ppm]: 112.5 (CH₂=), 136 (>C=), 120, 127, and 136.2 (Imidazole ring carbon atoms).

Analysis by mass spectrometry under EI mode showed a molecular ion peak at m/e 94 (M⁺).

EA: Calcd for C₅H₆N₂: C, 63.81; H, 6.43; N, 29.76. Found: C, 63.7; H, 6.32; N, 29.74.

9.3.7 Synthesis of poly(4-vinylimidazole)



A solution of 1.0 g. (0.01 mole) 4-vinylimidazole and 2 mg. (0.1 mole %) of AIBN in 125 ml. of benzene was heated (after degassed by several freeze-degas-thaw cycles and sealed under vacuum at -78°C) at reflux with stirring under argon for 42 hours. The precipitated polymer was removed by filtration and washed several times with benzene, giving 0.3 g. (30% conversion) of a white powder.

$M_n \sim 5.0 \times 10^3$ g/mol by Vapor Pressure Osmometry in ethanol.

IR (KBr) [cm^{-1}]: 1650 - 1570 (Imidazole ring stretching), 800 - 700 (double bond from imidazole ring), 3200 (N-H).

Anal. cal. for $[\text{C}_5\text{H}_6\text{N}_2]$: C, 58.23; H, 6.84; N, 27.17. Found: C, 58.07; H, 6.65; N, 27.05.

TGA/DSC (± 10 K/min): 260°C .

9.3.8 Tailoring quartz substrates for multilayer build up

Quartz substrate was cleaned by sequential ultrasonification for 15 minutes each in dichloromethane, acetone, ethanol, 10 % Hellmanex soap solution and finally in deionized MilliQ-filtered water. After washing, the substrate was dried under a slow stream of argon gas and then again dried in an oven at 120°C for two hours. The dried quartz substrates were plasma-etched in Harrick PCD 200G plasma cleaner with oxygen bleed for 5 min and exposed to 3-aminopropyldimethylethoxysilane for 3 hrs at 120°C . The resulting substrate was stored in ethanol prior to use.

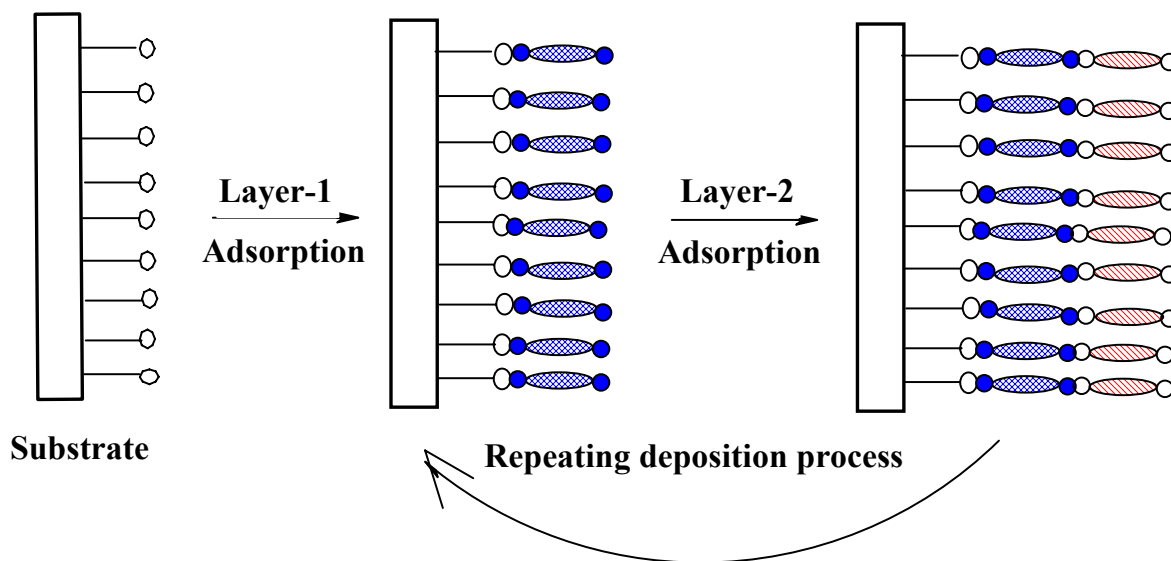


Fig. 1: Schematics of the Layer by layer assembly of PVPA and PBI

The substrate was first immersed in a proton donor polymer (0.02 M) such as PVPA, PVSA and PSSA in aqueous solution for 15 min to create acid layers on the substrate. After rinsing with Millipore water for five minutes and subsequent drying under argon purge, the substrate was transferred into proton acceptor polymer such as PBI and P4VIm in organic solution (0.02 M) and kept for 15 min. After washing with solvent for 5 minutes, the substrate was dried under an argon purge, and then again dipped into a proton donor polymer solution for 15 min to generate a second acid layer. A multilayer film could be obtained by repeating the above steps in a cyclic fashion as shown in fig. 1.

For PBI with PVPA multilayers: λ_{\max} : 355, 261, 213 nm. Absorbance maximum for 40 alternate layers: 0.375. Bilayer film thickness $\sim 3 \text{ \AA}$.

For PBI with PVSA multilayers: λ_{\max} : 353, 258, 209 nm. Absorbance maximum for 40 alternate layers: 0.325. Bilayer film thickness $\sim 2 \text{ \AA}$.

For PBI with PSSA multilayers: λ_{\max} : 353, 258, 220 nm. Absorbance maximum for 44 alternate layers: 0.27. Bilayer film thickness $\sim 2 \text{ \AA}$.

For P4VIm with PVPA multilayers: λ_{max} : 214 nm. Absorbance maximum for 16 alternate layers: 0.21. Bilayer thickness $\sim 3 \text{ \AA}$ up to 16 layers.

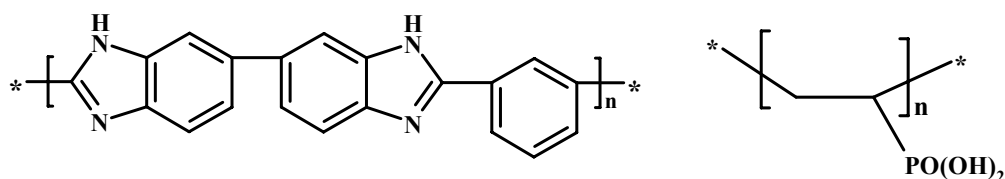
For P4VIm with PVSA multilayers: λ_{max} : 212 nm. Absorbance maximum for 16 alternate layers: 0.18. Bilayer thickness $\sim 4 \text{ \AA}$ up to 16 layers.

For P4VIm with PSSA multilayers: λ_{max} : 220 nm. Absorbance maximum for 16 alternate layers: 0.60. Bilayer thickness $\sim 4.25 \text{ \AA}$ up to 16 layers.

9.3.9 Surface modification of gold for multilayer fabrication

A quartz substrate (2.5 cm x 2.5 cm x 1 mm) was coated with an adhesive layer of 10 nm of chromium and 300 nm of gold using a thermal evaporator through a custom designed shadow mask of 3 mm width with 2.5 cm length. Gold was evaporated at $< 0.3 \text{ \AA/s}$ (slower rate), through thermal evaporator with water-cooling and used 90° offset evaporation to get ultra smooth surface. The substrates were exposed to a 0.03 M aqueous solution of 2-mercaptoethanesulfonic acid [pH ~ 1.7] for 3 hrs and washed with MilliQ water for five minutes and, dried under an argon purge.

9.3.10 Polybenzimidazole - poly(vinylphosphonic acid) multilayers on gold surface



The 2-mercaptoethanesulfonic acid modified gold substrate was first immersed in a 0.02 M polybenzimidazole [PBI] in DMAc and kept for 15 min. After washing with DMAc for 5 minutes, the substrate is dried under an argon purge, and then dipped into a 0.02M poly (vinylphosphonic acid) [PVPA] aqueous solution [pH ~ 2.2] for 15 min to create PVPA layers on the substrate. After rinsing with millipore water for five minutes and subsequent drying under an argon purge, the substrate was transferred PBI solution for 15 min to generate a second imidazole layer. A multilayer film could be obtained by repeating the above steps in a cyclic fashion.

Similarly, the above procedure was used to make PVIm-PVSA multilayers, PVIm-PVPA multilayers, PVIm-PSSA multilayers, PBI-PVSA multilayers and PBI-PSSA multilayers under 0.02 M concentration of both imidazole and acid solution.

9.3.11 Conductivity measurement of multilayers on top of gold electrode

During conductivity measurement, the system creates 2-electrode test beds of 9-mm² areas in which the LBL film is sandwiched between gold electrodes. Impedance spectroscopy was performed using a Solartron 1260 scanning from 1 MHz to 1 Hz. Because of noise at low frequency and high impedance, the lowest frequency included in analysis and typically greater than 1 Hz was chosen so that the measurement was within the <2% error region of impedance measurement for the instrument. The initial signal amplitude was 10 mV with no bias; amplitude was increased to 100 mV for each sample to reduce noise and increase the effective measurement range. Results at 100 mV amplitude were compared with the earlier 10 mV measurement to ensure no artifacts from increasing amplitude above kT (or approximately 25 mV at 25°C), which in some cases can cause nonlinearity in the impedance response, especially in the interfacial component. The absence of any cell shortening, even for rough samples, further substantiated that gold surfaces did not penetrate the LBL film.

9.3.12 Procedure for tailoring multilayers on Indium-tin oxide (ITO) glass for conductivity measurements

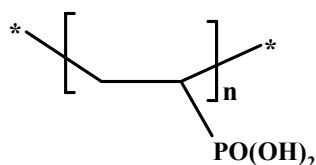
Substrates were 12.5 cm × 5 cm Indium-tin oxide (ITO) coated glass and patterned to form multiple 3-mm ITO stripes. ITO film resistance was measured to be 20 Ω/ square after patterning. The ITO substrates were cleaned by ultrasonification in solvents such as detergent, deionized MilliQ-filtered water, acetone, methanol, and 1,1,1-trichloroethane for 15 min each. Immediately before use, the ITO glass substrates were plasma-etched in a Harrick PCD 200G plasma cleaner with oxygen bleed for 5 min. Substrates were exposed to polymer solutions for 15 min, followed by rinsing in solvent baths.

9.3.13 Conductivity measurement of multilayers on top of ITO electrode

After assembly, films for proton conductivity evaluation were dried at 110 °C for 24 h, which has been shown to remove solvents from LBL assembled films. The drying was followed by thermal evaporation through a custom designed shadow mask of 2-mm wide, 1000 Å thick gold electrode perpendicular to the 3-mm wide patterned ITO stripes. This technique creates 2-electrode test beds of 9-mm² areas in which the LBL film is sandwiched between gold electrodes. The dimensions allowed 8 cells per substrate. The cells were profiled to verify the absence of significant gold penetration into the LBL film.

Impedance spectroscopy was performed using a Solartron 1260 scanning from 1 MHz to 1 Hz. Because of noise at low frequency and high impedance, the lowest frequency included in analysis was variable and typically greater than 1 Hz was chosen so that the measurement was within the < 2% error region of impedance measurement for the instrument. The initial signal amplitude was 10 mV with no bias; amplitude was increased to 100 mV for each sample to reduce noise and increase the effective measurement range. Results at 100 mV amplitude were compared with the earlier 10 mV measurement to ensure no artifacts from increasing amplitude above kT (or approximately 25 mV at 25°C), which in some cases can cause nonlinearity in the impedance response, especially in the interfacial component. The absence of any cell shortening, even for rough samples, further substantiated that evaporation deposited gold did not penetrate the LBL film.

9.3.14 Synthesis of polyvinylphosphonic acid in water medium



2 g of vinylphosphonic acid and 30 mg of K₂S₂O₈ were dissolved in water in a small polymerisation tube. The solution was degassed by several freeze-degas-thaw cycles and sealed under vacuum at -78 °C. The polymerisation was carried out by heating at 80–90 °C for 24 hr under argon atmosphere. After cooling, the poly(vinylphosphonic acid) was precipitated in acetone.

It was again dissolved in water and then precipitated in acetone. This procedure was repeated several times until to remove unreactive vinylphosphonic acid completely from the polymer. The polymer was dried in vacuum at 100 °C. Yield was ~ 40 %; The polymerisation was carried out with different amounts of initiator as described in table-6.1 of chapter-VI.

^1H NMR (250 MHz, D_2O , 298 K) δ [ppm]: 1.3 – 1.7 (broad, 3H).

IR (KBr) [cm^{-1}]: 1040 - 910 (P-OH asymmetric stretching), 1150 (P=O stretching), 2850 (O-H).

GPC (PS as a standard, Water)

M_n : 3.4×10^3 g/mol. $D = 1.5$ (The GPC data was obtained by converting PVPA into its sodium salt after treating with NaH, and then dissolved in water).

TGA (± 10 K/min): 175 °C (Decomposition temperature).

EA: Calcd for $[\text{C}_2\text{H}_5\text{O}_3\text{P}]_n$: C, 22.24; H, 4.66; P, 28.67. Found: C, 21.92; H, 4.53; P, 27.89.

9.3.15 Synthesis of poly(vinylphosphonate) in water medium

2 g of diethylvinylphosphonate and 30 mg of $\text{K}_2\text{S}_2\text{O}_8$ were dissolved in water in a small polymerisation tube. The solution was degassed by several freeze-degas-thaw cycles and sealed under vacuum at -78 °C. The polymerisation was carried out by heating at 80–90 °C for 24 hr under argon atmosphere. After cooling, the precipitated poly(vinylphosphonate) was dissolved in acetone. It was again precipitated in water and then dissolved in acetone. This procedure was repeated several times until to remove unreactive vinylphosphonate completely from the polymer. The polymer was dried in vacuum at 100 °C. Yield was ~ 30 %;

^1H NMR (250 MHz, d_6 -Acetone, 298 K) δ [ppm]: 1.1 – 1.9 (b, 9H), 3.8 (b, 4H).

IR (KBr) [cm^{-1}]: 1040 - 910 (P-O asymmetric stretching), 1145 (P=O stretching).

GPC (PS as a standard, DMF)

M_n : 1.8×10^3 g/mol, $D = 1.9$

TGA (± 10 K/min): 190 °C (Decomposition temperature).

EA: Calcd for $[\text{C}_6\text{H}_{13}\text{O}_3\text{P}]_n$: C, 43.90; H, 7.98; P, 18.87. Found: C, 43.08; H, 7.83; P, 18.14.

9.3.16 Polymerisation of vinylphosphonic acid in ethyl acetate-ethanol mixture

2 g of vinylphosphonic acid and 0.06 g of AIBN were dissolved in ethyl acetate in a small polymerisation tube. The solution was degassed by several freeze-degas-thaw cycles and sealed under vacuum at $-78\text{ }^{\circ}\text{C}$. The polymerisation was carried out by heating at $80 - 90\text{ }^{\circ}\text{C}$ for 24 hr under argon. After cooling, the PVPA was precipitated in acetone. It was again dissolved in water and then precipitated in acetone. This procedure was repeated several times until to remove unreactive vinylphosphonic acid completely from the polymer. The polymer was dried in vacuum at $100\text{ }^{\circ}\text{C}$. Yield $\sim 90\%$; The polymerisation was carried out with different amounts of initiator as described in table-6.2 of chapter-VI.

^1H NMR (250 MHz, D_2O , 298 K) δ [ppm]: 1.3 – 1.7 (broad, 3H).

IR (KBr) [cm^{-1}]: 1040 - 910 (P-OH asymmetric stretching), 1150 (P=O stretching), 2850 (O-H).

GPC (PS as a standard, Water)

M_n : 5.2×10^3 g/mol, $D = 8.7$ (The GPC data was obtained by converting PVPA into its sodium salt after treating with NaH, and then dissolved in water).

TGA (± 10 K/min): $175\text{ }^{\circ}\text{C}$ (Decomposition temperature).

EA: Calcd for $[\text{C}_2\text{H}_5\text{O}_3\text{P}]_n$: C, 22.24; H, 4.66; P, 28.67. Found: C, 22.03; H, 4.51; P, 27.94.

9.3.17 Anionic polymerisation of vinylphosphonate in THF

2 g of diethylvinylphosphonate and 30 mg of n-butyllithium were dissolved in 5 ml of dry THF in a small polymerisation tube. The solution was degassed by several freeze-degas-thaw cycles and sealed under vacuum at $-78\text{ }^{\circ}\text{C}$. The polymerisation was carried out at $-80\text{ }^{\circ}\text{C}$ for 24 hr under argon. After cooling, the PVPA was precipitated in water. It was again dissolved in acetone and then precipitated in water. This procedure was repeated several times until to remove unreactive vinylphosphonate completely from the polymer. The polymer was dried in vacuum at $100\text{ }^{\circ}\text{C}$. Yield $\sim 30\%$; The polymerisation was also carried out with different amounts of initiator as described in table-6.3 of chapter-VI.

^1H NMR (250 MHz, d_6 -Acetone, 298 K) δ [ppm]: 1.1 – 1.8 (b, 9H), 3.8 (b, 4H).

IR (KBr) [cm^{-1}]: 1040 - 910 (P-O asymmetric stretching), 1145 (P=O stretching).

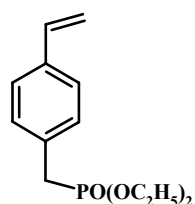
GPC (PS as a standard, DMF)

M_n : 1.9×10^3 g/mol, $D = 1.1$

TGA (± 10 K/min): 190 °C (Decomposition temperature).

EA: Calcd for $[\text{C}_6\text{H}_{13}\text{O}_3\text{P}]_n$: C, 43.90; H, 7.98; P, 18.87. Found: C, 43.27; H, 7.86; P, 18.55.

9.3.18 Preparation of p-vinylbenzylphosphonate diethyl ester (VBP)⁽¹⁷⁹⁻¹⁸²⁾



Synthesis of vinylbenzyl phosphonate was reported in the literature.⁽¹⁷⁹⁻¹⁸²⁾

However, it was synthesized with low yield due to high reaction temperature up to 145 °C. In order to synthesize VBP with high yield, a modified reaction procedure is given below: A modified synthetic procedure A 100 mL three-necked round-bottomed flask (fitted with a magnetic stirrer and reflux condenser connected to a calcium chloride tube) was charged with triethylphosphite (TEP) 60 mL (0.5 mol), vinylbenzyl chloride (VBC) 15 mL (0.1 mol), and 6-tert-butyl-2,4-dimethylphenol 0.2 mL. The reaction mixture was stirred vigorously at 95 °C for 72 h under argon. The resulting product was distilled at reduced pressure, and unreacted TEP was removed at 45 °C/8 mm Hg and unreacted VBC at 50-55 °C/0.5 mm Hg. VBP was collected at 115 °C/0.5 mm Hg with 70 % yield.

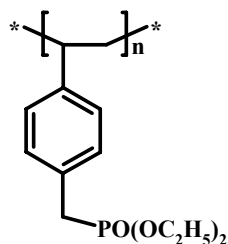
^1H NMR (250 MHz, CDCl_3 , 298 K) δ [ppm]: 1.2 (t, 6H), 3.0 (d, 2H), 3.9 (q, 4H), 5.1 (m, 1H), 5.68 (m, 1H), 6.5 (m, 1H) and 7.18 (m, 4H).

^{13}C NMR (62.5 MHz, CDCl_3 , 298 K) δ [ppm]: 8 (- CH_3), 17 (- $\text{CH}_2\text{-CH}_3$), 30 ($\text{C}_6\text{H}_4\text{-CH}_2\text{-}$), 110 ($\text{CH}_2\text{=}$), 136 (- C=), 126, 127, 131 and 135 (Ar).

MS (FD, 8kv): m/z (%) = 254.2 (100) [M^+].

EA: Calcd for $\text{C}_{13}\text{H}_{19}\text{O}_3\text{P}$: C, 61.41; H, 7.53; P, 12.18. Found: C, 61.38; H, 7.50; P, 12.07.

9.3.19 Polymerisation of diethyl p-vinylbenzylphosphonate¹⁷⁹⁻¹⁸²



Initiator (BPO or AIBN) was dissolved in vinylbenzyl phosphonate monomer, and the solution was degassed by several freeze-degas-thaw cycles and sealed under vacuum at $-78\text{ }^{\circ}\text{C}$. The polymerisation was carried out at $90\text{ }^{\circ}\text{C}$ under argon atmosphere. After few hours, polymer was dissolved in CHCl_3 , and then precipitated in excess of hexane. It was dried in vacuum for 48 hrs and yield was more than 90 %. The same polymerisation procedure was used in presence of TEMPO, however at $125\text{ }^{\circ}\text{C}$ for overnight. The molecular weight, polymerisation conditions were given in table-6.4 of chapter-6.

^1H NMR (250 MHz, CDCl_3 , 298 K) δ [ppm]: 1.1 (b, 8H), 2.1 (b, 1H), 2.96 (b, 2H), 3.9 (b, 4H), 6.4 - 6.9 (b, 4H).

^{13}C NMR (62.5 MHz, CDCl_3 , 298 K) δ [ppm]: 14 ($-\text{CH}_3$), 62 ($-\text{CH}_2-\text{CH}_3$), 31 ($\text{C}_6\text{H}_4-\text{CH}_2-$), 33 ($-\text{CH}_2-$), 37 ($-\text{C}<$), 125, 127.4, 131.6 and 136 (Ar).

GPC (PS as a standard, DMF):

M_n : 35.0×10^3 g/mol to 80.0×10^3 g/mol. $D = 1.2$ to 3.0 .

TGA(± 10 K/min): $310\text{ }^{\circ}\text{C}$ (Decomposition temperature).

DSC (± 10 K/min): $130\text{ }^{\circ}\text{C}$ (T_g)

EA: Calcd for $[\text{C}_{13}\text{H}_{19}\text{O}_3\text{P}]_n$: C, 61.41; H, 7.53; P, 12.18. Found: C, 60.23; H, 7.46; P, 11.71.

9.3.20 Synthesis of poly(diethyl vinylbenzylphosphonate) from PVBC¹⁸²

The poly(diethyl vinylbenzylphosphonate) was reported in the literature⁽¹⁸⁰⁾ from poly(vinylbenzylchloride) [PVBC] by Michaelis-Arbuzov reaction. However, the conversion from chloro to phosphonate derivative was in the range of 80 % at $120\text{ }^{\circ}\text{C}$. In order to get higher conversion, the reaction was carried out at $160\text{ }^{\circ}\text{C}$ in bis(2-ethoxyethyl) ether solvent.

A Michaelis-Arbuzov reaction was performed by the drop wise addition of a mixture of 180 mL bis(2-ethoxyethyl) ether and 180 mL triethylphosphite to a refluxing solution of 8.59 g poly(vinylbenzylchloride) in 150 mL bis(2-ethoxyethyl) ether over 4 hr. The resulting reaction mixture was refluxed for an additional 13 hr. The mixture was then cooled to room temperature and the polymer was precipitated in excess of hexane. The polymer was further purified by dissolving in acetone and then again precipitated in excess of hexane, followed by drying the white solid polymer under vacuum (4.0 g). Conversion: 100 %.

^1H NMR (250 MHz, CDCl_3 , 298 K) δ [ppm]: 1.2 (b, 8H), 2.0 (b, 1H), 2.9 (b, 2H), 3.92 (b, 4H), 6.2 - 7.1 (b, 4H).

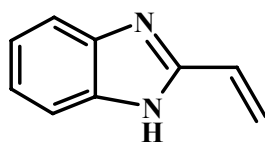
^{13}C NMR (62.5 MHz, CDCl_3 , 298 K) δ [ppm]: 13.8 ($-\text{CH}_3$), 62.4 ($-\text{CH}_2-\text{CH}_3$), 31 ($\text{C}_6\text{H}_4-\text{CH}_2-$), 33 ($-\text{CH}_2-$), 37 ($-\text{C}<$), 125.2, 127, 131.4 and 136.1 (Ar).

TGA(± 10 K/min): 316 $^\circ\text{C}$ (Decomposition temperature).

DSC (± 10 K/min): 127 $^\circ\text{C}$ (T_g)

EA: Calcd for $[\text{C}_{13}\text{H}_{19}\text{O}_3\text{P}]_n$: C, 61.41; H, 7.53; P, 12.18. Found: C, 60.17; H, 7.38; P, 11.42.

9.3.21 Synthesis of 2-vinylbenzimidazole⁽¹⁸³⁻¹⁸⁴⁾



Synthesis of 2-vinylbenzimidazole was briefly reported in the literature.⁽¹⁸³⁻¹⁸⁴⁾ However, it was carried out by multi steps synthetic process, which restricted yield of the product. In order to synthesize in high yield with minimum possible steps, the witting reaction was carried out as follows:

A solution of the 2-(chloromethyl)-1*H*-benzimidazole (5.0 g, 3.0 mM) and triphenylphosphine (7.9 g, 30 mM) in anhydrous dioxane (70 mL) was refluxed under an atmosphere of argon for 14 h. After being cooled, the resulting white precipitate was filtered, washed with dioxane (15 mL), and dried to give 11.1 g (86 %) of the phosphonium salt; mp 285 $^\circ\text{C}$.

A solution of 10 % sodium carbonate (13.6 mL, 12.8 mM) was added to a solution of phosphonium compound above (5.0 g, 11.7 mM) in chloroform (60 mL), followed by a 10 % aqueous solution of formaldehyde (7 mL, 23.3 mM), and stirring was continued at room temperature for 3 h. The chloroform layer was separated and extracted with 5N hydrochloric acid (3 × 5 mL). The acid extract was neutralized with solid sodium carbonate and the precipitate filtered, washed with water (2 X 5 mL), and dried. Sublimation at 120 °C under reduced pressure afforded 1.35 g (80 %) of 2-vinylbenzimidazole. m.p. 184 °C.

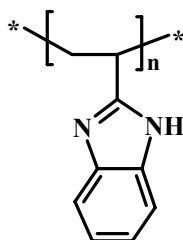
^1H NMR (250 MHz, d_6 -DMSO, 298 K) δ [ppm]: 5.74 (d, 1H), 6.35 (d, 1H), 6.77 (m, 1H), 7.23 (s, 2H), 7.5 (s, 2H), 12.66 (s, 1H).

^{13}C NMR (62.5 MHz, d_6 -DMSO, 298 K) δ [ppm]: 115.4, 118.3, 123, 136, 141.5.

Analysis by mass spectrometry under EI mode showed a molecular ion peak at m/e 144 (M^+).

EA: Anal. cal. for $[\text{C}_9\text{H}_8\text{N}_2]$: C, 74.98; H, 5.59; N, 19.43. Found: C, 74.89; H, 5.52; N, 19.40.

9.3.22 Polymerisation of 2-vinylbenzimidazole in CH_3OH ¹⁸⁴



Poly(2-vinylbenzimidazole)

Freshly sublimed monomer (0.3 g, 0.0021 mole) and 1 mole % AIBN (3 mg), were dissolved in 5 mL methanol in a small polymerisation tube. The solution was degassed by several freeze-degas-thaw cycles and sealed under vacuum at -78 °C. Polymerisation was carried out by heating at 70-80 °C for 48 hr. After cooling, the polymer was precipitated in hexane and dried. Dried sample was again washed several times in methanol solvent to remove unreactive monomer completely from polymer. The polymer was dried again in vacuo at 112 °C to give 0.25 g (83%) white powder, mp ~ 400 °C, with gradual softening and decomposition.

The polymerisation of 2-vinylbenzimidazole with different ratios of solvent and initiator was given in table-6.6 of chapter-VI.

The intrinsic viscosity in H₂SO₄ in a Cannon-Ubbelohde viscometer at 26 °C was 1.23 dl/g.

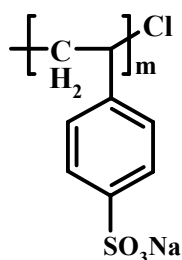
IR (KBr) [cm⁻¹]: 3200 - 3500 (N-H stretching), 1600 - 1500 (C=C stretching).

The NMR spectrum contained only broad resonance for the backbone protons.

TGA/DSC (± 10 K/min): 400 °C

EA: Anal. cal. for [C₉H₈N₂]: C, 74.98; H, 5.59; N, 19.43. Found: C, 72.21; H, 5.47; N, 16.83.

9.3.23 Synthesis of poly(4-styrenesulfonate) by ATRP reaction



The polymerisation was carried out as follows; a degassed ethylene glycol solution (10 ml), CuBr (0.02 mole), PMDETA (0.012 mole), 4-styrenesulfonate (2.0 g) and free initiator (0.02 mole) was sealed in a glass tube under vacuum for 1 hr and heated under argon atmosphere for a prescribed period of time at 90 °C. After polymerisation for few hours, it was precipitated in methanol-acetone mixture (40: 60) and dried well. Then, it was again washed with acetic acid solution to remove colour from the solution and dried under vacuum at 80 °C for 4 hrs. The yield was more than 90 %. The polymerisation was carried out with different ratios of solvent and initiator was given in table-6.6 of chapter-VI.

¹H NMR (250 MHz, D₂O, 298 K) δ [ppm]: 1.2 – 2.5 (b, 3H), 7.4 (b, 2H), 7.8 (b, 2H).

¹³C NMR (62.5 MHz, D₂O, 298 K) δ [ppm]: 32 (-CH₂-), 37 (-CH<), 126, 130.4, 140 and 142 (Ar).

IR (KBr) [cm^{-1}]: 1003 (p- substituted benzene ring), 1040 (SO_3^- stretching), 3400 (H-bonding).

GPC (PS as a standard, Water):

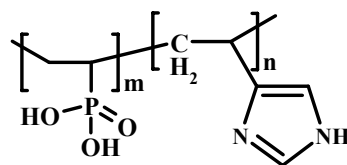
M_n : 5.5×10^4 g/mol to 6.5×10^4 g/mol. $D = 1.2$ to 1.4 .

TGA (± 10 K/min): 340 °C (Decomposition temperature).

DSC (± 10 K/min): 140 °C (T_g)

EA: Anal. cal. for $[\text{C}_8\text{H}_7\text{NaO}_3\text{S}]$: C, 46.60; H, 3.42; S, 15.55. Found: C, 45.51; H, 3.34; S, 15.19.

9.3.24 Polymerisation of vinylphosphonic acid and 4-vinylimidazole



4-vinylimidazole (1 g, 0.01 mol), vinylphosphonic acid (1.15 g, 0.01 mol), and initiator (30 mg) were dissolved in water (10 ml) in a small polymerisation tube. The solution was degassed by several freeze-degas-thaw cycles and sealed under vacuum at -78 °C. Polymerisation was carried out by heating at 80 °C for 24 hr. After cooling, the polymer was precipitated in acetone. Again, it was again dissolved in water and then precipitated in acetone. The polymer was dried in vacuum at 100 °C. Yield was ~ 55 %;

^1H NMR (250 MHz, D_2O , 298 K) δ [ppm]: 1.2 – 1.9 (b, 3H), 2.6 (b, 1H), 6.7 (b, 1H), 8.3 (b, 1H).

IR (KBr) [cm^{-1}]: 1617 (H-Im $^+$ -H), 3150 (N-H stretching), 3400 (H-bonding), 910 – 1200 (P-O $^-$).

GPC (PS as a standard, Water):

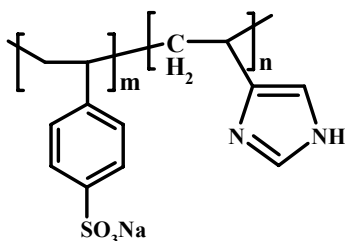
M_n : 3.2×10^4 g/mol. $D = 1.9$

TGA (± 10 K/min): 170 °C (Decomposition temperature).

DSC (± 10 K/min): 10 °C (T_g)

EA: Anal. cal. for $[\text{C}_2\text{H}_5\text{O}_3\text{P}]_x-[\text{C}_5\text{H}_6\text{N}_2]_y$: C, 40.12; H, 5.12; N, 20.43, P, 17.01.

9.3.25 Polymerisation of 4-vinylimidazole and 4-vinylstyrenesulfonate



4-vinylimidazole (1 g, 0.01 mol), 4-styrenesulfonate (2.062 g, 0.01 mol), and initiator (30 mg) were dissolved in water (10 ml) in a small polymerisation tube. The solution was degassed by several freeze-degas-thaw cycles and sealed under vacuum at $-78\text{ }^{\circ}\text{C}$. Polymerisation was carried out by heating at $80\text{ }^{\circ}\text{C}$ for 24 hr under argon. After cooling, the polymer was precipitated in acetone. Again, it was dissolved in water and then precipitated in acetone. The polymer was dried in vacuum at $100\text{ }^{\circ}\text{C}$. Yield: 65 %;

^1H NMR (250 MHz, D_2O , 298 K) δ [ppm]: 1.0 – 2.2 (b, 6H), 6.2 (b, 1H), 6.6 (b, 2H), 7.4 (b, 2H).

IR (KBr) [cm^{-1}]: 1007 (p- substituted benzene ring), 1040 (SO_3^- stretching), 3500 - 2800 (H-bonding), 1650 – 1570 (Imidazole stretching), 800 – 700 (C-H from Imidazole ring).

GPC (PS as a standard, Water):

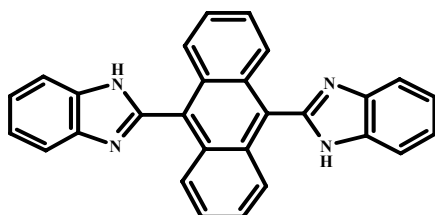
M_n : 6.5×10^4 g/mol. $D = 2.1$

TGA (± 10 K/min): $320\text{ }^{\circ}\text{C}$ (Decomposition temperature).

DSC (± 10 K/min): $132\text{ }^{\circ}\text{C}$ (T_g)

EA: Anal. cal. for $[\text{C}_8\text{H}_7\text{SO}_3\text{Na}]_x-[\text{C}_5\text{H}_6\text{N}_2]_y$: C, 70.17; H, 4.31; S, 18.32; N, 14.42.

9.3.26 Synthesis of 9,10-bis-(benzimidazole-2-yl)anthracene



9,10-Dicyanoanthracene (0.01 mol) was added to polyphosphoric acid at 75-80 °C, followed by the addition of orthophenylene diamine (0.02 mol). The mixture was heated to 200 °C and it was maintained until reaction was complete (2 h, monitored by thin-layer chromatography). The mixture was cooled at 80 °C, and crushed ice (about 200 g) was added with vigorous stirring when a yellow solid separated. The separated solid was filtered, washed with water until it was acid free, and then dried. Compound was purified by sublimating it at 300 °C; Yield 66 %, m.p. 360 °C.

^1H NMR (250 MHz, d_6 -DMSO, 298 K) δ [ppm]: 7.3 (m, 4H), 7.5 (m, 4H), 7.7 (m, 4H), 7.8 (m, 4H).

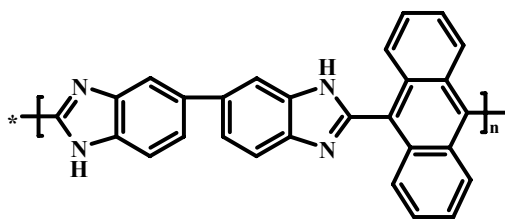
IR (KBr) [cm^{-1}]: 3400 (N-H stretching), 1520 – 1450 (Ar stretching), 700 – 1100 (bending frequency of Ar).

UV/vis: λ nm (max) = 257, 300, 400.

Analysis by FD mass showed a molecular ion peak at m/e 410 (M^+).

EA: Anal. cal. for $[\text{C}_{28}\text{H}_{18}\text{N}_4]$: C, 81.93; H, 4.42; N, 13.65. Found: C, 81.71; H, 4.36; N, 13.61.

9.3.27 Synthesis of poly(9,10-bis-(benzimidazole-2-yl)anthracene)



The polymerisation reaction was carried out as follows: 9,10-Dicyanoanthracene (0.01 mol) was added to polyphosphoric acid at 75-80 °C, followed by the addition of 3,3'-diaminobenzidine (0.02 mol). The mixture was heated to 200 °C and it was maintained until 48 hrs. The mixture was cooled till room temperature, and then, crushed ice (about 200 g) was added with vigorous stirring when a yellow solid separated. The separated solid was filtered, washed with water until it was acid free, and then dried. Yield ~ 85 %.

^1H NMR (250 MHz, d_6 -DMSO, 298 K) δ [ppm]: 3.3 (b, N-H), 6.5 – 8.0 (b, 14H).

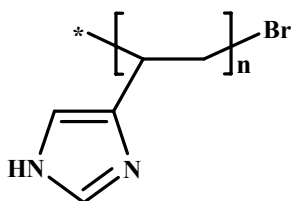
IR (KBr) [cm^{-1}]: 3400 (N-H stretching), 1520 – 1450 (Ar stretching), 700 – 1100 (bending frequency of Ar).

UV/vis: λ nm (max) = 257, 300, 403.

Intrinsic viscosity: 0.3 dl/g

EA: Anal. cal. for $[\text{C}_{28}\text{H}_{18}\text{N}_4]$: C, 81.93; H, 4.42; N, 13.65. Found: C, 78.73; H, 4.30; N, 16.41.

9.3.28 ATRP of 4-vinylimidazole



The polymerisation was carried out in a 250 ml dried flask equipped with a magnetic stirring bar under argon. The flask was charged with cyclohexane (10 ml), CuBr (0.00014 mole) and 2,2'-bipyridine (0.00028 mole). The flask was sealed with a rubber septum, and then cycled between vacuum and argon three times to remove oxygen. Degassed 4-vinylimidazole (0.007 mole in 2ml cyclohexane) was added via syringe. 1-phenylethylbromide (0.0000014 mole) was added and the flask was immersed in an oil bath held by a thermostat at 70 °C. After 10 hrs the heating was stopped, and the conversion was 8%. The reaction was poured into acetone and dried at 100 °C for two days.

^1H NMR (250 MHz, methanol, 298 K) δ [ppm]: 1.0 – 2.2 (b, 3H), 6.2 (b, 1H), 6.6 (b, 1H), 7.4 (b, 1H).

IR (KBr) [cm^{-1}]: 3500 - 2800 (H-bonding), 1650 – 1570 (Imidazole stretching), 800 – 700 (C-H from Imidazole ring).

GPC (PS as a standard, DMF):

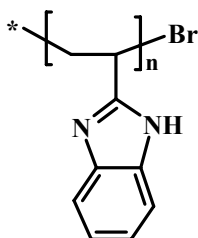
M_n : 8.0×10^2 g/mol. $D = 1.1$

TGA (± 10 K/min): 270 °C (Decomposition temperature).

DSC (± 10 K/min): 120 °C (T_g)

EA: Anal. cal. for $[C_5H_6N_2]_x$: C, 63.81; H, 6.43; N, 29.76. Found: C, 61.32; H, 6.12; N, 27.57.

9.3.29 ATRP of 2-vinylbenzimidazole



The polymerisation was carried out in a 250 ml dried flask equipped with a magnetic stirring bar under argon. The flask was charged with n-propanol (10 ml), CuBr (0.00014 mole) and Me₆TREN (0.0014 mole). The flask was sealed with a rubber septum, and then cycled between vacuum and argon three times to remove oxygen. Degassed 2-vinylbenzimidazole (0.014 mole in 2ml propanol) was added via syringe. 1-phenylethylbromide (0.0000014 mole) was added and the flask was immersed in an oil bath held by a thermostat at 70 °C. After 7 hrs the heating was stopped, and the conversion was 18%. The reaction was poured into hexane and dried at 100 °C for two days.

GPC (PS as a standard, DMF):

M_n : 3.8×10^3 g/mol. $D = 1.14$

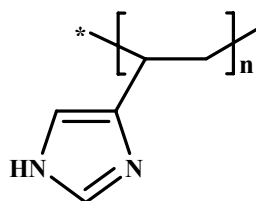
IR (KBr) [cm^{-1}]: 3200 - 3500 (N-H stretching), 1600 - 1500 (C=C stretching).

The NMR spectrum contained only broad resonance for the backbone protons.

TGA/DSC (± 10 K/min): 400 °C

EA: Anal. cal. for $[C_9H_8N_2]$: C, 74.98; H, 5.59; N, 19.43. Found: C, 72.75; H, 5.19; N, 16.38.

9.3.30 NMP of 4-vinylimidazole



4-vinylimidazole (0.01 mol), TEMPO (0.0001 mol), and AIBN (0.0002 mole) were dissolved in ethylene glycol (10 ml) in a small polymerisation tube. The solution was degassed by several freeze-degas-thaw cycles and sealed under vacuum at -78 °C. Polymerisation was carried out by heating at 125 °C for 15 hr under argon. After cooling, the polymer was precipitated in acetone. Then, it was dried at 100 °C for two days. The polymer was dried in vacuum at 100 °C. Yield: 8%;

^1H NMR (250 MHz, D_2O , 298 K) δ [ppm]: 1.0 – 2.2 (b, 6H), 6.2 (b, 1H), 6.6 (b, 2H), 7.4 (b, 2H).

IR (KBr) [cm^{-1}]: 3500 - 2800 (H-bonding), 1650 – 1570 (Imidazole stretching), 800 – 700 (C-H from Imidazole ring).

GPC (PS as a standard, DMF):

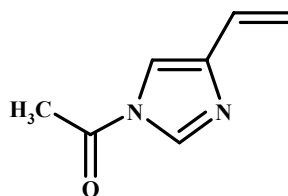
M_n : 3.0×10^3 g/mol. $D = 1.19$.

TGA (± 10 K/min): 275 °C (Decomposition temperature).

DSC (± 10 K/min): 122 °C (T_g)

EA: Anal. cal. for $[\text{C}_5\text{H}_6\text{N}_2]_x$: C, 63.81; H, 6.43; N, 29.76. Found: C, 62.21; H, 6.18; N, 28.15.

9.3.31 Synthesis of N-CO-CH₃ vinylimidazole



4-vinylimidazole (0.01 mol) and CH_3COCl (0.005 mol) were dissolved in benzene (5 ml) in a small tube. Then, the solution was stirred at 40 °C for 30 mins. Then it was cooled and recrystallized in benzene. Yield: 50 %; m.p. 138 °C;

^1H NMR (250 MHz, CDCl_3 , 298 K) δ [ppm]: 3.15 (s, 3H) 5.13 (dd, 1H), 5.68 (dd, 1H), 6.6 (m, 1H), 7.02 (s, 1H), 7.6 (s, 1H).

^{13}C NMR (62.5 MHz, CDCl_3 , 298 K) δ [ppm]: 112.5 ($\text{CH}_2=$), 136 ($>\text{C}=\text{}$), 120, 127, 136.2 (Imidazole ring carbon atoms), 24 (CH_3) and 172 (CO)

Analysis by mass spectrometry under EI mode showed a molecular ion peak at m/e 136.25 (M^+).

EA: Calcd for $\text{C}_5\text{H}_6\text{N}_2$: C, 61.75; H, 5.92; N, 20.57. Found: C, 61.71; H, 5.85; N, 20.14.

1. Ed Fontes, Eva Nilsson, *The Industrial Physicist*, 14, August/September, **2001**.
2. S. Gottesfeld, T.A. Zawodzinski, R.C. Alkire, H.Gerischer, D.M. Kolb, Tobias (Eds), *Advances in Electrochemical Science and Engineering*, Vol.5, Wiley-VCH, Weinheim, **1997**, pp.195.
3. B.K. Datta, G. Velayutham, A.P. Goud, *J. Power Sources* **2002**, 106 (1-2), 270.
4. S.J. Padidison, R. Paul, *Physical Chemisty Chemical Physics* **2002**, 4(7), 1158.
5. T.A. Zawodzinski, C. Derouin, S. Radzinski, R.J. Sherman, V.T. Smith, T.E. Springer, S. Gottesfeld, *J. Electrochem. Soc.*, **1993**, 140, 1041.
6. N.P. Chen, L. Hong, *Solid State Ionics* 2002, 146(3-4), 377.
7. K. Tsuruhara, K. Hara, M. Kawahara, M. Rikukawa, K. Sanui, N. Ogata, *Electrochim Acta* **2002**, 45, 1223.
8. J.L. Bredas, R.R. Chance, R. Silbey, *Phys Rev B*, **1982**, 26, 5843.
9. H. Kobayashi, H. Tomita, H. Moriyama, *J. Am. Chem. Soc.*, **1994**, 116, 3153.
10. F. Wand, J. Roovers, *Macromolecules* **1993**, 26, 5295.
11. C. Bailly, D.J. Williams, F.E. Karasz, W.J. Macknight, *Polymer* **1987**, 28, 1009.
12. S.J. Paddison, R. Paul, K.D. Kreuer, *Physical Chemistry Chemical Physics* **2002**, 4(7), 1151.
13. X. Glipa, M.E. Haddad, D.J. Jones, J. Rozieire, *Solid State Ionics* **1997**, 97, 323.
14. M. Kawahara, M. Rikukawa, K. Sanui, N. Ogata, *Polym. Adv. Technol*, **2000**, 11,1.
15. M. Kawahara, M. Rikukawa, K. Sanui, N. Ogata, *Proceedings of the sixth International Symposium on Polymer Electrolytes, Extended Abstracts*, **1998**, pp.98.
16. P. Donoso, W. Gorecki, C. Berthier, F. Dfendini, C. Poinsignon, M.B. Armand, *Solid State Ionics* **1988**, 28, 969.
17. J.T. Wang, S. Wasmus, R.F. Savinell, *J. Electrochem. Soc.*, **1996**, 123, 1233.

18. S.R. Samms, S. Wasmus, R.F. Savinell, *J. Electrochem. Soc.*, **1996**, 143, 1225.
19. M. Rikukawa, K. Sanui, *Prog. Polym. Sci.*, **2000**, 25,1463.
20. R.F. Savinell, E. Yeager, P. Tryk, U. Landau, J.S. Wainright, D. Weng, K. Lux, M. Litt, C. Rogers, *J. Electrochem. Soc.*, **1994**, 141, 46.
21. S.M. Aharoni and M.H. Litt, *J. Polym. Sci., Part A: Polym. Chem.*, **1974**, 12, 639.
22. J.S. Wainright, J.T. Wang, R.F.Savinell, and M.H. Litt, *J.Electrochem. Soc.*, **1995**, 142, 1, 121
23. J.J. Fontanella, M.C. Wintersgill, J.S. Wainright, R.F. Savinell, and M. Litt, *Electrochim. Acta* **1998**, 43, 1289.
24. D. Wang, J.S.Wainright, U.Landau, and R.F.Savinell, *J.Electrochem. Soc.*, **1996**, 143, 1260.
25. S.R. Samms, S.Wasmus, and R.F.Savinell, *J. Electrochem. Soc.*, **1996**, 143, 1225.
26. M. Litt, R. Ameri, Y.wang, R. Savinell, and J.Wainright, *Mater. Res. Soc.Symp. Proc.*, **1999**, 548, 313.
27. J.T. Wang, R.F. Savinell, J.S. Wainright, M.H. Litt, and H. Yu, *Electrochim. Acta* **1996**, 41, 193.
28. J.T. Wang, J.S. Wainright, R.F. Savinell, and M. Litt, *J. Appl. Electrochem.*, **1996**, 26, 751.
29. B. Xing and O. Savadogo, *J.New Mater. Electrochem. Syst.*, **1995**, 2, 95.
30. B. Xing and O.Savadogo, *Electrochem. Commun.*, **2000**, 2, 697.
31. P. Slaiti, M. Minuloli, and S. Hocevar, *J. Power Sources* **2000**, 90, 231.
32. P. Slaiti, F. Lufrano, A.S. Arico, E. Pasalacqua, and V. Anolonucci, *J. membr. Sci.*, **2001**, 188, 71.
33. H. Akita, M. Ichikawa, K. Nosaki, H. Oyanagi, and M. Iguchi, *U.S. Patent* **6,124.060 (2000)**.
34. C. Hasiotis, Q. F. Li, V. Deimede, J.K. Kallitsis, C.G. Kontoyannis, and N.J. Bjerrum, *J. Electrochem. Soc.*, **2001**, 148, A513.

35. C. Hasiotis, V. Deimede, and C. Kontoyannis, *Electrochim. Acta* **2001**, 46, 2401.
36. V. Deimede, G.A. Voyiatizis, J.K. Kallitsis, Q.F.Li, and N.J. Bjerrum, *Macromolecules* **2000**, 33, 7609.
37. J. Kerres, A. Ullrich, Th. Haring, W.Preidel, M.Baldauf, and U.Gebhardt, *J. New mater. Electrochem. Syst.*, **2000**, 3, 229.
38. J.A. Kerres, *J. Membr. Sci.*, **2001**, 185, 3.
39. J. Kerres, A. Ullrich, F. Meier, and T. Haring, *Solid State Ionics* **1999**, 125, 243.
40. L. Jorissen, V. Gogel, J. Kerres, and J. Garche, *J. Power Sources* **2002**, 105, 267.
41. J. Kerrers, W. Zhang, L. Jorissen, and V. Gogel, *J. New Mater. Electrochem. Syst.*, **2002**, 5, 97.
42. J. Roziere, D.J. Jones, M. Marrony, X. Glipa, and B. Mula, *Solid State Ionics* **2001**, 145, 61
43. X. Glipa, M. E. Hadda, D.J. Jones, and J. Roziere, *Solid State Ionics* **1997**, 97, 323.
44. J.M. Bae, I. Honma, M. Murata, T. Yamamoto, M. Rikukawa, and N. Ogata, *Solid State Ionics* **2002**, 147, 189.
45. M. Rikukawa and K. Sanui, *Prog. Polym. Sci.*, **2000**, 25, 1463.
46. C. Gavach and G. Pourcelly, in *Proton Conductors*, (Edited by Ph. Colomban) 487, Cambridge University Press, **1992**.
47. M. Rikukawa, K. Sanui, *Prog. Polym. Sci.*, **2000**, 25, 1463.
48. X. Jin, M.T. Bishop, T.S. Ellis, F.E.Br. Karasz, *Polymer J.* **1985**, 17, 4.
49. J.S. Wainrigh, J.- T. Wang, R. F. Savinell, M. Litt, H. Moadell, C. Rogers, *Proc. ECS 94/23 (Electrode Materials and Processes)*, **1994**, 255.
50. K.D. Kreuer, *J. Membr. Sci.* **2001**, 185, 29-39.
51. K. Miyatake, E. Shouji, K. Yamamoto, E. Tsuchida, *Macromolecules* **1997**, 30, 2941

52. A. Bozkurt, W.H. Meyer, *Solid State Ionics* **2001**, 138, 259-265.
53. P. Donoso, W. Gorecki, C. Berthier, F. Defendini, C. Poinignon, M.B. Armand, *Solid State Ionics* **1988**, 28, 969-74.
54. A. Bozkurt, W.H. Meyer, *Journal of Polymer Science: Part B: Polymer Physics* **2001**, 39, 1987-1994.
55. D.T. Chin, H.H. Chang, *J. Appl. Electrochem.*, **1989**, 19(1), 95-99.
56. R.A. Munson, M.E. Lazarus, *J. Phys. Chem.*, **1967**, 71(10), 3245-48.
57. T. Dippel, K.D. Kreuer, J.C. Lassegues, D. Rodriguez, *Solid State Ionics* **1993**, 61 (1-3); 41-46.
58. K.D. Kreuer, *Chem. Mater.*, **1996**, 8(3): 610-41.
59. K.D. Kreuer, *Solid State Ionics* **2000**, 136-137: 149-60.
60. H. Pu, W.H. Meyer, G. Wegner, *Journal of Polymer Science: Part B: Polymer Physics* **2002**, 40, 663 - 669.
61. R. Bouchet, E. Siebert, *Solid State Ionics* **1999**, 118, 287.
62. M.L. Bender, G.R. Schonbaum, G.A. Hamilton, B. Zerner, *J. Am. Chem. Soc.*, **1961**, 83, 4656.
63. R. Ianniello, V.M. Schmidt, U. Stimming, J. Stumper, A. Wallan, *Electrochim. Acta* **1994**, 39, 1863.
64. J.T. Daycock, G.P. Jones, J.R.N. Evans, J.M. Thomas, *Nature* **1968**, 218, 673.
65. A. Kawada, A.R. McGhie, M.M. Labes, *J. Chem. Phys.* **1970**, 52, 3121.
66. B.S. Hickman, M. Mascal, J.J. Titman, I.G. Wood, *J. Am. Chem. Soc.* **1999**, 121, 11486.
67. D. Hoel, E. Grunwald, *J. Phys. Chem.* **1977**, 81, 2135.
68. R.W. Singleton, H.D. Noether, J.F. Tracy, *J. Polym. Sci. Polym. Symp.*, **1967**, 19, 65-76.
69. J.K. Gillham, *Rev. Macromol. Sci.* **1972**, 1, 83.
70. M. Armand, *Solid State Ionics* **1983**, 9, 745.
71. *Polymer Electrolyte Reviews 1; MacCallum, J.R.; Vincent, C.A., Eds.; Elsevier Applied Science: Newyork, 1987.*
72. J.J. Fontanella, M.C. Wintersgill, J.S. Wainright, R.F. Savinell, M.Litt, *Electrochim Acta* **1998**, 43, 1289.

73. H. Pu, W.H. Meyer, G. Wegner, *Macromol.Chem.Phys.* **2001**, 202, 1478-1482.
74. A. Bozkurt, W.H. Meyer, *Solid State Ionics* **2000**, 138, 259.
75. H. Pu, *Polym Int* **2003**, 52, 1540-1545.
76. G. Zlatka, G.A. Yuri, P.T. David, G.B. Peter, *Nature* **2001**, 412, 520-523.
77. A. Kawada, A.R. McGhie, M.M. Labes, *J. Chem. Phys.* **1970**, 52, 3121-3125.
78. Y. Masanori, H. Itaru, *J. Phys. Chem .B*, **2004**, 108, 5522-5526.
79. J. M. Lehn, *Science* **1985**, 227, 849
80. R. Maoz, L. Netzer, J. Gun, J. Sagiv, *J. Chem. Phys.* **1988**, 85, 1059
81. J. M. Lehn, *Angew. Chem.* **1990**, 102, 1347.
82. G. Decher, H. Ringsdorf, *Liq. Cryst.* **1993**, 13, 57.
83. K. B. Blodgett, *J. Am. Chem. Soc.* **1934**, 56, 495.
84. K. B. Blodgett, Langmuir, I. *Phys. Rev.* **1937**, 51, 964.
85. H. Kuhn, D. Möbius, *Angew. Chem.* **1971**, 83, 672.
86. G. Decher, J. D. Hong, J. Schmitt, *Thin Solid Films* **1992**, 210/211, 831.
87. J. Gun, G. Sagiv, *J. Colloid Interface Sci.* **1986**, 112, 457.
88. G. G. *Langmuir-Blodgett Films; Plenum Press: New York*, **1990**, p420.
89. S. S. Shiratori, M. F. Rubner, *Macromolecule* **2000**, 33, 4213.
90. D. M. Delongchamp, P. T. Hammond, *Chemistry of Materials* **2003**, 15, 1165.
91. Y. Lvov, G. Decher, G. Sukhorukov, *Macromolecule* **1993**, 26, 5396.
92. Y. M. Lvov, Z. Lu, J. B. Schenkman, J. F. Rusling, *J. Am. Chem. Soc.* **1998**, 120, 4073.
93. E. R. Kleinfield, G. S. Ferguson, *Science* **1994**, 265, 370.
94. S. Watanabe, S. L. Regan, *J. Am. Chem. Soc.* **1994**, 116, 8855.
95. D.L. Feldheim, K. C. Grabar, M. J. Natan, T. C. Mallouk, *J. Am. Chem. Soc.* **1996**, 118, 7640.
96. Y. Lvov, K. Ariga, M. Onda, I. Ichinose, T. Kunitake, *Langmuir* **1997**, 13, 6195.
97. N.A. Kotov, I. Dekany, J. H. Fendler, *J. Phys. Chem.* **1995**, 99, 13065.
98. J.H. Cheung, A. F. Fou, M. F. Rubner, *Thin Solid Films* **1994**, 244, 985.

-
99. P. Stroeve, V. Vasquez, M. A. N. Coelho, J. F. Rabolt, *Thin Solid Films* **1996**, 284, 708.
100. J. Levasalmi, T.J. McCarthy, *Macromolecules* **1997**, 30, 1752.
101. M. Onda, Y. Lvov, K. Ariga, T. Kunitake, *Biotechnol. Bioeng.* **1996**, 51, 163.
102. Y. Sun, X. Zhang, C. Sun, B. Wang, J. Shen, *J. Macromol. Chem. Phys.* **1996**, 197, 147.
103. A. C. Fou, O. Onitsuka, M. Ferreira, M. F. Rubner, B. R. Hsieh, *J. Appl. Phys.* **1996**, 79, 7501.
104. P.T. Hammond, G. M. Whitesides, *Macromolecules* **1995**, 28, 7569.
105. J. Stepp, J. B. Schlenoff, *J. Electrochem. Soc.* **1997**, 144, L155.
106. D. Laurent, J. B. Schlenoff, *Langmuir* **1997**, 13, 1552.
107. A. Laschewsky, B. Mayer, E. Wischerhoff, X. Arys, P. Bertrand, A. Delcorte, A. Jonas, *Thin Solid Films* **1996**, 284, 334.
108. M. F. Durstock, M. F. Rubner, *Langmuir* **2001**, 17, 7865.
109. S. Toyota, T. Nogami, H. Mikawa, *Solid State Ionics* **1984**, 13, 243.
110. A.S. Michaels, *Ind. Eng. Chem.* **1965**, 57, 32.
111. T.R. Farhat, J. B. Schlenoff, *Langmuir* **2001**, 17, 1184.
112. J.F. LeNest, A. Gangini, *In Second International Symposium on Polymer Electrolytes; Scrosati, B., Ed.; Elsevier Science Publishing Co., Inc.: New York, 1990*, pp 129-141.
113. C. Berthier, W. Gorecki, M. Minier, M.B. Armand, J.M. Chabagno, P. Rigaud, *Solid State Ionics* **1986**, 18-9, 300-305.
114. D.M. DeLongchamp, P. T. Hammond, *Chemistry of Materials* **2003**, 15, 1165.
115. D.M. DeLongchamp, P. T. Hammond, *Langmuir* **2004**, 20, 5403.
116. W.B. Stockton, M. F. Rubner, *Macromolecules* **1997**, 30, 2717.
117. L.Y. Wang, Z. Q. Wang, X. Zhang, J.C. Shen, L.F. Chi, H. Fuchs, *Macromol. Rapid Commun.* **1997**, 18, 509.
118. L.Y. Wang, Y. Fu, Z. Q. Wang, Y. Wang, C.Q. Sun, Y.G. Fan, X. Zhang, *Macromol. Chem. Phys.* **1999**, 200, 1523.

119. L.Y. Wang, Y. Fu, Z.Q. Wang, Y.G. Fan, X. Zhang, *Langmuir* **1999**, 15, 1360.
120. L.Y. Wang, S.X. Cui, Z.Q. Wang, X. Zhang, M. Jiang, F.L. Chi, H. Fuchs, *Langmuir* **2000**, 16, 10490.
121. S.A. Sukhishvilli, S. Granick, *J. Am. Chem. Soc.* **2000**, 122, 9550.
122. S.A. Sukhishvilli, S. Granick, *Macromolecules* **2002**, 35, 301.
123. S.Y. Yang, M. F. Rubner, *J. Am. Chem. Soc.* **2002**, 124, 2100.
124. S.T. Dubas, J. B. Schlenoff, *Macromolecules* **2001**, 34, 3736.
125. D.M. DeLongchamp, P.T. Hammond, *Langmuir* **2004**, 20, 5403.
126. I. Yamaguchi, K. Osakada, T. Yamamoto, *Macromolecules* **1997**, 30, 4288.
127. M.B. Gieselman, J.R. Reynolds, *Macromolecules* **1992**, 25, 4832.
128. I. Yamaguchi, K. Osakada, T. Yaamoto, *Macromolecules* **2000**, 33, 2315.
129. X. Glipa, M.E. Hoddad, D.J. Jones, J. Roziere, *Solid State Ionics* **1997**, 97, 323.
130. J.H. Cho, M. Park, J.H. Choi, B.C. Ji, S. Soohan, W. Seoklyoo, *J. Polym. Sci., Part B: Polym. Phys.*, **2001**, 39, 1778.
131. M. Hu, Eli.M. Pearce, T.K. Kwei, *J. Polym. Sci., Part A: Polym. Chem.*, **1993**, 31, 553.
132. T. Brock, D.C. Sherrington, H.G. Tang, *Polymer* **1991**, 32, 353.
133. B. Gordon, R.J. Kumpf, P.C. Painter, *J. Polym. Sci., Part A: Polym. Chem.*, **1988**, 26, 1689.
134. F.D. Trischler, *US Patent 3 578 644 (1971)*.
135. A.H. Gerber, *US Patent 3 943 125 (1976)*.
136. E.W. Choe, *US Patent 4 579 915 (1986)*.
137. M.J. Sansone, *US Patent 4 868 249 (1989)*.
138. M.J. Sansone, *US Patent 4 933 397 (1990)*.
139. M.J. Sansose, *US Patent 4 997 892 (1991)*.

140. H. Pu, Q. Liu, G. Liu, *Journal of Membrane Science* **2004**, 241, 169.
141. Weicheng Wu, *Ph.D-Thesis* **2003**, Max-Planck Institute for Polymer Research, Mainz, Germany.
142. Z. Gadjourova, Y.G. Andreev, D.P. Tunstall, P.G. Bruce, *Nature* **2001**, 412, 520.
143. A. Kawada, A.R. Mcghie, M.M. Labes, *J. Chem. Phys.* **1970**, 52, 3121.
144. G. Decher, J.D. Hong, J. Schmitt, *Thin Solid Films* **1992**, 210/211, 831.
145. G. Decher, J.D. Hong, *Makromol. Chem., Macromol. Symp.* **1991**, 46, 321.
146. F. Saremi, E. Maassen, B. Tieke, G. Jordan, W. Rammensee, *Langmuir* **1995**, 11, 1068.
147. F. Saremi, B. Tieke, *Advanced Materials* **1995**, 7, 378.
148. F. Sevil, A. Bozkurt, *J. Phys. Chem. Solids* **2004**, 65, 1659.
149. W. Münch, K. D. Kreuer, W. Silvestri, J. Maier, G. Seifert, *Soild State Ionics* **2001**, 145, 437.
150. A. Kawada, A. R. Mcghie, M.M. Labes, *J. Chem. Phys.* **1970**, 52, 3121.
151. D. Hoel, E. Grunwald, *J. Phys. Chem.* **1977**, 81, 2135.
152. D.P. Rutger, Y.S. Dotsevi, *Macromolecules* **1997**, 30, 7050
153. S.R. Samms, S. Wasmus, R. F. Savinell, *J. Electrochem. Soc.*, **1996**, 143, 1225.
154. G. Guerra, S. Choe, D.J. Williams, F.E. Karasz, W.J. Macknight, *Macromolecules* **1988**, 21, 231.
155. P. Musto, F.E. Karasz, W.J. Macknight, *Polymer* **1993**, 34, 2934.
156. P. Musto, F.E. Karasz, W.J. Macknight, *Polymer* **1989**, 30, 1012.
157. C. G. Overberger, N. Vorchheimer, *J. Am. Chem. Soc.* **1963**, 85, 951.
158. S. L. Clark, P. T. Hammond, *Langmuir* **2000**, 16, 10206.
159. A. Kudelski, *Langmuir* **2003**, 19, 3805.
160. M. F. Durstock, M. F. Rubner, *Langmuir* **2001**, 17, 7865.
161. D. M. DeLongchamp, P. T. Hammond, *Chem. Mater.* **2003**, 15, 1165.
162. F. Sevil, A. Bozkurt, *J. Phy. Chem. Solids* **2004**, 65, 1659.

-
163. W. Münch, K. D. Kreuer, W. Silvestri, J. Maier, G. Seifert, *Solid State Ionics* **2001**, 145, 437.
164. A. Bozkurt, W. H. Meyer, *Solid State Ionics* **2001**, 138, 259.
165. A. Bozkurt, W. H. Meyer, J. Guttman, G. Wegner, *Solid State Ionics* **2003**, 164, 169.
166. M.F.H. Schuster, W.H. Meyer, *Annual Review Materials Research* **2003**, 33, 233-261.
167. G. Alberti, M. Casciola, *Solid State Ionics* **2001**, 125, 3-16.
168. A. Bozkurt, W.H. Meyer, *Solid State Ionics* **2001**, 138, 259-265.
169. A. Bozkurt, W.H. Meyer, *Journal of Polymer Science: Part B: Polymer Physics* **2001**, 39, 1987-1994.
170. N. Inagaki, K. Goto, K. Katsuura, *Polymer* **1975**, 16, 641.
171. G. M. Kosolapoff., *J. Am. Chem. Soc.*, **1948**, 70, 1971.
172. L.A. Hamilton, *U.S. Pat. 2,365,466*, **1944**.
173. R.M. Pike, R.A. Cohen, *Journal of Polymer Science* **1960**, 531-538.
174. C.S. Marvel, J.C. Wright, *Journal of Polymer Science* **1952**, 8, 255.
175. C.L. Arcus, R.J.S. Matthews, *J. Chem. Soc.*, **1956**, 4607.
176. A. Bozkurt, W.H. Meyer, J. Guttman, G. Wegner, *Solid State Ionics* **2003**, 164, 169.
177. Q. Wu, R.A. Weiss, *J. Polym. Sci., Part-B: Polym. Physics* **2004**, 42, 3628.
178. L. Vinogradova, L. Fedorova, H.J.P. Adler, G. Wegner, *J. Macromol. Sci.- Pure Appl. Chem.*, **2001**, A38 (5&6), 577.
179. B. Boutevin, B. Hamoui, J.P. Parisi, B. Ameduri, *Eur. Polym. J.* **1996**, 32, 159.
180. Z. Yu, W. Zhu, I. Cabasso, *J. Polym. Sci., Part A: Polym. Chem.* **1990**, 28, 227.
181. C. Carbonneau, R. Frantz, J.O. Durant, G.F. Lanneau, R.J.P. Corriu, *Tetrahedron Lett.* **1999**, 40, 5855.
182. R. Frantz, J.O. Durand, F. Carre, G.F. Lanneau, J.L. Bideau, B. Alonso, D. Massiot, *Chem. Eur. J.* **2003**, 9, 770.

183. C.G. Overberg, B. Kusters, T.S. Pierre, *J. Polym. Sci. Part A-1-Polym. Chem.*, **5 (8PA1): 1967**, 1987.
184. C.G. Overberg, K. Gerberdi, *J. Poly. Sci. Part C-Polym. Lett.*, **1973**, 11(7): 465.
185. N.G. Kumar, *J. Polym. Sci. Part C-Polym. Lett.*, **1973**, 11(7), 461.
186. J.B. Lando, M. Litt, T. Shimko, N.G. Kumar, *Polym. Engin. And Sci.*, **1976**, 16(5), 361.
187. C.G. Overberger, L.J. Mathias, *J. Polym. Sci. Part A-Polym. Chem.* **1978**, 16(3), 627.
188. E. Alcalde, L. Perezgarcia, I. Dinares, J. Frigola, *J. Org. Chem.*, **1991**, 56(23), 6516.
189. R.C. Boruah, E.B. Skibo, *J. Org. Chem.*, **1993**, 58(27), 7797.
190. J.S. Wang, K. Matyjaszewski, *Macromolecules* **1995**, 28, 7901.
191. J.S. Wang, K. Matyjaszewski, *J. Am. Chem. Soc.*, **1995**, 117, 5614.
192. T.E. Patten, T. Abernathy, K. Matyjaszewski, *Science* **1996**, 272, 866.
193. K. Matyjaszewski, T. Patten, J. Xia, *J. Am. Chem. Soc.*, **1997**, 119, 674.
194. M. Sawamoto, M. Kamigaito, *Trends in Polymer Science* **1996**, 4, 371.
195. D.A. Shipp, J.L. Wang, K. Matyjaszewski, *Macromolecules* **1998**, 31(23), 8005.
196. K. Matyjaszewski, V. Coessens, Y. Nakagawa, J. Xia, J. Qiu, S. Gaynor, S. Coca, C. Jasieczek, *ACS Symposium Series* **1998**, 704, 16.
197. K. Matyjaszewski, Y. Nakagawa, S.G. Gaynor, *Macromol. Rapid Commun.*, **1997**, 30, 7697.
198. A.J. Applady, R.L. Foulkes, *Fuel cell Handbook; Van Nostrand: New York*, **1989**.
199. L.W. Niedrach, W.T. Grubb, *In fuel cells, Academic Press; New York*, **1963**, p 259.
200. K.D. Kreuer, Th. Dippel, W.H. Meyer, J. Maier, *Mater. Res. Soc. Symp. Proc.* **1993**, 29, 273.
201. K.D. Kreuer, *New proton conducting polymers for fuel cell applications, in: B.V.R. Chowdari, et al. (Eds.), Solid State Ionics: Science and Technology, World Science Publishing, Singapore*, **1998**, 263.

-
202. J.C. Lassegues, in: P. Colomban (Ed.), *Proton Conductors: Solids, Membranes and Gels: Materials and Devices*, Cambridge Univ. Press, Cambridge, **1992**, 311.
203. A. Bozkurt, M. Ise, K.D. Kreuer, W.H. Meyer, G. Wegner, *Solid State Ionics* **1999**, 125, 225.
204. A. Bozkurt, W.H. Meyer, *Solid State Ionics* **2001**, 138, 259.
205. K.D. Kreuer, *J. Memb. Sci.* **2001**, 185, 29.
206. M. Schuster, W.H. Meyer, G. Wegner, H.G. Hertz, M. Ise, K.D. Kreuer, J. Maier, *Solid State Ionics* **2001**, 145, 85.
207. K. D. Kreuer, *Chem. Mater.* **1996**, 8, 610-641.
208. K. D. Kreuer, *J. Membr. Sci.* **2001**, 185, 29-39.
209. C. Yang, P. Costamagna, S. Srinivasan, J. Benziger, A. B. Bocarsly, *J. Power Sources* **2001**, 103, 1-9.
210. B. C. H. Steele, A. Heinzl, *Nature* **2001**, 414, 345-352.
211. P. Jannasch, *Curr. Opin. Colloid Interface Sci.* **2003**, 8, 96-102.
212. J. T. Wang, R. F. Savinell, J. Wainright, M. Litt, H. Yu, *Electrochim. Acta* **1996**, 41, 193-197.
213. A. Bozkurt, M. Ise, K. D. Kreuer, W. H. Meyer, G. Wegner, *Solid State Ionics* **1999**, 125, 225-233.
214. K. D. Kreuer, S. J. Paddison, E. Spohr, M. Schuster, *Chem. Rev.* **2004**, 104, 4637-4678.
215. M. Schuster, W. H. Meyer, G. Wegner, H. G. Herz, M. Ise, K. D. Kreuer, J. Maier, *Solid State Ionics* **2001**, 145, 85-92.
216. M. F. H. Schuster, W. H. Meyer, M. Schuster, K. D. Kreuer, *Chem. Mater.* **2004**, 16, 329-337.
217. J. C. Persson, P. Jannasch, *Chem. Mater.* **2003**, 15, 3044-3045.
218. H. G. Herz, K. D. Kreuer, J. Maier, G. Scharfenberger, M. F. H. Schuster, W. H. Meyer, *Electrochim. Acta* **2003**, 48, 2165-2171.
219. H. Pu, W. H. Meyer, G. Wegner, *Macromol. Chem. Phys.* **2001**, 202, 1478-1282.
220. J. Gao, D. Lee, Y. Yang, S. Holdcroft, B. J. Frisken, *Macromolecules* **2005**, 38, 5854.

221. T. R. Farhat, P. T. Hammond, *Adv. Funct. Mater.* **2005**, 15, 945.
222. C. Hamcuic, M. Klapper, K. Mullen, Synthesis of PEEK with anthracene structural units **2005**. (Manuscript would be submitted).
223. H. Sun, J. E. Mark, N. Venkatasubramanian, M. D. Houtz, S. C. Tan, F. E. Arnold, C. Y. C. Lee, *J. Macro. Mol. Sci., Part A- Pure and Applied Chemistry*, **2004**, 9, 981.
224. D. D. Jiang, S. H. Goh, S. Y. Lee, K. L. Tan, *Polymer* **1997**, 38, 5333.
225. S. Samitsu, T. Shimomura, K. Ito, *Applied Physics Letters* **2005**, 86, 233103.
226. J. Ding, C. Chuy, S. Holdcroft, *Chem. Materials* **2001**, 13(7), 2231.
227. N. G. McCrum, B. E. Read, G. Williams, *Anelastic and Dielectric Effects in Polymeric Solids*, Dover, New York, 1991.
228. H. PU, W. H. Meyer, G. Wegner *J. Polym. Science; Part B: Polym. Phys.* **2002**, 40, 663.
229. K. Toyoji, N. Atsushi, M. Yutaka, M. Soh, S. Naoya, S. Toshifumi, K. Harumi, *Macromolecules* **2003**, 36(12), 4302.
230. R. Bouchet, E. Siebert, *Solid State Ionics* **1999**, 118, 287.
231. J. S. Wainright, J. T. Wang, D. Weng, R. F. Savinell, M. Litt, *J. Electrochem. Soc.* **1995**, 142, L 121.
232. H. Ming, M. Eli, T. K. Kwei, *J. Poly. Sci. Part A: Poly. Chem.*, **1993**, 31, 553.
233. B. Bauer, D. J. Jones, J. Roziere, L. Tchicaya, G. Alberti, *J. New Mater. Electrochem. Syst.* **2000**, 3, 17.
234. G. Alberti, M. Casciola, L. Massinelli, B. Bauer, *J. Membr. Sci.* **2001**, 185, 73.
235. A. Kudelski, W. Hill, *Langmuir* **1999**, 15, 3162.
236. A. Kudelski, *Surf. Sci.* **2002**, 502, 219.
237. A. Kudelski, *Langmuir* 2002, 18, 4714.
238. C. H. Lee, H. B. Park, R. D. Lee, *Ind. Eng. Chem. Res.* **2005**, 44, 7617.
239. H. Jianying, L. Jian, L. Minghua, L. Qiang, D. Lizong, Z. Yousi, *J. Poly. Sci. Part A: Poly. Chem.*, **2005**, 43, 5246.
240. S. OH, K. Kim, B. H. Lee, S. E. Shim, S. Choe, *J. Poly. Sci. Part A: Poly. Chem.*, **2006**, 44, 62.
241. K. O. Siegenthaler, A. Studer, *Macromolecules* **2006**, 39, 1347.

-
242. J. H. Xia, X. Zhang, K. Matyjaszewski, *Macromolecules* **1999**, 32, 3531.
243. T. Cakir, I. E. Serhatli, A. Önen, *J. App. Polym. Sci.*, **2006**, 99, 1993.
244. R. Yang, Y. Wang, X. Wang, W. He, C. Pan, *Euro. Polym. Journal* **2003**, 39, 2029.
245. J. Bibiao, F. Jianbo, Y. Yang, R. Qiang, W. Wenyun, H. Jianjun, *Euro. Polym. Journal* **2006**, 42, 179.
246. J. Chiefari, Y. K. Chong, F. Ercole, J. Krstina, J. Jeffery, T. P. T. Le, R. T. A. Mayadunne, G. F. Meijs, C. L. Moad, G. Moad, E. Rizzardo, S. H. Thang, *Macromolecules* **1998**, 31, 5559.
247. S. W. Prescott, M. J. Ballard, E. Rizzardo, R. G. Gilbert, *Macromolecules* **2002**, 35, 5417.
248. J. Sun, L. R. Jordan, M. Forsyth, D. R. MacFarlane, *Electrochim. Acta* **2001**, 46, 1703.
249. R. A. Munson, M. E. Lazarus, *J. Phys. Chem.* **1967**, 10, 3245.
250. G. K. R. Senadeera, M. A. Careem, S. Skaarup, K. West, *Solid State Ionics* **1996**, 85, 37.
251. J. C. Lassegues, J. Grondin, M. Hernandez, B. Maree, *Solid State Ionics* **2001**, 145, 37.

-

Prabakaran Reguna Sukumar

Max-Planck Institute for Polymer Research,
Ackermannweg 10, D-55128 Mainz, Germany.

Tel: (+49) 6131-379154 (office)

Mobile : (+49) 1601431665

E.mail: prabakaran.sukumar@ge.com

rs.prabakaran@gmail.com



Personal Details

Date of Birth : March 5th, 1973

Nationality : Indian

Marital status : Married

Academic Record

- Ph. D in Polymer Chemistry (January 2002 – June 2006) in the research group of Prof. Klaus Müllen at the Max Planck Institute for Polymer Research, Mainz, Germany.

Thesis Title : *“New proton conducting membranes for fuel cell application.”*

- Master of Technology (M.Tech.) in Polymer Science and Technology (1998-1999), Indian Institute of Technology, New Delhi.

Dissertation Title : *“Chemical modification of polypropylene”*

- Master of Science (M.Sc) in Chemistry (1995-1997), Bharathidasan university, India
- Bachelor of science (B.Sc) in Chemistry (1992-1995), Bharathidasan university, India

Work Experience

July 2006 onwards: IP analyst, GE Technology Center, Bangalore, India

